2015

DESIGNED SYNTHESIS OF NANOPOROUS ORGANIC POLYMERS FOR SELECTIVE GAS UPTAKE AND CATALYTIC APPLICATIONS

Pezhman Arab
Virginia Commonwealth University, arabp@vcu.edu

DESIGNED SYNTHESIS OF NANOPOROUS ORGANIC POLYMERS FOR SELECTIVE GAS UPTAKE AND CATALYTIC APPLICATIONS

A dissertation submitted in partial fulfillment of the requirements for the degree of Doctor of Philosophy at Virginia Commonwealth University.

By
Pezhman Arab

Bachelor of Science
University of Arak, 2007

Master of Science
University of Tehran, 2010

Director: Hani M. El-Kaderi, Associate
Professor, Department of Chemistry

Virginia Commonwealth University
Richmond, Virginia
December, 2015

Acknowledgment

I would like to acknowledge the support and guidance of Dr. Hani M. El-Kaderi whose ideas and encouragement helped me to successfully complete this work. I would also like to express my sincere appreciation for my committee members, Dr. M. Samy El-Shall, Dr. Massimo F. Bertino, and Dr. Indika U. Arachchige, for their invaluable input in pursuit of my Ph.D degree. I am very thankful to Dr. Dmitry Pestov for training me how to operate various characterization instruments used in my research. I wish to thank the members of Dr. El-Kaderi group who have been a great pleasure to work with. I would also like to acknowledge Nanoscience and Nanotechnology program of Virginia Commonwealth University for providing me the opportunity of pursing my Ph.D studies. I wish to thank Chemistry Department of Virginia Commonwealth University for providing a great atmosphere for completing my research. Finally, I would especially like to thank my family for all their love and care. This research was supported by the U.S. Department of Energy, Office of Basic Energy Sciences, under Award DE-SC0002576.

Dedication

This work is dedicated to my parents who have been my first teachers, and to my sisters who have been my best friends.

Table of Contents

Abstract

DESIGNED SYNTHESIS OF NANOPOROUS ORGANIC POLYMERS FOR SELECTIVE GAS UPTAKE AND CATALYTIC APPLICATIONS

By Pezhman Arab, Ph.D.

A dissertation submitted in partial fulfillment of the requirements for the degree of Doctor of Philosophy at Virginia Commonwealth University.

Virginia Commonwealth University, 2015

Director: Hani M. El-Kaderi, Associate Professor, Department of Chemistry

Design and synthesis of porous organic polymers have attracted considerable attentions during the past decade due to their wide range of applications in gas storage, gas separation, energy conversion, and catalysis. Porous organic polymers can be pre-synthetically and post-synthetically functionalized with a wide variety of functionalities for desirable applications. Along these pursuits, we introduced new synthetic strategies for preparation of porous organic polymers for selective CO_2 capture and catalytic applications.

Porous azo-linked polymers (ALPs) were synthesized by an oxidative reaction of amine-based monomers using copper(I) as a catalyst which leads to azo-linkage formation. ALPs exhibit high surface areas of up to 1200 $m^2 g^{-1}$ and have high chemical and thermal stabilities. The nitrogen atoms of the azo group can act as Lewis bases and the carbon atom of CO_2 can act as a Lewis acid. Therefore, ALPs show high CO_2 uptake capacities due to this Lewis acid-based interaction. The potential applications of ALPs for selective CO_2 capture from flue gas, natural gas, and landfill gas under pressure-swing and vacuum swing separation settings were studied. Due to their high CO_2 uptake capacity, selectivity, and regenerability, ALPs are among the best porous organic frameworks for selective CO_2 capture.

In our second project, a new bis(imino)pyridine-linked porous polymer (BIPLP-1) was synthesized and post-synthetically functionalized with $Cu(BF_4)_2$ for highly selective CO_2 capture. BIPLP-1 was synthesized via a condensation reaction between 2,6-pyridinedicarboxaldehyde and 1,3,5-tris(4-aminophenyl)benzene, wherein the bis(imino)pyridine linkages are formed *in-situ* during polymerization. The functionalization of the polymer with $Cu(BF_4)_2$ was achieved by treatment of the polymer with a solution of $Cu(BF_4)_2$ via complexation of copper cations with bis(imino)pyridine moieties of the polymer. BF_4^- ions can act Lewis base and CO_2 can act as a Lewis acid; and therefore, the functionalized polymer shows high binding affinity for CO_2 due to this Lewis acid-based interaction. The functionalization of the pores with $Cu(BF_4)_2$ resulted in a significant enhancement in CO_2 binding energy, CO_2 uptake capacity, and CO_2 selectivity values. Due to high reactivity of bis(imino)pyridines toward transitions metals, BIPLP-1 can be post-synthetically functionalized with a wide variety of inorganic species for CO_2 separation and catalytic applications.

Chapter 1

Introduction

1.1 Porous Organic Polymers as a New Class of Porous Materials

Owing to their high surface areas, porous materials have attracted considerable attention for a wide variety of applications such as separation, chromatography, catalysis, gas storage, and sensing.[1-3] Because of their ability to interact with atoms and ions in both gas phase and liquid phase, porous materials have been used for a large number of scientific and technological applications.[4] According to IUPAC classification, porous materials care classified into three main categories based on their pore sizes.[4-5] Materials with pore sizes of below 2 nm are called microporous.[4-5] If the size of the pores is in the range of 2-50 nm, the solid is classified as a mesoporous material.[4-5] Solid materials with pore sizes greater than 50 nm are denoted as macroporous materials.[4-5] The performance of porous materials for a particular application is a function of pore size, pore shape, pore volume, and chemical nature of the pores.[4, 6] Moreover, pore accessibility and pore connectivity should be controlled to achieve desired properties in porous materials.[6] Therefore, a lot of synthetic strategies have been developed for synthesis of porous structures with different textural properties.[7-10]

Zeolites are crystalline microporous solids which are widely used in catalysis and separation for industrial applications; however, the small size of the pores (<1 nm) in zeolites imposes diffusion limitations which lead to potential complications for practical applications.[9] In order to circumvent this issue, several classes of porous silica and carbon materials with large pores (>2nm) have been recently synthesized.[9, 11] However, the surface chemistry of these conventional porous solids is mainly determined by the nature of the material although they can be modified via post-synthetic approaches to some extent.[7] This lack of chemical tunability can limit the applicability of porous carbon and silica materials.[7] As a result, to overcome these limitations, development of synthetic protocols for preparation of porous structures with tunable physical and chemical properties is highly desirable.[7] Very recently, metal-organic frameworks (MOFs) were introduced as a new class of porous materials with ultra-high surface areas of up to 6000 m^2 g^{-1}.[12] MOFs can be synthesized through reaction of a metallic node with an organic linker via a coordination bond to form a porous coordination framework.[12] Due to crystallinity of MOFs, their pore size, pore volume, and pore shape can be easily tuned.[12] Moreover, thanks to availability of a wide variety of organic linkers and metallic nodes, the chemical nature of the pores in MOFs can be easily controlled for a desired function.[13] However, metal organic frameworks usually exhibit low chemical stabilities which limit the application of this class of materials.[1] Very recently, porous organic polymers (POPs) have begun to emerge as a novel class of porous materials having high porosity and physicochemical stability.[5] POPs are synthesized through polymerization of rigid organic monomers having star-shaped topology.[3] Due to the large number of reactions available for polymerization of organic molecules, different synthetic protocols for preparation of POPs with desirable chemical pore environments have been developed.[5] Different functional groups can be incorporated into POP structure through

pre-synthetic and post-synthetic approaches.[5, 7, 14] This high degree of chemical tunability allows for targeted design and synthesis of POPs for a specific application.[5] Moreover, high physicochemical stability of POPs make them promising materials in industrial applications where harsh conditions such as high temperature and acidic media are normally involved.[15] POPs exhibit high surface areas of up to 6500 m^2 g^{-1},[16] and they can be designed to have microporous or mesoporous structures via appropriate choice of monomers.[17-18] Porous organic polymers might have crystalline or amorphous structures depending on the polymerization reactions and conditions.[5] While the chemical environment of the pores in all classes of POPs can be easily controlled, the complete control over pore size and pore shape is only achievable for crystalline POPs.[5] Since POPs are synthesized using a bottom-up approach via connecting molecular building blocks, their physical and chemical properties can be engineered for a desired property.[3] To synthesize a porous organic polymer, one could imagine constructing a molecular scaffold by connecting rigid monomers to form a web-like structure upon polymerization.[3] Due to their hyper-cross-linked structures, POPs are inherently insoluble in common organic solvents.[5] While this inherent insolubility is advantageous for many applications, the characterization of POPs is more challenging than that of linear polymers since conventional polymer analysis techniques such as gel permeation chromatography cannot be applied for analysis of POPs.[5]

1.2 Synthesis of Porous Organic Polymers via a Topology-Directed Approach

Yaghi and coworkers were the first to apply a topology-directed approach for synthesis of crystalline porous organic polymers.[2] For topological design of porous organic frameworks, atoms and bonds are considered to be vertices and edges respectively.[3] As a result, by appropriate choice of rigid monomers, POPs having well-defined structures can be designed

since the location of atoms and bonds in the porous framework could be predicted before synthesis of the material (Figure 1.1).[3] Due to the geometry of monomers, the pores are formed upon reaction between nodes and struts.[19] For synthesis of POPs using this strategy, star-shaped monomers acting as nodes are usually linked by linear monomers for formation of a porous framework.[19] This approach allows for a total control over the pore size and pore shape of crystalline porous organic polymers.[5] However, the porosity parameters of amorphous POPs cannot be predicted based on the geometry of the building blocks due to uncontrolled framework interpenetration.[7] As a result, due to the bottom-up approach used for the synthesis of POPs, both amorphous and crystalline POPs have well-defined chemical structures while the physical nature of the pores can be fully controlled only in crystalline POPs.[5]

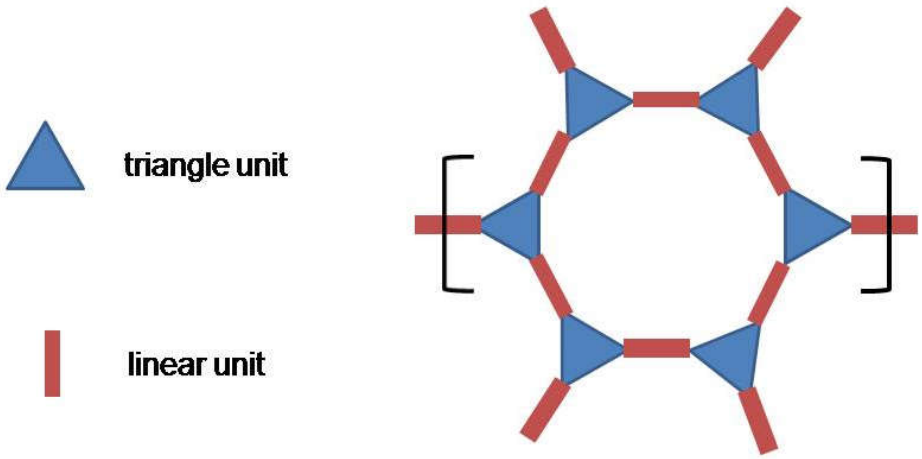

Figure 1.1: Synthesis of a porous organic polymer using the topology-directed. approach.[3]

Figure 1.2 shows the synthesis of COF-5, a crystalline porous organic polymer which is synthesized by boronate linkage formation upon a condensation reaction between 2,3,6,7,10,11-hexahydroxytriphenylene (HHTP) and 1,4-benzenediboronic acid (BDBA).[2] COF-5 has the BET surface are of 1590 m^2 g^{-1}, and its XRD pattern reveals that it has a crystalline eclipsed structure.[2] This strategy has been successfully adopted for synthesis of different classes of POPs with different linkages such as imine,[20] amide,[21] benzimidazole,[22] acetal,[23] and imide.[24]

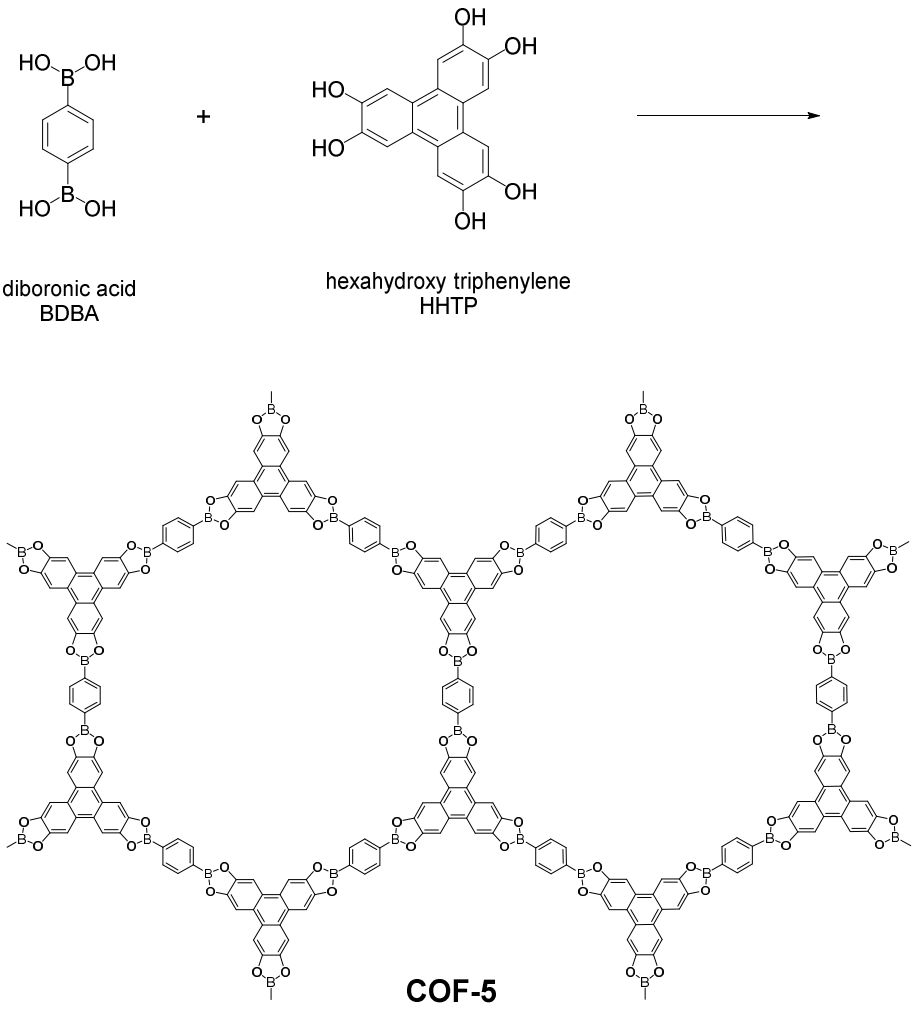

Figure 1.2: Synthesis of a COF-5, a two-dimensional porous organic polymer. [2, 25]

1.3 Carbon Dioxide Separation

Anthropogenic emission of carbon dioxide to the atmosphere has been drastically increased due to industrial development over the past century.[1] This increase in atmospheric CO_2 level has resulted in global warming and climate changes in the past few decades.[26] Due to the increasing demand for energy especially in developing countries, global CO_2 emission is expected to increase in the future.[1] Around 80% of CO_2 emission is due to the combustion of fossil fuels; and therefore, development of alternative clean energy sources is necessary for mitigating climate change.[1] However, the proposed technologies for implementation of alternative renewable clean energy sources are not yet efficient enough for practical applications.[1] As a result, carbon dioxide capture and sequestration (CCS) has been considered as one of the promising solutions for global warming until alternative clean energy sources become widely accessible.[26] In order to reduce the CO_2 emissions to the atmosphere, CO_2 should be separated and sequestrated at stationary point sources such as fossil fuel-based power plants.[1] Electricity generation is responsible for approximately 60 % of total CO_2 emission worldwide, and therefore the implementation of CO_2 capture technologies in power plants can result in a significant reduction in CO_2 emission.[1] Another solution to decrease CO_2 emissions to atmosphere is the removal of CO_2 from natural gas.[27] Natural gas typically consists of ~15% CO_2 which should be separated from methane before transportation.[27] Demand for natural gas is continuously increasing since natural gas has higher energy density and causes lower CO_2 emissions than conventional liquid fossil fuels.[27] Different scenarios have been suggested for permanent sequestration of the captured CO_2.[1] Carbon dioxide can be injected into underground geological formations such as empty oil wells.[1] The use of carbon dioxide as a chemical feedstock in chemical transformation can be considered as an alternative sequestration strategy.[1]

However, this might not be considered as a long-term solution since the market for such commodities would rapidly be saturated due to the large amount of CO_2 produced worldwide.[1] Conversion of the captured CO_2 into a fuel using renewable energy sources can be considered as the most promising scenario for CO_2 sequestration.[28] However, the processes for production of fuel from CO_2 have not been developed enough for practical applications.[1, 28] Regardless of the sequestration strategy used in a CCS system, carbon dioxide needs to be captured from gas mixtures in such systems before sequestration.[1, 27] Currently, the most efficient separation technology used for separation of CO_2 from flue gas involves chemical absorption of CO_2 by aqueous amine solutions.[29] The main drawback of amine scrubbing is the high energy input needed for desorption of the captured CO_2 and regeneration of amine solutions.[29] Due to formation of a strong bond between the carbon atom of CO_2 and a nitrogen atom of amine molecules, the liberation of the captured CO_2 takes place at high temperatures.[29] Because of high water content of such amine solutions and high heat capacity of water, regeneration of scrubbing solutions are energy-intensive.[29] As a result, porous sorbents having much lower heat capacities than that of scrubbing solutions can offer promising strategy to reduce the energy penalty needed for regeneration of a CSS system.[30] In order to be efficient for real-world applications, a CO_2 sorbent needs to selectively capture carbon dioxide over other species present in flue gas such as N_2, H_2O, and O_2.[30] However, due to low concentration of CO_2 (~ 15 %) in flue gas when compared to that of N_2 (~ 75 %), development of highly selective porous sorbents is challenging.[27] Highly selective CO_2 sorbents can provide the opportunity for separation of pure CO_2 for subsequent sequestration.[27] While amine solutions are highly selective for CO_2, their applications can be limited due to the high energy penalty for their regeneration.[29] On the other hand, porous sorbents offering less energy penalty needed for release of captured CO_2 do not

have high CO_2 uptake capacity and selectivity crucial for practical applications.[14] In addition, due to presence of moisture in gas mixtures, porous sorbents might be filled with water after few cycles; and therefore, their performance for CO_2 capture will be reduced significantly.[1] Accordingly, in order to achieve a carbon dioxide capture technology, there is an urgent need for development of new sorbents having high CO_2 uptake capacity, high selectivity, and low regeneration energy penalty.[14] In order to reduce CO_2 emissions from power plants, three strategies can be sought including post-combustion, pre-combustion and oxy-fuel combustion processes.[1] In a post-combustion process, CO_2 is separated from flue gas after combustion of fuel.[14] The separation process mainly involves selective CO_2 capture over N_2 due to high nitrogen content of air used for burning of the fuel.[1, 14] Separation of CO_2 via a post-combustion process using different CO_2 sorbents has been widely explored since this strategy can be easily employed in existing power plants.[1] Alternatively, in a pre-combustion process, the fossil-fuel is first converted to a mixture of H_2 and CO_2 which is followed by separation of CO_2 and combustion of H_2.[1] Due to very low polarizability of H_2 compared to N_2, separation of carbon dioxide from a CO_2/H_2 mixture is much easier than that from a CO_2/N_2 mixture. Oxy-fuel combustion is another possible CO_2 capture process for reducing CO_2 emissions from power plants.[26] In this process, the nitrogen is first removed from air, and then the pure oxygen obtained from removal of N_2 from air will be diluted with CO_2 for combustion of the fossil-fuel.[26] The flue gas resulted from an oxy-fuel combustion is a mixture of carbon dioxide and water.[1] Separation of carbon dioxide from this CO_2/H_2O mixture can be effectively achieved using current technologies.[1] Different CO_2 separation processes suggested for reduction of CO_2 emissions from power plants are schematically illustrated in Figure 1.3.

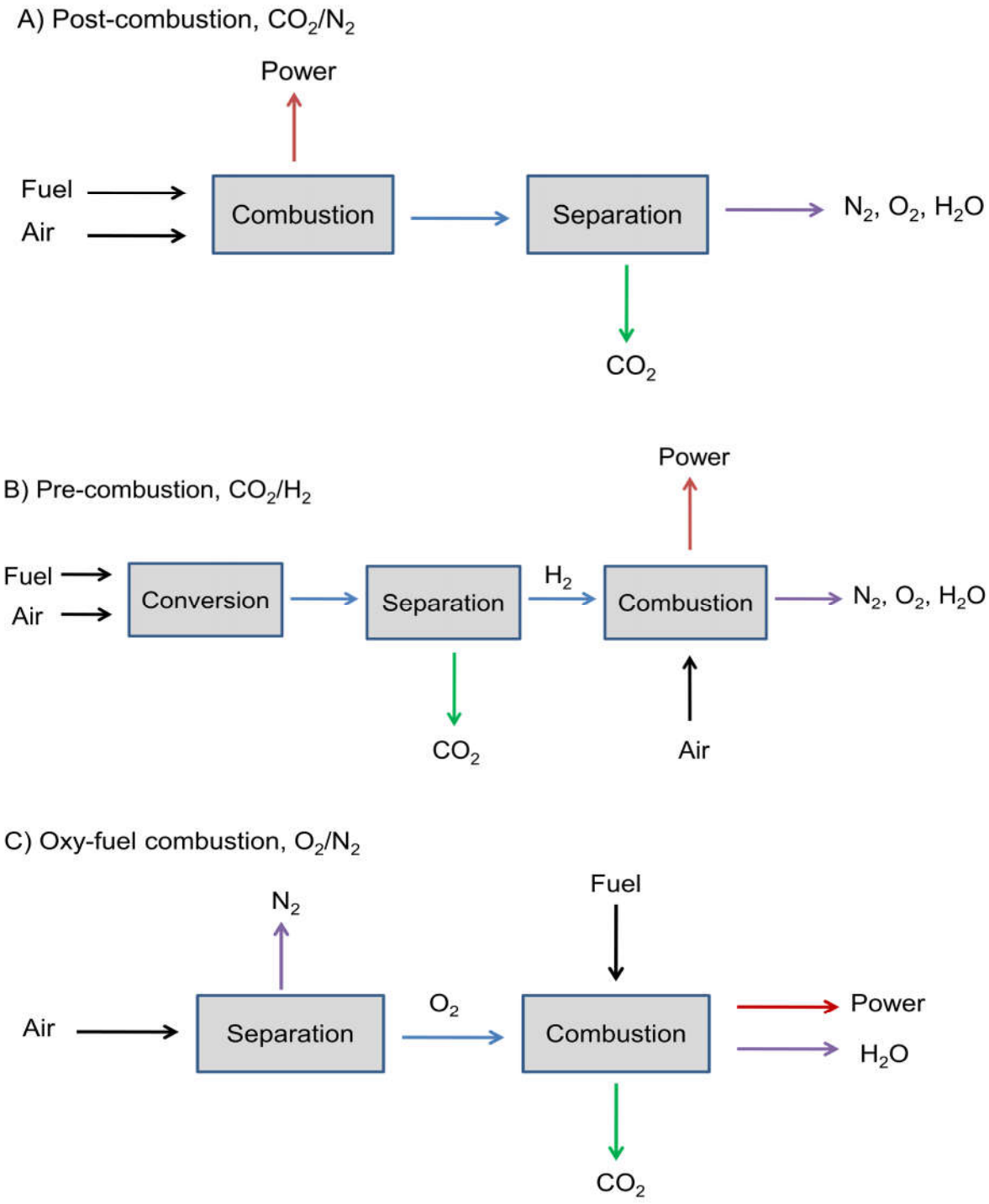

Figure 1.3: Schematic representation of CO_2 separation in post-combustion, pre-combustion and oxy-fuel combustion processes in a power plant.[1]

1.4 Current Sorbents for CO_2

Design and synthesis of new materials for selective CO_2 capture has recently attracted a great deal of attention.[14, 26, 31] Depending on the CO_2 separation conditions for real-world applications, porous sorbents with different properties are required.[27, 30] In order to reduce the energy penalty and cost of CO_2 separation systems, the properties of CO_2 sorbents should be optimized individually for each separation condition.[30] An ideal CO_2 sorbent should have high CO_2 uptake capacity and should selectively capture CO_2 from a gas mixture.[30] Sorbents with high binding affinity for CO_2 usually exhibit high CO_2 uptake capacity and selectivity.[14] However, high binding affinity values result in high energy penalty and cost for desorption of the captured CO_2.[32] On the other hand, low binding energy levels of sorbents for CO_2 can lead to low CO_2 uptake capacity and low selectivity values toward CO_2.[14] Moreover, CO_2 sorbents should have high physicochemical stabilities to retain their performance for infinite number of adsorption-desorption cycles.[1, 14] Several classes of materials such as amine solutions, zeolites, porous carbons, metal-organic frameworks, and porous organic polymers have been explored as CO_2 sorbents; however, none of them could fulfill all requirements for a cost-effective CO_2 capture system.[1]

1.4.1 Amine Solutions

Currently, separation of CO_2 using alkanolamine solutions is the most widely used technology for CO_2 capture in power plants.[29] In this process, amine solutions chemically react with CO_2 to form carbamate or bicarbonate depending on amine type (Figure 1.4).[29] These systems exhibit very high enthalpy of absorption of up to -100 kJ mol^{-1} at 298 K leading to high selectivity values toward CO_2 over other component of gas mixtures.[1] However, due to such

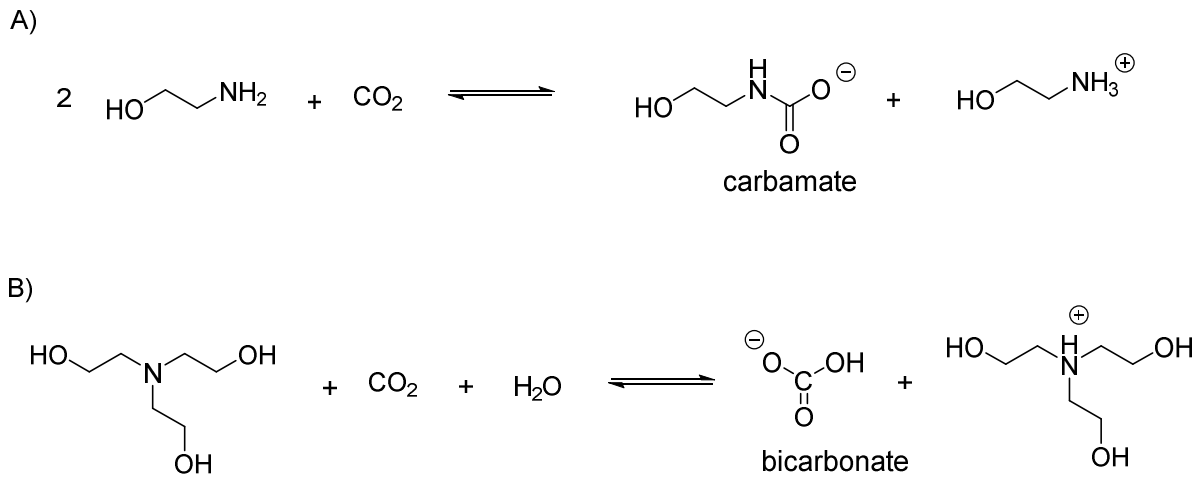

Figure 1.4: Reaction of CO_2 with two different aqueous amine solutions to form carbamate and bicarbonate.[1]

strong interactions between CO_2 molecules and amine functionalities, the liberation of the captured CO_2 and regeneration of sorbents are associated with large energy penalty.[1, 29] Moreover, these aqueous amine solutions contain large percentage of water (~ 60 %) which results in increase in the energy penalty for the regeneration process due to the high heat capacity of water.[1, 29] Aqueous amine solutions have other limitations as CO_2 sorbents for practical applications.[1] First, the regeneration temperature for complete desorption of the captured CO_2 is limited by low thermal stabilities of amine solutions.[1] Moreover, amine solutions decompose over time which leads to decrease in their CO_2 capturing ability by time.[29] In addition, amine solutions are volatile, toxic, and corrosive which limit their applications in real-world applications due to environmental concerns.[29]

1.4.2 Porous Adsorbents

Due to disadvantages of amines solutions, design and synthesis of new CO_2 capturing materials have attracted a lot of attention.[1, 14] In this regard, because of their low heat capacity and high accessible surface for adsorption of CO_2, porous materials have been explored as new sorbents for separation of CO_2 from natural gas and flue gas.[27] The strength of interactions between gas molecules and porous sorbents depends on physical properties of gases such as kinetic diameter, polarizability, and quadrupole moment.[1] This difference in binding affinity of porous sorbents toward different gas molecules present in gas mixtures allows for thermodynamic gas separation via selective adsorption.[1] The gas uptake capacity of a porous sorbent depends on the physical properties of the sorbate.[1] Porous materials exhibit high gas uptake capacities for molecules with high polarizability values and high quadrupole moments.[1] The gas components of a gas mixture have different physical properties and enthalpy of adsorption; and therefore porous sorbents usually show selective adsorption of a certain gas over other components in a gas mixture.[1] If a porous sorbent shows significant differences in binding affinity for the components of a binary gas mixture, selective adsorption of the component with higher enthalpy of adsorption takes place.[1] High difference in enthalpy of adsorptions of components of a binary gas mixture will result in highly selective adsorption of one species over the other one.[1] For example, porous materials can show high CO_2/N_2 selectivity values due to higher polarizability and quadrupole moment of CO_2 (Table 1.1).[1, 14] As expected, porous sorbents usually show lower selectivity values for CO_2/CH_4 separation than that for CO_2/N_2 separation due to higher polarizability of CH_4 than that of N_2 (Table 1.1).[22, 33]

Table 1.1: Physical parameters of selected gases.[1]

Gas	Kinetic Diameter (Angestrom)	Polarizability ($\times 10^{-25}$ cm^3)	Quadrupole Moment ($\times 10^{-26}$ esu cm^2)
He	2.55	2.0	0.0
Ar	3.54	16.4	0.0
N_2	3.64	17.4	1.5
CH_4	3.82	25.9	0.0
CO_2	3.30	29.1	4.3

1.4.2.1 Zeolites

Thanks to development of synthetic strategies for synthesis of zeolites with different porosity parameters and chemical compositions, the relationship between CO_2 capturing ability of this class of materials and their structure can be studied.[1, 27] Due to their microporous structure and high surface areas, zeolites can exhibit high CO_2 uptake capacities.[27] For example, zeolite 13X, having CO_2 uptake capacity of 16.4 wt % at 0.8 bar and room temperature, is one of the most promising CO_2 sorbents among all classes of porous materials.[1, 27] It has been shown that zeolites can offer much faster CO_2 adsorption and lower energy penalty than aqueous amine solutions in post-combustion CO_2 capture processes.[1] However, due to their hydrophilic nature, zeolites adsorb water from flue gas and their CO_2 adsorption capacity will decrease over time due to pore filling with water.[34] Moreover, high temperatures (~ 130 ºC) are required for regeneration of zeolites because of their high binding affinity for CO_2.[35] Although the synthetic strategies for preparation of zeolites have been significantly developed, precise control over porosity parameters of this class of materials still remains a great challenge.[9] Therefore, tuning the physical and chemical nature of the pores in zeolites might be challenging for tuning their

binding affinity toward CO_2.[1] However, owing to their high physicochemical stability, low cost, and well-defined crystalline structure, zeolites are promising materials for CO_2 capture and separation.

1.4.2.2 Porous Carbons

Porous carbons are another class of promising solid sorbents for CO_2 capture due their exceptionally high surface area, high physicochemical stability, and hydrophobic surface.[36] The binding affinity of porous carbons for CO_2 is lower than that of zeolites; and therefore, porous carbons exhibit lower CO_2 uptake capacities than zeolites at low pressures.[27] On the other hand, the exceptionally high surface areas of porous carbons can lead to high CO_2 uptake capacities at high pressure settings.[1] As a result, porous carbons can be efficient CO_2 sorbents in high-pressure separation systems such as pre-combustion CO_2 capture.[37] Moreover, the CO_2 uptake capacity of porous carbons do not usually decrease under hydrated conditions, making them promising candidates for real-world applications where gas streams typically contain considerable water contents.[38] In addition, porous carbons have lower binding affinities toward CO_2 when compared to zeolites; and therefore, the regeneration of porous carbons can take place at relatively low temperatures.[1]

1.4.2.3 Metal-Organic Frameworks

Metal-organic frameworks are emerging as a new class of materials for selective carbon dioxide capture and separation.[26, 30] Due to high crystallinity of MOFs as well as a wide diversity of organic linkers available for synthesis of MOFs, the physical and chemical nature of the pores in MOF can be easily tuned.[26] This allows for a precise control over gas-framework interactions

to achieve desired separation capabilities.[26] Thanks to the building block approach employed for the synthesis of MOFs, porous structures functionalized with CO_2-philic groups can be easily synthesized and explored for CO_2 separation applications.[26] Moreover, MOFs are among the most porous structures and have high surface areas of up to 7000 m^2 g^{-1}. As a result, MOFs can provide a high number of adsorption sites because of their significantly high surface areas.[27] A great number of MOFs with different pore sizes, surface areas, and chemical functionalities have been synthesized and studied for CO_2 separation.[27] The structure of MOFs can be predicated prior to their synthesis; and therefore, MOFs featuring desired binding affinities for CO_2 can be synthesized based on the requirements needed for each separation condition.[1, 27] However, MOFs usually have low chemical and thermal stabilities which limit their applications as CO_2 sorbents.[1] For practical applications, MOF having high CO_2 uptake capacities with high stabilities toward moisture as well as high thermal stabilities in high temperatures should be developed.[1]

1.4.2.4 Porous Organic Polymers

Targeted synthesis of porous organic polymers (POPs) for separation of CO_2 from flue gas, natural gas, and landfill gas have recently attracted considerable attention.[14] In order for POPs to be considered as efficient adsorbents for large scale CO_2 capture and separation, they should show high CO_2 uptake capacity and high selectivity toward CO_2.[14] In addition, an ideal POP should have a moderate binding affinity for CO_2 to minimize the energy input required in the regeneration step.[32] POPs are among the most porous materials and have high physicochemical stabilities in harsh conditions such as acidic and basic conditions as well as high temperatures.[16] Moreover, the physical and chemical nature of the pores in POPs can be easily tuned by appropriate choice of monomers and polymerization reactions.[3, 19] This high

degree of control over the chemical nature of POPs is considered to be the main advantage of POPs over conventional porous CO_2 sorbents such as porous silica and carbon materials. Functionalization of the pores with polar groups such as nitrogen-rich and oxygen-rich groups can result in high binding affinity of the framework for CO_2.[5] Therefore, POPs featuring such functional groups usually show high CO_2 uptake capacities and selectivities.[5] This offers the opportunity of tuning gas-framework interactions in POPs for selective CO_2 capture over other gases present in industrial gas mixtures.[14] Three main strategies can be used to tune the physical and chemical properties of POPs to increase their CO_2 capturing properties.[14] These approaches include: 1) synthesis of ultra-high surface area POPs; 2) increasing binding affinity of POPs for CO_2 via pore size engineering; 3) pore functionalization with CO_2-philic groups.[14] Due to their high surface areas (up to 6500 m^2 g^{-1}), porous organic polymers provide a high number of adsorption sites for gas molecules.[16] CO_2 uptake capacity of POPs especially at high pressures usually increases with surface area.[14] For example, PPN-4 which is a porous organic polymer with surface area of 6460 m^2 g^{-1} exhibits high CO_2 uptake capacity of 39 mmol g^{-1} at 295 K and 50 bar.[16] The CO_2 uptake capacity of microporous polymers at atmospheric pressure is also a function of surface areas. For example, BILP-12 having the highest surface areas among benzimidazole-linked polymers exhibits the highest CO_2 uptake capacity among this class of POPs at 1 bar and 298 K.[39] It should be noted that POPs with ultra-high surface area do not necessary show high CO_2 uptake capacities at low pressures although they usually have very high CO_2 uptake capacities at high pressures.[14] This originates from the low binding affinity of ultra-high surface areas POPs.[14] For example, PAFs having high surface areas (~5000 m^2 g^{-1}) show low binding affinities for CO_2 (~15 kJ mol^{-1}) which result in their low CO_2 uptake capacities at 1 bar.[40] On the other hand, BILPs which are microporous polymers with moderate

surface areas have high binding affinity for CO_2 (~30 kJ mol^{-1}); and therefore they show high CO_2 uptake capacities of up to 5.3 mmol g^{-1} at 1 bar and 273 K.[22] This highlights the more important role of binding affinity in CO_2 capture at low pressures than that of surface area. Pore functionalization of POPs with polar groups can result in high binding affinity of the framework toward CO_2.[41] This is due to dipole-quadrupole interactions between individual CO_2 molecules and Lewis basic sites of the pores.[41] The carbon atom in a CO_2 molecule is electron deficient and can act as a Lewis acid.[42] Therefore, incorporation of Lewis basic sites into porous organic frameworks can lead to high binding affinity values for CO_2 which can result in high CO_2 uptake capacity of such functionalized POPs.[14] Porous organic polymers functionalized with Lewis basic sites can be synthesized by pre-synthetic or post-synthetic functionalization approaches.[14] In the pre-synthetic modification strategy, POPs with polar functional groups are synthesized by judicious choice of nitrogen-, oxygen-, and sulfur- rich monomers.[14] For example, imine-linked,[43] benzimidazole-linked,[33] benzoxazole-linked,[44] and triazole-linked[45] polymers have been synthesized via pre-synthetic approaches where the functionalities are created in-situ during polymerization. On the other hand, in post-synthetic functionalization protocols, functional groups are incorporated into POPs' framework after synthesis of the porous framework.[41] Several porous organic polymers which are post-synthetically functionalized with nitro, amino, and sulfonic groups have shown enhanced CO_2 uptake capacity and selectivity.[14, 41] The binding affinity of POPs for CO_2 can be also tuned via pore size engineering. Porous organic polymers with ultra-small pores (< 7 nm) usually show high binding affinity for CO_2 leading to high CO_2 uptake capacity especially at low pressures.[46] An adsorbed CO_2 in an ultra-small pore can have multiple interactions with pore walls which result in strong framework-CO_2 interactions.[14] Due to high binding affinity and high CO_2 uptakes at low pressures, microporous organic polymers

are promising candidates for CO_2 separation under low pressure settings such as post-combustion processes.[46]

1.4.2.4.1 Synthesis of Nitrogen-Rich Porous Organic Polymers for Selective CO_2 Capture

Theoretical and experimental studies have shown that the lone pair electrons of nitrogen atoms in nitrogen-rich porous organic polymers usually show high Lewis basicity toward CO_2.[47-48] This leads to high binding affinity for such polymers for CO_2 which results in high CO_2 uptake capacity and selectivity values.[47-48] The nitrogen based functional groups can be incorporated into POPs via pre-synthetic or post-synthetic approaches.[41] A large number of nitrogen-rich POPs have been synthesized via polymerization of nitrogen-rich monomers (Figure 1.5).[49] In pre-synthetic approaches, the nitrogen-based functionalities can be created in-situ during polymerization.[25] For example, benzimidazole functional groups can be incorporated into a POP structure in situ upon reaction of aldehyde-based monomers with diamine-based monomers (Figure 1.5).[22] The use of monomers containing nitrogen-based functional groups is also a useful means for synthesis of nitrogen rich POPs.[25] For example, porous organic polymers functionalized with triazine and tertiary amine moieties have been successfully prepared by suitable choice of monomers and reaction conditions (Figure 1.5).[25]

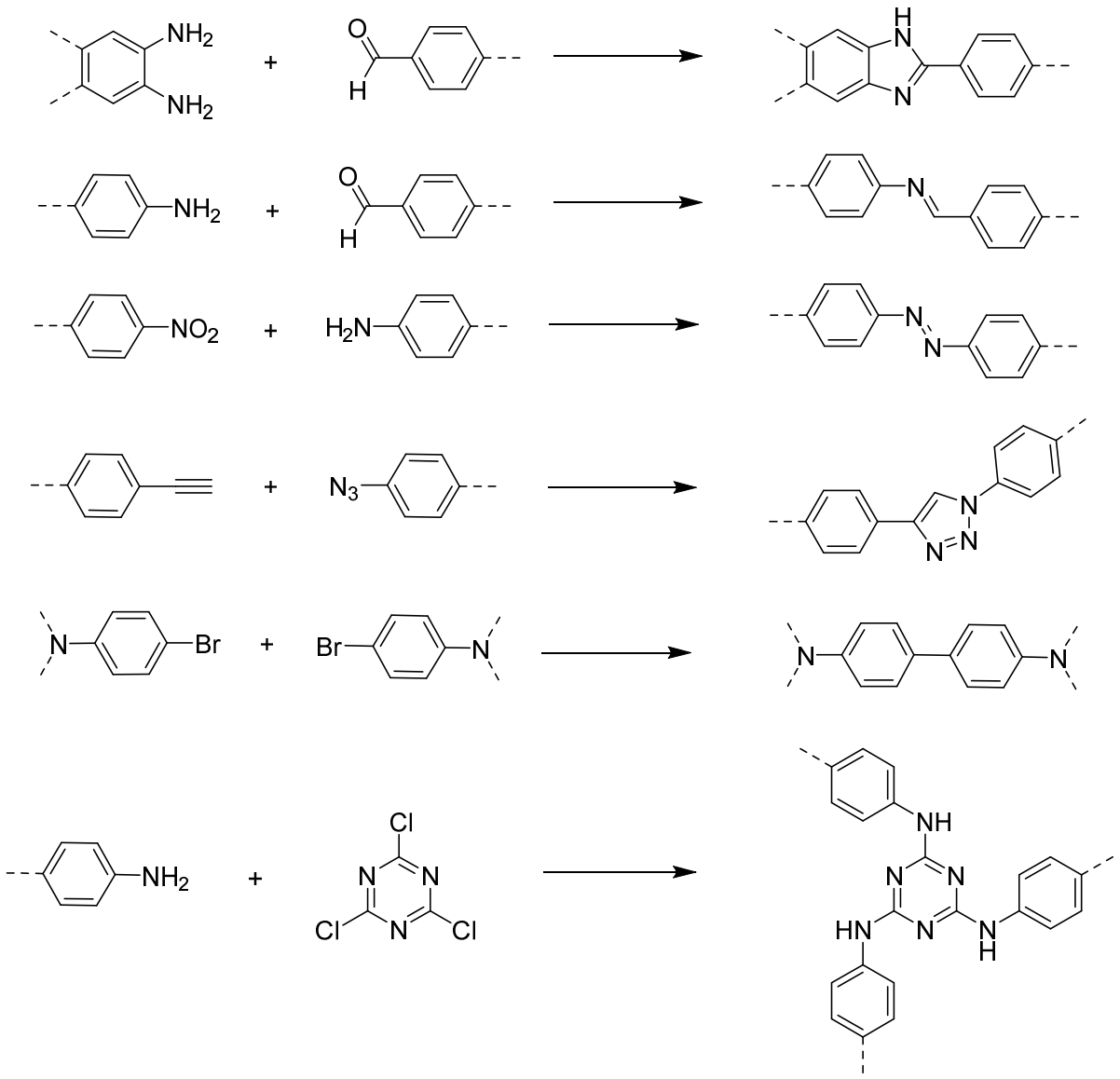

Figure 1.5: Synthesis of different nitrogen rich porous organic polymers.[25]

1.5 Regeneration Processes for Solid CO_2 Sorbents

In any CO_2 capture system, the sorbent needs to be regenerated after each CO_2 sorption cycle to be used for the next run.[27] Solid sorbents can be regenerated using different processes such as temperature swing adsorption (TSA), vacuum swing adsorption (VSA), and pressure swing adsorption (PSA).[27] In a TSA process, after adsorption takes place, the captured CO_2 will be desorbed by increasing the temperature.[27] TSA can be an efficient process for CO_2 capture systems in power-plants due to availability of low-grade heat accessible during electricity generation.[1] In a TSA cycle, in order to release the captured CO_2, the sorbent is heated in ambient pressure followed by purging the system to remove the desorbed CO_2 from the void spaces of the sorbent.[1] Finally, the system should be cooled down to ambient temperature to be prepared for the next separation cycle.[1] In VSA cycles, after CO_2 is adsorbed at ambient temperature and pressure, the sorbent is regenerated by lowing the pressure of the system to ~ 0.1 for desorption of CO_2.[27] VSA can be an appropriate regeneration process for CO_2 capture systems in post-combustion applications due to atmospheric pressure of flue gas.[27] Similar to VSA, in a PSA process the sorbent is regenerated upon lowering the pressure of the system; however, in PSA cycles the adsorption takes place at high pressures (~5 bar) and the regeneration of the sorbent is achieved by reducing the pressure of the system to atmospheric pressure.[27] The adsorption of CO_2 in pre-combustion process takes place at high pressures; and therefore, PSA process is more promising for regeneration of the sorbents in pre-combustion CO_2 capture systems.[1, 27] The adsorption/desorption parameters such as temperature and pressure in regeneration cycles should be optimized for each system to minimize the total cost of CO_2 separation.[27, 30] Moreover, the choice of adsorbent should be based on the type of the regeneration process.[30] For example, sorbents with moderate surface area and high binding

affinity are more suitable for CO_2 separation by VSA processes.[30] On the other hand, sorbents with high surface area and moderate binding energy for CO_2 are more promising for PSA systems.[30]

1.6 Porous Organic Polymers in Heterogeneous Catalysis

Porous organic polymers have recently attracted a lot of attention as new supports for preparation of heterogeneous catalysts.[7] Due to the bottom-up approach used for preparation of POPs, the chemical nature of POPs can be easily controlled by judicious choice of monomers.[3] This high degree of surface tunability is considered as the main advantage of POPs over conventional catalyst supports such as zeolites and porous carbons.[7] Moreover, the topological approach used for synthesis of POPs allows for an atomic level control over the surface chemistry of POPs.[3] As a result, a wide variety of functional groups can be incorporated into POPs for desirable catalytic applications.[50] POPs constructed from nitrogen-, sulfur-, and phosphorous-rich monomers have been widely used for encapsulation of metal nanoparticles for preparation of highly stable heterogeneous catalysts.[7, 50] Due to their strong nanoparticle-heteroatom interactions, POPs having electron rich groups can stabilize nanoparticles against agglomerations during a catalytic reaction.[50] In addition, porous organic polymers are promising supports for immobilization of molecular catalysts.[51] POPs functionalized with chelating sites have been successfully used for immobilization of a wide variety of molecular catalysts.[50-51] Both pre-synthetic and post-synthetic approaches can be applied for incorporation of molecular catalysts into POPs' structure.[50] In a pre-synthetic strategy, metal-containing monomers are linked together to form a porous polymer functionalized with a molecular catalyst.[7] On the other hand, in post-synthetic approaches, porous organic polymers with free metal binding sites are

synthesized by polymerization of monomers containing chelating sites.[7] These polymers will be post-synthetically functionalized with molecular catalysts via complexation of their chelating sites to metallic species after treatment with a solution of desirable molecular catalyst.[51] Various porous organic polymers functionalized with different transition metals such as Pt(II), Pd(II), Ru(II), and Rd(II) have shown high catalytic activity and stability.[50-51] Because of their high surface area, high physicochemical stability, and tunability of their surface chemistry, porous organic polymers are promising supports for preparation of heterogeneous catalysts.[50-51]

1.7 Porosity and Gas Uptake Measurements

The specific surface area and porosity parameters of solid materials can be determined by their gas adsorption isotherms. The crude data are obtained by adsorption of an adsorbate such as N_2 gas on the surface of a solid in a constant temperature. The surface area of solid materials can be estimated by determination of the amount of gas which can be adsorbed on their surfaces. For surface area measurements, the sample is loaded in a cell and the cell is submerged in a liquid bath to provide a constant temperature during the measurement. The gas isotherms show the amount of gas adsorbed on the surface of the sorbent as a function of pressure. For surface area and porosity measurements, gas isotherms are usually collected at a pressure range of 10^{-6} – 1 bar. After applying vacuum over the cell, the adsorption/desorption isotherms are constructed by point-by-point admission and withdrawal of a known amount of a gas. In order to measure the amount of gas adsorbed by the sorbent, the instrument doses small quantities of the sorbate to the cell until the desired requested pressure is achieved. Since the volume of the cell is known, the amount of the gas needed to reach a certain pressure in an empty cell can be calculated. On the other hand, solid materials can adsorb large quantities of the gas introduced to the cell; and

therefore, the gas amount needed to reach a desired pressure in a cell filled with solid sorbents is higher than that of an empty cell. As a result, the instrument can calculate the quantity of the gas adsorbed on the surface of the sample by using the gas uptake data of the sample and void volume of the empty cell. In order to measure the amount of the adsorbed gas at a desired pressure, the instrument introduces small amount of gas to the cell and waits for the gas to equilibrate after adsorption takes place. This dosing process will be repeated for several times until the desired pressure in the cell in reached. Then, the instrument will record the total amount of the gas introduced to the cell to reach the requested pressure. The same process will take place for recording the gas uptake of the sample for each desired pressure until the adsorption isotherm is complete. To obtain desorption isotherms, the instrument applies vacuum in a stepwise fashion to the cell after adsorption curve is completed. The instrument removes the adsorbed gas molecules using a fine vacuum and record the volume of the gas desorbed at each pressure to provide a desorption curve. Using this approach, the gas uptake capacity of porous sorbent for different gas molecules such as CO_2, N_2, CH_4, Kr, and H_2 at different temperatures can be measured. At early stages of adsorption, each gas molecule occupies an adsorption site on the surface of the solid. In other words, each molecule is directly adsorbed on the surface, forming a monolayer of gas on the surface of the solid. Then, another layer of gas molecules can form on the top of the first layer, followed by adsorption of other layers on the top of existing layers.[52] This adsorption behavior is usually observed for adsorption of Ar and N_2 gases at cryogenic temperatures and is called multilayer adsorption.

The specific surface area can be obtained by determining the number of gas molecules needed to form a monolayer on the surface of adsorbent. The amount of gas forming a monolayer on the surface of a solid material is called monolayer capacity. After determination of

monolayer capacity, the surface area can be calculated by multiplying the number of gas molecules forming the monolayer by the area occupied by each molecule. Langmuir and BET models are typically used for assessment of surface area of solid materials.[53] In Langmuir model, it is assumed that: i) adsorbed molecules do not have any interactions with each other, ii) all adsorbate molecules are adsorbed with the same adsorption mechanism, and iii) adsorbates form a single layer one surface of the sorbent, and multilayer adsorption doses not take place. However, in reality, gas molecules usually interact with each other, and multilayer adsorption generally takes place. This results in different adsorption mechanism in early stage and final stage of the gas adsorption. As a result, the use of Langmuir model usually leads to overestimation of measured surface areas of solid sorbents. In 1938, Brunauer, Emmett, and Teller developed another model, called BET, for measurement of surface area of solid materials where they considered the possible scenario for multilayer adsorptions.[52] As a result, the BET model is considered to reflect more realistic results than Langmuir model.[52]

The size of the pores of porous materials can also be determined using gas isotherms. Depending on the pore size, porous materials can show different types of isotherms due to differences in adsorbate-sorbent as well as adsorbate-adsorbate interactions. As a result, by fitting experimentally collected isotherms into developed models for pore size determination, the size of the pores can be measured. . Barrett-Joyner-Halenda (BJH) and Non-Local Density Functional Theory (NLDFT) models are typically used for pore size measurements.[54] BJH can underestimate the size of the pores by 25 % and is not used in our research.

References

1. Sumida, K.; Rogow, D. L.; Mason, J. A.; McDonald, T. M.; Bloch, E. D.; Herm, Z. R.; Bae, T.-H.; Long, J. R., Carbon Dioxide Capture in Metal–Organic Frameworks. *Chemical Reviews,* **2011**, *112*, 724-781.

2. Côté, A. P.; Benin, A. I.; Ockwig, N. W.; O'Keeffe, M.; Matzger, A. J.; Yaghi, O. M., Porous, Crystalline, Covalent Organic Frameworks. *Science,* **2005**, *310*, 1166-1170.

3. Zou, X.; Ren, H.; Zhu, G., Topology-Directed Design of Porous Organic Frameworks and their Advanced Applications. *Chemical Communications,* **2013**, *49*, 3925-3936.

4. Davis, M. E., Ordered Porous Materials for Emerging Applications. *Nature,* **2002**, *417*, 813-821.

5. Dawson, R.; Cooper, A. I.; Adams, D. J., Nanoporous Organic Polymer Networks. *Progress in Polymer Science,* **2012**, *37*, 530-563.

6. Vilela, F.; Zhang, K.; Antonietti, M., Conjugated Porous Polymers for Energy Applications. *Energy & Environmental Science,* **2012**, *5*, 7819-7832.

7. Kaur, P.; Hupp, J. T.; Nguyen, S. T., Porous Organic Polymers in Catalysis: Opportunities and Challenges. *ACS Catalysis,* **2011**, *1*, 819-835.

8. Lee, J.; Kim, J.; Hyeon, T., Recent Progress in the Synthesis of Porous Carbon Materials. *Advanced Materials,* **2006**, *18*, 2073-2094.

9. Tao, Y.; Kanoh, H.; Abrams, L.; Kaneko, K., Mesopore-Modified Zeolites: Preparation, Characterization, and Applications. *Chemical Reviews,* **2006**, *106*, 896-910.

10. Long, J. R.; Yaghi, O. M., The Pervasive Chemistry of Metal-organic Frameworks. *Chemical Society Reviews,* **2009**, *38*, 1213-1214.

11. Stein, A.; Wang, Z.; Fierke, M. A., Functionalization of Porous Carbon Materials with Designed Pore Architecture. *Advanced Materials,* **2009**, *21*, 265-293.

12. Zhou, H.-C.; Long, J. R.; Yaghi, O. M., Introduction to Metal–Organic Frameworks. *Chemical Reviews,* **2012**, *112*, 673-674.

13. Rowsell, J. L. C.; Yaghi, O. M., Metal–Organic Frameworks: a New Class of Porous Materials. *Microporous and Mesoporous Materials,* **2004**, *73*, 3-14.

14. Dawson, R.; Cooper, A. I.; Adams, D. J., Chemical Functionalization Strategies for Carbon Dioxide Capture in Microporous Organic Polymers. *Polymer International,* **2013**, *62*, 345-352.

15. Arab, P.; Rabbani, M. G.; Sekizkardes, A. K.; İslamoğlu, T.; El-Kaderi, H. M., Copper(I)-Catalyzed Synthesis of Nanoporous Azo-Linked Polymers: Impact of Textural Properties on Gas Storage and Selective Carbon Dioxide Capture. *Chemistry of Materials,* **2014**, *26*, 1385-1392.

16. Yuan, D.; Lu, W.; Zhao, D.; Zhou, H.-C., Highly Stable Porous Polymer Networks with Exceptionally High Gas-Uptake Capacities. *Advanced Materials,* **2011**, *23*, 3723-3725.

17. Chen, X.; Huang, N.; Gao, J.; Xu, H.; Xu, F.; Jiang, D., Towards Covalent Organic Frameworks with Predesignable and Aligned Open Docking Sites. *Chemical Communications,* **2014**, *50*, 6161-6163.

18. Ding, S.-Y.; Gao, J.; Wang, Q.; Zhang, Y.; Song, W.-G.; Su, C.-Y.; Wang, W., Construction of Covalent Organic Framework for Catalysis: Pd/COF-LZU1 in Suzuki–Miyaura Coupling Reaction. *Journal of the American Chemical Society,* **2011**, *133*, 19816-19822.

19. Feng, X.; Ding, X.; Jiang, D., Covalent Organic Frameworks. *Chemical Society Reviews,* **2012**, *41*, 6010-6022.

20. Rabbani, M. G.; Sekizkardes, A. K.; Kahveci, Z.; Reich, T. E.; Ding, R.; El-Kaderi, H. M., A 2D Mesoporous Imine-Linked Covalent Organic Framework for High Pressure Gas Storage Applications. *Chemistry – A European Journal,* **2013**, *19*, 3324-3328.

21. Weber, J.; Su, Q.; Antonietti, M.; Thomas, A., Exploring Polymers of Intrinsic Microporosity – Microporous, Soluble Polyamide and Polyimide. *Macromolecular Rapid Communications,* **2007**, *28*, 1871-1876.

22. Rabbani, M. G.; El-Kaderi, H. M., Synthesis and Characterization of Porous Benzimidazole-Linked Polymers and Their Performance in Small Gas Storage and Selective Uptake. *Chemistry of Materials,* **2012**, *24*, 1511-1517.

23. Zhao, Y.-C.; Zhang, L.-M.; Wang, T.; Han, B.-H., Microporous Organic Polymers with Acetal Linkages: Synthesis, Characterization, and Gas Sorption Properties. *Polymer Chemistry,* **2014**, *5*, 614-621.

24. Farha, O. K.; Bae, Y.-S.; Hauser, B. G.; Spokoyny, A. M.; Snurr, R. Q.; Mirkin, C. A.; Hupp, J. T., Chemical Reduction of a Diimide Based Porous Polymer for Selective Uptake of Carbon Dioxide Versus Methane. *Chemical Communications,* **2010**, *46*, 1056-1058.

25. Xu, C.; Hedin, N., Microporous Adsorbents for CO_2 Capture – a Case for Microporous Polymers? *Materials Today,* **2014**, *17*, 397-403.

26. Li, J.-R.; Ma, Y.; McCarthy, M. C.; Sculley, J.; Yu, J.; Jeong, H.-K.; Balbuena, P. B.; Zhou, H.-C., Carbon Dioxide Capture-Related Gas Adsorption and Separation in Metal-Organic Frameworks. *Coordination Chemistry Reviews,* **2011**, *255*, 1791-1823.

27. Bae, Y.-S.; Snurr, R. Q., Development and Evaluation of Porous Materials for Carbon Dioxide Separation and Capture. *Angewandte Chemie International Edition,* **2011**, *50*, 11586-11596.

28. Kumar, B.; Smieja, J. M.; Kubiak, C. P., Photoreduction of CO_2 on p-type Silicon Using Re(bipy-But)$(CO)_3$Cl: Photovoltages Exceeding 600 mV for the Selective Reduction of CO_2 to CO. *The Journal of Physical Chemistry C,* **2010**, *114*, 14220-14223.

29. Rochelle, G. T., Amine Scrubbing for CO_2 Capture. *Science,* **2009**, *325*, 1652-1654.

30. Wilmer, C. E.; Farha, O. K.; Bae, Y.-S.; Hupp, J. T.; Snurr, R. Q., Structure-Property Relationships of Porous Materials for Carbon Dioxide Separation and Capture. *Energy & Environmental Science,* **2012**, *5*, 9849-9856.

31. Jiang, J.-X.; Cooper, A., Microporous Organic Polymers: Design, Synthesis, and Function. In *Functional Metal-Organic Frameworks: Gas Storage, Separation and Catalysis*, Schröder, M., Ed. Springer Berlin Heidelberg: 2010; Vol. 293, pp 1-33.

32. Sung, S.; Suh, M. P., Highly Efficient Carbon Dioxide Capture with a Porous Organic Polymer Impregnated with Polyethylenimine. *Journal of Materials Chemistry A,* **2014**, *2*, 13245-13249.

33. Rabbani, M. G.; Sekizkardes, A. K.; El-Kadri, O. M.; Kaafarani, B. R.; El-Kaderi, H. M., Pyrene-Directed Growth of Nanoporous Benzimidazole-Linked Nanofibers and their Application

to Selective CO_2 Capture and Separation. *Journal of Materials Chemistry,* **2012**, *22*, 25409-25417.

34. Li, G.; Xiao, P.; Webley, P.; Zhang, J.; Singh, R.; Marshall, M., Capture of CO_2 from High Humidity Flue Gas by Vacuum Swing Adsorption with Zeolite 13X. *Adsorption,* **2008**, *14*, 415-422.

35. Konduru, N.; Lindner, P.; Assaf-Anid, N. M., Curbing the Greenhouse Effect by Carbon Dioxide Adsorption with Zeolite 13X. *AIChE Journal,* **2007**, *53*, 3137-3143.

36. Lu, A.-H.; Hao, G.-P.; Zhang, X.-Q., Porous Carbons for Carbon Dioxide Capture. In *Porous Materials for Carbon Dioxide Capture*, Lu, A.-H.; Dai, S., Eds. Springer Berlin Heidelberg: 2014; pp 15-77.

37. D'Alessandro, D. M.; Smit, B.; Long, J. R., Carbon Dioxide Capture: Prospects for New Materials. *Angewandte Chemie International Edition,* **2010**, *49*, 6058-6082.

38. Plaza, M. G.; García, S.; Rubiera, F.; Pis, J. J.; Pevida, C., Post-Combustion CO_2 Capture with a Commercial Activated Carbon: Comparison of Different Regeneration Strategies. *Chemical Engineering Journal,* **2010**, *163*, 41-47.

39. Sekizkardes, A. K.; Islamoglu, T.; Kahveci, Z.; El-Kaderi, H. M., Application of Pyrene-Derived Benzimidazole-Linked Polymers to CO_2 Separation under Pressure and Vacuum Swing Adsorption Settings. *Journal of Materials Chemistry A,* **2014**, *2*, 12492-12500.

40. Ben, T.; Pei, C.; Zhang, D.; Xu, J.; Deng, F.; Jing, X.; Qiu, S., Gas Storage in Porous Aromatic Frameworks (PAFs). *Energy & Environmental Science,* **2011**, *4*, 3991-3999.

41. Islamoglu, T.; Gulam Rabbani, M.; El-Kaderi, H. M., Impact of Post-Synthesis Modification of Nanoporous Organic Frameworks on Small Gas Uptake and Selective CO_2 Capture. *Journal of Materials Chemistry A,* **2013**, *1*, 10259-10266.

42. Nagaraja, C. M.; Haldar, R.; Maji, T. K.; Rao, C. N. R., Chiral Porous Metal–Organic Frameworks of Co(II) and Ni(II): Synthesis, Structure, Magnetic Properties, and CO_2 Uptake. *Crystal Growth & Design,* **2012**, *12*, 975-981.

43. Pandey, P.; Katsoulidis, A. P.; Eryazici, I.; Wu, Y.; Kanatzidis, M. G.; Nguyen, S. T., Imine-Linked Microporous Polymer Organic Frameworks. *Chemistry of Materials,* **2010**, *22*, 4974-4979.

44. Patel, H. A.; Ko, D.; Yavuz, C. T., Nanoporous Benzoxazole Networks by Silylated Monomers, Their Exceptional Thermal Stability, and Carbon Dioxide Capture Capacity. *Chemistry of Materials,* **2014**, *26*, 6729-6733.

45. Plietzsch, O.; Schilling, C. I.; Tolev, M.; Nieger, M.; Richert, C.; Muller, T.; Brase, S., Four-Fold Click Reactions: Generation of Tetrahedral Methane- and Adamantane-Based Building Blocks for Higher-Order Molecular Assemblies. *Organic & Biomolecular Chemistry,* **2009**, *7*, 4734-4743.

46. Sekizkardes, A. K.; Culp, J. T.; Islamoglu, T.; Marti, A.; Hopkinson, D.; Myers, C.; El-Kaderi, H. M.; Nulwala, H. B., An Ultra-Microporous Organic Polymer for High Performance Carbon Dioxide Capture and Separation. *Chemical Communications,* **2015**, *51*, 13393-13396.

47. Altarawneh, S.; Behera, S.; Jena, P.; El-Kaderi, H. M., New Insights into Carbon Dioxide Interactions with Benzimidazole-Linked Polymers. *Chemical Communications,* **2014**, *50*, 3571-3574.

48. Patel, H. A.; Je, S. H.; Park, J.; Chen, D. P.; Jung, Y.; Yavuz, C. T.; Coskun, A., Unprecedented High-Temperature CO_2 Selectivity in N_2-Phobic Nanoporous Covalent Organic Polymers. *Nature Communications,* **2013**, *4*, 1357.

49. Xu, Y.; Jin, S.; Xu, H.; Nagai, A.; Jiang, D., Conjugated Microporous Polymers: Design, Synthesis and Application. *Chemical Society Reviews,* **2013**, *42*, 8012-8031.

50. Rose, M., Nanoporous Polymers: Bridging the Gap between Molecular and Solid Catalysts? *ChemCatChem,* **2014**, *6*, 1166-1182.

51. Zhang, Y.; Riduan, S. N., Functional Porous Organic Polymers for Heterogeneous Catalysis. *Chemical Society Reviews,* **2012**, *41*, 2083-2094.

52. Brunauer, S.; Emmett, P. H.; Teller, E., Adsorption of Gases in Multimolecular Layers. *Journal of the American Chemical Society,* **1938**, *60*, 309-319.

53. Gómez-Serrano, V.; González-García, C. M.; González-Martín, M. L., Nitrogen Adsorption Isotherms on Carbonaceous Materials. Comparison of BET and Langmuir Surface Areas. *Powder Technology,* **2001**, *116*, 103-108.

54. Luisa Ojeda, M.; Marcos Esparza, J.; Campero, A.; Cordero, S.; Kornhauser, I.; Rojas, F., On Comparing BJH and NLDFT Pore-Size Distributions Determined from N_2 Sorption on SBA-15 Substrata. *Physical Chemistry Chemical Physics,* **2003**, *5*, 1859-1866.

Chapter 2

Copper(I)-Catalyzed Synthesis of Nanoporous Azo-linked Polymers: Impact of Textural Properties on Gas Storage and Selective Carbon Dioxide Capture

This chapter is mainly taken from my recent article.[1] Adapted with permission from *Chemistry of Materials,* **2014**, *26*, 1385-1392.

2.1 Abstract

A new facile method for synthesis of porous azo-linked polymers (ALPs) is reported. The synthesis of ALPs was accomplished by homocoupling of aniline-like building units in the presence of copper(I) bromide and pyridine. The resulting ALPs exhibit high surface areas (SA_{BET} = 862-1235 $m^2 g^{-1}$), high physiochemical stability, and considerable gas storage capacity especially at high-pressure settings. Under low pressure conditions, ALPs have remarkable CO_2 uptake (up to 5.37 mmol g^{-1} at 273 K and 1 bar), as well as moderate CO_2/N_2 (29-43) and CO_2/CH_4 (6-8) selectivity. Low pressure gas uptake experiments were used to calculate the binding affinities of small gas molecules and revealed that ALPs have high heats of adsorption for hydrogen (8 kJ mol^{-1}), methane (18-21 kJ mol^{-1}), and carbon dioxide (28-30 kJ mol^{-1}). Under high pressure conditions, the best performing polymer, ALP-1, stores significant amounts of H_2 (24 g L^{-1}, 77 K/70 bar), CH_4 (67 g L^{-1}, 298 K/70 bar), and CO_2 (304 g L-1, 298 K/40 bar).

2.2 Introduction

The surface modification of porous organic polymers with polar groups can significantly enhance their CO_2 binding energy, resulting in enhancement in CO_2 uptake and/or CO_2 selectivity over nitrogen and methane.[2-4] Stronger CO_2-framework interaction is expected due to hydrogen bonding and/or dipole-quadrupole interactions between CO_2 and the functional groups of porous polymers.[5] Moderate porosity, small pore size, and polar functional groups such as amine, hydroxyl and halogen etc. are favorable for selective CO_2 binding and CO_2 separation from N_2 and CH_4.[6] Therefore, synthesis of new porous organic polymers and the incorporation of polar groups into their frameworks through post-modification methods or directly by synthesizing porous polymers using nitrogen- and/or oxygen-rich monomers have obtained a lot of attention.[7] Several polymeric systems having nitrogen-functionalized pores have shown enhanced CO_2 uptake and/or selectivity.[8-13] A recent study by Patel *et al.*, has shown that nitrogen-nitrogen double bonds (azo-bond) in porous polymer backbone can play important roles in small gas storage and separation applications.[14] They reported very high CO_2 selectivity over azo-linked covalent organic polymers (azo-COPs); however, low surface area of azo-COPs results in relatively low CO_2 uptake capacities (85-108 mg g^{-1} at 273 K/1 bar), which might limit the applications of azo-COPs in CO_2 capture and CO_2 separation.[14]

In this study, we report an alternative route to construct azo-linked porous organic polymers (ALPs) with high porosity and remarkable CO_2 uptake. We also investigated the performance of ALPs in small gas (H_2, CO_2, CH_4) uptake applications under low and high pressure conditions.

2.3 Experimental Section

2.3.1 Materials and Methods

All chemicals were purchased from commercial suppliers (Acros Organics, Sigma Aldrich, or Frontier Scientific) and used without further purification, unless otherwise noted. 1,3,5,7-tetrakis(4-aminophenyl)adamantane[15] (TAPA), 2,6,12-triaminotriptycene[16] (TAT), tetrakis(4-aminophenyl)methane[17] (TAM) and 1,3,5-tris(4-aminophenyl)benzene[18] (TAB) were synthesized according to published methods. Solution ^{1}H NMR spectra were taken by Varian Mercury-300 MHz NMR spectrometer (75 MHz carbon frequency). Solid-state ^{13}C cross-polarization magic angle spinning (CP-MAS) NMR spectra of solid samples were obtained by Spectral Data Services, Inc. Spectra were obtained using Tecmag-based NMR spectrometer, operated at a H-1 frequency of 363 MHz, using contact time of 1 ms and delay of three seconds for CP-MAS experiments. All samples were spun at 7.0 kHz. Thermogravimetric analysis (TGA) was carried out by a TA Instruments Q-5000IR series thermal gravimetric analyzer using 50 μL platinum pans under flow of N_2 gas with heating rate of 5 °C/min. To obtain Scanning Electron Microscopy (SEM) images, each sample was dispersed onto a sticky carbon surface attached to a flat aluminum sample holder. Then, the sample was coated with platinum at pressure of 1×10^{-5} mbar in nitrogen atmosphere for 90 seconds before imaging. SEM images were taken by a Hitachi SU-70 Scanning Electron Microscope. Powder X-ray diffraction patterns were collected on a Panalytical X'pert pro multipurpose diffractometer (MPD) with Cu Kα radiation. FT-IR spectra were obtained by a Nicolet-Nexus 670 spectrometer having an attenuated total reflectance accessory. Porosity and gas sorption experiments were carried out using a Quantachrome Autosorb iQ volumetric analyzer using UHP grade adsorbates. All samples were degassed at 120 °C under vacuum before gas sorption measurements. Pore Size Distribution (PSD) was calculated from Ar isotherms using cylindrical pore (zeolite) NLDFT adsorption branch model. High pressure sorption measurements

were carried out using a VTI HPVA-100 volumetric analyzer. Before data collection, in order to establish appropriate cold zone compensation factors, free space measurements were performed by using ultra-high purity helium, and the skeletal density of the material was found in the course of analysis for appropriate density correction factorization.[19] High pressure excess total gas uptakes were calculated according to literature methods by using NIST Thermochemical Properties of Fluid Systems.[19]

2.3.2 Synthetic Aspects

The synthesis of ALPs was accomplished by homocoupling of 2D and 3D aniline-like building units using copper(I)-catalyzed oxidative coupling reaction that leads to azo-linkage formation (Figure 2.1).

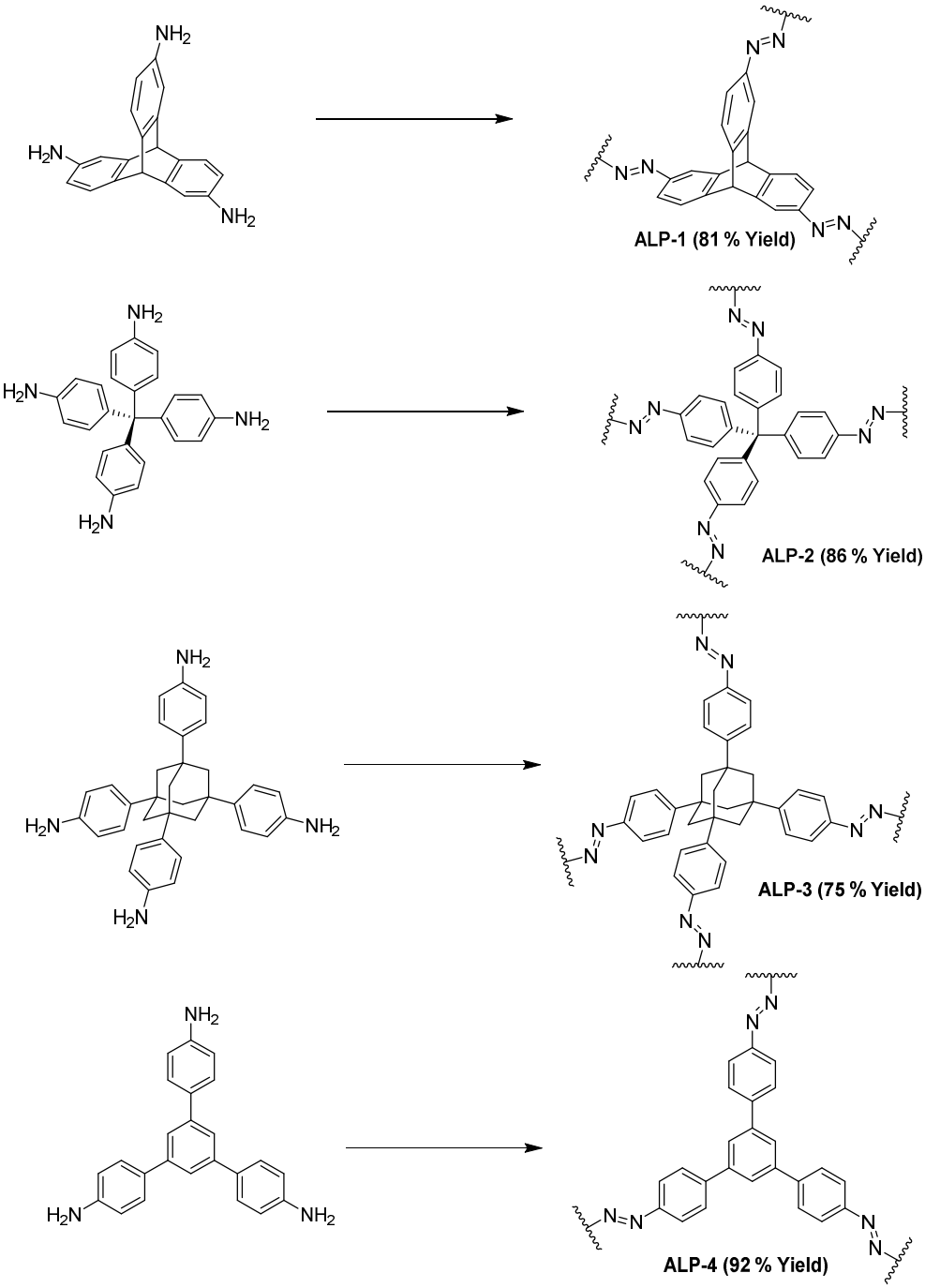

Figure 2-1: Synthesis of azo-linked porous organic polymers (ALPs) by using CuBr as a catalyst. Reaction conditions: CuBr, pyridine, THF/toluene (25-80 °C, 48 h).

Synthesis of ALP-1. 2,6,12-triaminotriptycene (100 mg, 0.334 mmol) was added to a 22 mL solvent mixture of THF/toluene (v:v = 1:1). CuBr (23.5 mg, 0.164 mmol) and pyridine (94 mg, 1.19 mmol) were added. The resulting mixture was stirred under air atmosphere at room temperature for 24 h, at 60 °C for 12 h, and then at 80 °C for 12 h. Afterwards, the mixture was filtered and washed with THF and water. The resulting powder was soaked in HCl (100 mL, 4M) for 24 h and then filtered and washed with water. The resulting powder was further washed with NaOH (200 mL, 1M), water, and ethanol. After drying at 110 °C and 150 mTorr, ALP-1 was isolated as a brownish red powder (70 mg, 81% yield). Elemental analysis calcd (%) for $C_{20}H_{11}N_3$: C, 81.89; H, 3.78; N, 14.33. Found: C, 76.22; H, 3.57; N, 12.46.

Synthesis of ALP-2. This polymer was synthesized following the same method described above for ALP-1, using tetrakis(4-aminophenyl)methane (100 mg, 0.26 mmol), CuBr (25 mg, 0.174 mmol) and pyridine (107 mg, 1.35 mmol). After drying, a brownish powder was obtained and denoted as ALP-2 (84 mg, 86% yield). Elemental analysis calcd (%) for $C_{25}H_{16}N_4$: C, 80.63; H, 4.33; N, 15.04. Found: C, 76.58; H, 5.12; N, 12.08.

Synthesis of ALP-3. This polymer was prepared following the same synthetic method used for synthesis of ALP-1, using 1,3,5,7-Tetrakis(4-aminophenyl)adamantane (100 mg, 0.2 mmol), CuBr (19 mg, 0.132 mmol) and pyridine (81 mg, 1.02 mmol). After drying, a brownish powder was obtained and denoted as ALP-3 (74 mg, 75% yield). Elemental analysis calcd (%) for $C_{34}H_{28}N_4$: C, 82.90; H, 5.73; N, 11.37. Found: C, 76.06; H, 5.73; N, 9.29.

Synthesis of ALP-4. This polymer was synthesized following the same method described above for ALP-1, using1,3,5-tris(4-aminophenyl)benzene (100 mg, 0.28 mmol), CuBr (20 mg, 0.139 mmol), and pyridine (80 mg, 1.01 mmol). After drying, a brownish powder was obtained

and denoted as ALP-4 (91 mg, 92% yield). Elemental analysis calcd (%) for $C_{24}H_{15}N_3$: C, 83.46; H, 4.38; N, 12.17. Found: C, 79.27; H, 5.30; N, 9.51.

2.4 Result and Discussion

2.4.1 Synthesis and Characterization of ALPs

The synthetic route for ALPs preparation reported in this study is based on copper(I)-catalyzed homocoupling of 3D and 2D aniline-like building units via azo bond formation. Recently, Zhang *et al.* reported a convenient approach for homocoupling of anilines through azo bond formation, using copper(I) as catalyst and air as an oxidant.[20] In this work, we have successfully adopted a similar approach for the synthesis of ALPs. Notably, the use of mixed solvents consisting of toluene and THF was essential for optimizing the porosity of ALPs. The synthetic conditions were first optimized for the synthesis of ALP-4 and then were used for the preparation of other ALPs (Table 2.1 and 2.2).

Table 2.1: The effect of different solvents in synthesis of ALP-4. Reaction conditions; monomer (100 mg), CuBr (20 mg), pyridine (80 mg), solvent (22 ml), 60 °C, 48h.

Entry	Solvent	Surface Area ($m^2\ g^{-1}$)[a]	Comment
1	Toluene	205	
2	THF	N/A	No polymer formed.
3	Chloroform	83	
4	THF/ Toluene (50:50)	597	
5	Chloroform/ Toluene (50:50)	376	

[a]BET Surface areas were calculated from N_2 adsorption isotherms at 77 K measured by NOVA-4200e (Quantachrome).

Table 2.2: Different conditions for synthesis of ALP-4. Reaction conditions; monomer (100 mg), THF/toluene (22 ml v:v=1:1).

entry	CuBr (mg)	Pyridine (mg)	Reaction Temperature and Time	Surface Area (m^2 g^{-1})[a]
1	20	80	RT for 48 h	223
2	10	80	60 ºC for 48 h	351
3	20	80	60 ºC for 48 h	597
4	20	80	(1) RT for 24 h (2) 60 ºC for 24 h	648
5	20	80	80 ºC for 48 h	628
6	20	80	(1) RT for 24 h (2) 60 ºC for 12 h (3) 80 ºC for 12 h	800
7	30	80	(1) RT for 24 h (2) 60 ºC for 24 h	670
8	20	120	(1) RT for 24 h (2) 60 ºC for 24 h	668
9	20	45	(1) RT for 24 h (2) 60 ºC for 24 h	562

[a]BET Surface areas were calculated from N_2 sorption isotherms measured by NOVA (Quantachrome).

Our initial attempts involved the use of single solvents such as toluene, THF, and chloroform. Toluene has been reported as the best solvent for the formation of azo bond in copper-catalyzed oxidative coupling of anilines.[20] However, the use of toluene resulted in the formation of a porous polymer having low surface area (205 m^2 g^{-1}). Unlike previously reported small anilines coupled by copper(I) catalyst [20], the monomer used for the synthesis of ALP-4 has very low solubility in toluene, and this low solubility can hinder the polymerization process. Although the monomer has

high solubility in polar solvents, the use of THF led to almost no polymerization while the use of chloroform resulted in a very low surface area polymer (83 m^2 g^{-1}). These observations are consistent with the fact that the CuBr-pyridine catalyst has low catalytic activity in polar solvents as previously reported.[20] Therefore, toluene was mixed with a polar solvent to both maintain high catalytic activity of CuBr-pyridine and to enhance the solubility of the monomer. The surface area of ALP-4 increased to 376 m^2 $g^{-1}$and 597 m^2 g^{-1} when chloroform/toluene and THF/toluene were used, respectively. We should also note that the use of mixed solvent systems such as dioxane/mesitylene was very effective in enhancing the porosity of 2D and 3D covalent organic frameworks (COFs).[21-22] As such, the porosity of ALP-4 was further optimized using THF/toluene solvent system as summarized in Table 2.2. A recent study by Yuan *et al.*, has shown that covalent bond formation at ambient temperature can lead to very high surface area porous polymer networks (PPN-4).[23] However, in our case when the polymerization was carried out at room temperature, the surface area decreased from 597 m^2 g^{-1} to 223 m^2 g^{-1}. This decrease in surface area could be ascribed to the low catalytic activity of CuBr-pyridine at low temperature. Therefore, the effect of polymerization temperature on the porosity of the polymer was further studied (Table 2.2). We carried out the polymerization at 60 °C and 80 °C and found that both temperatures lead to similar porosity levels. Finally, we investigated the impact of stepwise increase of temperature on the porosity of the polymer. Polymerization at ambient temperature can minimize unwanted side reactions and allow for more uniform pore formation, while incomplete polymerization of building units can be minimized by increasing the catalytic activity of the catalyst at higher temperatures (60-80 °C). As such, the reaction was carried out at room temperature for 24 hours and then at higher temperatures (60 °C, 80 °C) for 24 further hours. When the reaction was carried out in three steps (room temperature for 24 h, 60 °C for 12 h, and 80 °C for 12 h), the surface area of the

polymer increased to 800 m^2 g^{-1} and therefore, other ALPs were synthesized using the same synthetic strategy.

ALPs were characterized by spectral and analytical methods, while porosity was investigated by argon sorption measurements prior to gas uptake and selectivity studies. ALPs are insoluble in common organic solvents such as THF, DMF, DCM, methanol, and acetone, suggesting that they have hyper-cross-linked networks as expected. It is worth noting that ALPs are chemically stable under harsh acidic (4M HCl) and basic (4M NaOH) conditions. The thermal stability of ALPs was confirmed by TGA and all polymers remain stable up to ~400 °C under N_2 while the initial weight loss at below 100 °C is due to adsorbed moisture (Figure 2.2).

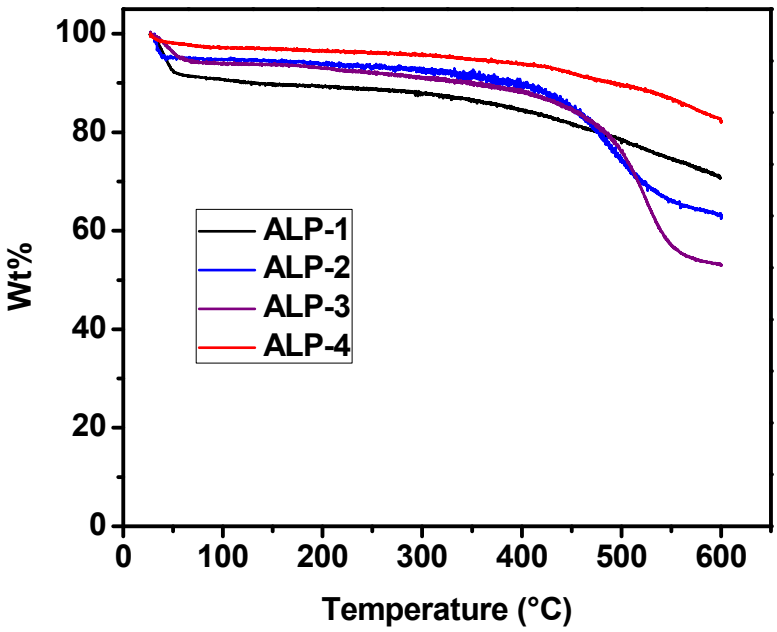

Figure 2.2: TGA traces of ALPs.

SEM studies on as-synthesized ALPs revealed different morphologies (Figure 2.3). The SEM images of ALP-1 and ALP-4 reveal uniform spherical particles having diameters of ~200 nm (ALP-1) and ~400 nm (ALP-4). In case of ALP-2, nanoscale fibers (~30 nm diameter) are randomly aggregated to form spongy spheres having ~800 nm diameter while ALP-3 shows agglomerated ribbon-like particles of variable sizes.

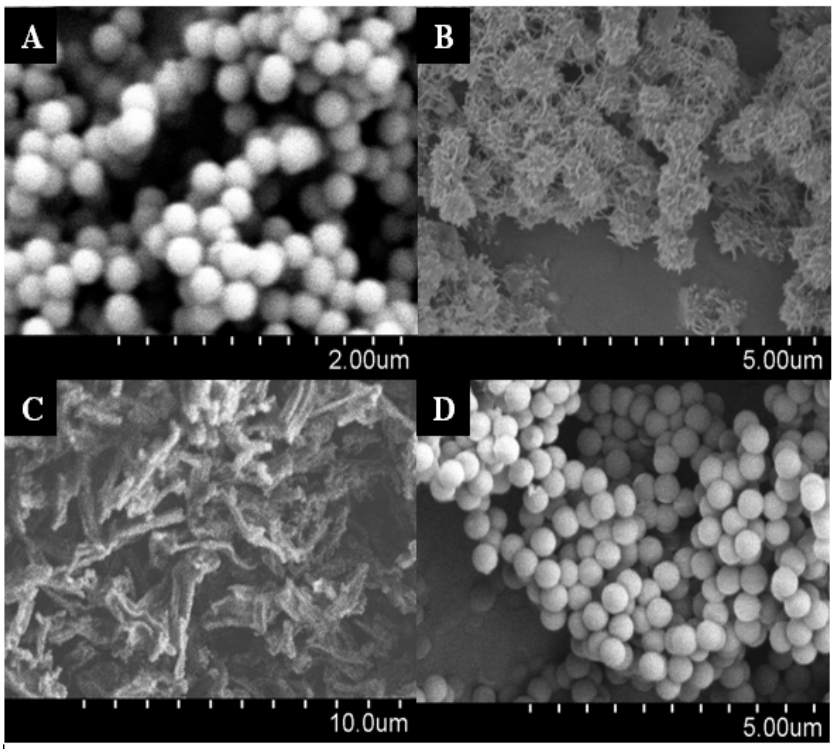

Figure 2.3: Scanning electron microscopy (SEM) images of as- prepared ALP-1 (A), ALP-2 (B), ALP-3 (C), and ALP-4 (D).

Powder X-ray diffraction analysis of ALPs indicates that ALPs are amorphous as evidenced by their featureless PXRD patterns (Figure 2.4). The formation of azo bond was first confirmed by FT-IR; the appearance of new bands at 1419 cm^{-1}, 1404 cm^{-1}, 1480 cm^{-1}, and 1437 cm^{-1}, in FT-IR spectra of ALP-1, ALP-2, ALP-3, and ALP-4, respectively, can be attributed to asymmetric vibration of N=N bond (Figure 2.5). The IR spectra of ALPs also show strongly attenuated N-H stretches that are present in the spectra of starting monomers.

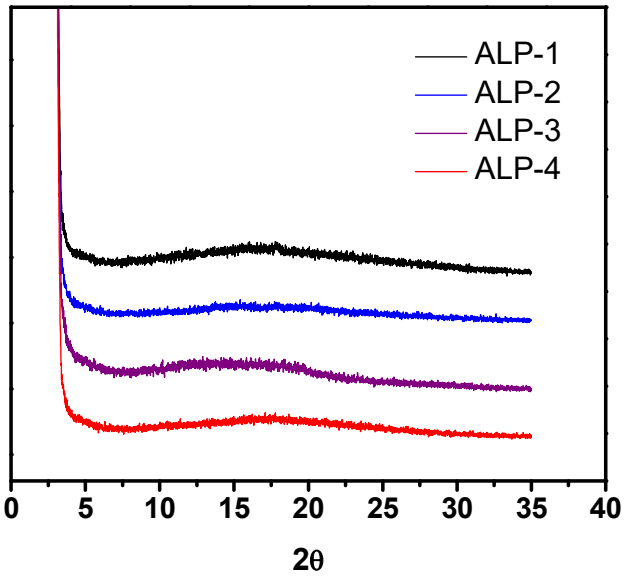

Figure 2.4: .PXRD pattern of ALPs.

Additionally, the azo-linkage formation was further confirmed by the presence of characteristic signals for the –*C*-N=N-*C*– bond at around 152 ppm in ^{13}C CP-MAS NMR spectra of ALPs as well as other signals that correspond to the other carbon atoms in building units (Figures 2.6 - 2.9).

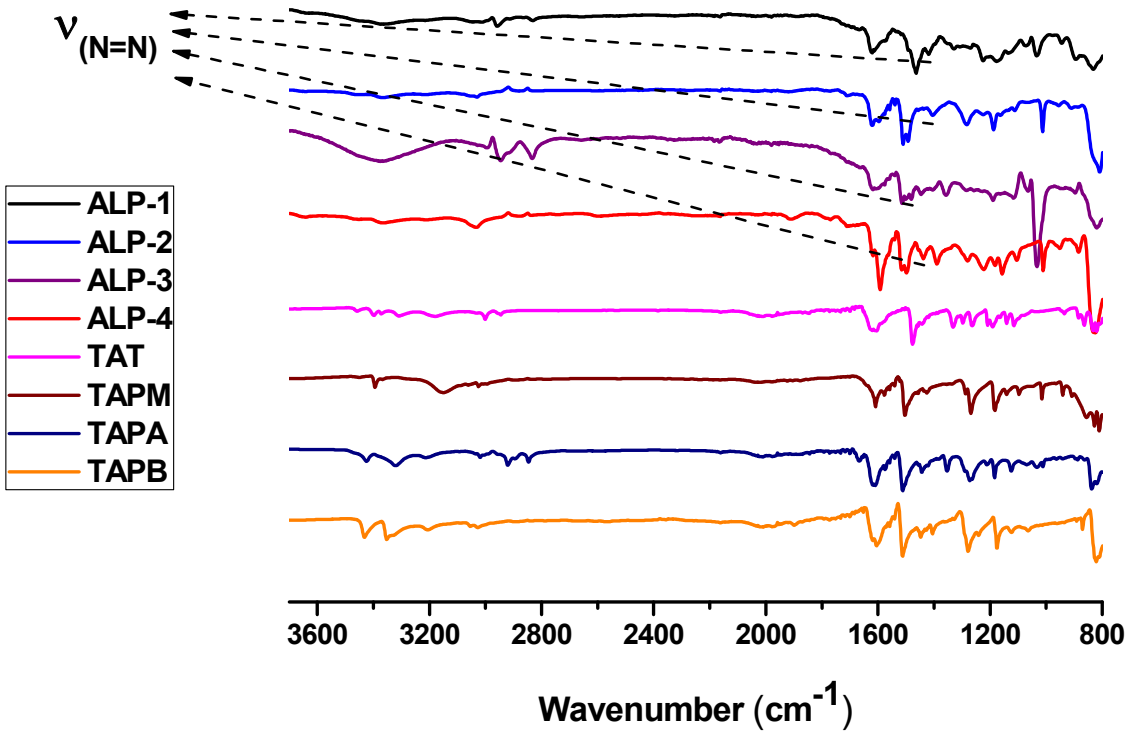

Figure 2.5: FT-IR spectra of ALPs and starting materials.

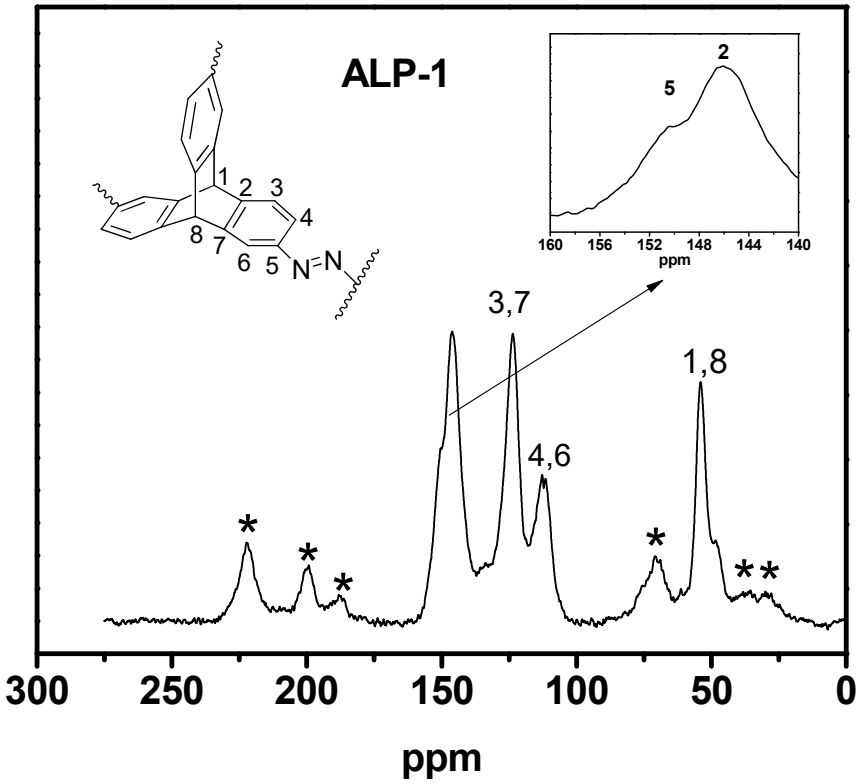

Figure 2.6: Solid-state ^{13}C CP-MAS NMR spectrum of ALP-1. Asterisks denote spinning side-bands.

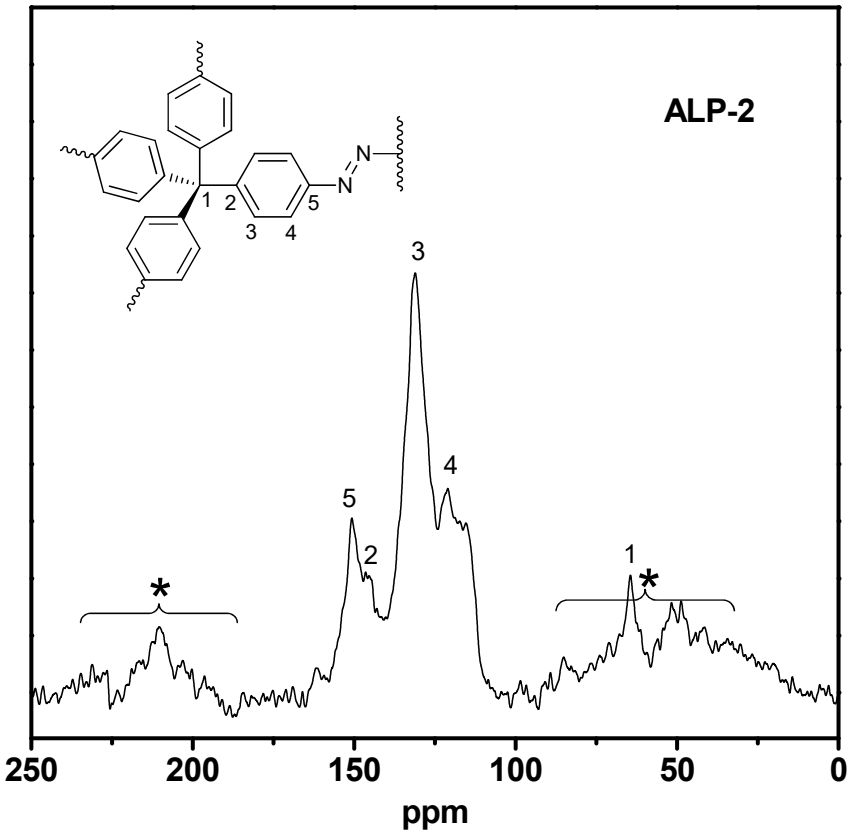

Figure 2.7: Solid-state ^{13}C CP-MAS NMR spectrum of ALP-2. Asterisks denote spinning side-bands.

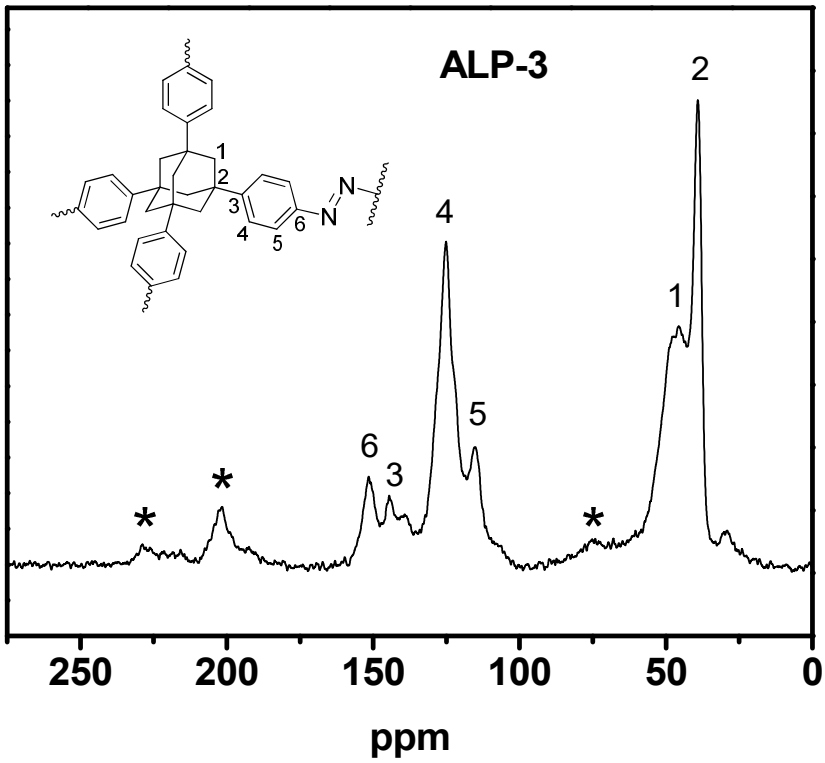

Figure 2.8: Solid-state ^{13}C CP-MAS NMR spectrum of ALP-3. Asterisks denote spinning side-bands

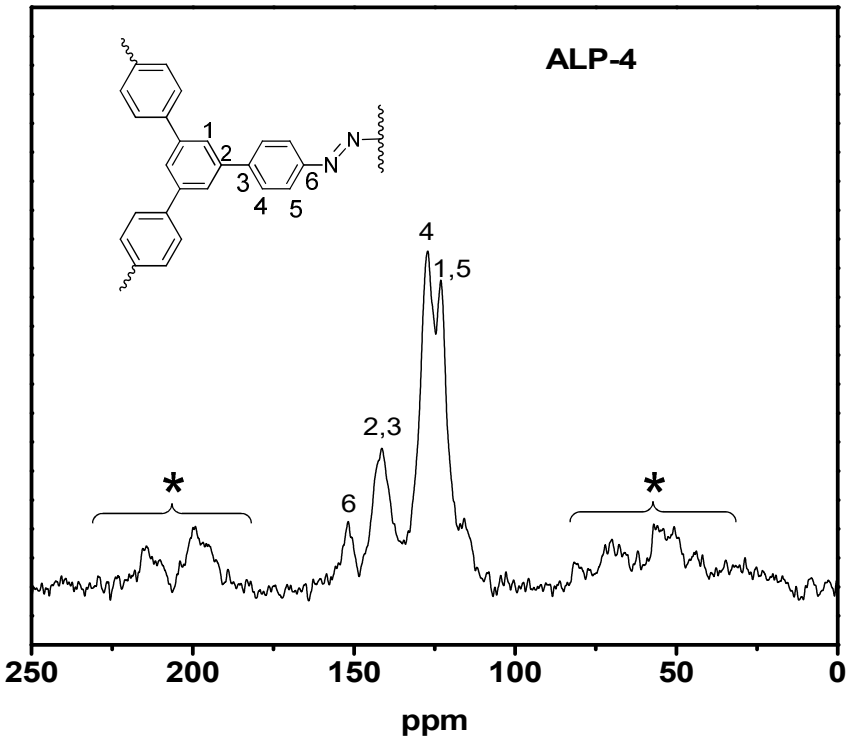

Figure 2.9: Solid-state ^{13}C CP-MAS NMR spectrum of ALP-4. Asterisks denote spinning side-bands

The elemental analysis of ALPs shows some deviations from theoretical values. The difference between the observed and theoretical elemental analysis is common for porous organic polymers[13] that can be caused by incomplete polymerization as well as the adsorption of water and gases from air during handling, as previously reported for CTFs,[13, 24] MPIs,[25] COF-300,[26] SNU-C1,[27] and BILPs.[28] Porosity parameters of ALPs were studied by argon adsorption-desorption measurements at 87 K. The Ar isotherms of ALPs, depicted in Figure 2.10, exhibit a rapid Ar uptake at very low relative pressures indicating their predominant microporosity followed by the gradual increase in Ar uptake (*P/Po* = 0.05 to 0.9) due to the presence of mesopores in the polymers. The increase in Ar uptake at relative pressures above 0.9 can be ascribed to Ar condensation in interparticle voids formed by the aggregation of the polymers' particles. The minor hysteresis observed for all ALPs is consistent with the powdery nature of all ALPs.

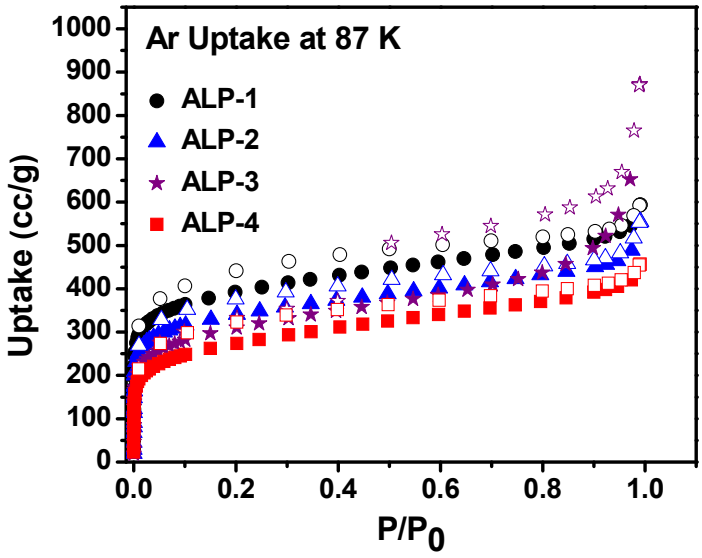

Figure 2.10: Ar isotherms for ALPs at 87 K.

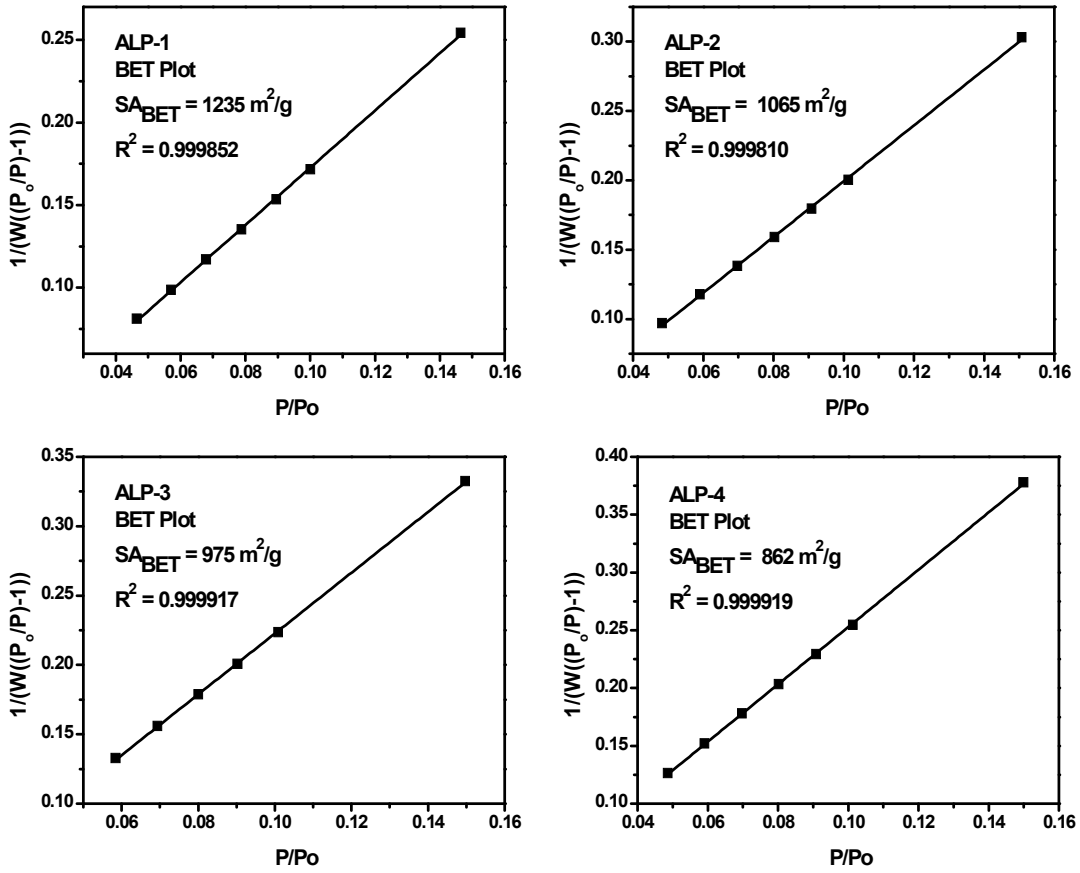

Figure 2.11: BET plots for ALPs.

The specific surface areas were estimated from the Ar adsorption branch using the Brunauer-Emmett-Teller (BET) model, ranging from 862 m^2 g^{-1} to 1235 m^2 g^{-1} (Figure 2.11). The surface areas of ALPs are considerably higher than those of azo-COPs (493−729 m^2 g^{-1}).[14] Notably, the surface area of ALP-2 (1065 m^2 g^{-1}) is much higher than that of azo-COP-1 (635 m^2 g^{-1}) which was constructed from the same building unit.[14] The surface areas of ALPs are in line with those of wide range of amorphous porous organic networks such as BILPs (599-1172 m^2 g^{-1})[28], MPIs (586-1454 m^2 g^{-1})[25], POFs (466−1521 m^2 g^{-1})[29], PIMs (618−1760 m^2 g^{-1})[30], and CMPs (522−1043 m^2

g^{-1})[31]. Pore size distributions (PSDs) were estimated from the adsorption branch of Ar isotherms by NLDFT, (Figures 2.12 – 2.16). PSD studies show that ALP-1 has one major peak centered at around 10 Å and some other peaks below 50 Å. Pore size distributions of ALP-2 and ALP-4 are similar; both having a major peak centered at around 11 Å with significantly broad distribution in the mesoporous range. PSD of ALP-3 shows one major peak centered at around 12.6 Å. Broad pore size distributions may result from uncontrolled pore formation during polymerization steps. Pore volumes of ALPs were calculated from single point Ar uptake at *P/Po* = 0.90 and found to be 0.66 cc g-1, 0.57 cc g^{-1}, 0.63 cc g^{-1}, and 0.50 cc g^{-1} for ALP-1, ALP-2, ALP-3, and ALP-4, respectively. The porosity parameters of ALPs are summarized in Table 2.3.

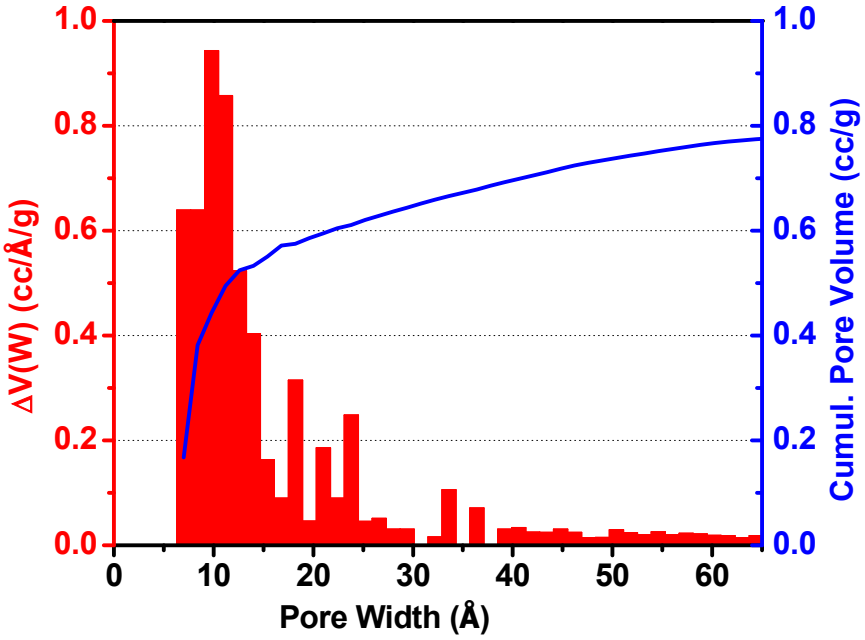

Figure 2.12: Pore size distribution for ALP-1.

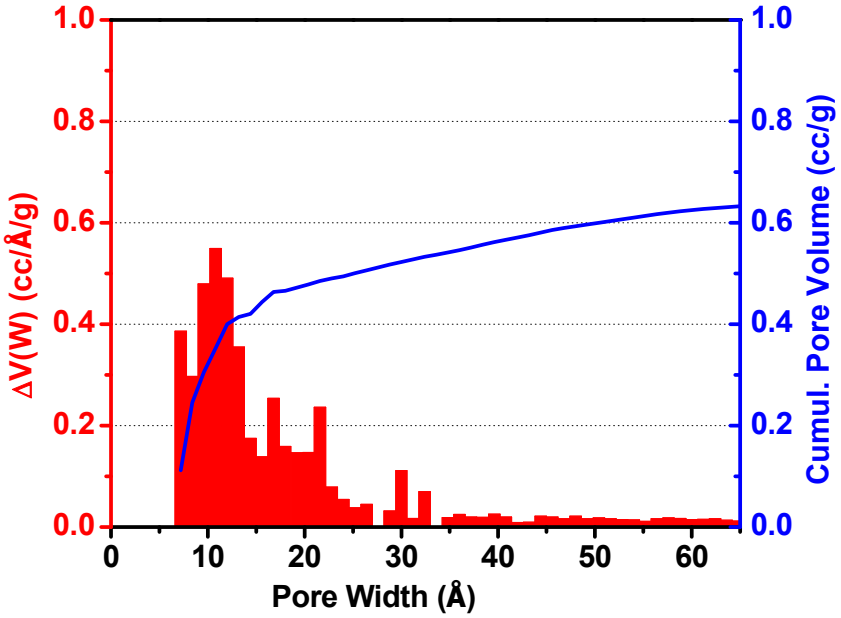

Figure 2.13: Pore size distribution for ALP-2.

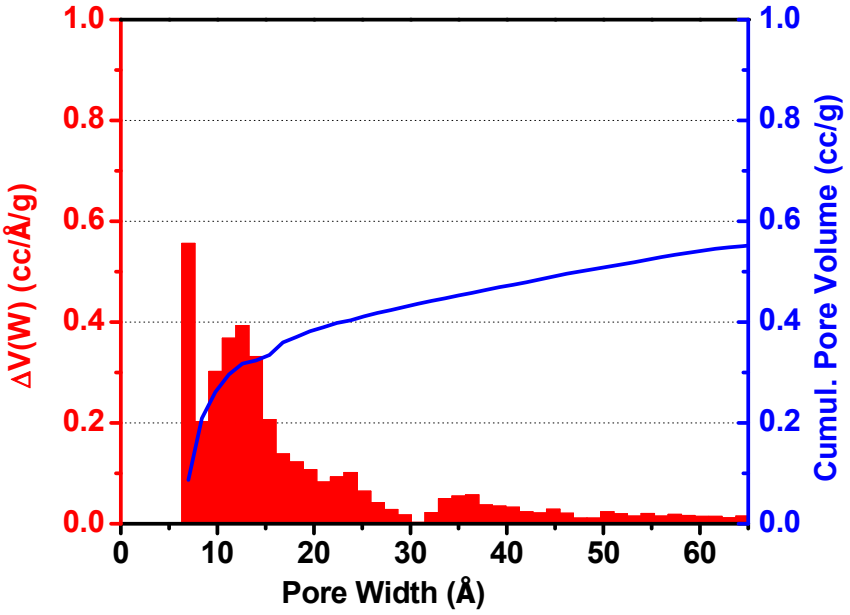

Figure 2.14: Pore size distribution for ALP-3.

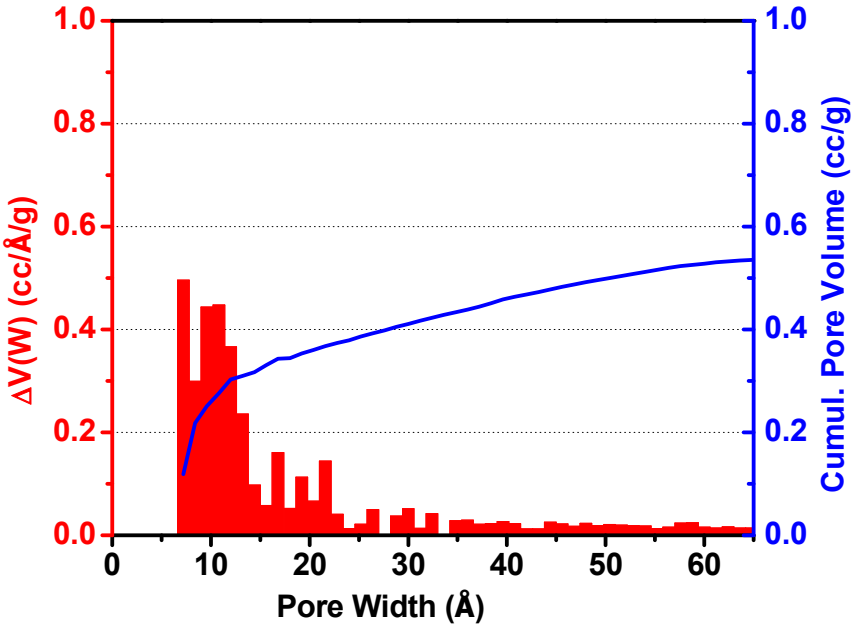

Figure 2.15: Pore size distribution for ALP-4.

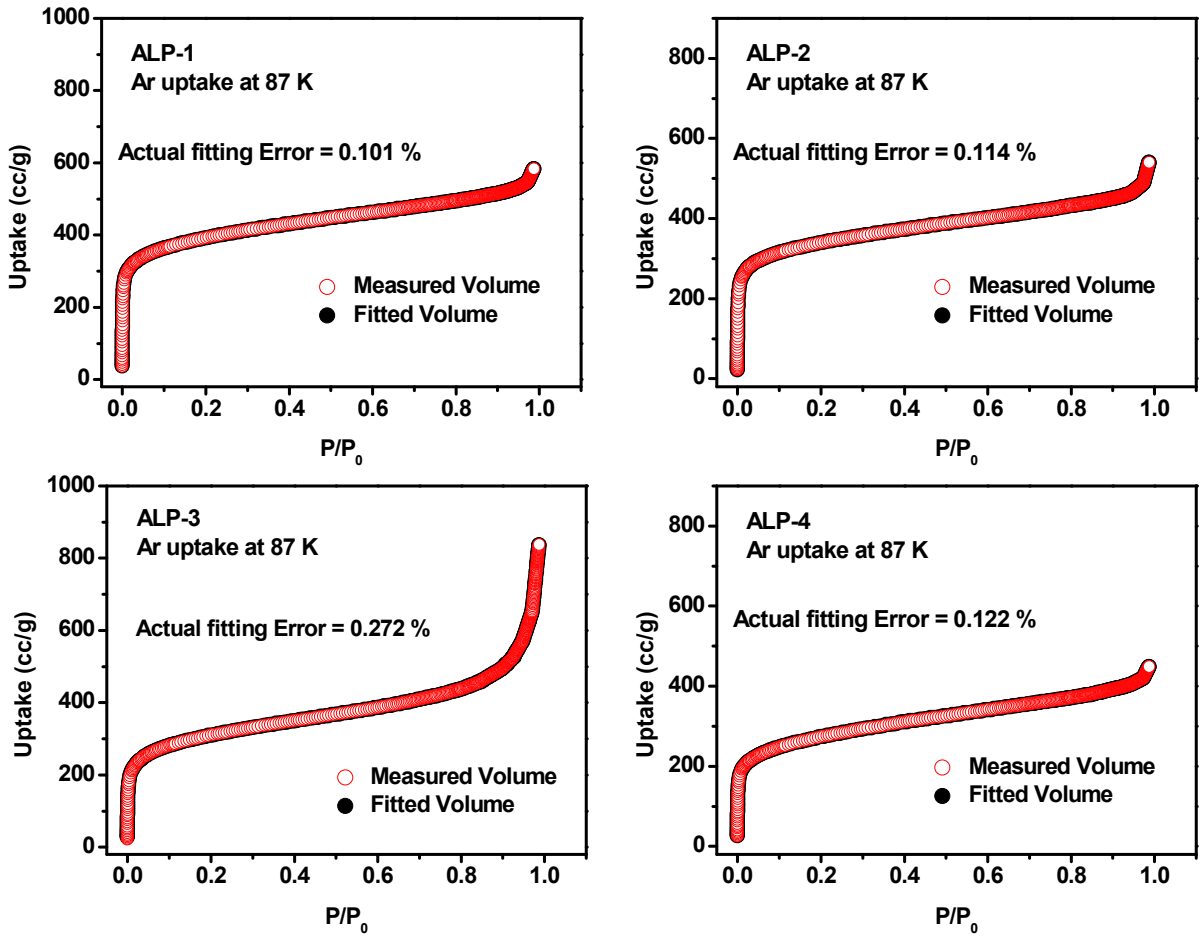

Figure 2.16:. Experimental argon adsorption isotherm for ALPs at 87 K and their corresponding calculated NLDFT isotherms.

Table 2.3: Porosity parameters for ALPs.

Polymer	SA_{BET}[a]	SA_{Lang}[b]	V_{total}[c]
ALP-1	1235	1669	0.66
ALP-2	1065	1444	0.57
ALP-3	975	1365	0.63
ALP-4	862	1209	0.50

[a]Surface area (m^2 g^{-1}) calculated from the argon adsorption branch according to the BET model. [b]Surface area (m^2 g^{-1}) calculated from the argon adsorption branch based on the Langmuir model. [c]The total pore volume (cm^3 g^{-1}) calculated from single point argon uptake at *P/Po*= 0.90.

2.4.2 Low Pressure Gas Storage of H_2, CO_2, and CH_4

Because of considerable porosity and nitrogen-rich nature of ALPs, we were interested in assessing their performance in gas storage in general and CO_2 in particular. Thus, we collected CO_2, CH_4, and H_2 isotherms (Figure 2.17) and calculated their isosteric heats of adsorption (Q_{st}) by using the virial method; the overall results are presented in (Table 2.4). The virial fittings are shown in Figures 2.18 – 2.20. The CO_2 sorption isotherms are completely reversible, indicating that the interactions between CO_2 and ALPs are weak enough to allow material regeneration without heating (Figure 2.17 A). All ALPs show high CO_2 uptake at 273 K and 1.0 bar (153-236 mg g^{-1}). Importantly, these values are almost twice those of azo-COPs (85-108 mg g^{-1})[14] and similar to the uptake of BILPs (128-235 mg g^{-1})[28] which are among the best performing porous

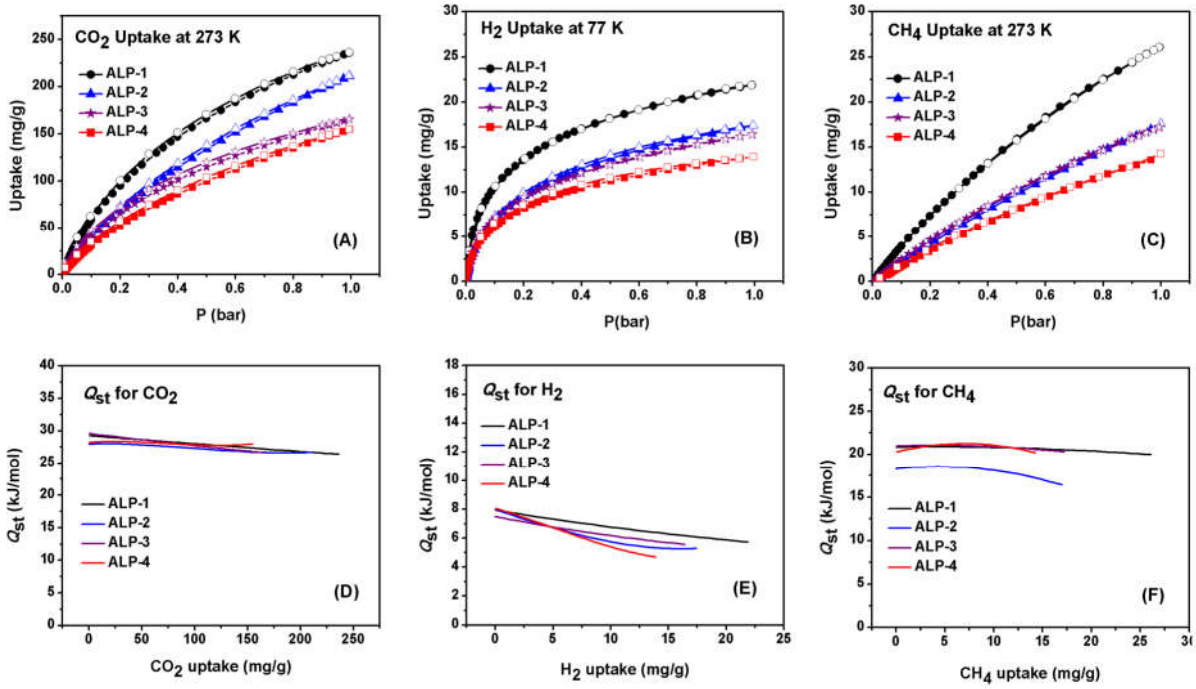

Figure 2.17: CO_2 uptake isotherms (A), H_2 uptake isotherms (B) and CH_4 uptake isotherms (C) of ALPs, and isosteric heats of adsorption for CO_2 (D), H_2 (E), and CH_4 (F).

polymers in CO_2capture and separation. The Q_{st} of ALPs toward CO_2 at zero coverage was found to be very similar and ranges between 27.9-29.6 kJ mol^{-1} (Figure 2.17 D) and within the desirable range for CO_2 sorbents according to recent findings by Wilmer *et al.*[32]

Table 2.4: H_2, CO_2, and CH_4 uptakes, and isosteric heats of adsorption for ALPs.

Polymer	H_2 at 1 bar[a]			CO_2 at 1 bar[a]			CH_4 at 1 bar[a]		
	77K	87K	Q_{st}	273K	298 K	Q_{st}	273 K	298K	Q_{st}
ALP-1	21.9	17.2	7.9	236	143	29.2	26.0	15.0	20.8
ALP-2	17.4	13.9	8.0	211	108	27.9	17.6	10.7	18.5
ALP-3	16.5	12.6	7.5	166	101	29.6	17.2	9.6	21.0
ALP-4	13.9	10.2	8.0	155	81	28.2	14.3	8.3	21.2

[a]Gas uptake in mg g^{-1} and the isosteric enthalpies of adsorption (Q_{st}) in kJ mol^{-1}.

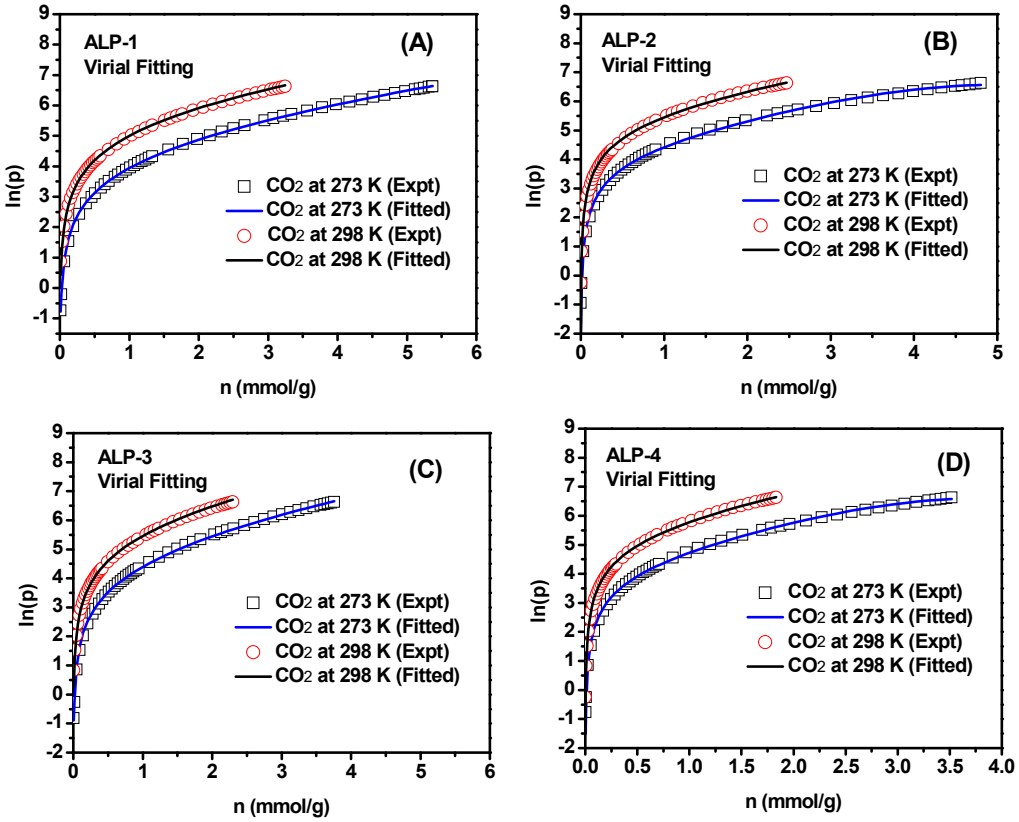

Figure 2.18: Virial fittings for CO_2 isotherms of ALPs.

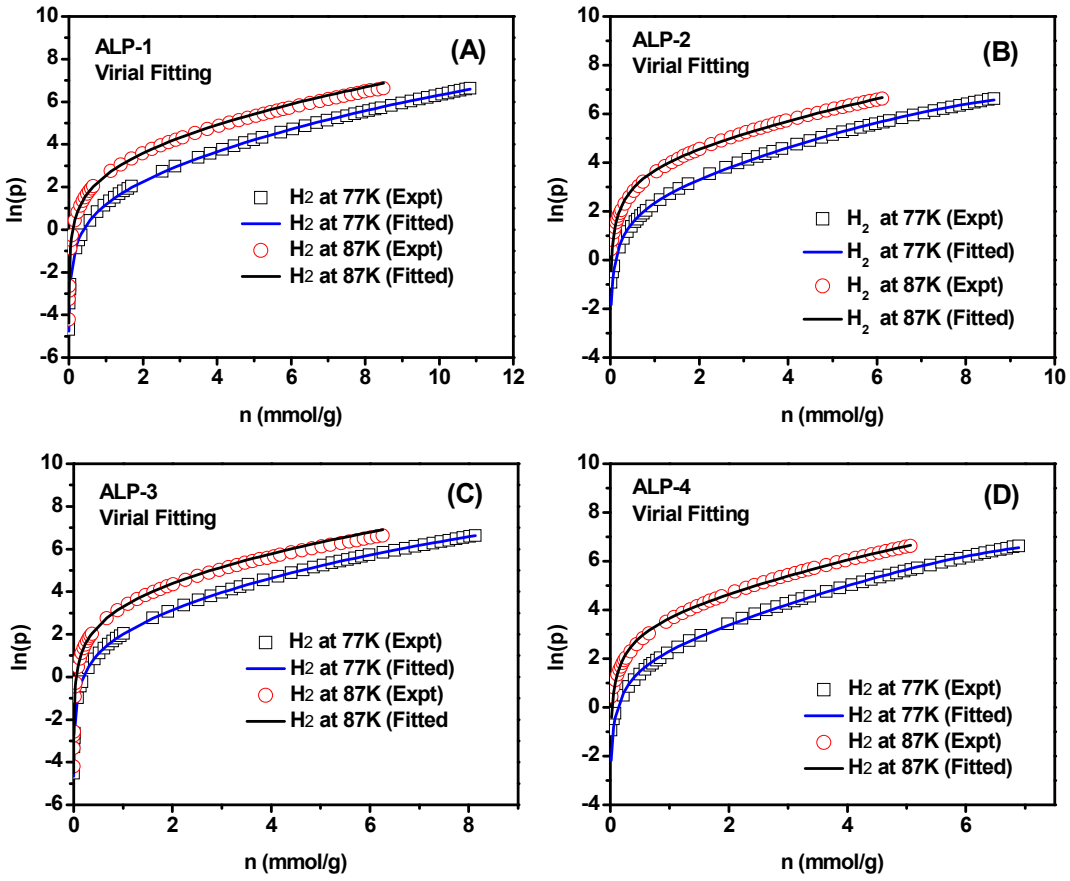

Figure 2.19: Virial fittings for H_2 isotherms of ALPs.

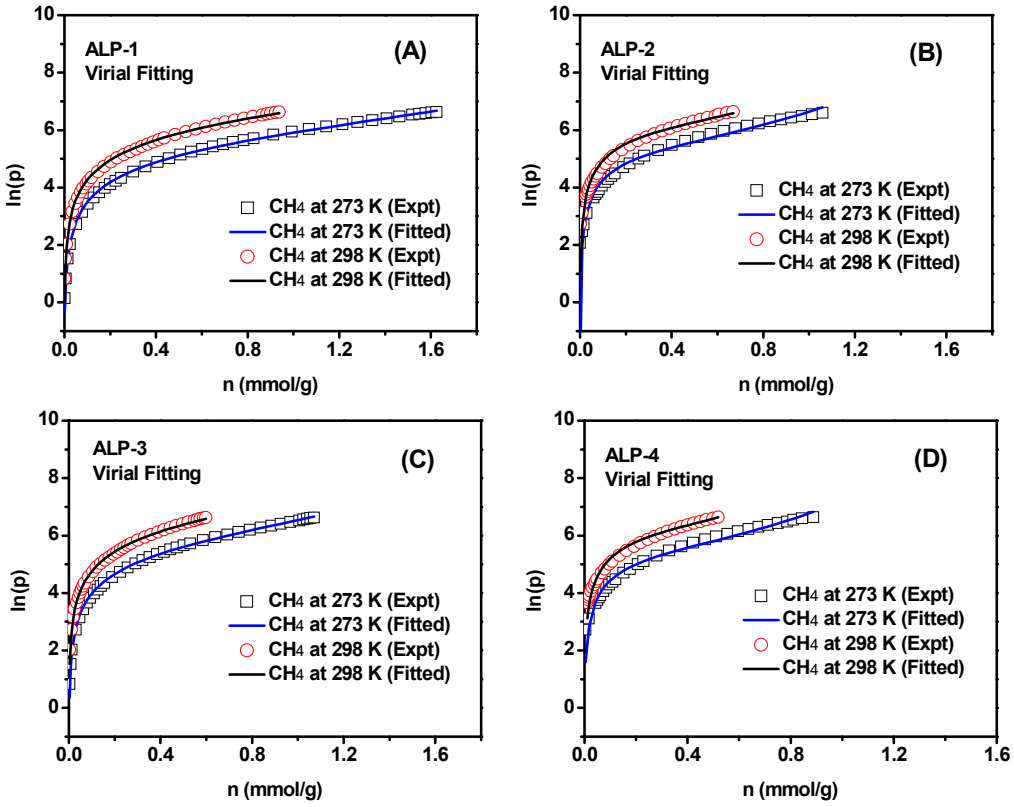

Figure 2.20: Virial fittings for CH_4 isotherms of ALPs.

The CO_2 uptake of ALP-1 at 273 K and 1.0 bar is substantial (236 mg g^{-1}) and represents one of the highest values for all known porous organic polymers reported to date (Table 2.5). For example, the recently reported BILP-4 stores 235 mg g^{-1} under similar conditions.[28] As summarized in Table 2.4, ALP-1 outperforms other ALPs in CO_2 uptake. The remarkable uptake of CO_2 by the triptycene-based ALP-1 can be attributed to several factors such as high internal molecular free volume (IMFV), high surface area, and high nitrogen content.[8] Very recently, both theoretical and experimental studies have shown that high CO_2 uptake can be obtained by azo-functionalized porous frameworks due to dipole–quadrupole interactions between polarizable CO_2

molecules and azo groups.[14, 33] The azo group can act as a Lewis basic site, and the electron deficient carbon atom in CO_2 can act as a Lewis acid; therefore, a strong interaction between CO_2 and azo groups has been observed. In general, nitrogen-rich porous polymers have high CO_2 affinity and adsorption capacity due to dipole–quadrupole interactions between CO_2 and nitrogen sites.[34]

Table 2.5: Low-pressure gas uptakes by selected porous organic materials.

polymer	CO_2 uptake at 1 bar (mmol g^{-1})			H_2 uptake at 1 bar (wt %)		CH_4 uptake at 1 bar (wt %)			Ref.
	273 K	298 K	Q_{st}[a]	77 K	Q_{st}[a]	273 K	298 K	Q_{st}[a]	
ALP-1	5.37	3.24	29.2	2.2	7.9	2.6	1.5	20.8	This Work
ALP-2	4.80	2.47	27.9	1.7	7.8	1.7	1.1	18.5	This Work
ALP-3	3.80	2.30	29.6	1.6	7.5	1.7	0.96	21.0	This Work
ALP-4	3.52	1.83	28.2	1.4	8.0	1.4	0.83	21.2	This Work
BILP-3	5.11	3.3	28.6	2.1	8.0	2.4	1.7	16.6	28
BILP-4	5.34	3.59	28.7	2.3	7.8	2.6	1.8	13.0	28
PAF-3	3.48	1.81	19.2	2.1	6.6	1.9	-	-	35
COF-300	3.29	-	-	-	-	-	-	-	36
HCP 4	3.92	1.6	21.6	-	-	-	-	-	37
COF-6	3.84	-	-	1.22	7	-	-	-	38
PPN-3	-	-	-	1.58	5.51	-	-	-	39
Azo-COP-2	2.6	1.53	24.8	-	-	-	-	-	14
NPOF-4-NH_2	2.9	1.9	30.1	1.15	8.1	1.2	0.7	20.7	4
POF1B	4.09	-	-	-	-	-	-	-	40
P6M	4.17	-	-	-	-	-	-	-	41
BINOL-4	3.96	2.27	29.8	-	-	-	-	-	42
CPOP-1	4.82	-	27	2.8	-	-	-	-	11
MOP-C	3.86	2.2	33.7	-	-	-	-	-	36

[a]The isosteric enthalpies of adsorption (Q_{st}) in kJ mol^{-1}.

We have also studied H_2 and CH_4 storage since both are considered as potential alternative fuels for automotive applications due to their abundance and clean nature. While ALP-1 shows a relatively high hydrogen uptake (2.2 wt%) at 77 K and 1 bar, other ALPs store moderate amounts of hydrogen (1.4−1.7 wt%) as shown in Figure 2.17 B. The Q_{st} of ALPs toward H_2 at zero coverage

was found to be in the range of 7.5-8.0 kJ mol^{-1} which is higher than the values reported for non-functionalized porous organic polymers but similar to those of BILPs (7.8−9.3 kJ mol^{-1})[28], OH-functionalized POFs (8.3 kJ mol^{-1})[40], and tetrazine-based organic frameworks (7.8−8.2 kJ mol^{-1})[43]. Similarly, we investigated the CH_4 uptakes at 273 and 298 K up to 1 bar (Figure 2.17 C). Again, all isotherms are completely reversible and exhibit a steep rise then reach maxima of 14−26 mg g^{-1} at 273 K. The corresponding Q_{st} values for CH_4 were calculated by the virial method and found to range from 18 to 21 kJ mol^{-1} at zero coverage. In general, these values are higher than those of non-functionalized porous organic polymers and comparable to the values reported for organic polymers functionalized with polar groups.[4]

2.4.3 Selective CO_2 Capture over N_2 and CH_4 at Low Pressure

Once the porosity and gas uptake properties of ALPs were studied, we considered their performance in selective CO_2 capture over N_2 and CH_4 for potential use in gas separation applications. A recent study by Patel *et al.* reported a very high CO_2/N_2 selectivity for azo-COPs due to the "N_2-phobicity" of the azo-linkage.[14] ALPs and azo-COPs have similar functional sites (azo-linkage) but have different porosity parameters (surface area and pore size), which can affect their application in gas separation. In order to study the potential use of ALPs in gas separation applications, single component adsorption isotherms for CO_2, N_2 and CH_4 were collected at 273 and 298 K up to 1.0 bar (Figure 2.20 and 2.21).

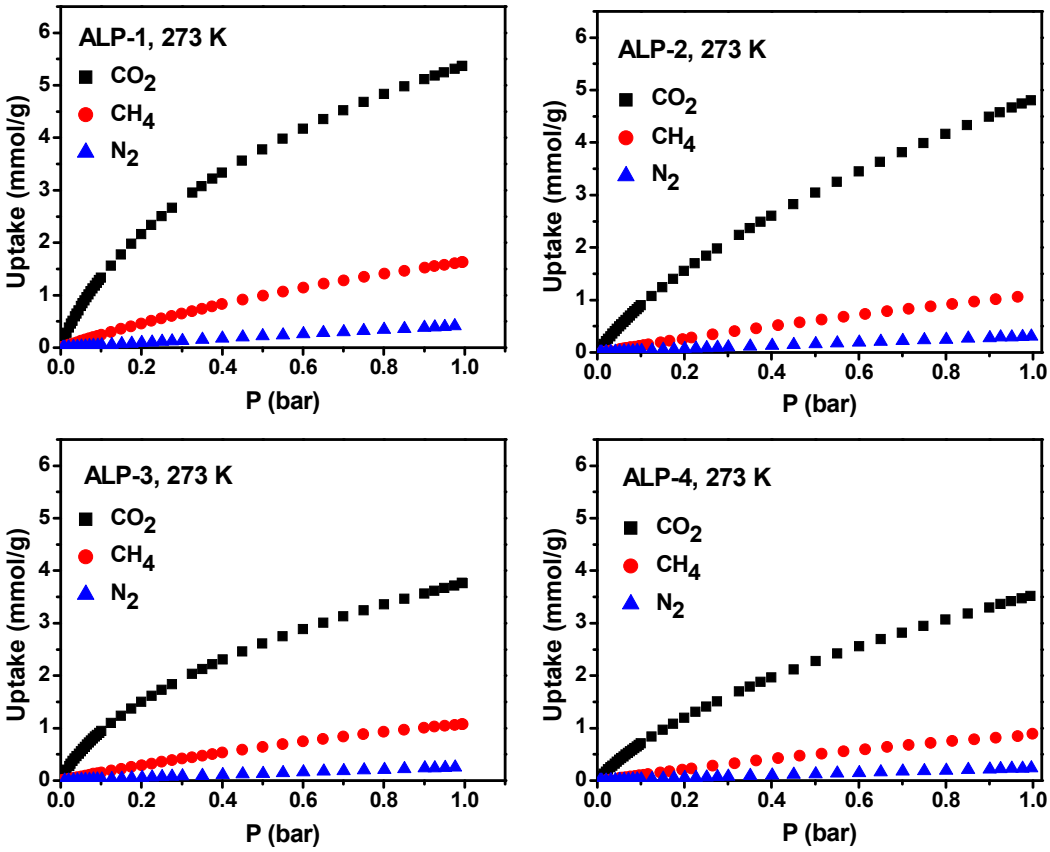

Figure 2.20: CO_2, CH_4, and N_2 adsorption isotherms of ALPs at 273 K.

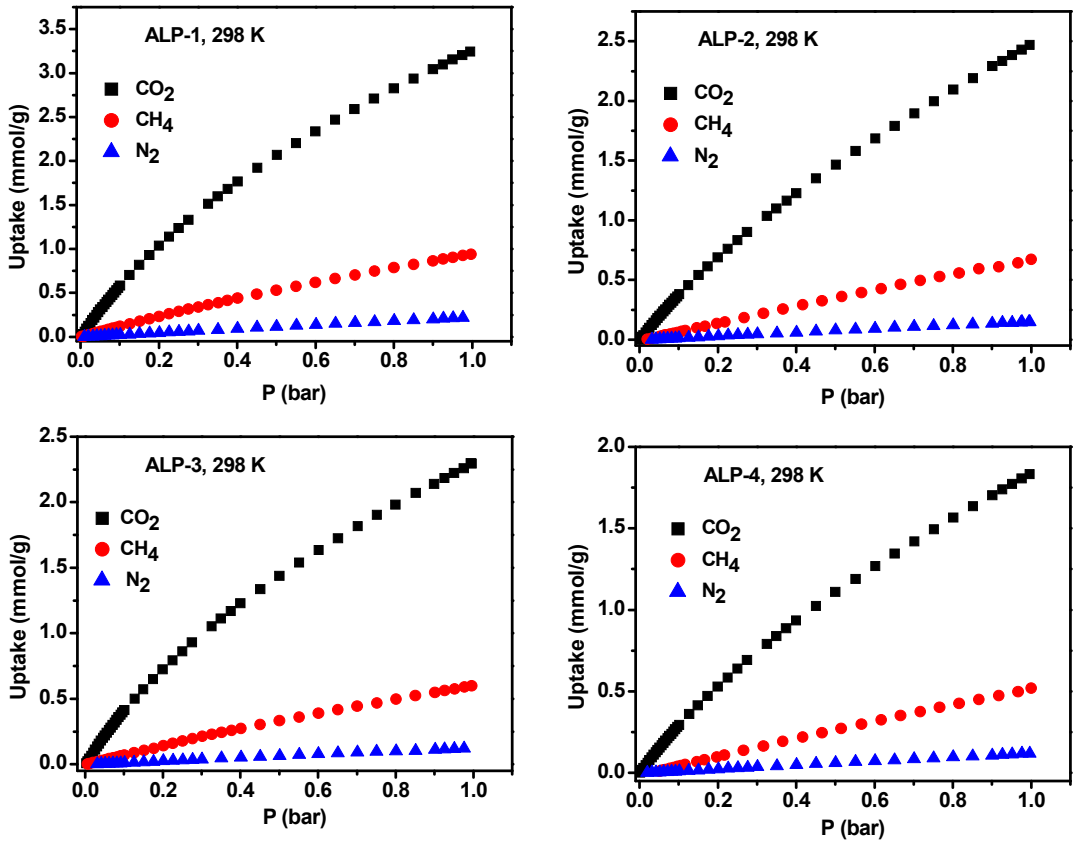

Figure 2.21: CO_2, CH_4, and N_2 adsorption isotherms of ALPs at 298 K.

CO_2/N_2 and CO_2/CH_4 selectivities were first estimated by the use of initial slope ratios estimated from Henry's law constants for single-component adsorption isotherms collected at 273 and 298 K as summarized in Table 2.6 and Figures 2.22 – 2.25.

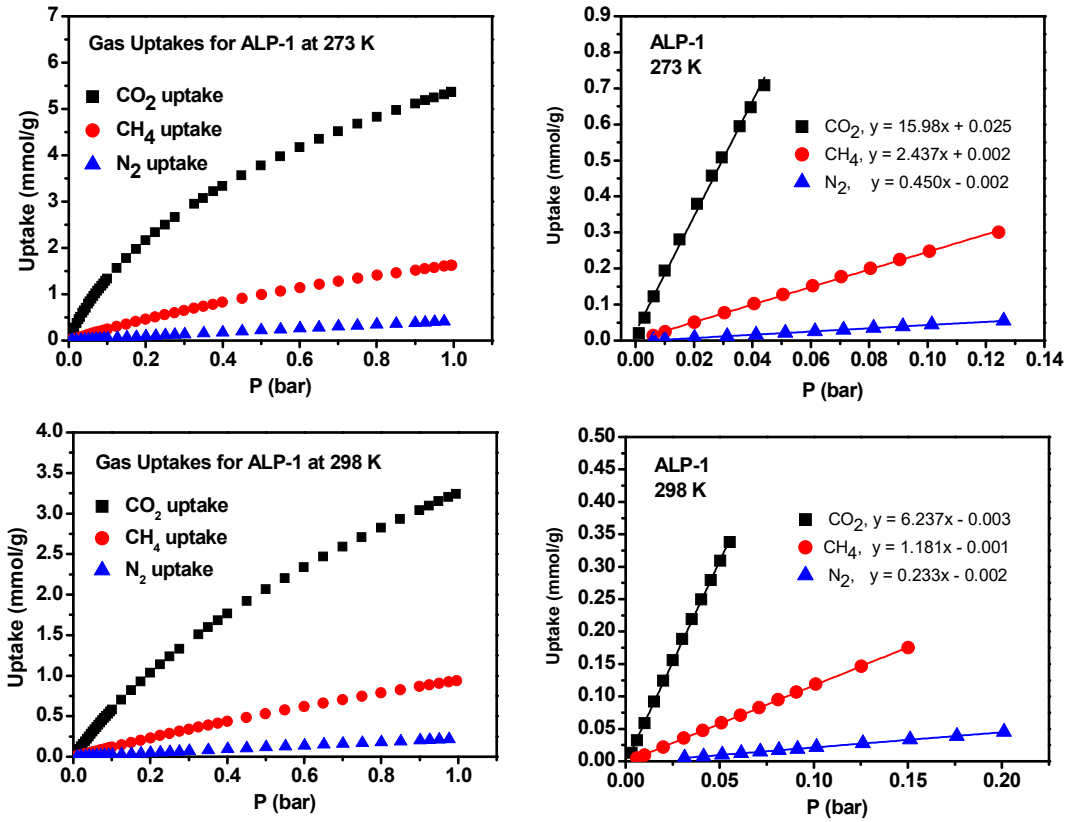

Figure 2.22: CO_2/N_2 and CO_2/CH_4 initial slope selectivity studies for ALP-1.

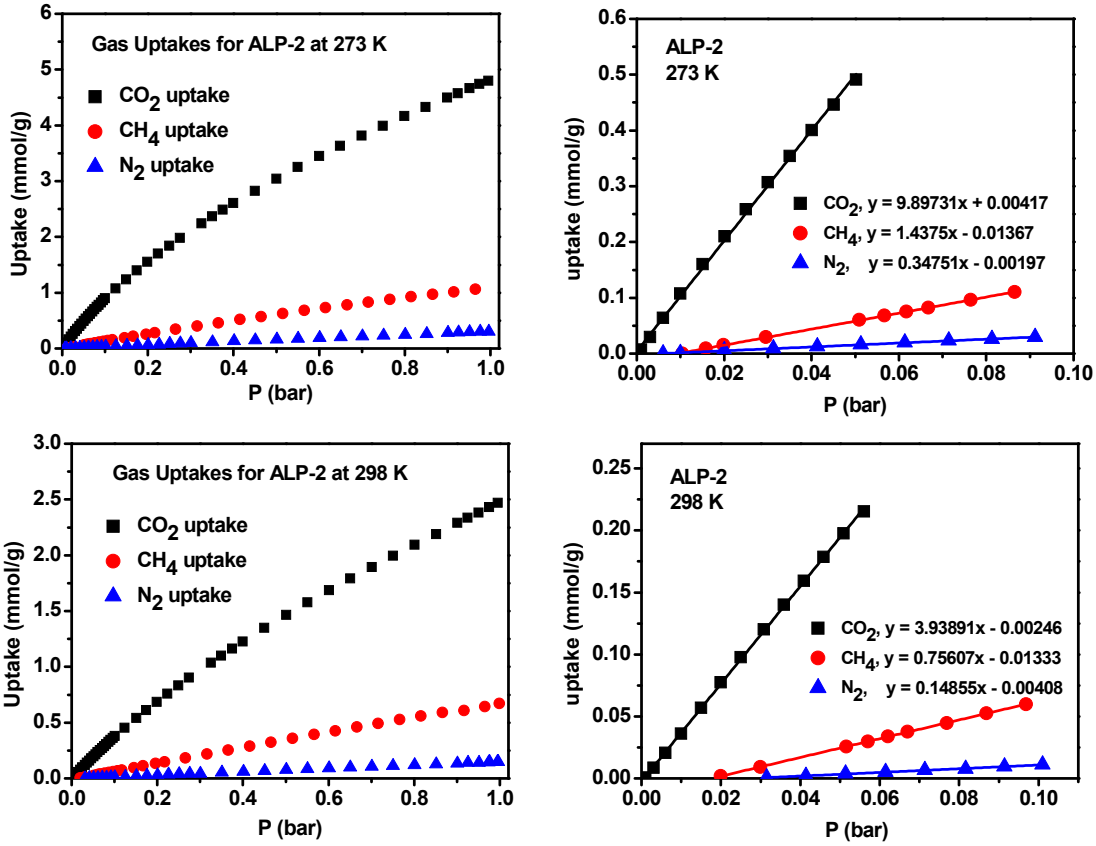

Figure 2.23: CO_2/N_2 and CO_2/CH_4 initial slope selectivity studies for ALP-2.

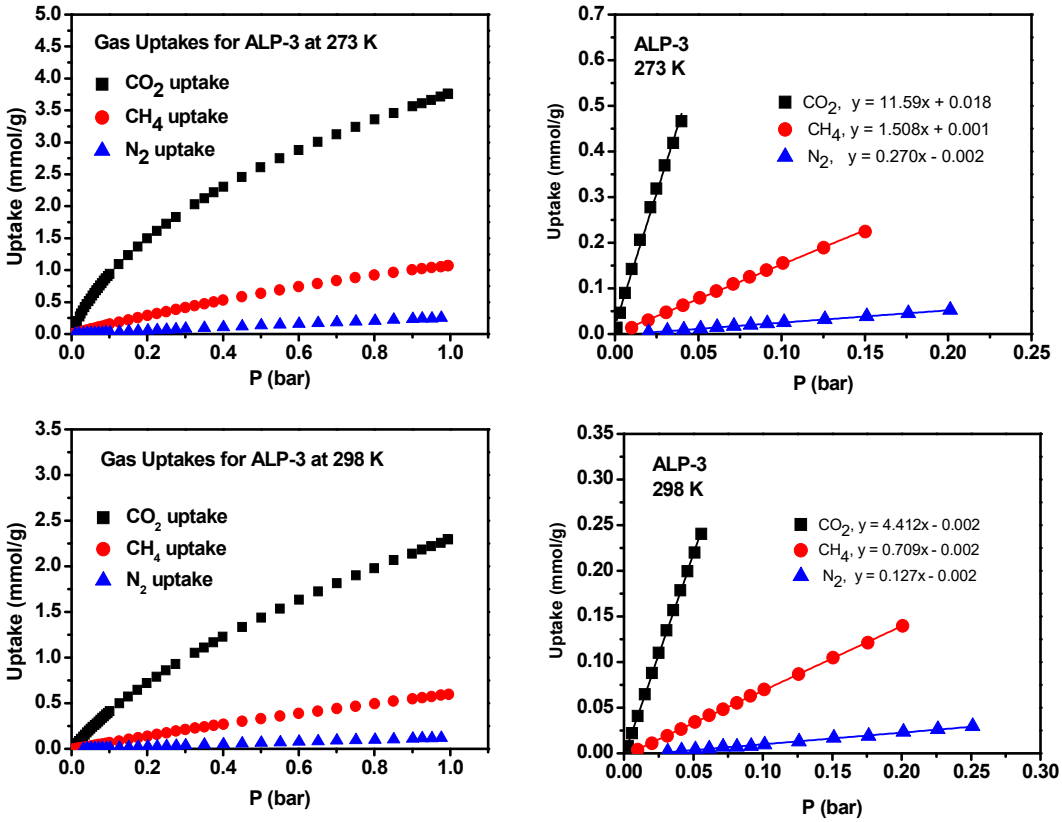

Figure 2.24: CO_2/N_2 and CO_2/CH_4 initial slope selectivity studies for ALP-3.

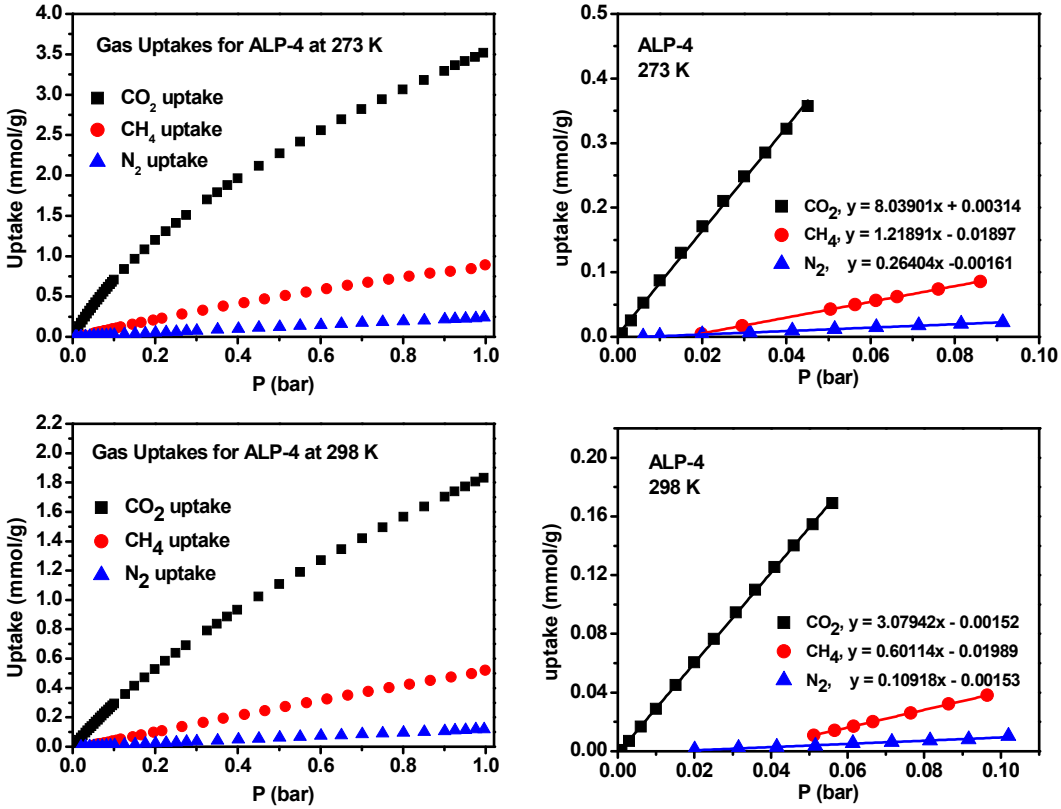

Figure 2.25: CO_2/N_2 and CO_2/CH_4 initial slope selectivity studies for ALP-4.

Table 2.6: CO_2/N_2 and CO_2/CH_4 selectivity of ALPs.

Polymer	Selectivity [Initial Slope][a]		Selectivity [IAST][b]	
	CO_2/N_2	CO_2/CH_4	CO_2/N_2	CO_2/CH_4
ALP-1	35 (27)	6 (5)	40 (28)	9(6)
ALP-2	29 (27)	7 (5)	34 (26)	8(5)
ALP-3	43 (35)	8 (6)	44 (35)	9(6)
ALP-4	30 (28)	7 (5)	35 (26)	8(5)

[a]Selectivity (mol mol^{-1}) was calculated by initial slope method at 273 K and (298 K).

[b]Selectivity (mol mol^{-1}, 1 bar) was calculated by IAST method at mole ratio of 15:85 for CO_2/N_2 and mole ratio of 50:50 for CO_2/CH_4 at 273 K and (298 K).

The CO_2/N_2 selectivity of ALPs was found to be only 29−43 at 273 K and 27−35 at 298 K. Surprisingly, the calculated CO_2/N_2 selectivities for ALPs are significantly lower than those reported for azo-COPs which can reach up to124 at 273 K and 142 at 298 K, although both ALPs and azo-COPs have the same functional groups (azo-linkage).[14] Moreover, in contrast to azo-COPs which display enhanced CO_2/N_2 selectivity upon increasing temperature, the selectivity of ALPs decreases as temperature increases. As stated above, ALPs have higher surface areas, larger pores, and broader pore size distributions than azo-COPs. These differences in CO_2/N_2 selectivities between ALPs and azo-COPs suggest that in addition to the function of the azo-linkage, the surface area and pore size are very important factors that affect the CO_2/N_2 selectivity of this class of material. Our results suggest that the N_2-phobocity of the azo-linkage in azo-COPs, might stem from the sieving effect of the very narrow pore aperture of azo-COPs. As such, the pores of azo-COPs become less accessible by N_2 molecules as temperature increases. Our findings are also

consistent with the general notion that higher porosity levels in porous organic polymers generally compromise the CO_2/N_2 selectivity.[6]

The selectivity studies described above were also supported by results from the ideal adsorbed solution theory (IAST)[44] . IAST method can be used to predict gas mixture behaviour in porous materials from single-component isotherms. This method allows for the prediction of selectivities as a function of pressure and has been reported to provide good predictions of gas mixture behaviour for many zeolites and MOFs.[45] Very recently, IAST has been widely used to study gas selectivity of several porous organic polymers such as MOPs,[46] POPs,[10, 47] COPs,[48] APOPs,[49] NPOFs,[4] BLP-10(Cl),[50] and azo-COPs [14]. Accordingly, we used IAST to predict binary gas mixture behavior in ALPs at 273 K and 298 K, with gas mixture compositions similar to those of flue gas (CO_2/N_2: 15/85) and landfill gas (CO_2/CH_4: 50/50). For IAST studies, the pure component isotherms of CO_2 measured at 273 and 298 K were fitted with the dual-site Langmuir (DSL) model:

$$q = q_A + q_B = q_{sat,A}\frac{b_A p}{1 + b_A p} + q_{sat,B}\frac{b_B p}{1 + b_B p}$$

with T-dependent parameters b_A and b_B

$$b_A = b_{A0}\, exp\left(\frac{E_A}{RT}\right), \qquad b_B = b_{B0}\, exp\left(\frac{E_B}{RT}\right)$$

where, q is molar loading of adsorbate (mol kg^{-1}), q_{sat} is saturation loading (mol kg^{-1}) , b is parameter in the pure component Langmuir isotherm (bar^{-1}), p is bulk gas phase pressure (bar), $-E$ is heat of adsorption (J mol^{-1}), R is ideal gas constant (8.314 J mol^{-1} K^{-1}), T is absolute temperature (K), subscripts A and B refers to site A and site B, respectively.[51]

Since the pure component isotherms of CH_4 and N_2 do not show any inflection characteristic they were fitted with the single-site Langmuir (SSL) model:

$$q = q_{sat,A} \frac{b_A p}{1 + b_A p}$$

with T-dependent parameter b_A

$$b_A = b_{A0}\, exp\left(\frac{E_A}{RT}\right)$$

Pure-component isotherm fitting parameters were then used for calculating Ideal Adsorbed Solution Theory (IAST)[44] binary-gas adsorption selectivities, S_{ads},defined as

$$S_{ads} = \frac{q_1/q_2}{p_1/p_2}$$

The fitting parameters for gas uptake isotherms are summarized in the following tables and graphs.

Table 2.7: Langmuir fitting parameters of CO_2, CH_4, and N_2 adsorption isotherms of ALP-1 at 273 and 298 K.

Gas	$q_{sat,A}$ (mol/kg)	b_{A0} (bar^{-1})	E_A (J/mol)	$q_{sat,B}$ (mol/kg)	b_{B0} (bar^{-1})	E_B (J/mol)	Reduced χ^2	Adj. R^2
CO_2	9.31868	1.44E-05	24802.34	1.36358	4.06E-06	33187.76	1.40E-05	0.99999
CH_4	4.5197	6.77E-05	20487.59				1.12E-05	0.99995
N_2	5.68371	2.84E-05	18012.55				2.08E-06	0.99984

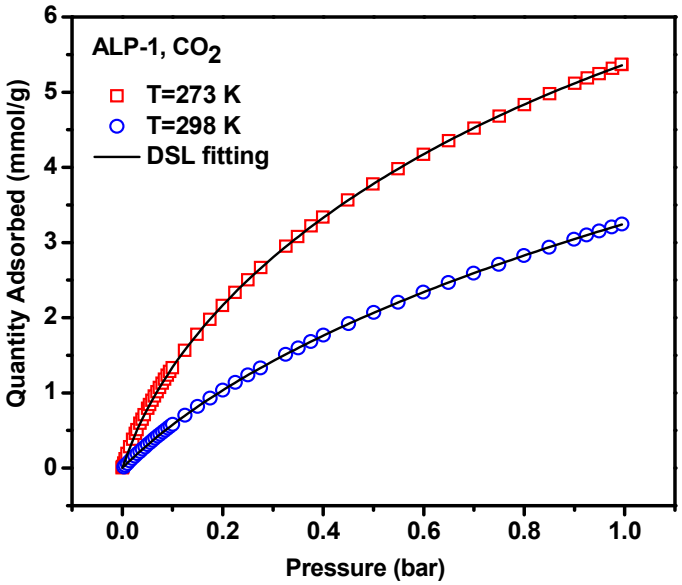

Figure 2.26: Experimental data and corresponding DSL fittings for CO_2 adsorption of ALP-1 at 273 and 298 K.

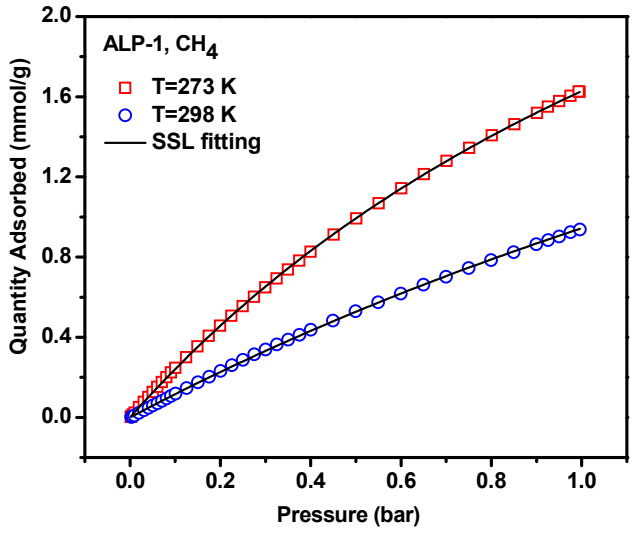

Figure 2.27: Experimental data and corresponding SSL fittings for CH_4 adsorption of ALP-1 at 273 and 298 K.

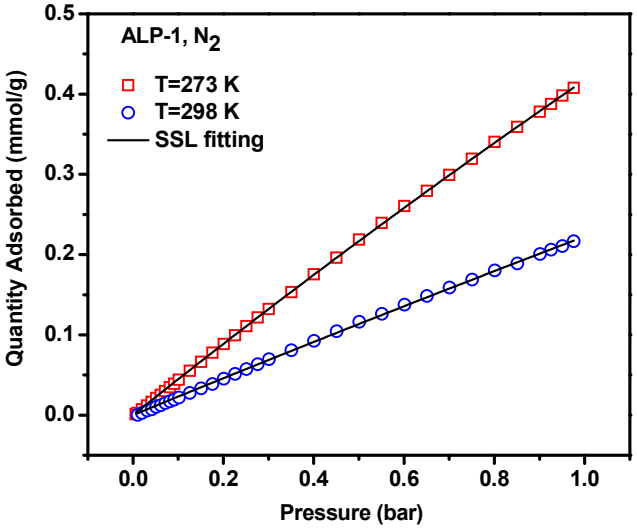

Figure 2.28: Experimental data and corresponding SSL fittings for N_2 adsorption of ALP-1 at 273 and 298 K.

Table 2.8: Langmuir fitting parameters of CO_2, CH_4, and N_2 adsorption isotherms of ALP-2 at 273 and 298 K

Gas	$q_{sat,A}$ (mol/kg)	b_{A0} (bar^{-1})	E_A (J/mol)	$q_{sat,B}$ (mol/kg)	b_{B0} (bar^{-1})	E_B (J/mol)	Reduced χ^2	Adj. R^2
CO_2	15.09636	2.81E-06	26531.02	1.23102	2.22E-05	27928.80	1.11E-05	0.99999
CH_4	5.98893	1.90E-04	16059.83				6.17E-05	0.99932
N_2	4.29767	8.66E-06	20632.84				4.08E-06	0.99946

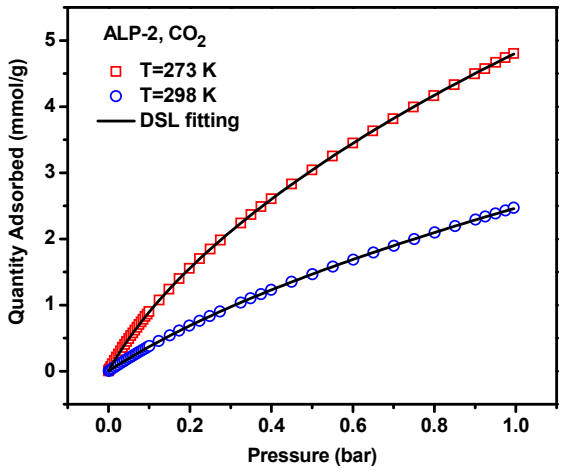

Figure 2.29: Experimental data and corresponding DSL fittings for CO_2 adsorption of ALP-2 at 273 and 298 K.

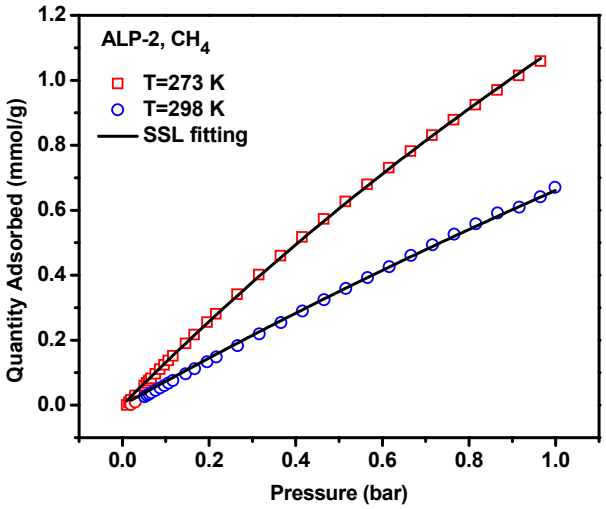

Figure 2.30: Experimental data and corresponding SSL fittings for CH_4 adsorption of ALP-2 at 273 and 298 K.

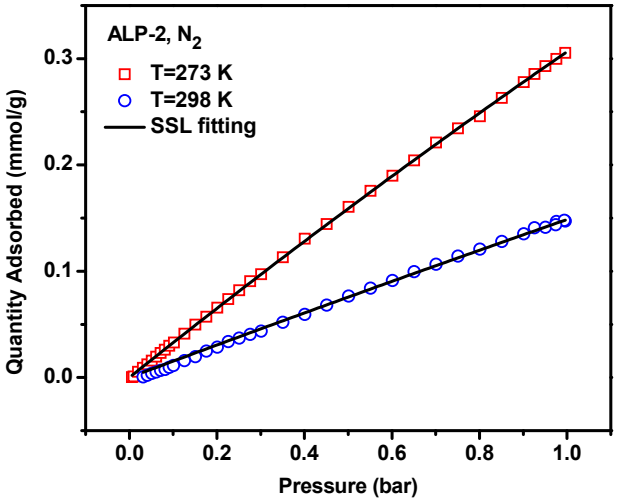

Figure 2.31: Experimental data and corresponding SSL fittings for N_2 adsorption of ALP-2 at 273 and 298 K.

Table 2.9: Langmuir fitting parameters of CO_2, CH_4, and N_2 adsorption isotherms of ALP-3 at 273 and 298 K.

Gas	$q_{sat,A}$ (mol/kg)	b_{A0} (bar^{-1})	E_A (J/mol)	$q_{sat,B}$ (mol/kg)	b_{B0} (bar^{-1})	E_B (J/mol)	Reduced χ^2	Adj. R^2
CO_2	7.20044	2.37E-05	23235.15	0.97805	1.35E-06	35909.01	3.11E-05	0.99997
CH_4	3.3775	4.58E-05	20958.05				8.21E-06	0.99992
N_2	6.18507	5.39E-06	20407.12				3.73E-06	0.99926

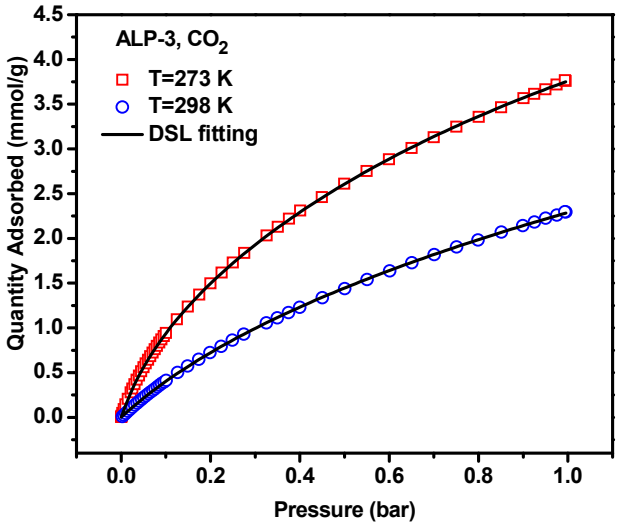

Figure 2.32: Experimental data and corresponding DSL fittings for CO_2 adsorption of ALP-3 at 273 and 298 K.

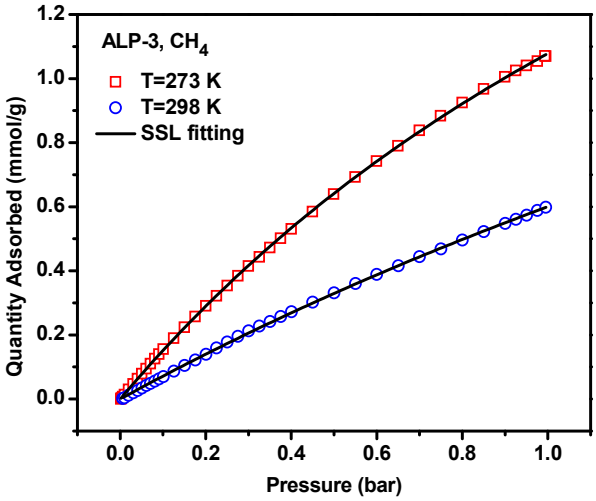

Figure 2.33: Experimental data and corresponding SSL fittings for CH_4 adsorption of ALP-3 at 273 and 298 K.

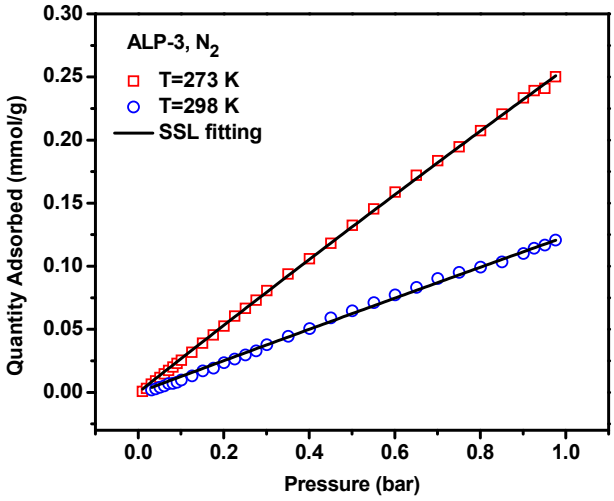

Figure 2.34: Experimental data and corresponding SSL fittings for N_2 adsorption of ALP-3 at 273 and 298 K.

Table 2.10: Langmuir fitting parameters of CO_2, CH_4, and N_2 adsorption isotherms of ALP-4 at 273 and 298 K.

Gas	$q_{sat,A}$ (mol/kg)	b_{A0} (bar^{-1})	E_A (J/mol)	$q_{sat,B}$ (mol/kg)	b_{B0} (bar^{-1})	E_B (J/mol)	Reduced χ^2	Adj. R^2
CO_2	10.9653	2.21E-06	26891.67	1.12282	1.28E-05	29234.33	7.84E-06	0.99999
CH_4	4.58847	8.98E-05	17909.35				1.05E-04	0.99835
N_2	3.60292	1.21E-05	19679.61				1.84E-06	0.9996

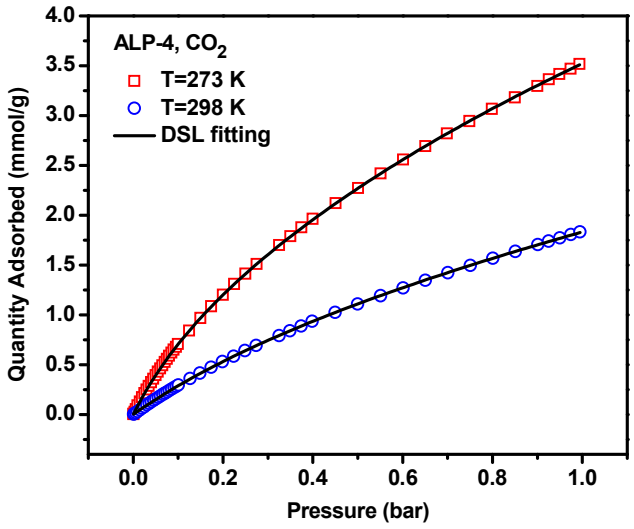

Figure 2.35: Experimental data and corresponding DSL fittings for CO_2 adsorption of ALP-4 at 273 and 298 K.

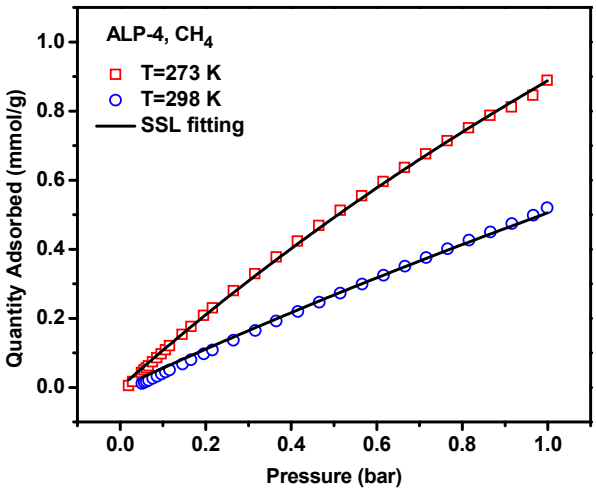

Figure 2.36: Experimental data and corresponding SSL fittings for CH_4 adsorption of ALP-4 at 273 and 298 K.

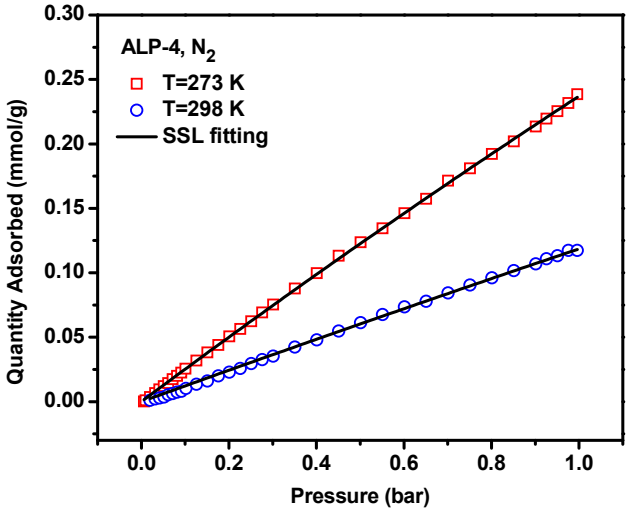

Figure 2.37: Experimental data and corresponding SSL fittings for N_2 adsorption of ALP-4 at 273 and 298 K.

The IAST selectivity results are summarized in Figure 2.38 and Table 2.6. The overall results from IAST calculations are in a good agreement with those obtained from the initial slope method. The IAST CO_2/N_2 selectivity of ALPs at 273 K and 1 bar was found to be 34-44 which are much lower than those of azo-COPs (64-110)[14]. The impact of temperature on the CO_2/N_2 selectivity can be seen in Figures 2.38 A and B, which clearly indicate a decrease in the selectivity of all ALPs. The IAST CO_2/N_2 selectivities at 298 K and 1 bar were found to be 26-35, which are lower than those at 273 K (Table 2.6). Again, these values are significantly lower than those of azo-COPs (97-131)[14]. At 273 K, ALP-3 has the highest CO_2/N_2 selectivity, which starts at 54 at low coverage and then drops slightly with increased pressure to reach 44 at 1 bar. Other ALPs have similar CO_2/N_2 selectivities that remain almost constant with pressure. The CO_2/CH_4 selectivity of ALPs at 273 K is very similar reaching ~9 at 1 bar. Increasing the temperature to 298 K reduces the CO_2/CH_4 selectivity of ALPs to 5-6, which again is consistent with our results from the initial slope calculations. The CO_2/CH_4 selectivity of ALPs is considerably lower than that of CO_2/N_2 since CH_4 has much higher adsorption potential than N_2 because of the higher polarizability of CH_4 (26 × 10-25 cm^3) compared to that of N_2 (17.6 × 10^{-25} cm^3).[52]

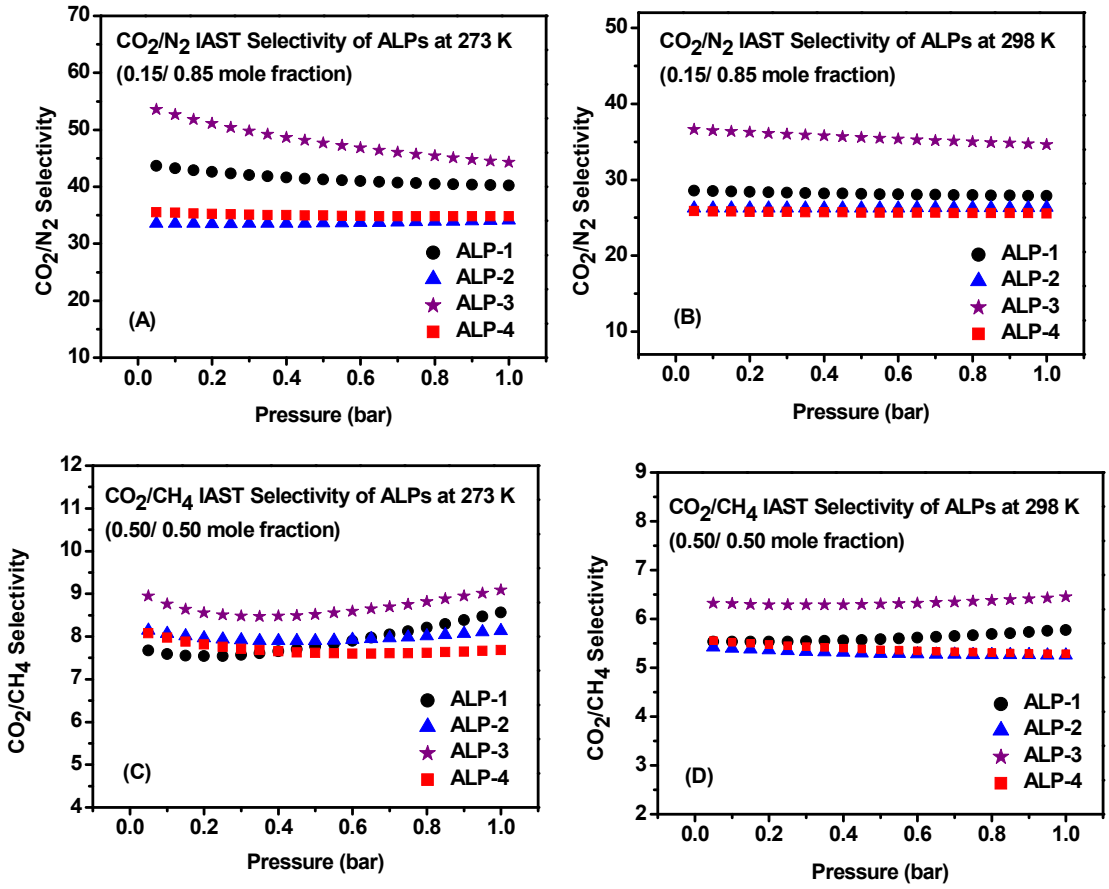

Figure 2.38: CO_2/N_2 selectivity of ALPs for mole ratio of 15:85 at 273 K (A) and 298 K(B), and CH_4/N_2 selectivity of ALPs for mole ratio of 50:50 at 273 K (C) and 298 K (D).

2.4.4 High Pressure Gas Storage Studies for ALPs

Because our low pressure gas sorption studies on ALPs indicate that ALPs are far from saturation at 1 bar, high pressure gas sorption measurements for H_2, CH_4, and CO_2 were performed to evaluate gas storage capacity of ALPs under high pressure and the results are summarized in Figure 2.39, Figure 2.40, and Table 2.11.

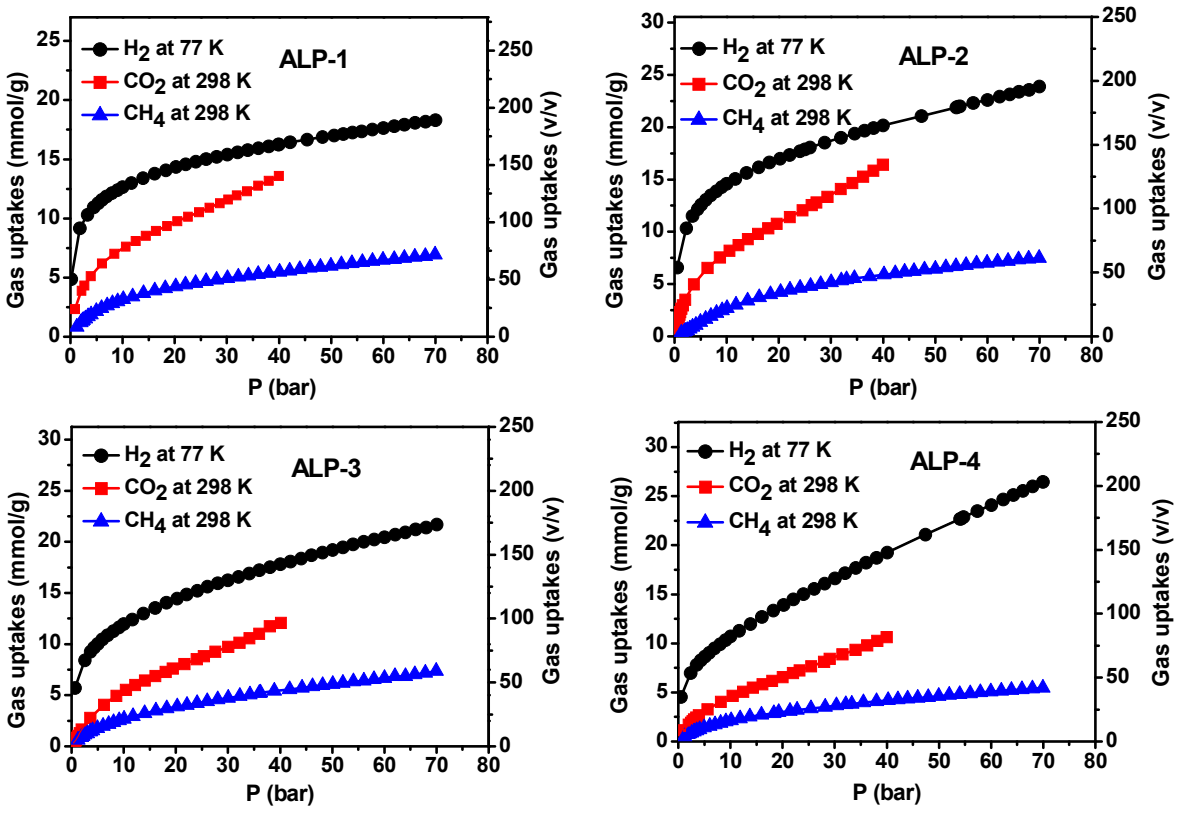

Figure 2.39: High pressure excess gas sorption uptake capacities of ALPs for H_2, CO_2, and CH_4.

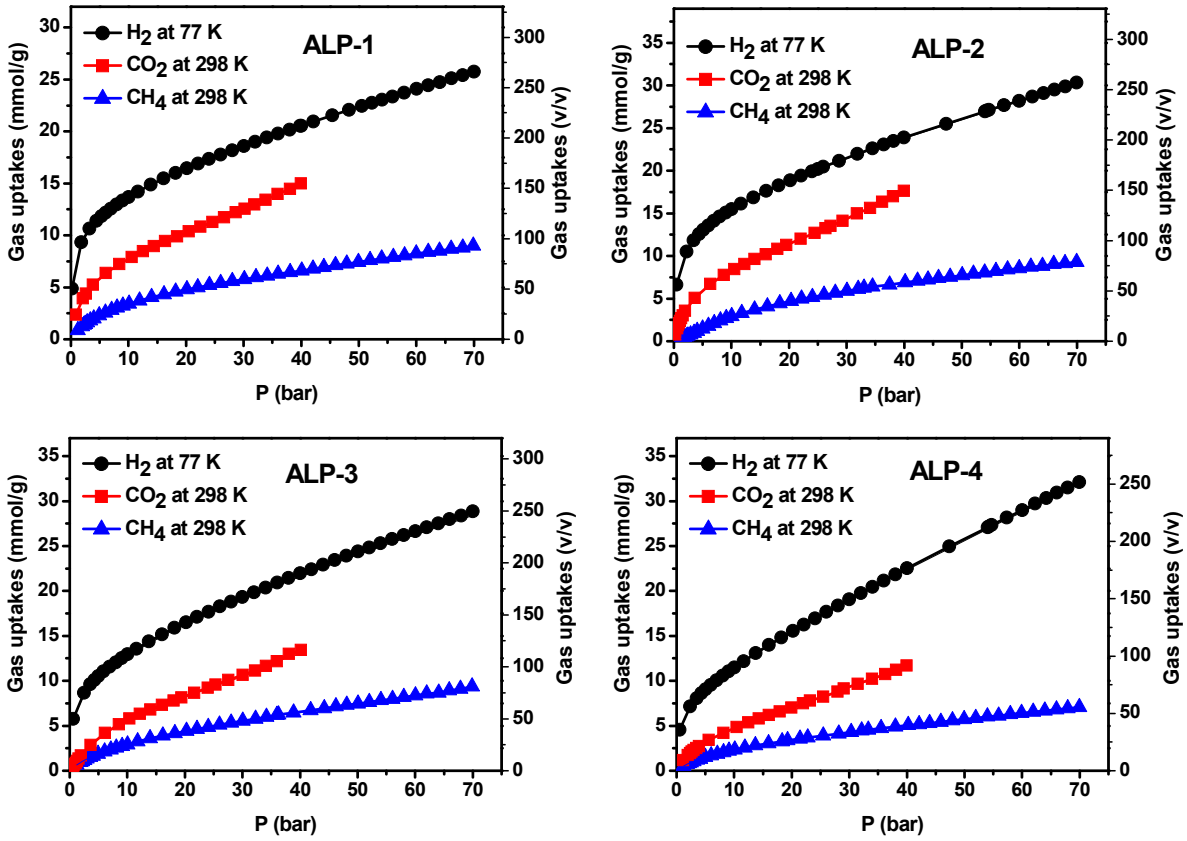

Figure 2.40: High pressure total gas uptake capacities of ALPs for H_2, CO_2, and CH_4.

Table 2.11: H_2, CO_2, and CH_4 high pressure gas sorption data for ALPs.

Polymer	Excess H_2 Uptake[a,*]	Total H_2 Uptake[a,*]	Excess CO_2 Uptake[b,*]	Total CO_2 Uptake[b,*]	Excess CH_4 Uptake[c,*]	Total CH_4 Uptake[c,*]
ALP-1	18.3	25.7	13.6	15.0	6.9	9.0
ALP-2	23.9	31.3	16.4	17.8	7.5	9.6
ALP-3	21.7	30.8	12.1	13.8	7.4	9.9
ALP-4	26.4	32.5	10.6	11.8	5.5	7.2

[*]All gas uptakes are in mmol g^{-1}. [a]At 77 K and 70 bar. [b]At 298 K and 40 bar. [c]At 298 K and 70 bar.

The hydrogen uptake by ALPs at 77 K shows a gradual increase with pressure and the hydrogen surface excess uptake at 70 bar reaches 18.3, 23.9, 21.7, and 26.4 mmol g^{-1} for ALP-1, ALP-2, ALP-3 and ALP-4, respectively. The corresponding gravimetric surface excess uptakes were found to be 3.6, 4.6, 4.2, and 5.1 wt% for ALP-1, ALP-2, ALP-3, and ALP-4, exceeding the hydrogen uptake capacities for most organic polymers having similar surface area (Table 2.12). The surface excess CO_2 uptake of ALPs was significant reaching 10.6−16.4 mmol g^{-1} at 298 K and 40 bar. These values exceed the reported values for HCPs (10.6−13.3 mmol g^{-1}, 30 bar and 298 K)[37] as well as PPN-1 (11 mmol g^{-1} at 295 K/60 bar)[39] but are lower than those of PPN-2 (19 mmol g^{-1} at 295 K/60 bar)[39], PAF-1 (29.6 mmol g^{-1}, 298 K/40 bar)[53] and PPN-4 (~39 mmolg^{-1}, 295 K/50 bar)[23]. The methane gravimetric surface excess uptakes of ALPs at 298 K and 70 bar were found to be 6.9, 7.5, 7.4, and 5.5 mmol g^{-1} for ALP-1, ALP-2, ALP-3 and ALP-4, respectively. These values are comparable to the reported values for PPN-1 and PPN-2.[39]

Table 2.12: High-pressure excess gas uptake by selected porous organic materials.

Polymer	CO_2 Uptake (wt%)	H_2 Uptake (wt%) at 77 K	CH_4 Uptake (wt%)	Ref.
ALP-1	37(40 bar, 298 K)	3.6 (70 bar)	10.0 (70 bar, 298 K)	This Work
ALP-2	42 (40 bar, 298 K)	4.6 (70 bar)	10.7 (70 bar, 298 K)	This Work
ALP-3	35 (40 bar, 298 K)	4.2 (70 bar)	10.6(70 bar, 298 K)	This Work
ALP-4	32 (40 bar, 298 K)	5.1 (70 bar)	8.1 (70 bar, 298 K)	This Work
COF-1	19 (55 bar, 298 K)	1.5 (Sat[a])	4.2 (85 bar, 298 K)	[38]
COF-6	24 (55 bar, 298 K)	2.2 (Sat[a])	6.4 (85 bar, 298 K)	[38]
COF-8	39 (55 bar, 298 K)	3.5 (Sat[a])	10.2 (85 bar, 298 K)	[38]
BILP-10	35 (40 bar, 298 K)	3.4 (40 bar)	6.2 (40 bar, 298 K)	[54]
PPN-3	53 (60 bar, 295 K)	4.3 (42 bar)	16.7 (70 bar, 295 K)	[39]
HCP 4	32 (30 bar, 298 K)	-	-	[37]
PAF-1	56 (40 bar, 298 K)	7.0 (48 bar)	-	[55]
PS4TH	-	3.6 (60 bar)	-	[56]

High volumetric gas storage capacity of adsorbents is also one of the desired features, especially for on-board hydrogen and methane storage, in order to reduce fuel tank size. In general, attaining high volumetric gas uptake capacity for low density adsorbents such as organic polymers remains a considerable challenge. Since significant amounts of compressed gas can be accommodated inside the voids of porous materials under high pressures, the total amount of gas stored at high pressures is higher than the amount of adsorbed gas. Therefore, for high pressure storage applications, the total volumetric storage capacity of porous organic materials which typically have low densities should be investigated to evaluate their efficiency for practical use. Accordingly,

total (absolute) amounts of gas adsorbed by ALPs were calculated from experimentally determined surface excess adsorptions (Figure 2.40), and are summarized in Table 2.11. The total volumetric hydrogen uptakes of ALPs at 77 K and 70 bar were found to be 23.9 g L^{-1} (ALP-1), 23.0 g L^{-1} (ALP-2), 22.2 g L^{-1} (ALP-3), and 22.5 g L^{-1} (ALP-4). Similarly, the total methane uptakes at 298 K and 70 bar for ALPs in volumetric units were estimated to be 93, 78, 80, and 55 L L^{-1} for ALP-1, ALP-2, ALP-3, and ALP-4 respectively. These values are lower than the 2015 DOE target which emphasizes the need for high pore volume and surface area materials for both hydrogen and methane storage under high pressure conditions. The volumetric CO_2 sorption capacity for ALPs at 298 K and 40 bar was found to be in the range of 90-155 L L^{-1}. The volumetric CO_2 sorption capacity of ALP-1 (304 g L^{-1}, 298 K/40 bar) is higher than other ALPs and is more than three times (3.3) the density of CO_2 at the same temperature and pressure.[57]

2.5 Conclusions

We have introduced a new synthetic route to synthesize highly porous azo-linked polymers (ALPs) by homocoupling of 2D and 3D aniline-like monomers using copper(I) as a catalyst. ALPs have high BET surface area up to 1235 m^2 g^{-1} and exhibit high thermal and chemical stability. Notably, ALPs have higher porosity and larger pores than azo-COPs and as a result they perform well in gas uptake under high pressure conditions. One of the polymers, ALP-1, has remarkable CO_2 uptake (5.37 mmol g^{-1} at 273 K and 1.0 bar) which is among the highest by porous organic polymers. ALPs also exhibit good CO_2/N_2 selectivity that can reach up to 43 at 273 K and moderate CO_2/CH_4 selectivity (5-8). The CO_2/N_2 selectivity of ALPs decreases upon increase in gas uptake temperature in contrast to the behavior of reported azo-COPs. Because of their high gas uptake capacities, chemical heterogeneity, as well as high physicochemical stability, ALPs show promise in small gas storage and separation applications.

References

1. Arab, P.; Rabbani, M. G.; Sekizkardes, A. K.; İslamoğlu, T.; El-Kaderi, H. M., Copper(I)-Catalyzed Synthesis of Nanoporous Azo-Linked Polymers: Impact of Textural Properties on Gas Storage and Selective Carbon Dioxide Capture. *Chemistry of Materials,* **2014**, *26*, 1385-1392.

2. Lu, W.; Sculley, J. P.; Yuan, D.; Krishna, R.; Wei, Z.; Zhou, H.-C., Polyamine-Tethered Porous Polymer Networks for Carbon Dioxide Capture from Flue Gas. *Angewandte Chemie International Edition,* **2012**, *51*, 7480-7484.

3. Lu, W.; Yuan, D.; Sculley, J.; Zhao, D.; Krishna, R.; Zhou, H.-C., Sulfonate-Grafted Porous Polymer Networks for Preferential CO_2 Adsorption at Low Pressure. *Journal of the American Chemical Society,* **2011**, *133*, 18126-18129.

4. Islamoglu, T.; Gulam Rabbani, M.; El-Kaderi, H. M., Impact of Post-Synthesis Modification of Nanoporous Organic Frameworks on Small Gas Uptake and Selective CO_2 Capture. *Journal of Materials Chemistry A,* **2013**, *1*, 10259-10266.

5. Rabbani, M. G.; El-Kaderi, H. M., Template-Free Synthesis of a Highly Porous Benzimidazole-Linked Polymer for CO_2 Capture and H_2 Storage. *Chemistry of Materials,* **2011**, *23*, 1650-1653.

6. Dawson, R.; Cooper, A. I.; Adams, D. J., Chemical Functionalization Strategies for Carbon Dioxide Capture in Microporous Organic Polymers. *Polymer International,* **2013**, *62*, 345-352.

7. Xie, L.-H.; Suh, M. P., High CO_2-Capture Ability of a Porous Organic Polymer Bifunctionalized with Carboxy and Triazole Groups. *Chemistry – A European Journal,* **2013**, *19*, 11590-11597.

8. Rabbani, M. G.; Reich, T. E.; Kassab, R. M.; Jackson, K. T.; El-Kaderi, H. M., High CO_2 Uptake and Selectivity by Triptycene-Derived Benzimidazole-Linked Polymers. *Chemical Communications,* **2012**, *48*, 1141-1143.

9. Xu, C.; Hedin, N., Synthesis of microporous organic polymers with high CO_2-over-N_2 selectivity and CO_2 adsorption. *Journal of Materials Chemistry A,* **2013**, *1*, 3406-3414.

10. Farha, O. K.; Spokoyny, A. M.; Hauser, B. G.; Bae, Y.-S.; Brown, S. E.; Snurr, R. Q.; Mirkin, C. A.; Hupp, J. T., Synthesis, Properties, and Gas Separation Studies of a Robust Diimide-Based Microporous Organic Polymer. *Chemistry of Materials,* **2009**, *21*, 3033-3035.

11. Chen, Q.; Luo, M.; Hammershøj, P.; Zhou, D.; Han, Y.; Laursen, B. W.; Yan, C.-G.; Han, B.-H., Microporous Polycarbazole with High Specific Surface Area for Gas Storage and Separation. *Journal of the American Chemical Society,* **2012**, *134*, 6084-6087.

12. Pandey, P.; Farha, O. K.; Spokoyny, A. M.; Mirkin, C. A.; Kanatzidis, M. G.; Hupp, J. T.; Nguyen, S. T., A "Click-Based" Porous Organic Polymer from Tetrahedral Building Blocks. *Journal of Materials Chemistry,* **2011**, *21*, 1700-1703.

13. Ren, S.; Bojdys, M. J.; Dawson, R.; Laybourn, A.; Khimyak, Y. Z.; Adams, D. J.; Cooper, A. I., Porous, Fluorescent, Covalent Triazine-Based Frameworks Via Room-Temperature and Microwave-Assisted Synthesis. *Adv. Mater.,* **2012**, *24*, 2357-2361.

14. Patel, H. A.; Je, S. H.; Park, J.; Chen, D. P.; Jung, Y.; Yavuz, C. T.; Coskun, A., Unprecedented High-Temperature CO_2 Selectivity in N_2-Phobic Nanoporous Covalent Organic Polymers. *Nature Communications,* **2013**, *4*, 1357.

15. Plietzsch, O.; Schilling, C. I.; Tolev, M.; Nieger, M.; Richert, C.; Muller, T.; Brase, S., Four-Fold Click Reactions: Generation of Tetrahedral Methane- and Adamantane-Based Building Blocks for Higher-Order Molecular Assemblies. *Organic & Biomolecular Chemistry,* **2009**, *7*, 4734-4743.

16. Cheng, L.; Xu, Z.; Xiong, X.-q.; Wang, J.-x.; Jing, B., A Facile Synthesis of Hyperbranched Polyimides from 2,6,12-triaminotriptycene. *Chinese Journal of Polymer Science,* **2010**, *28*, 69-76.

17. Moon, S.-Y.; Bae, J.-S.; Jeon, E.; Park, J.-W., Organic Sol–Gel Synthesis: Solution-Processable Microporous Organic Networks. *Angewandte Chemie International Edition,* **2010**, *49*, 9504-9508.

18. Bao, C.; Lu, R.; Jin, M.; Xue, P.; Tan, C.; Xu, T.; Liu, G.; Zhao, Y., Helical Stacking Tuned by Alkoxy Side Chains in π-Conjugated Triphenylbenzene Discotic Derivatives. *Chemistry – A European Journal,* **2006**, *12*, 3287-3294.

19. Rabbani, M. G.; Sekizkardes, A. K.; Kahveci, Z.; Reich, T. E.; Ding, R.; El-Kaderi, H. M., A 2D Mesoporous Imine-Linked Covalent Organic Framework for High Pressure Gas Storage Applications. *Chemistry – A European Journal,* **2013**, *19*, 3324-3328.

20. Zhang, C.; Jiao, N., Copper-Catalyzed Aerobic Oxidative Dehydrogenative Coupling of Anilines Leading to Aromatic Azo Compounds using Dioxygen as an Oxidant. *Angewandte Chemie International Edition,* **2010**, *49*, 6174-6177.

21. El-Kaderi, H. M.; Hunt, J. R.; Mendoza-Cortés, J. L.; Côté, A. P.; Taylor, R. E.; O'Keeffe, M.; Yaghi, O. M., Designed Synthesis of 3D Covalent Organic Frameworks. *Science,* **2007**, *316*, 268-272.

22. Côté, A. P.; El-Kaderi, H. M.; Furukawa, H.; Hunt, J. R.; Yaghi, O. M., Reticular Synthesis of Microporous and Mesoporous 2D Covalent Organic Frameworks. *Journal of the American Chemical Society,* **2007**, *129*, 12914-12915.

23. Yuan, D.; Lu, W.; Zhao, D.; Zhou, H.-C., Highly Stable Porous Polymer Networks with Exceptionally High Gas-Uptake Capacities. *Advanced Materials,* **2011**, *23*, 3723-3725.

24. Katekomol, P.; Roeser, J.; Bojdys, M.; Weber, J.; Thomas, A., Covalent Triazine Frameworks Prepared from 1,3,5-Tricyanobenzene. *Chemistry of Materials,* **2013**, *25*, 1542-1548.

25. Li, G.; Wang, Z., Microporous Polyimides with Uniform Pores for Adsorption and Separation of CO_2 Gas and Organic Vapors. *Macromolecules,* **2013**, *46*, 3058-3066.

26. Uribe-Romo, F. J.; Hunt, J. R.; Furukawa, H.; Klöck, C.; O'Keeffe, M.; Yaghi, O. M., A Crystalline Imine-Linked 3-D Porous Covalent Organic Framework. *Journal of the American Chemical Society,* **2009**, *131*, 4570-4571.

27. Zhang, Q.; Yang, Y.; Zhang, S., Novel Functionalized Microporous Organic Networks Based on Triphenylphosphine. *Chemistry – A European Journal,* **2013**, *19*, 10024-10029.

28. Rabbani, M. G.; El-Kaderi, H. M., Synthesis and Characterization of Porous Benzimidazole-Linked Polymers and Their Performance in Small Gas Storage and Selective Uptake. *Chemistry of Materials,* **2012**, *24*, 1511-1517.

29. Pandey, P.; Katsoulidis, A. P.; Eryazici, I.; Wu, Y.; Kanatzidis, M. G.; Nguyen, S. T., Imine-Linked Microporous Polymer Organic Frameworks. *Chemistry of Materials,* **2010**, *22*, 4974-4979.

30. Ghanem, B. S., et al., Triptycene-Based Polymers of Intrinsic Microporosity: Organic Materials That Can Be Tailored for Gas Adsorption. *Macromolecules,* **2010**, *43*, 5287-5294.

31. Dawson, R.; Adams, D. J.; Cooper, A. I., Chemical Tuning of CO_2 Sorption in Robust Nanoporous Organic Polymers. *Chemical Science,* **2011**, *2*, 1173-1177.

32. Wilmer, C. E.; Farha, O. K.; Bae, Y.-S.; Hupp, J. T.; Snurr, R. Q., Structure-Property Relationships of Porous Materials for Carbon Dioxide Separation and Capture. *Energy & Environmental Science,* **2012**, *5*, 9849-9856.

33. Nagaraja, C. M.; Haldar, R.; Maji, T. K.; Rao, C. N. R., Chiral Porous Metal–Organic Frameworks of Co(II) and Ni(II): Synthesis, Structure, Magnetic Properties, and CO_2 Uptake. *Crystal Growth & Design,* **2012**, *12*, 975-981.

34. Li, P.-Z.; Zhao, Y., Nitrogen-Rich Porous Adsorbents for CO_2 Capture and Storage. *Chemistry – An Asian Journal,* **2013**, *8*, 1680-1691.

35. Ben, T.; Pei, C.; Zhang, D.; Xu, J.; Deng, F.; Jing, X.; Qiu, S., Gas Storage in Porous Aromatic Frameworks (PAFs). *Energy & Environmental Science,* **2011**, *4*, 3991-3999.

36. Dawson, R.; Stockel, E.; Holst, J. R.; Adams, D. J.; Cooper, A. I., Microporous Organic Polymers for Carbon Dioxide Capture. *Energy & Environmental Science,* **2011**, *4*, 4239-4245.

37. Martin, C. F.; Stockel, E.; Clowes, R.; Adams, D. J.; Cooper, A. I.; Pis, J. J.; Rubiera, F.; Pevida, C., Hypercrosslinked organic polymer networks as potential adsorbents for pre-combustion CO_2 capture. *Journal of Materials Chemistry,* **2011**, *21*, 5475-5483.

38. Furukawa, H.; Yaghi, O. M., Storage of Hydrogen, Methane, and Carbon Dioxide in Highly Porous Covalent Organic Frameworks for Clean Energy Applications. *Journal of the American Chemical Society,* **2009**, *131*, 8875-8883.

39. Lu, W., et al., Porous Polymer Networks: Synthesis, Porosity, and Applications in Gas Storage/Separation. *Chemistry of Materials,* **2010**, *22*, 5964-5972.

40. Katsoulidis, A. P.; Kanatzidis, M. G., Phloroglucinol Based Microporous Polymeric Organic Frameworks with −OH Functional Groups and High CO_2 Capture Capacity. *Chemistry of Materials,* **2011**, *23*, 1818-1824.

41. Ren, S.; Bojdys, M. J.; Dawson, R.; Laybourn, A.; Khimyak, Y. Z.; Adams, D. J.; Cooper, A. I., Porous, Fluorescent, Covalent Triazine-Based Frameworks Via Room-Temperature and Microwave-Assisted Synthesis. *Advanced Materials,* **2012**, *24*, 2357-2361.

42. Dawson, R.; Stevens, L. A.; Drage, T. C.; Snape, C. E.; Smith, M. W.; Adams, D. J.; Cooper, A. I., Impact of Water Coadsorption for Carbon Dioxide Capture in Microporous Polymer Sorbents. *Journal of the American Chemical Society,* **2012**, *134*, 10741-10744.

43. Zhang, D.-S.; Chang, Z.; Lv, Y.-B.; Hu, T.-L.; Bu, X.-H., Construction and Adsorption Properties of Microporous Tetrazine-Based Organic Frameworks. *RSC Advances,* **2012**, *2*, 408-410.

44. Myers, A. L.; Prausnitz, J. M., Thermodynamics of Mixed-Gas Adsorption. *AIChE Journal,* **1965**, *11*, 121-127.

45. Liu, B.; Smit, B., Comparative Molecular Simulation Study of CO_2/N_2 and CH_4/N_2 Separation in Zeolites and Metal−Organic Frameworks. *Langmuir,* **2009**, *25*, 5918-5926.

46. Dawson, R.; Ratvijitvech, T.; Corker, M.; Laybourn, A.; Khimyak, Y. Z.; Cooper, A. I.; Adams, D. J., Microporous Copolymers for Increased Gas Selectivity. *Polymer Chemistry,* **2012**, *3*, 2034-2038.

47. Farha, O. K.; Bae, Y.-S.; Hauser, B. G.; Spokoyny, A. M.; Snurr, R. Q.; Mirkin, C. A.; Hupp, J. T., Chemical Reduction of a Diimide Based Porous Polymer for Selective Uptake of Carbon Dioxide Versus Methane. *Chemical Communications,* **2010**, *46*, 1056-1058.

48. Xiang, Z.; Zhou, X.; Zhou, C.; Zhong, S.; He, X.; Qin, C.; Cao, D., Covalent-Organic Polymers for Carbon Dioxide Capture. *Journal of Materials Chemistry,* **2012**, *22*, 22663-22669.

49. Song, W.-C.; Xu, X.-K.; Chen, Q.; Zhuang, Z.-Z.; Bu, X.-H., Nitrogen-Rich Diaminotriazine-Based Porous Organic Polymers for Small Gas Storage and Selective Uptake. *Polymer Chemistry,* **2013**, *4*, 4690-4696.

50. Reich, T. E.; Behera, S.; Jackson, K. T.; Jena, P.; El-Kaderi, H. M., Highly Selective CO_2/CH_4 Gas Uptake by a Halogen-Decorated Borazine-Linked Polymer. *Journal of Materials Chemistry,* **2012**, *22*, 13524-13528.

51. Mason, J. A.; Sumida, K.; Herm, Z. R.; Krishna, R.; Long, J. R., Evaluating Metal-Organic Frameworks for Post-Combustion Carbon Dioxide Capture via Temperature Swing Adsorption. *Energy & Environmental Science,* **2011**, *4*, 3030-3040.

52. Yang, R. T., *Adsorbents: fundamentals and applications*; Wiley-Interscience, 2003.

53. Ben, T., et al., Targeted Synthesis of a Porous Aromatic Framework with High Stability and Exceptionally High Surface Area. *Angewandte Chemie International Edition,* **2009**, *48*, 9457-9460.

54. Rabbani, M. G.; Sekizkardes, A. K.; El-Kadri, O. M.; Kaafarani, B. R.; El-Kaderi, H. M., Pyrene-Directed Growth of Nanoporous Benzimidazole-Linked Nanofibers and their Application to Selective CO_2 Capture and Separation. *Journal of Materials Chemistry,* **2012**, *22*, 25409-25417.

55. Ben, T., et al., Targeted Synthesis of a Porous Aromatic Framework with High Stability and Exceptionally High Surface Area. *Angewandte Chemie,* **2009**, *121*, 9621-9624.

56. Yuan, S.; Kirklin, S.; Dorney, B.; Liu, D.-J.; Yu, L., Nanoporous Polymers Containing Stereocontorted Cores for Hydrogen Storage. *Macromolecules,* **2009**, *42*, 1554-1559.

57. NIST Chemistry WebBook (Thermophysical Properties of Fluid Systems):

. *NIST Chemistry WebBook (Thermophysical Properties of Fluid Systems): http://webbook.nist.gov/chemistry/fluid/.*

Chapter 3

Synthesis and Evaluation of Porous Azo-Linked Polymers for Highly Selective Carbon Dioxide Capture under Pressure Swing and Vacuum Swing Separation Settings

This chapter is mainly taken from my recent article.[1] Reproduced from Ref. 1 with permission from The Royal Society of Chemistry.

3.1 Abstract

A series of new azo-linked polymers (ALPs) was synthesized via copper(I)-catalyzed oxidative homocoupling of 2D and 3D aniline-like monomers. ALPs have moderate surface areas (SA_{BET} = 412-801 m^2 g^{-1}), narrow pore sizes (< 1nm), and high physiochemical stability. The potential applications of ALPs for selective CO_2 capture from flue gas and landfill gas at ambient temperature were studied. ALPs exhibit high isosteric heats of adsorption for CO_2 (28.6-32.5 kJ mol^{-1}) and high CO_2 uptake capacities of up to 2.94 mmol g^{-1} at 298 K and 1 bar. Ideal adsorbed solution theory (IAST) selectivity studies revealed that ALPs have good CO_2/N_2 (56) and CO_2/CH_4 (8) selectivities at 298 K. The correlation between the performance of ALPs in selective CO_2 capture and their properties such as surface area, pore size, and heat of adsorption was investigated. Moreover, the CO_2 separation ability of ALPs from flue gas and landfill gas under pressure-swing adsorption (PSA) and vacuum-swing adsorption (VSA) processes were evaluated.

3.2 Introduction

Very recently, azo-linked POPs have emerged as a new class of CO_2 adsorbents with exceptional physicochemical stability and high CO_2 uptake capacity.[2-5] Both theoretical[6] and experimental[2-3] studies have shown that porous frameworks functionalized with azo groups exhibit high CO_2 uptake capacity and/or selectivity due to Lewis acid-base interactions between CO_2 and azo groups. In addition, the photo-responsive nature of the azo-linkage could be utilized for CO_2 release via *trans-to-cis* isomerization by UV.[7] Patel *et al.* have recently reported very high CO_2/N_2 selectivity values (up to 131 at 298 K) for azo-linked covalent organic polymers (azo-COPs); however, the low porosity of azo-COPs resulted in modest CO_2 uptake capacities (1.2 - 1.5 mmol g^{-1}, 298 K and 1 bar) which could limit their applications in CO_2 capture.[3] To address this drawback, we have introduced a facile synthetic route for the synthesis of highly porous azo-linked polymers (ALPs) with remarkable CO_2 uptake capacities of up to 3.2 mmol g^{-1} (298 K and 1 bar).[2] However, the CO_2/N_2 selectivities of ALPs (26-35 at 298K) are much lower than those of azo-COPs (96-131 at 298 K).[2] ALPs[2] have higher surface area, greater pore volume, and larger pore width than azo-COPs[3] which affect their performance in selective CO_2 capture.[2] Azo-linked polymers with different structural properties (pore size, surface area, and pore volume) can be synthesized from diverse building units and different synthetic routes.[2-4] Therefore, it is necessary to investigate the dependence of CO_2 separation ability of azo-linked polymers on their structural properties. To be practical, a porous sorbent must be highly selective toward CO_2 and also have high CO_2 uptake capacity[8-9]; however, all previously reported azo-linked porous polymers might only meet one of these criteria at best.[2-3] Accordingly, design and synthesis of new azo-linked POPs should be aimed at achieving both high CO_2 uptake capacity and selectivity simultaneously. Moreover, CO_2 uptake capacity and selectivity do not provide enough information for evaluation

of a sorbent's effectiveness since they do not consider the cyclic nature of CO_2 separation processes.[10-11] Any CO_2 capturing system needs to be coupled with a regeneration technology for desorption of the captured CO_2 and recovery of the sorbent for the next runs. Therefore, other critical criteria such as regenerability, working capacity, and sorbent selection parameters should also be evaluated for comprehensive assessment of CO_2 sorbents in a cyclic separation process.[10-11] Pressure-swing adsorption (PSA) and vacuum-swing adsorption (VSA) processes are now used as efficient technologies for regeneration of adsorbents for a number of applications.[10] In a PSA or VSA process, after adsorption takes place, the adsorbent is regenerated by desorption of CO_2 under a reduced pressure without applying heat.[11] In a PSA process, CO_2 is adsorbed from a gas mixture at a high pressure (>1 bar), and the regeneration takes place upon reducing the pressure to 1 bar. On the other hand, in a VSA process, the adsorption pressure is ~ 1 bar, and the adsorbent is regenerated by reducing the pressure to ~ 0.1 bar.

With these considerations in mind, we applied new nitrogen-rich building units to synthesize new ALPs in an attempt to combine both high CO_2 uptake capacity and selectivity. One of the polymers, ALP-5, was successful in meeting both of these criteria simultaneously. Moreover, the new ALPs were evaluated for selective CO_2 removal from flue gas and landfill gas under PSA and VSA processes. Our study highlights the influence of properties (surface area, pore size, and heat of adsorption) of azo-linked polymers on their CO_2 separation ability. We demonstrate that the optimization of such variables can lead to remarkable CO_2 capturing properties fort his class of porous organic polymers.

3.3 Experimental Section

3.3.1 Materials and Methods

All chemicals were purchased from commercial suppliers (Acros Organics, Sigma Aldrich, or Frontier Scientific) and used without further purification, unless otherwise noted. N,N,N′,N′,tetrakis(4-aminophenyl)-1,4-phenylenediamine (TAPPA) was purchased from Combi-Blocks. 2,2′,7,7′-Tetraamino-9,9′-spirobifluorene[12] (TASBF), tris(4-aminophenyl)amine[13] (TAPA), and 1,1,2,2-tetrakis(4-aminophenyl)ethene[14] (TAPE) were synthesized according to literature procedures. Solid-state ^{13}C cross-polarization magic angle spinning (CP-MAS) NMR spectra of polymers were taken at Spectral Data Services, Inc. Elemental analyses were performed by Midwest Microlab LLC. Thermogravimetric analysis (TGA) was carried out by a Perkin-Elmer Pyris 1 thermogravimetric analyzer under a nitrogen atmosphere with a heating rate of 10 °C min^{-1}. For Scanning Electron Microscopy (SEM) imaging, the samples were prepared by dispersing each polymer onto the surface of a sticky carbon attached to a flat aluminum sample holder. Then, the samples were coated with platinum at a pressure of 1×10^{-5} mbar in a N_2 atmosphere for 60 seconds before SEM imaging. The images were taken by a Hitachi SU-70 scanning electron microscope. Powder X-ray diffraction patterns were obtained by using a Panalytical X'pert pro multipurpose diffractometer (MPD) with Cu Kα radiation. FT-IR spectra of the samples were obtained by a Nicolet-Nexus 670 spectrometer having an attenuated total reflectance accessory. Low pressure gas sorption measurements were carried out by a Quantachrome Autosorb iQ volumetric analyzer using UHP grade adsorbates. High pressure gas sorption measurements were performed using a VTI HPVA-100 volumetric analyzer. High pressure total gas uptakes were calculated according to literature methods using NIST Thermochemical Properties of Fluid Systems.[15] The samples were degassed at 120 °C under vacuum for 24 hours before gas sorption measurements.

3.3.2 Synthetic Aspects

Synthesis of ALP-5. This polymer was synthesized following a modified procedure described in our recent work.[2] CuBr (25 mg, 0.174 mmol) and pyridine (110 mg, 1.391 mmol) were added to 11 mL toluene. The mixture was stirred at 25 °C for 3 h in an open air atmosphere. The resulting mixture was added to a solution of 2,2′,7,7′-tetraamino-9,9′-spirobifluorene (100 mg, 0.266 mmol) in 11 mL THF. The mixture was stirred in an open air atmosphere at 25 °C for 24 h, at 60 °C for 12 h, and then at 80 °C for 12 h. The resulting brownish solid was isolated by filtration over a medium glass frit funnel and subsequently washed with THF and water. The obtained powder was stirred in HCl (100 mL, 2 M) for 12 h, then filtered and washed with water. The powder was further washed with NaOH (2 M), water, ethanol, THF, and chloroform. Finally, the obtained product was dried at 120 ºC under vacuum (150 mTorr) to give ALP-5 as a brownish fluffy powder (79 mg, 81%). Elemental analysis calcd (%) for $C_{25}H_{12}N_4$: C, 81.51; H, 3.28; N, 15.21. Found (%): C, 74.88; H, 3.86; N, 13.34.

Synthesis of ALP-6. This polymer was synthesized by following the same synthetic method described above for ALP-5 using N,N,N′,N′-tetrakis(4-aminophenyl)-1,4-phenylenediamine (100 mg, 0.212 mmol), CuBr (40 mg, 0.279 mmol), and pyridine (160 mg, 2.023mmol). The final product was obtained as a brown powder which was denoted as ALP-6 (88 mg, 90%). Elemental analysis calcd (%) for $C_{30}H_{20}N_6$: C, 77.57; H, 4.34; N, 18.09. Found (%): C, 69.52; H, 4.18; N, 14.66.

Synthesis of ALP-7. This polymer was prepared following the same method described above for ALP-5 using tris(4-aminophenyl)amine (100 mg, 0.344 mmol), CuBr (40 mg, 0.279 mmol), and pyridine (160 mg, 2.023 mmol). The final product was obtained as a brownish powder, denoted as ALP-7 (85 mg, 87%). Elemental analysis calcd (%) for $C_{18}H_{12}N_4$: C, 76.04; H, 4.25; N, 19.71. Found (%): C, 71.07; H, 4.20; N, 16.46.

Synthesis of ALP-8. This polymer was synthesized following the synthetic method described above for ALP-5 using 1,1,2,2-tetrakis(4-aminophenyl)ethane (100 mg, 0.255 mmol), CuBr (25 mg, 0.174 mmol) and pyridine (110 mg, 1.391 mmol). The final product was obtained as a brown powder, denoted as ALP-8 (77 mg 79%). Elemental analysis calcd (%) for $C_{26}H_{16}N_4$: C, 81.23; H, 4.20; N, 14.57. Found (%): C, 74.36; H, 4.47; N, 12.60.

3.4 Result and Discussion

3.4.1 Synthesis and Characterization of ALPs

The synthesis of ALPs was carried out according to our previously reported procedure via oxidative homocoupling reaction of aniline-like monomers that leads to azo bond formation as depicted in Scheme 1.[2] The monomers used for the synthesis of new ALPs were selected based on the topology-directed approach developed for preparation of POPs using rigid star-shaped monomers.[16] A recent study has shown that the incorporation of tertiaryamines into POPs can result in enhanced CO_2/N_2 selectivities.[17] Therefore, we used tertiaryamine-based monomers for the synthesis of ALP-6 and ALP-7 in an attempt to achieve high selectivity values. It is worth noting that the synthesis of ALP-7 using the same amount of catalyst reported in our recent work[2] resulted in low surface area of 60 m^2 g^{-1} (entry 1 in Table 3.1). This could be attributed to incomplete polymerization caused by low activity of the CuBr-pyridine catalyst due to coordination of the tertiaryamine of the monomer to copper cations. In fact, doubling the amount of catalyst resulted in much higher surface area of 400 m^2 g^{-1} (entry 2 in Table 3.1). Further increase in catalyst amount led to a low surface area of 100 m^2 g^{-1} (entry 3 in Table 3.1). This can be attributed to a fast polymerization rate which results in higher degree of framework interpenetration.[18]

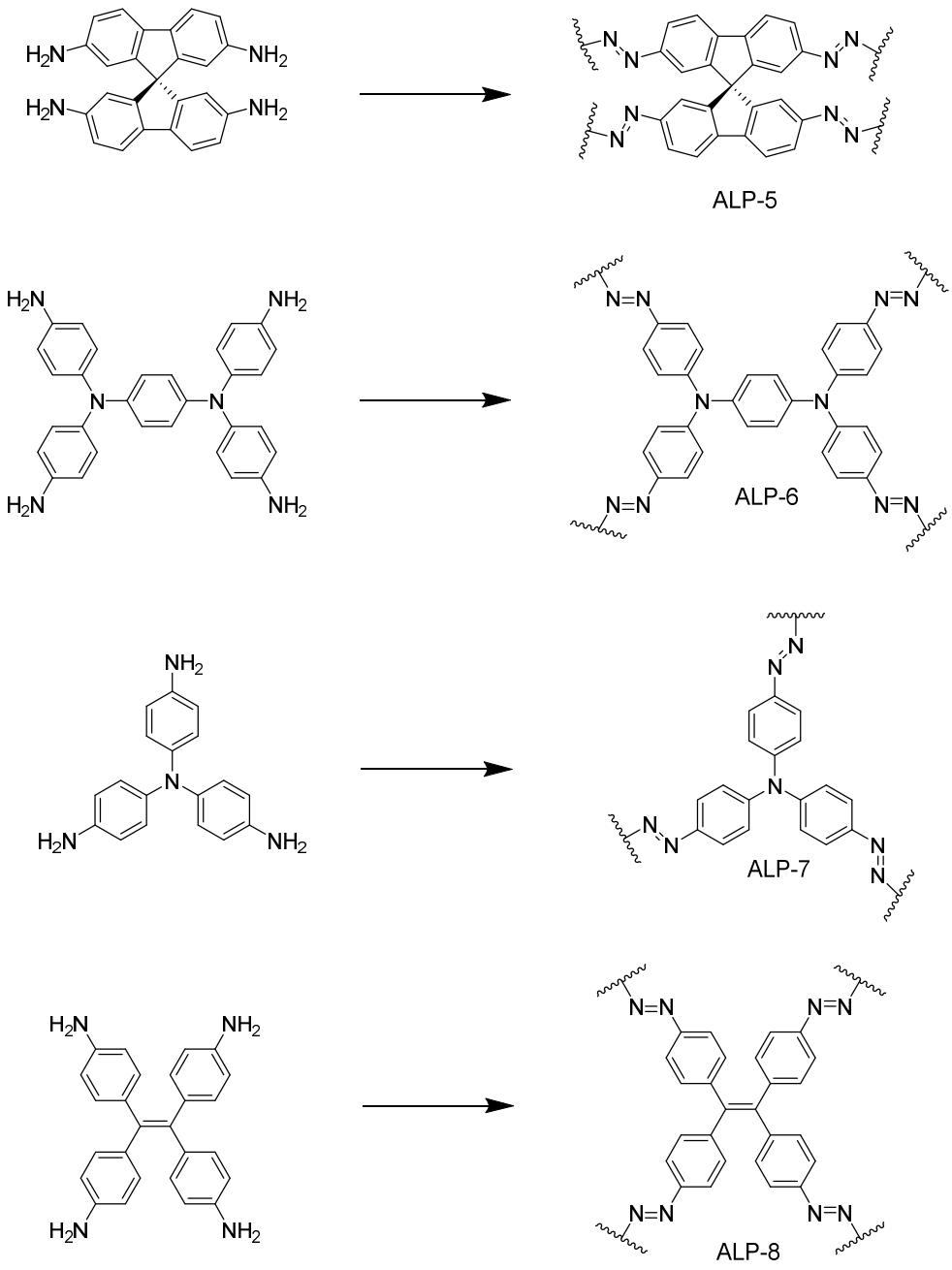

Figure 3.1: Synthesis of azo-linked porous polymers (ALPs). Reaction conditions: CuBr, pyridine, THF/toluene (25-80 °C, 48 h).

Table 3.1: The effect of amount of catalyst on surface area of ALP-7.[a]

Entry	CuBr (mg)	Pyridine (mg)	Surface area (m^2 g^{-1})[b]
1	20	80	60
2	40	160	400
3	80	320	100
4	80	160	390
5	60	160	380
6	60	120	240
7	40	120	370
8	30	80	230

[a]Reaction conditions: monomer (100 mg), THF (11 ml), toluene (11 ml), stirred at 25 °C for 24 h, at 60 °C for 12 h, and at 80 °C for 12 h. [b]BET surface areas were calculated from N_2 adsorption isotherms collected by NOVA (*Quantachrome*).

Since the monomer used for synthesis of ALP-6 contains tertiary amine, the synthesis of ALP-6 was carried out using the synthetic conditions optimized for ALP-7. FTIR studies reveal the successful polymerization of monomers by appearance of characteristic bands for N=N vibrations at 1415-1400 cm^{-1} (Figures 3.2 – 3.5).[2-3] Upon polymerization, the intensity of the band resulting from N-H stretches (3200-3450 cm^{-1}) significantly decreased (Figures 3.2 – 3.5). The residual signals at this region can be attributed to the presence of terminal amines on the surface of ALPs' particles. In addition, ^{13}C CP-MAS NMR spectra of ALPs were collected to confirm the expected structures of ALPs (Figures 3.6 – 3.9).

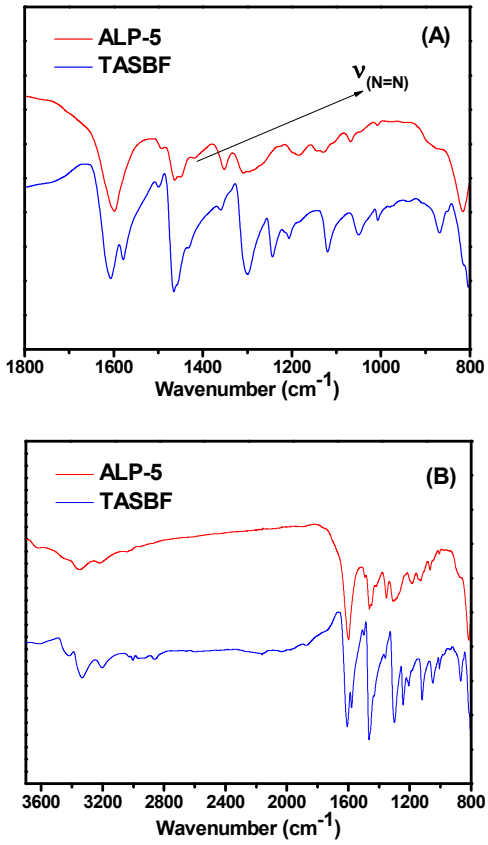

Figure 3.2: FT-IR spectra of ALP-5 and its corresponding monomer (TASBF).

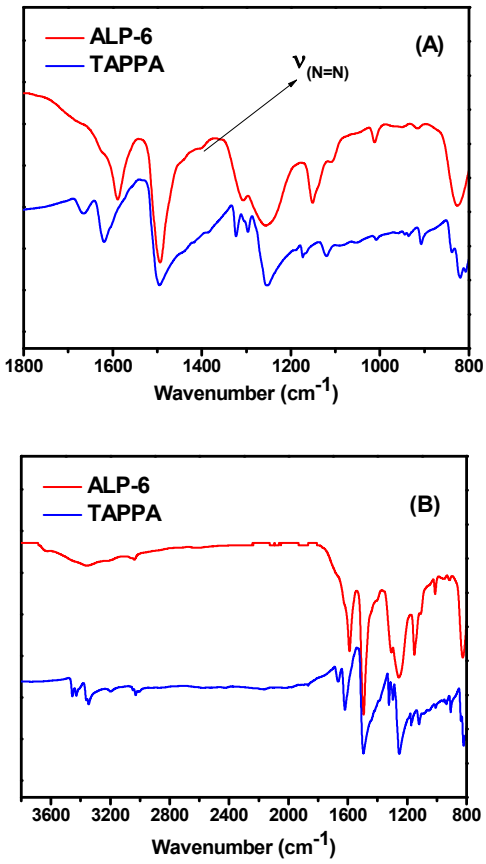

Figure 3.3: FT-IR spectra of ALP-6 and its corresponding monomer (TAPPA).

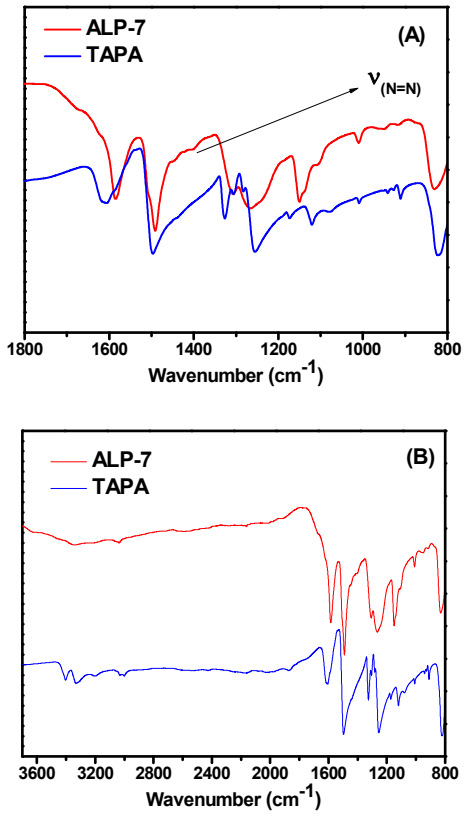

Figure 3.4: FT-IR spectra of ALP-7 and its corresponding monomer (TAPA).

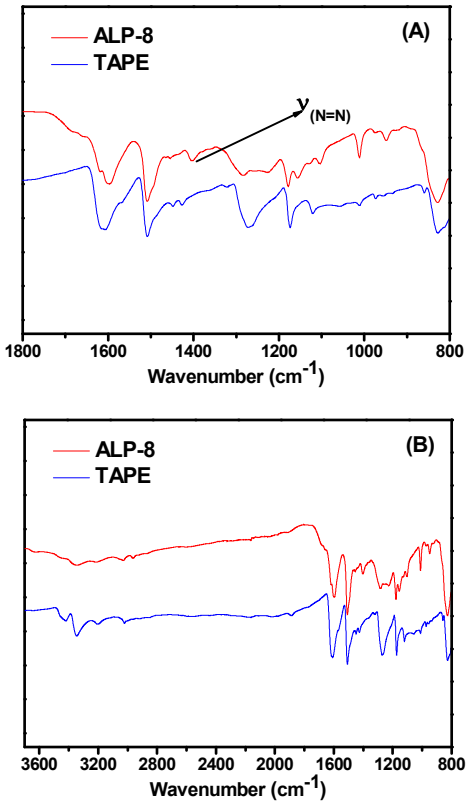

Figure 3.5: FT-IR spectra of ALP-8 and its corresponding monomer (TAPE).

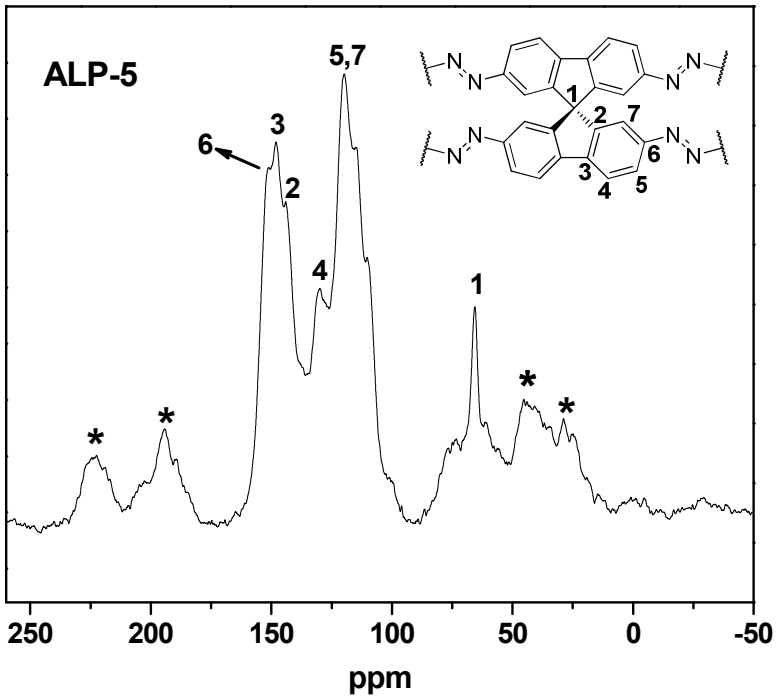

Figure 3.6 Solid state ^{13}C CP-MAS NMR spectrum of ALP-5. Asterisks denote spinning side-bands.

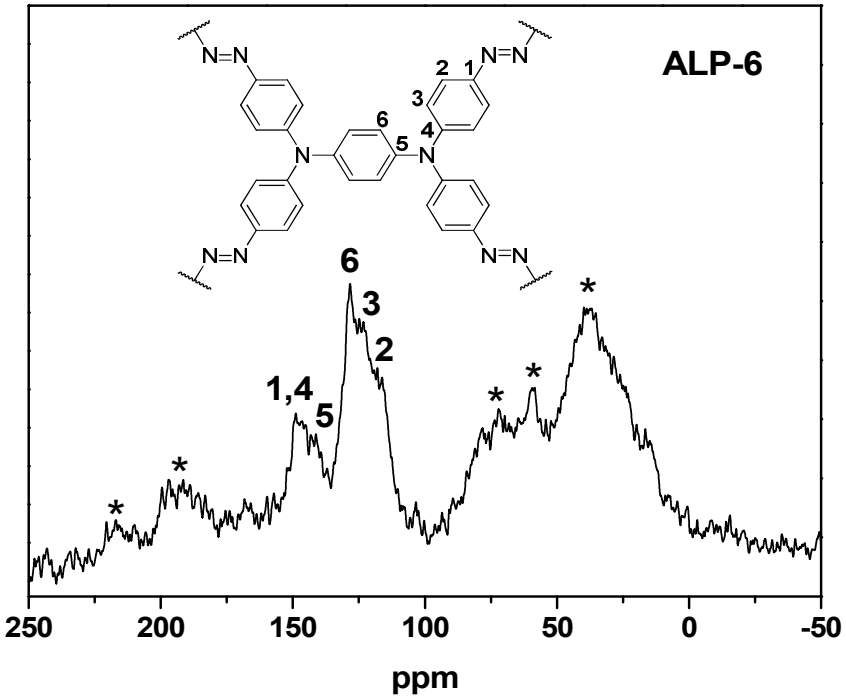

Figure 3.7: Solid state ^{13}C CP-MAS NMR spectrum of ALP-6. Asterisks denote spinning side-bands.

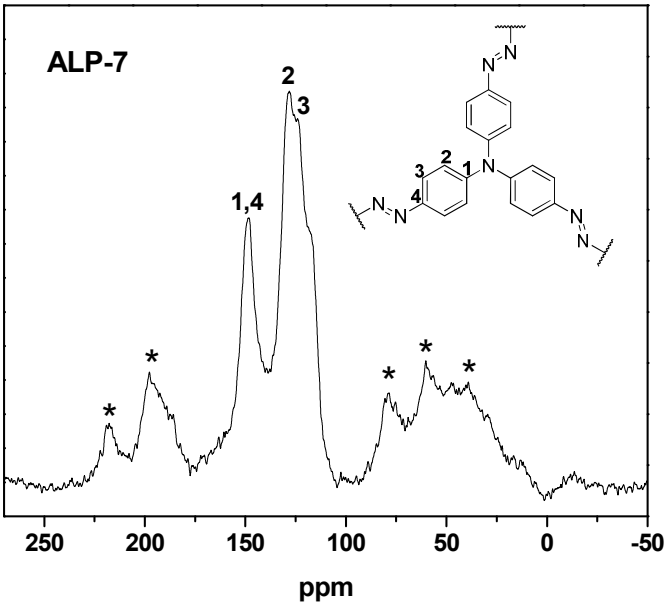

Figure 3.8: Solid state^{13} C CP-MAS NMR spectrum of ALP-7. Asterisks denote spinning side-bands.

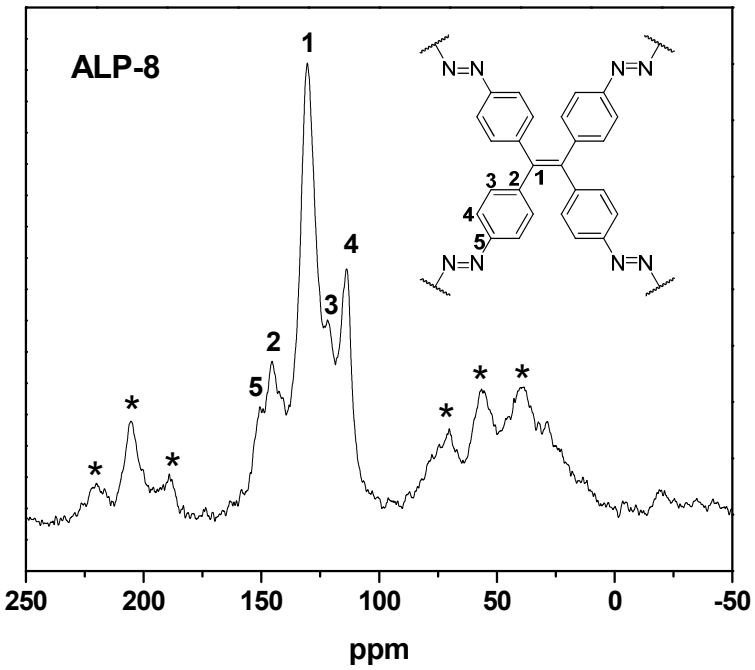

Figure 3.9: Solid state^{13} C CP-MAS NMR spectrum of ALP-8. Asterisks denote spinning side-bands.

All ALPs are insoluble in organic solvents such as DCM, DMF, THF, and DMSO, showing their expected hyper-cross-linked networks.[19] Elemental analysis studies of ALPs show some deviations from expected values for hypothetical networks. These deviations are common for POPs, and are mainly attributed to incomplete polymerization as well as adsorption of moisture during handling.[2, 20] SEM images of ALPs show aggregated spherical particles of variable size (200-800 nm) as shown in Figures 3.10 – 3.13.

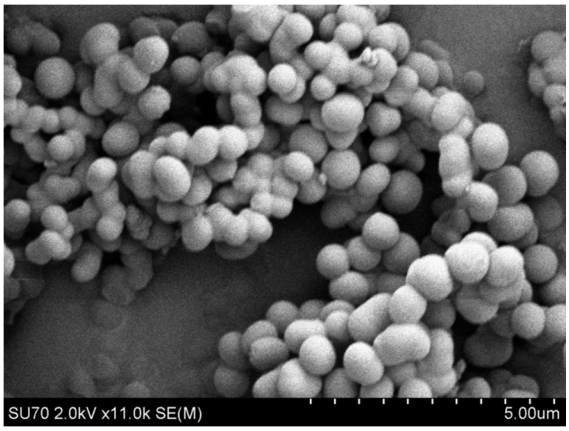

Figure 3.10: SEM image of ALP-5.

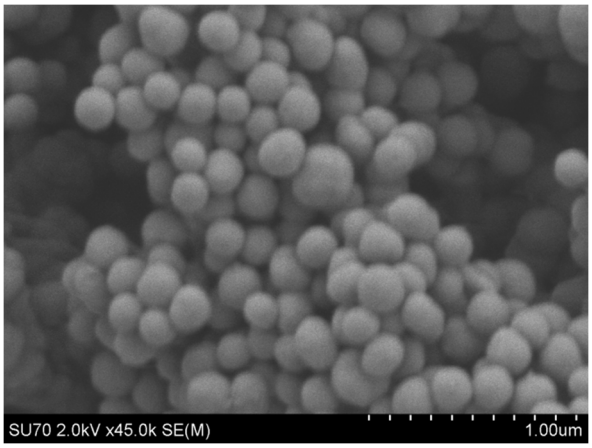

Figure 3.11: SEM image of ALP-6.

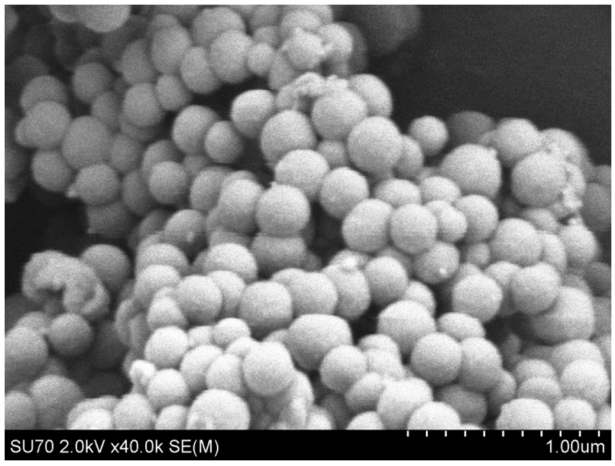

Figure 3.12: SEM image of ALP-7.

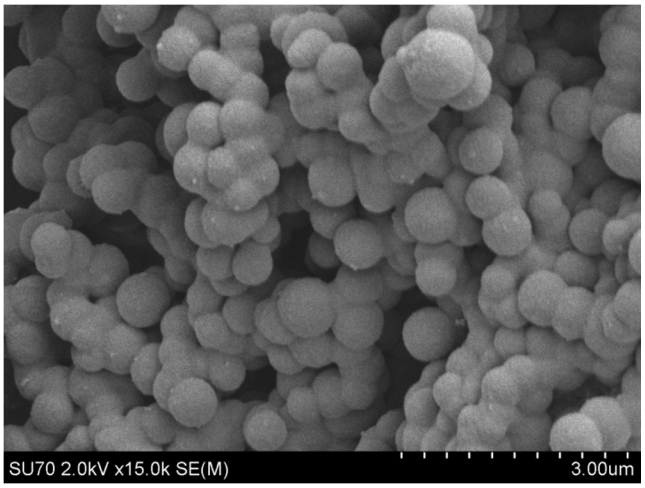

Figure 3.13: SEM image of ALP-8.

The XRD patterns of ALPs are featureless (Figure 3.14), indicating their amorphous structure which is caused by the rapid and irreversible formation of the azo linkage.[21] Thermogravimetric analysis (TGA) shows that ALPs are stable up to ~400 °C under nitrogen while initial weight loss below 100 °C can be attributed to desorption of adsorbed moisture (Figure 3.15). It should also be noted that porous azo-linked polymers have high chemical stability toward water.[3, 5] In order to check the water stability of ALPs, their surface areas were measured after they were stirred in boiling water for 48 h. No noticeable change in surface areas was observed, indicating the high water stability of ALPs. It is noteworthy that ALPs have high chemical stability in acidic (2 M HCl) and basic (2 M NaOH) conditions.

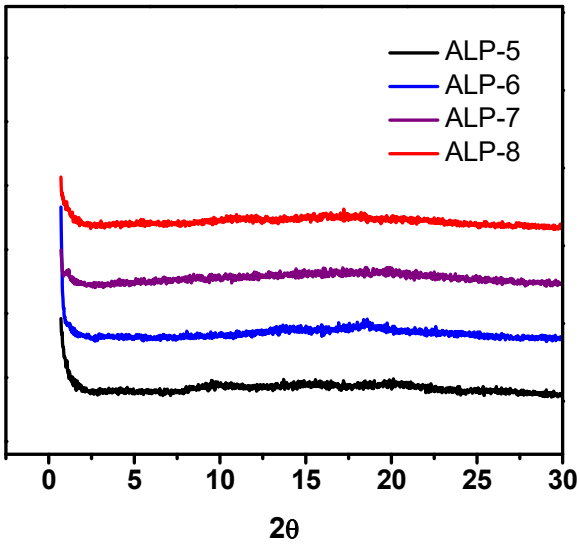

Figure 3.14: PXRD patterns of ALPs.

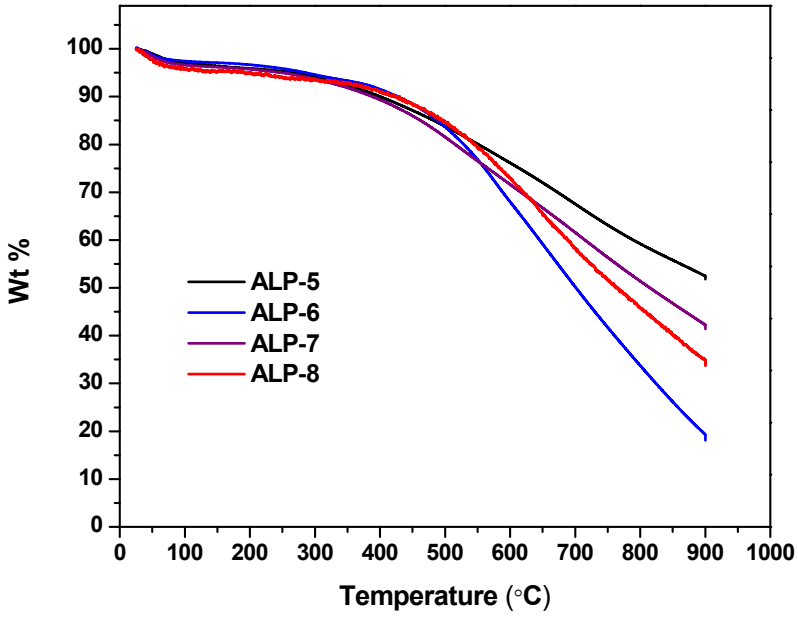

Figure 3.15: TGA traces of ALPs.

3.4.2 Porosity Measurements and CO_2 Uptake Studies

The porosity of ALPs was studied by Ar adsorption isotherms collected at 87 K as shown in Figure 3.16. All Ar adsorption isotherms exhibit a rapid uptake at very low relative pressures of below 0.04 due to the permanent microporosity of the polymers.[22] The gradual increase in Ar uptake at higher relative pressures (0.04-0.9) can be attributed to the presence of a small portion of mesoporosity.[22-23] The specific surface areas of ALPs were calculated from adsorption branch of Ar isotherms using the Brunauer-Emmett-Teller (BET) method and were found to be 801, 698, 412, and 517 $m^2 g^{-1}$ for ALP-5, ALP-6, ALP-7, and ALP-8, respectively (Figure 3.17). The surface area of ALP-5 (801 $m^2 g^{-1}$) is higher than those of azo-COPs (493-729 $m^2 g^{-1}$)[3] and azo-POFs (439-712 $m^2 g^{-1}$)[4] but lower than those of our previously reported ALPs (862-1235 $m^2 g^{-1}$).[2]

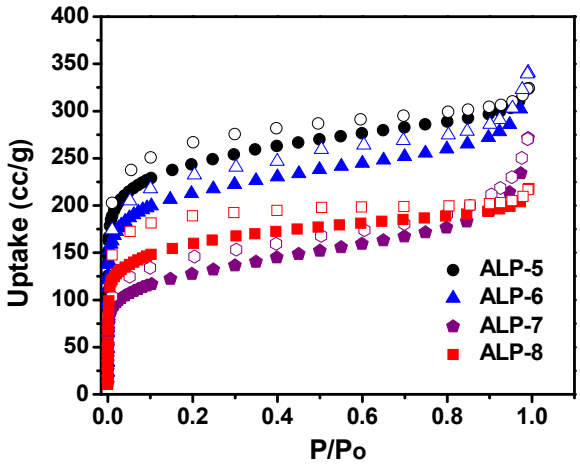

Figure 3.16: Ar uptake isotherms of ALPs collected at 87 K.

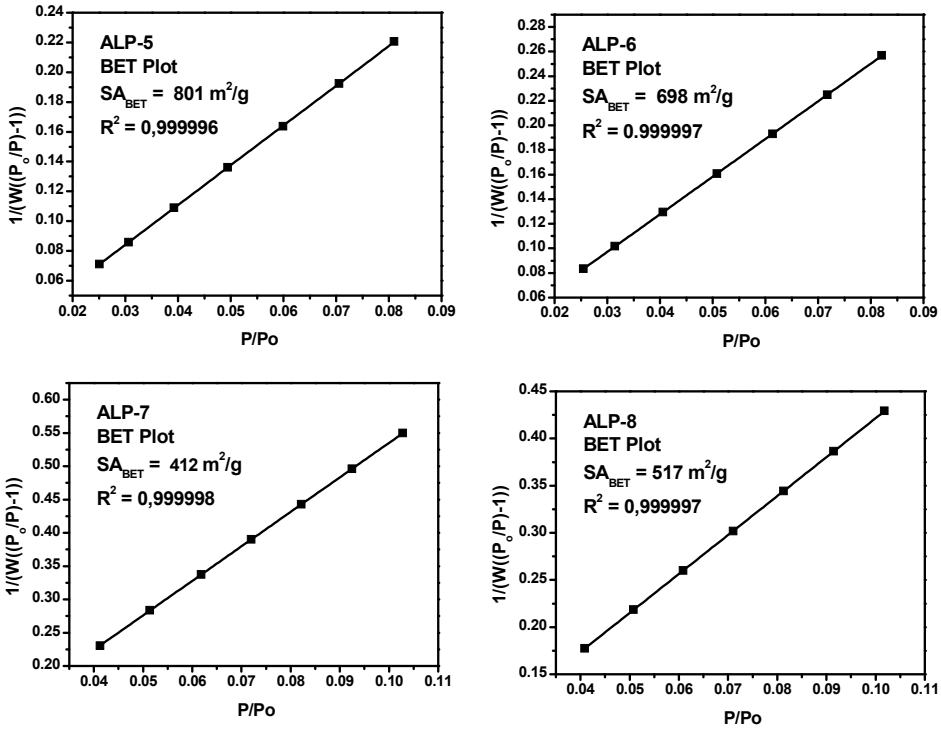

Figure 3.17: BET plots of ALPs.

Pore size distributions (PSD) of ALPs were calculated from Ar adsorption branch using nonlocal density functional theory (NLDFT), and are depicted in Figure 3.18. The overall PSDs of ALPs are similar, showing a major peak centred at around 8-9 Å and broadly distributed pores below 25 Å. The total pore volumes of ALPs were estimated from single point Ar uptake at P/P_o of 0.9 and found to be 0.25−0.39 cm^3g^{-1}. The porosity parameters of ALPs are summarized in Table 3.2.

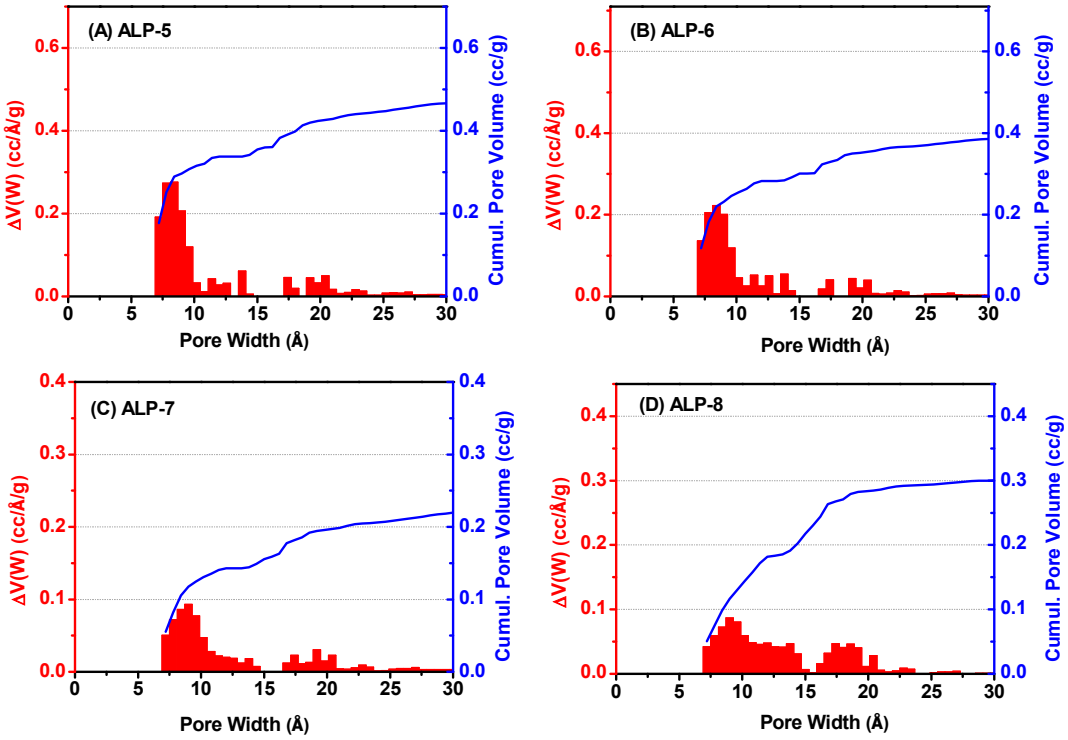

Figure 3.18: Pore size distribution of ALPs calculated from Ar adsorption branch using NLDFT (spherical/cylindrical model).

Table 3.2: Porosity parameters of ALPs.

Polymer	SA_{BET}[a]	Dominant Pore Size[b]	V_{total}[c]
ALP-5	801	0.80	0.39
ALP-6	698	0.85	0.36
ALP-7	412	0.90	0.27
ALP-8	517	0.92	0.25

[a]Surface area ($m^2\ g^{-1}$) calculated from the Ar adsorption branch based on the BET model. [b]Pore size distribution (nm) estimated from the adsorption branch of the Ar isotherm using NLDFT. [c]Total pore volume ($cm^3\ g^{-1}$) calculated from single point Ar uptake at P/P_o= 0.90.

It has been reported that microporous sorbents having pore size below 1.0 nm are very useful for CO_2 capture and separation.[24] In order to study the CO_2 uptake capacity of ALPs, single component CO_2 isotherms were collected at 273 and 298 K (Figure 3.19). The CO_2 isotherms of ALPs are completely reversible and exhibit a steep rise at low pressures as seen in Figure 3.19. While the steep rise at low pressures shows strong dipole-quadrupole integrations between CO_2 and azo groups of ALPs, the reversible nature of CO_2 isotherms indicates that ALPs can be readily regenerated by simply reducing the pressure at ambient temperature. ALP-5 exhibits the highest CO_2 uptake among new ALPs, reaching 4.46 and 2.94 mmol g^{-1} at 273 K and 298 K respectively (Table 3.3). The CO_2 uptake capacity of ALP-5 at 298 K (2.94 mmol g-1) is higher than that of azo-COPs (1.2- 1.5 mmol g^{-1})[3] and azo-POFs (1.2- 1.9 mmol g^{-1})[4] but slightly lower than that of the best performing azo-linked polymer ALP-1 (3.2 mmol g^{-1}).[2]

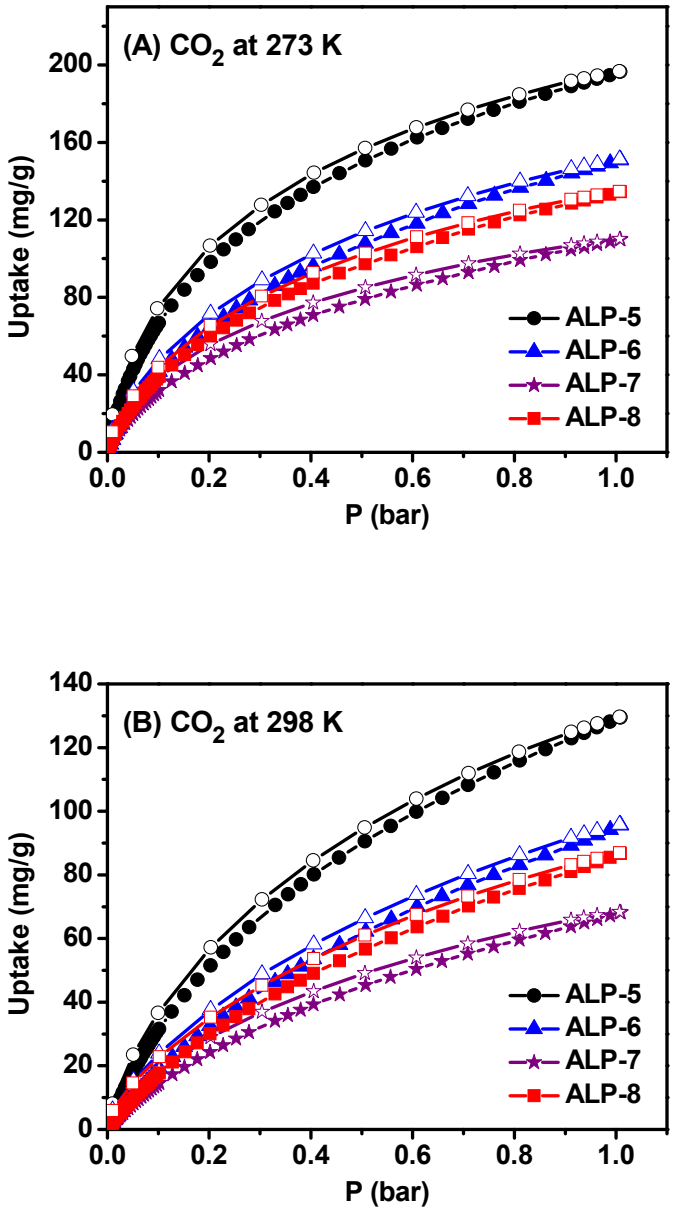

Figure 3. 19: CO_2 uptake isotherms for ALPs at 273 K (A) and 298 K (B).

Table 3.3: Gas uptake, selectivity, and isosteric heat of adsorption for ALPs.

Polymer	Surface Area[a]	CO_2 at 1.0 bar[b]			CH_4 at 1.0 bar[b]			Selectivity[c]	
		273K	298 K	Q_{st}	273 K	298K	Q_{st}	CO_2/N_2	CO_2/CH_4
ALP-1	1235	5.37	3.24	29.2	1.63	0.94	20.8	44 (28)	8 (6)
ALP-5	801	4.46	2.94	32.5	1.44	0.85	22.4	60 (47)	14 (8)
ALP-6	698	3.42	2.17	28.6	1.02	0.60	19.0	45 (48)	10 (7)
ALP-7	412	2.50	1.55	30.7	0.73	0.40	22.2	52 (56)	12 (8)
ALP-8	517	3.05	1.97	29.4	0.91	0.53	20.04	51 (44)	11 (7)

[a]Surface area ($m^2\ g^{-1}$) calculated from the Ar adsorption branch based on the BET model. [b]Gas uptake in mmol g^{-1}, and isosteric heat of adsorption (Q_{st}) at zero coverage in kJ mol^{-1}. [c]Selectivity (mol mol^{-1}, at 1.0 bar) calculated by IAST method at mole ratio of 10:90 for CO_2/N_2, and mole ratio of 50:50 for CO_2/CH_4 at 273 K and (298 K).

The Q_{st} of CO_2 was calculated by the virial method (Figure 3.20) and found to be 28.6-32.5 kJ mol^{-1} at zero coverage (Figures 3.21). Notably, ALP-5 exhibits the highest value (32.5 kJ mol^{-1}) among all previously reported classes of azo-linked porous polymers, including ALPs (27.9-29.6 kJ mol^{-1})[2], azo-POFs (26.2- 27.5 kJ mol^{-1})[4], and azo-COPs (24.8-32.1 kJ mol^{-1})[3]. The higher binding affinity of ALP-5 for CO_2, when compared to other ALPs, can be attributed to its narrower pores (~8 Å), as shown in Table 3.4.[8-9] In general, stronger CO_2-framework interactions can be expected in POPs having narrow pores due to higher number of interactions between the adsorbed CO_2 and pore walls.[8] For the same reason, ALP-5 has the highest Q_{st} for CH_4 when compared to other ALPs (Figure 3.23 and Table 3.4).[25] Moreover, the CO_2 uptake capacity of microporous organic polymers usually increases with surface area.[2, 8, 26] Consequently, the high CO_2 uptake capacity of ALP-5 when compared to other ALPs can be attributed to the combined effects of its narrow pores and high surface area.[27]

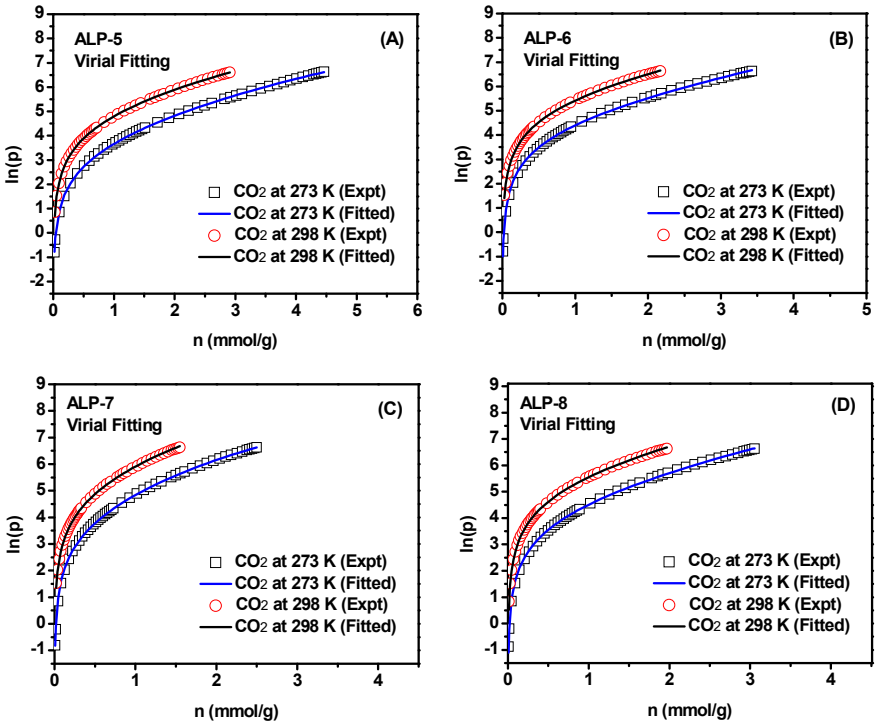

Figure 3.20: Virial fitting for CO_2 isotherms of ALPs.

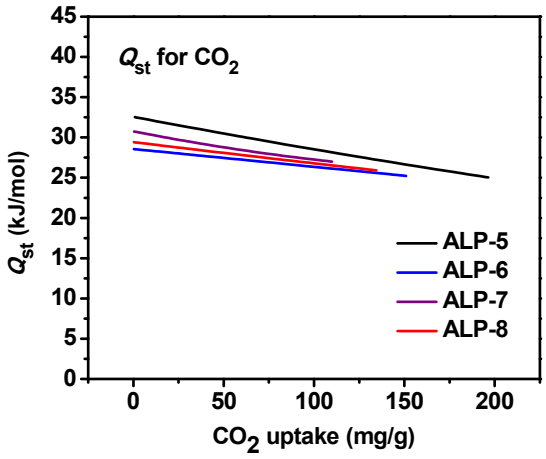

Figure 3.21: Isosteric heat of adsorption (Q_{st}) for CO_2.

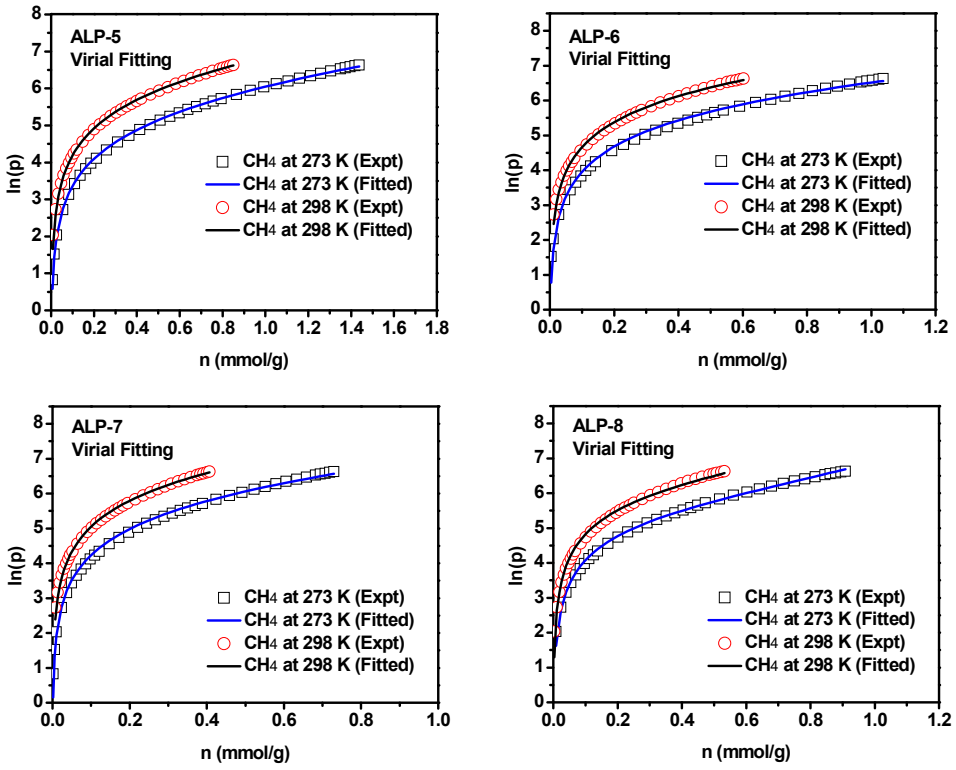

Figure 3.22: Virial fitting for CH_4 isotherms of ALPs.

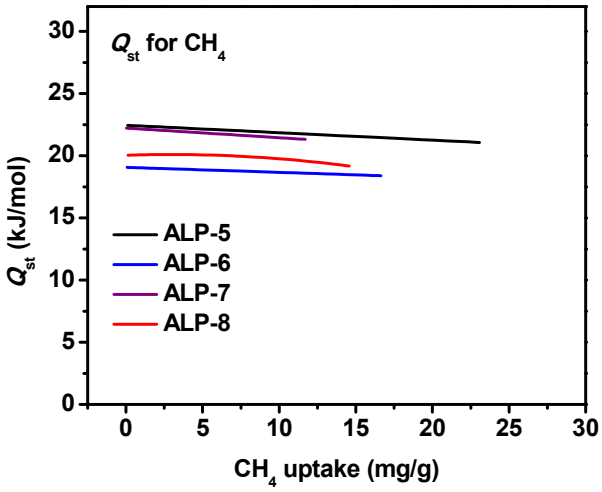

Figure 3.23: Isosteric heat of adsorption (Q_{st}) for CH_4.

Table 3.4: CO_2, CH_4, and N_2 uptakes, and isosteric heats of adsorption (Q_{st}) for ALPs.

Polymer	CO_2 Uptake at 1 bar[a]			CH_4 Uptake at 1 bar[a]			N_2 Uptake at 1 bar[a]		Ref.
	273 K	298 K	Q_{st}[b]	273 K	298 K	Q_{st}[b]	273 K	298 K	
ALP-1	5.4	3.3	29.2	1.6	0.94	20.8	0.41	0.21	2
ALP-2	4.8	2.4	27.9	1.1	0.67	18.5	0.31	0.14	2
ALP-3	3.8	2.3	29.6	1.1	0.60	21.0	0.25	0.12	2
ALP-4	3.5	1.8	28.2	0.89	0.52	21.2	0.24	0.12	2
ALP-5	4.5	2.9	32.5	1.4	0.85	22.4	0.40	0.18	This Work
ALP-6	3.4	2.2	28.6	1.0	0.60	19.0	0.25	0.10	This Work
ALP-7	2.5	1.5	30.7	0.73	0.40	22.2	0.19	0.06	This Work
ALP-8	3.0	2.0	29.4	0.90	0.53	20.0	0.21	0.10	This Work

[a]Uptake in mmol g^{-1}.[b]Isosteric enthalpies of adsorption (Q_{st}) in kJ mol^{-1}at zero coverage.

Despite its high nitrogen content and high Q_{st} for CO_2, ALP-7 exhibits the lowest CO_2 uptake capacity among ALPs due to its lower surface area (Table 3.3).[8, 10] It is important to note that a high CO_2 uptake capacity at 1.0 bar does not necessarily reflect the effectiveness of the sorbent in post-combustion CO_2 capture applications since the partial pressure of CO_2 in flue gas is only ~0.1-0.15 bar.[27-30] Therefore, the CO_2 uptake capacity at low pressure is more relevant for CO_2 separation from the flue gas.[27-29] To provide a better evaluation of the new ALPs for CO_2 separation, we compared their low-pressure CO_2 uptake to that of ALP-1, which has the highest CO_2 uptake at 1 bar among all previously reported azo-linked polymers (Figure 3.24). ALP-5 exhibits CO_2 uptake capacity of 0.95

mmol g^{-1} at 0.15 bar and 298 K, outperforming all other ALPs (Figure 3.24). Interestingly, although the surface area of ALP-5 (801 m^2 g^{-1}) is much lower than that of ALP-1 (1235 m^2 g^{-1}), it adsorbs more CO_2 at low pressure. This can be attributed to the higher Q_{st} value of ALP-5 for CO_2 (Table 3.3).[9] On the other hand, the CO_2 uptake capacity of ALP-5 at 298 K and 1.0 bar (2.94 mmol g^{-1}) is lower than that of ALP-1 (3.2 mmol g^{-1}), which indicates that the effect of surface area on CO_2 uptake capacity becomes more dominant at 1.0 bar.[9] These results show that the effect of Q_{st} on CO_2 uptake at low pressures is more significant than that of surface area; while CO_2 uptake at high pressures correlates more with surface area.[9, 31] The CO_2 uptake capacity of ALP-7 at 0.15 bar is much lower than that of ALP-1 despite its higher Q_{st} for CO_2. This poor performance of ALP-7 for CO_2 uptake arises from its low surface area (412 m^2 g^{-1}).[8, 10] Accordingly, the high CO_2 uptake of ALP-5 at low pressure can be attributed to the combined effects of its high surface area and high Q_{st} for CO_2.[10, 27]

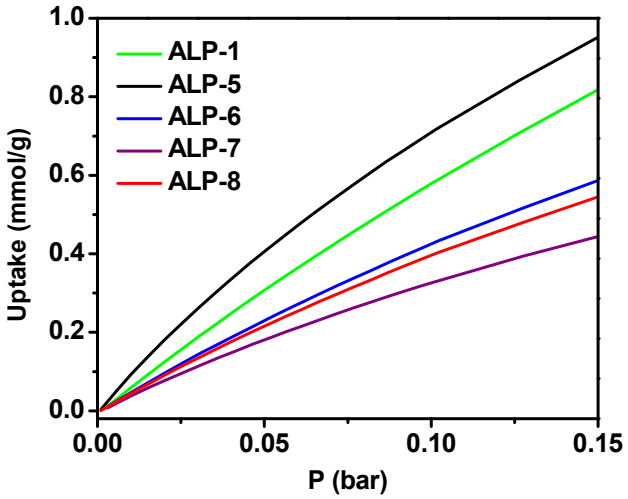

Figure 3.24: Low-pressure CO_2 uptake capacity of ALPs at 298 K.

It should be noted that the unreacted terminal amine groups on the surface of ALPs' particles can contribute to CO_2 adsorption. However, their contributions to CO_2 uptake capacity of ALPs can be considered to be negligible due to the much lower concentration of terminal amines compared to that of azo groups.

3.4.3 Selective CO_2 Capture over N_2 and CH_4

Because of their high Q_{st} for CO_2, narrow pore size, and moderate surface area, we expected high CO_2/N_2 and CO_2/CH_4 selectivity values for the new ALPs. To study the selective carbon dioxide capture over nitrogen and methane, single component CO_2, CH_4 and N_2 isotherms were collected at 273 and 298 K (Figures 3.25 and 3.26). The adsorption behaviour of gas mixtures in porous materials can be predicted from single-component gas isotherms by the ideal adsorbed solution theory (IAST) method that predicts the selectivity values of porous sorbents as a function of the total pressure of gas mixtures.[10] Previous studies have shown that the IAST can provide a good prediction of gas mixtures adsorption behaviour in many zeolites and MOFs.[32] Furthermore, IAST has been widely used to predict CO_2/N_2 and CO_2/CH_4 selectivity of many POPs using gas mixture composition similar to those of flue gas, natural gas, and landfill gas.[33-39] Therefore, we calculated CO_2/N_2 and CO_2/CH_4 selectivities for flue gas (CO_2:N_2 = 10:90) and landfill gas (CO_2:CH_4 = 50:50). For IAST studies, the pure component CO_2 isotherms were fitted with the dual-site Langmuir (DSL) model. On the other hand, pure component isotherms of CH_4 and N_2 were fitted with the single-site Langmuir (SSL) model. Experimental data and corresponding fittings of gas isotherms for ALPs are summarized in Figures 3.27 – 3.30.

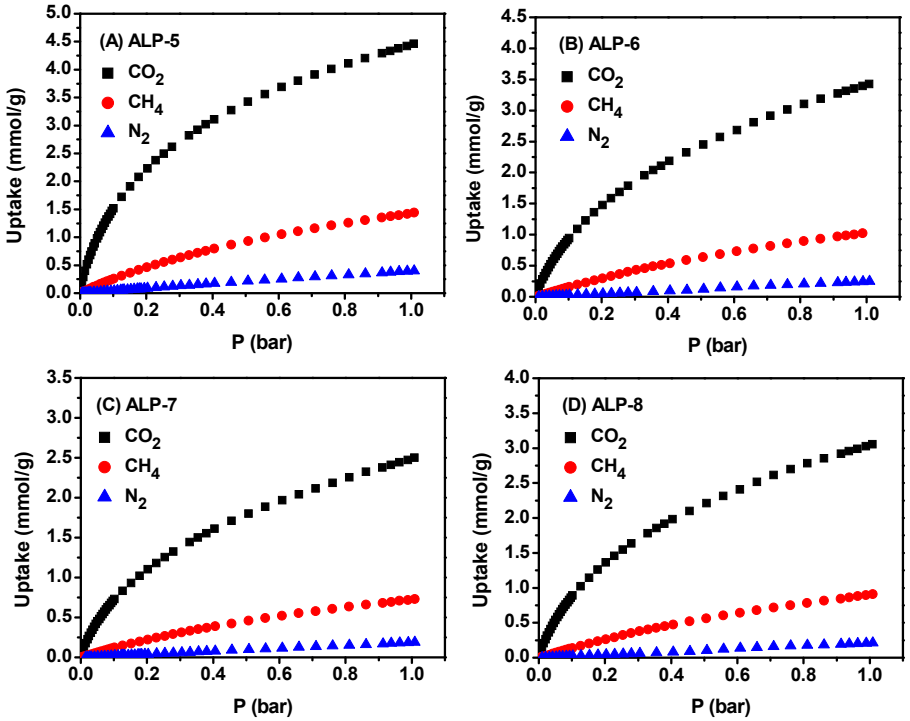

Figure 3.25: CO_2, CH_4, and N_2 adsorption isotherms of ALPs at 273 K.

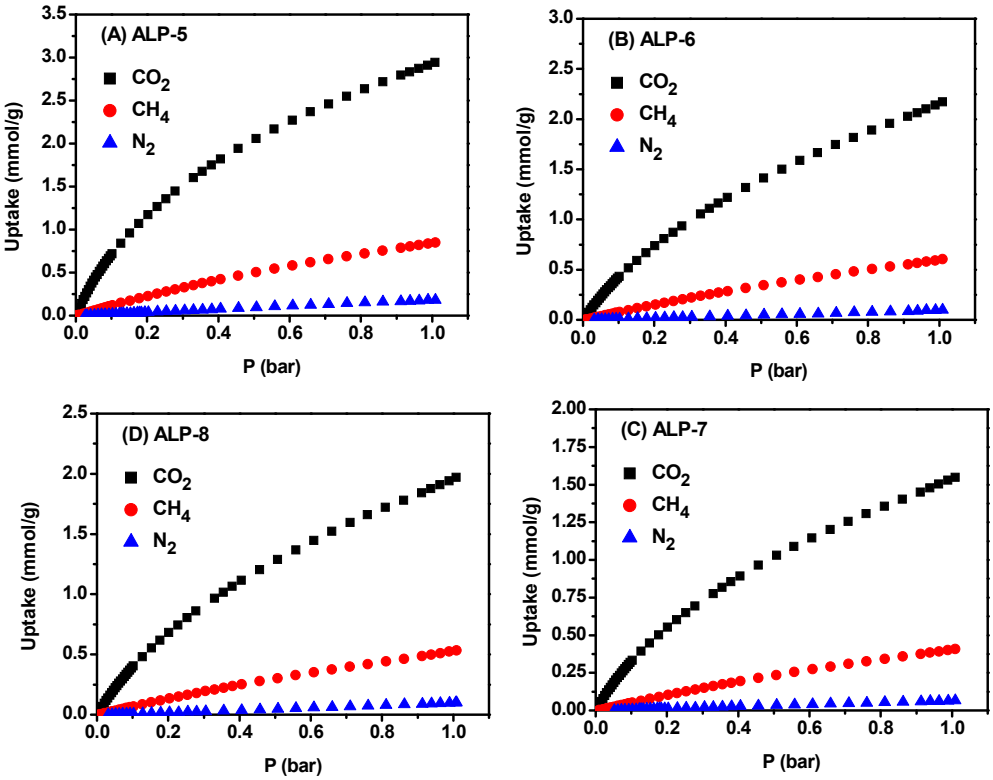

Figure 3.26: CO_2, CH_4, and N_2 adsorption isotherms of ALPs at 298 K.

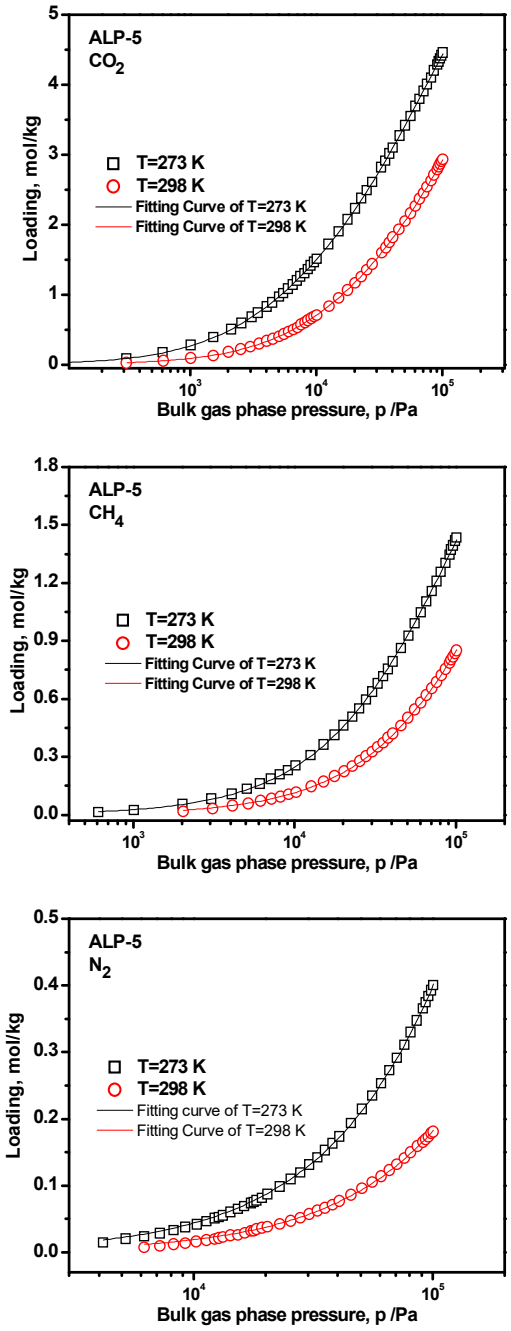

Figure 3.27: Experimental data and corresponding fittings of gas isotherms for ALP-5. (Dual site Langmuir-Freundlich for CO_2, and single site Langmuir-Freundlich for CH_4 and N_2 with temperature dependent parameter at 273 and 298 K).

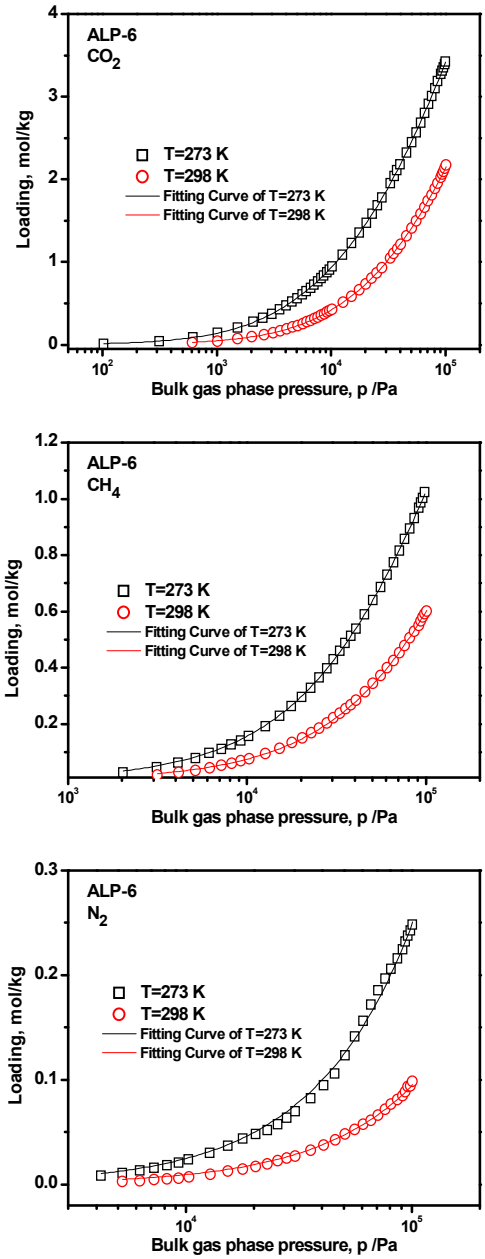

Figure 3.28: Experimental data and corresponding fittings of gas isotherms for ALP-6. (Dual site Langmuir-Freundlich for CO_2, and single site Langmuir-Freundlich for CH_4 and N_2 with temperature dependent parameter at 273 and 298 K).

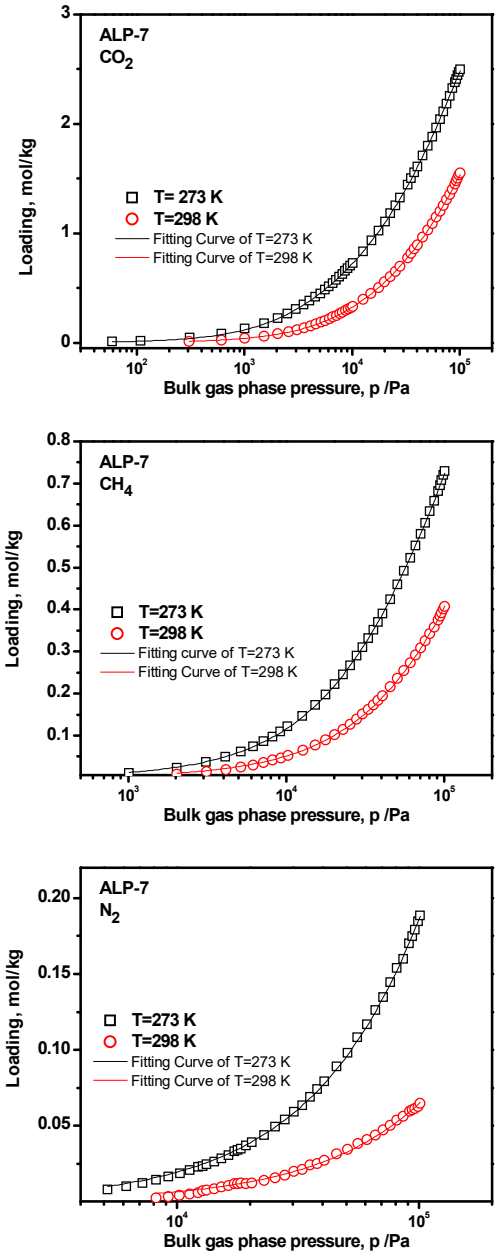

Figure 3.29: Experimental data and corresponding fittings of gas isotherms for ALP-7. (Dual site Langmuir-Freundlich for CO_2, and single site Langmuir-Freundlich for CH_4 and N_2 with temperature dependent parameter at 273 and 298 K).

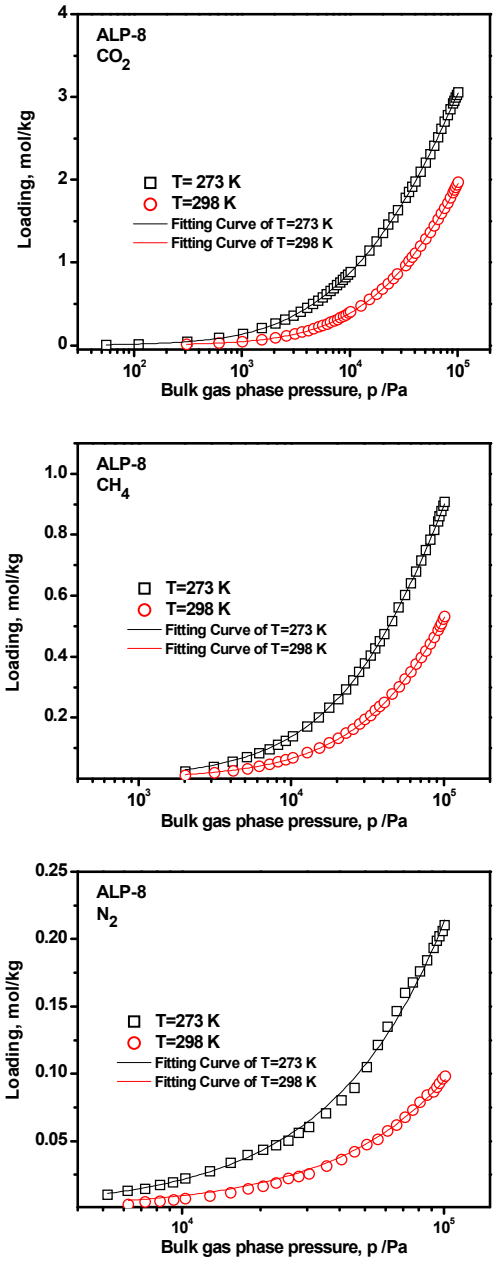

Figure 3.30: Experimental data and corresponding fittings of gas isotherms for ALP-8. (Dual site Langmuir-Freundlich for CO_2, and single site Langmuir-Freundlich for CH_4 and N_2 with temperature dependent parameter at 273 and 298 K).

The IAST selectivities of new ALPs are summarized in Figure 3.31 and Table 3.3. As seen in Table 3.3, all new ALPs have higher CO_2/N_2 and CO_2/CH_4 selectivity values than ALP-1, which has the highest surface area and CO_2 uptake capacity among all classes of azo-linked POPs. This can be due to their lower surface area and narrower pores which result in lower N_2 uptake compared to ALP-1.[2, 27] At 298 K, the CO_2/N_2 selectivities of new ALPs (44-56) reach higher values than those of azo-POFs (37-42)[4] and are comparable to those of BILPs (31-57)[26] and functionalized NPOFs (38-59)[40].

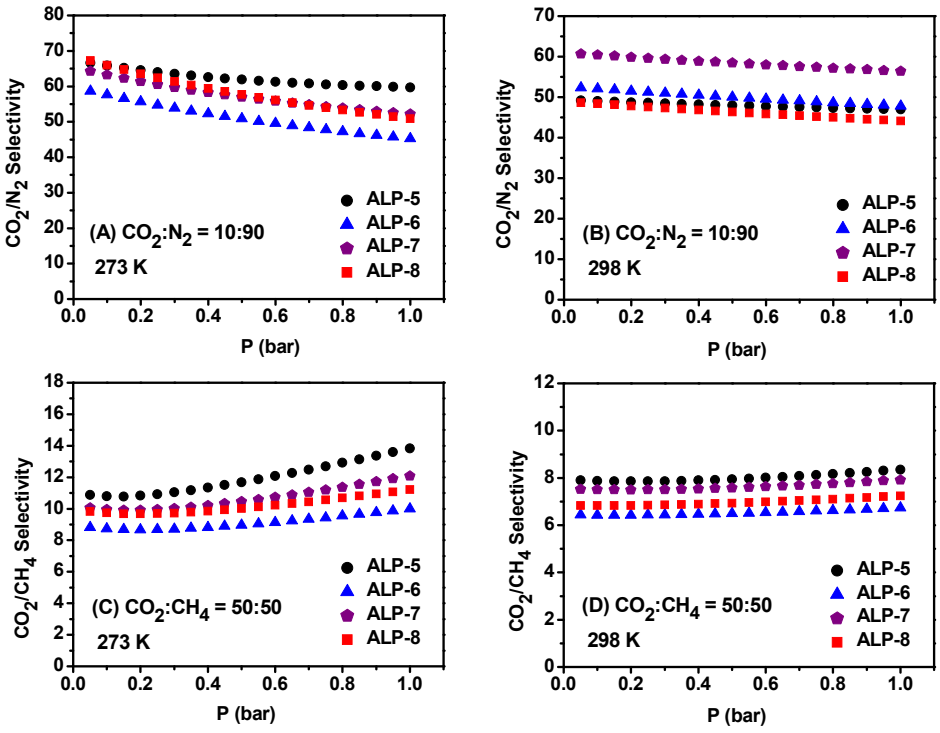

Figure 3.31: IAST CO_2/N_2 selectivity of ALPs for CO_2:N_2 molar ratio of 10:90 at 273 K (A) and 298 K (B), and IAST CO_2/CH_4 selectivity of ALPs for CO_2:CH_4 molar ratio of 50:50 at 273 K (C) and 298 K (D).

At 273 K, ALP-5 shows the highest CO_2/N_2 and CO_2/CH_4 selectivities among all ALPs (Table 3.3). This can be attributed to its high Q_{st} for CO_2 which leads to high CO_2 uptake at low pressures. In general, porous polymers with high Q_{st} for CO_2 show higher CO_2 uptake capacity and selectivity.[8] ALP-7 shows high CO_2/N_2 selectivity of 56 at 298 K, outperforming all other ALPs. This originates from the low surface area of ALP-7 which leads to very low N_2 uptake at 298 K.[8] These results are consistent with our previous findings that the structural characteristics (e.g. pore size, surface area, and pore volume) of azo-linked porous polymers play important roles in their performance in selective CO_2 capture.[2, 4] The higher porosity levels in POPs leads to enhanced CO_2 uptake capacities while the CO_2/N_2 selectivity values decrease with increasing surface area.[2] Generally, there is a trade-off between CO_2 uptake capacity and CO_2/N_2 selectivity, that is, porous materials having high CO_2 uptake capacity exhibit lower selectivity values than those with low CO_2 uptake capacity although this trend is not always followed by all materials.[8] It should also be mentioned that the nitrogen content of ALP-7 (16.46 wt %) is higher than that of other ALPs (9.51-14.66 wt%) which can be another factor playing role in high CO_2/N_2 selectivity of ALP-7 at 298 K. Due to dipole-quadrupole interactions between CO_2 and nitrogen atoms, nitrogen-rich POPs generally exhibit high CO_2/N_2 selectivity values.[41] The CO_2/N_2 selectivities of new ALPs (44-56 at 298 K) are lower than those of azo-COPs (96-131, 298 K)[3] due to larger size of the pores in ALPs.[2] It is worth noting that azo-COP-2 which has the smallest pore size (~0.5 nm) among azo-COPs, outperforms other azo-COPs in CO_2/N_2 selectivity.[3] Moreover, the high CO_2/N_2 of azo-COPs[3, 5] at 298 K has been explained by the new concept of nitrogen-phobicity,[3, 42-43] which is the enhancement in CO_2/N_2 selectivity values upon rise in adsorption temperature. While azo-COPs[3] show enhanced CO_2/N_2 selectivities at higher adsorption temperatures, the selectivities of ALPs decrease or remain almost constant upon the rise in the temperature (Table 3.5).

Table 3.5: IAST selectivity of different classes of azo-linked porous polymers.

Polymer	CO_2/N_2 selectivity at 1 bar		Reference
	273 K	298 K	
ALP-1[a]	40	28	[2]
ALP-2[a]	34	26	[2]
ALP-3[a]	44	35	[2]
ALP-4[a]	35	26	[2]
ALP-5[b]	60	47	This Work
ALP-6[b]	45	48	This Work
ALP-7[b]	52	56	This Work
ALP-8[b]	51	44	This Work
azo-COP-1[a]	64	97	[3]
azo-COP-2[a]	110	131	[3]
azo-COP-3[a]	79	96	[3]
azo-POF-1[a]	52	37	[4]
azo-POF-2[a]	55	42	[4]

[a]For CO_2:N_2 mole ratio of 15:85. [b]For CO_2:N_2 mole ratio of 10:90.

This inconsistency can be attributed to the differences in porosity parameters of ALPs and azo-COPs. In fact, we and others have recently shown that the nitrogen-phobicity of porous polymers can be due to the physical nature of the pores rather than their chemical nature.[2, 42-43] Several studies have shown that porous polymers having the same functional groups but different porosity parameters can exhibit different behaviors in terms of N_2-phobicity.[2, 42-43] Very recently, Choi *et al.* have shown that the N_2-phobicity in porous polymers can be due to the relatively large portion of mesoporosity in polymers.[43] Their results suggest that the N_2 uptake capacity of materials having larger mesopore portions decrease significantly upon the rise in adsorption temperature.[43]

This leads to enhanced CO_2/N_2 selectivity values at higher temperatures.[43] Their findings can explain the different behavior of ALPs and azo-COPs[3] in terms of the change in CO_2/N_2 selectivities with adsorption temperature. As evidenced by their N_2 isotherms at 77 K, azo-COPs[3] have relatively large portion of mesopores while ALPs have lower degree of mesoporosity, as can be concluded from their Ar isotherms by their gradual increase in Ar uptake at P/P_o = 0.04-0.90. Very recently, Lu and Zhang have reported on the synthesis of azo-POFs via Zn-induced reductive homocoupling of aromatic nitro monomers and studied their performance in selective CO_2 capture.[4] Similar to ALPs, azo-POFs[4] exhibit lowered CO_2/N_2 selectivities upon rise in adsorption temperature, confirming the role of porosity parameters on N_2-phobicity behavior (Table 3.5). The surface area of azo-POFs (440-710 $m^2\ g^{-1}$)[4] are much lower than that of ALP-1 (1240 $m^2\ g^{-1}$)[2]; and therefore, azo-POFs have much lower CO_2 uptake capacities (1.2- 1.9 mmol g^{-1}, 298 K and 1 bar) than ALP-1 (3.2 mmol g^{-1}, 298 K and 1 bar). As expected, azo-POFs show higher CO_2/N_2 selectivity (37-42, 298 K)[4] values than ALP-1 (28, 298 K), further supporting our finding that CO_2/N_2 selectivity of azo-linked porous polymers depends on the structural characteristics of this class of materials.[2] The IAST CO_2/CH_4 selectivity of new ALPs was found to be 11-14 at 273 K which decreases to 7-8 at 298 K. ALP-5 shows the highest CO_2/CH_4 selectivity values among all ALPs during the entire loading (Figure 3.31), due to its high Q_{st} for CO_2. The CO_2/CH_4 selectivities of ALPs are much lower than CO_2/N_2 selectivity values. This is due to higher CH_4 uptakes of ALPs compared to their N_2 uptakes, which originates from the higher polarizability of CH_4 (26×10^{-25} cm^3) than that of N_2 (17.6×10^{-25} cm^3).[44] We also calculated the selectivities of ALPs by initial slope method using the ratios of Henry's law constants (Figures 3.32 – 3.35). Consistent with IAST studies, all new ALPs show higher initial slope CO_2/N_2 selectivity values than ALP-1 (Table 3.6). This can attributed to lower surface areas and narrower pores of new ALPs.[8]

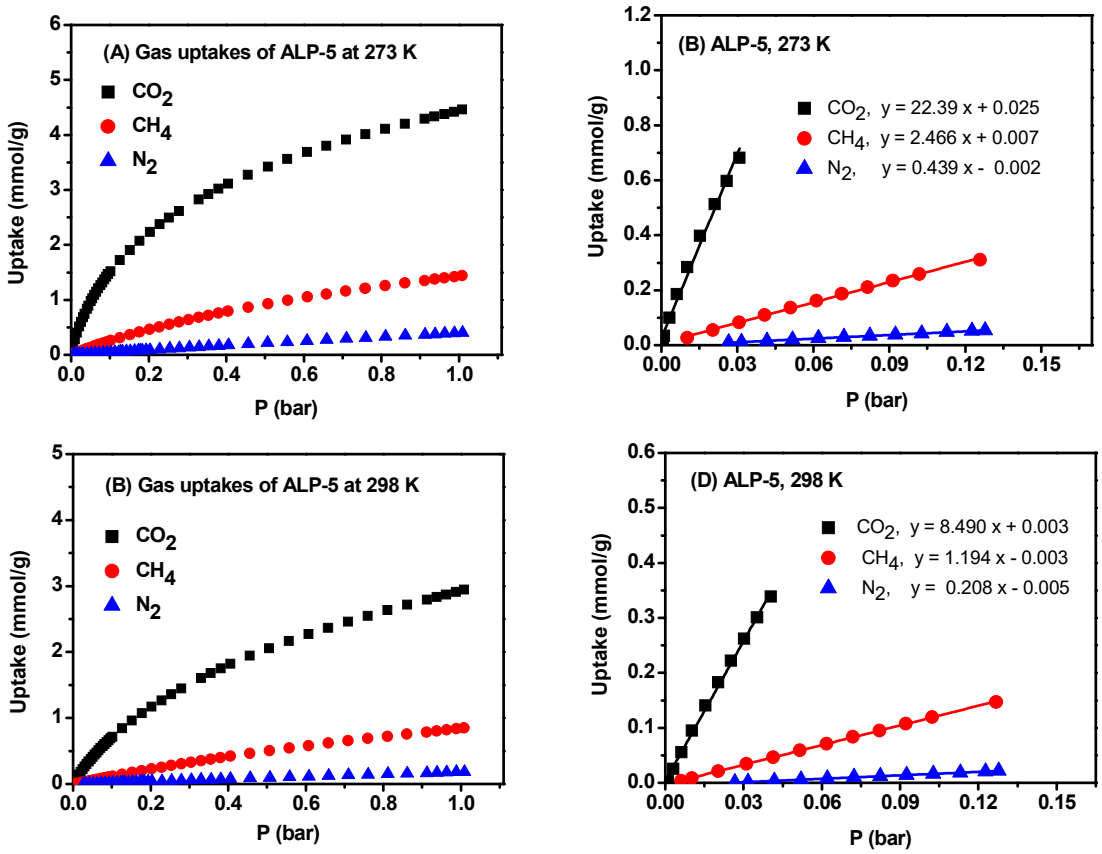

Figure 3.32: Gas uptakes and initial slope selectivity studies of ALP-5.

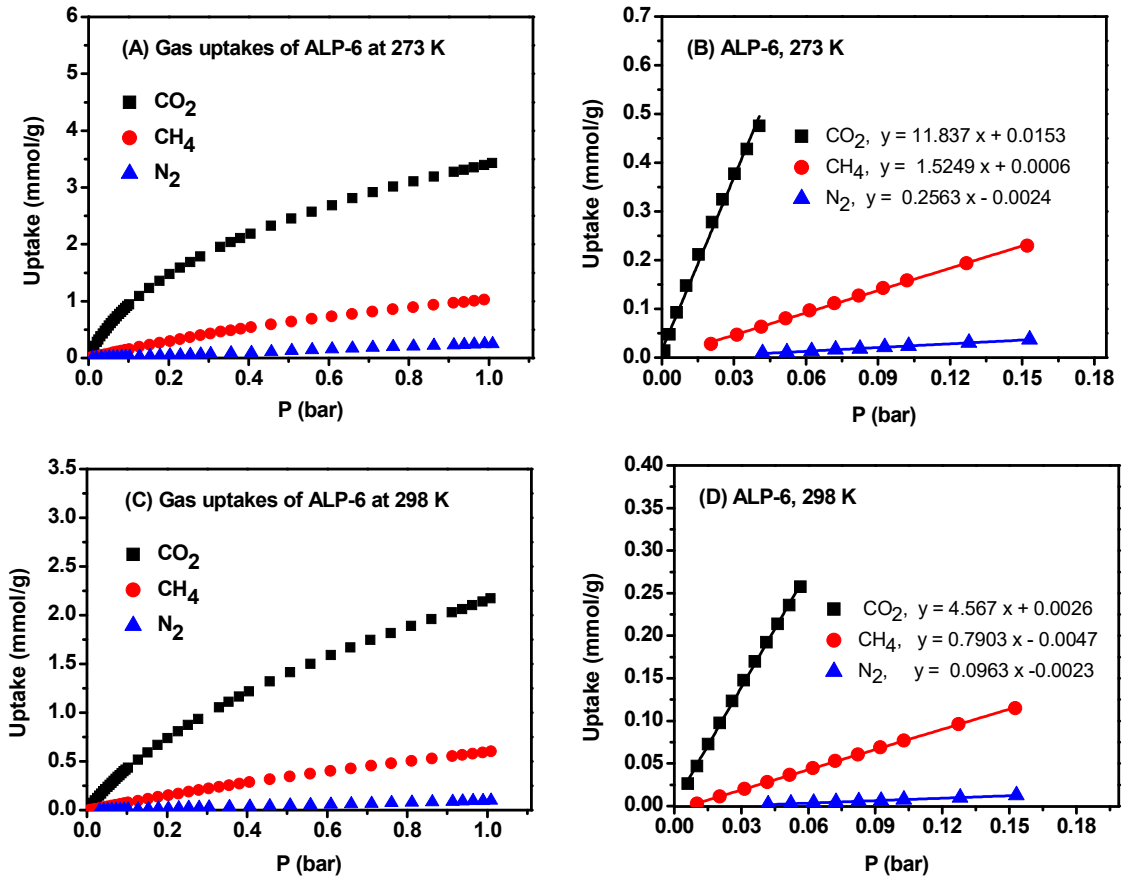

Figure 3.33: Gas uptakes and initial slope selectivity studies of ALP-6.

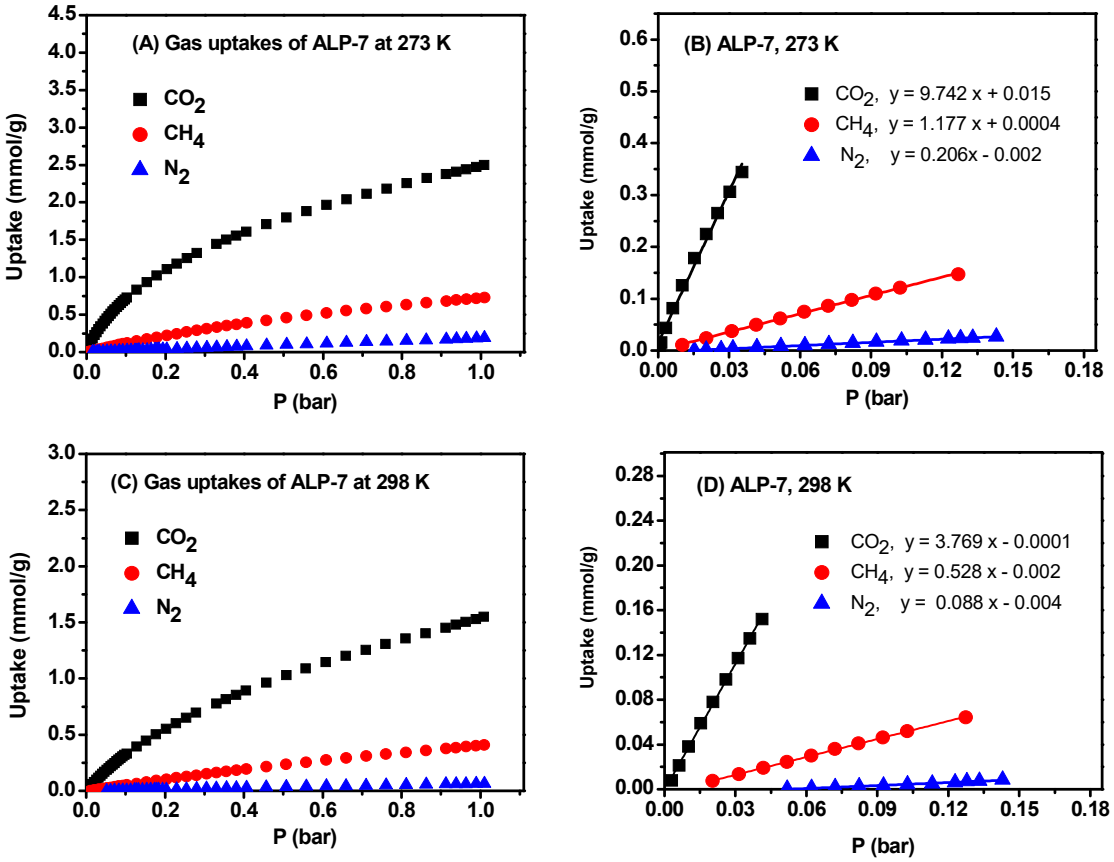

Figure 3.34: Gas uptakes and initial slope selectivity studies of ALP-7.

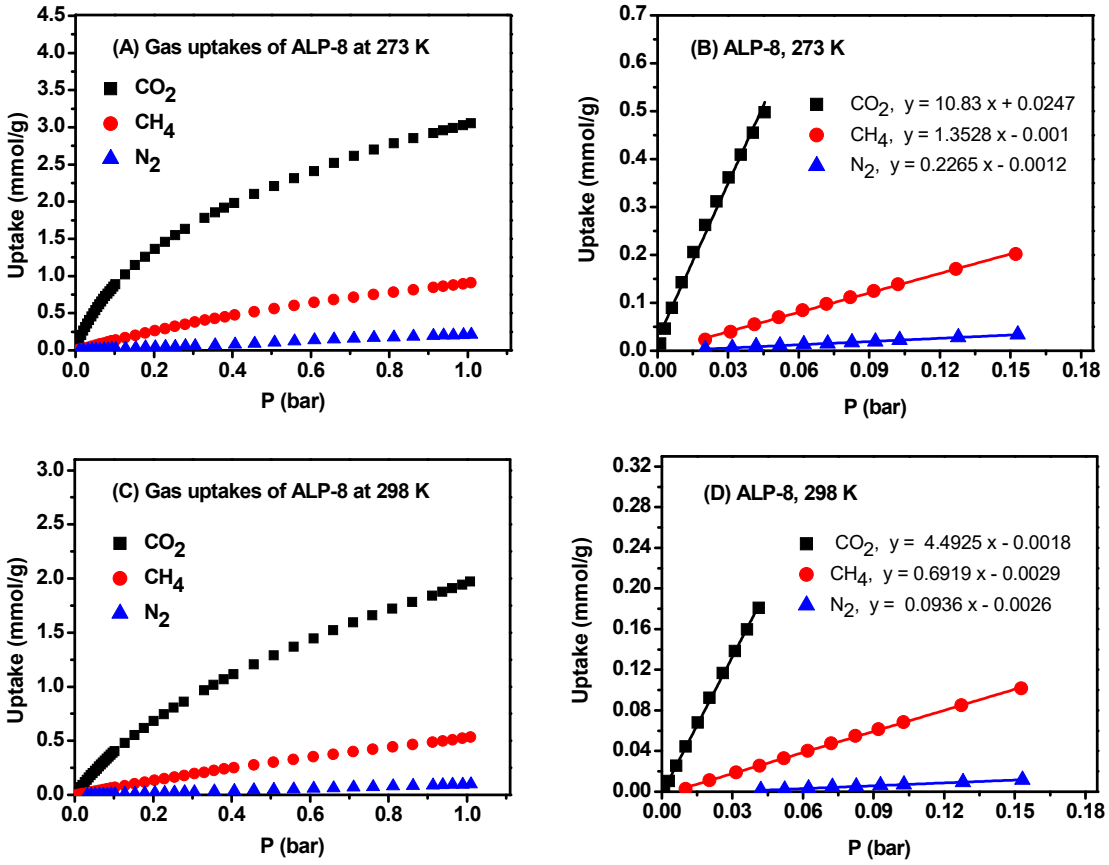

Figure 3.35: Gas uptakes and initial slope selectivity studies of ALP-8.

Table 3.6: Initial slope selectivity of ALPs.

Polymer	CO_2/N_2 Selectivity[a]		CO_2/CH_4 Selectivity[a]		Reference
	273 K	298 K	273 K	298 K	
ALP-1	35	27	6	5	[2]
ALP-5	51	41	9	**7**	This Work
ALP-6	46	47	8	6	This Work
ALP-7	47	43	8	7	This Work
ALP-8	48	48	8	6	This Work

[a](mol mol^{-1}).

3.4.4 Evaluation of ALPs for PSA and VSA Processes

For comprehensive evaluation of porous adsorbents for VSA and PSA processes, five criteria have been recently developed by Bae and Snurr,[10] which are defined in the following and summarized in Table 3.7. *CO_2 uptake under adsorption conditions* (N_1^{ads}) is defined as the CO_2 uptake capacity of the sorbent when the partial pressure of CO_2 in a binary gas mixture is taken into account. *Working CO_2 capacity (ΔN_1)*, defined as $\Delta N_1 = N_1^{ads} - N_1^{des}$, shows the difference between CO_2 uptake capacity at the adsorption pressure (N_1^{ads}) and the desorption pressure (N_1^{des}) when the partial pressure of CO_2 in a binary gas mixture is considered. *Regenerability (R),* which is defined as $R = (\Delta N_1/N_1^{ads}) \times 100$ %, shows the percentage of adsorption sites that can be regenerated upon lowering the pressure during the desorption step. S*electivity under adsorption conditions* (α_{12}^{ads}) is defined as $(\alpha_{12}^{ads}) = (N_1^{ads}/N_2^{ads}) \times (y_2/y_1)$, where N ^{ads} and y are the adsorbed amount and the mole fraction of each component in a binary gas mixture respectively, subscripts 1 and 2 indicate the strongly adsorbed component (CO_2) and the weakly adsorbed component (CH_4 or N_2) respectively. *Sorbent selection parameter (S)* is defined as $S = (\alpha_{12}^{ads})^2/(\alpha_{12}^{des}) \times (\Delta N_1/\Delta N_2)$

where superscripts ads and des represent the adsorption and desorption conditions, respectively. The *S* value combines the selectivity values at adsorption and desorption pressures with working capacity of both components of the gas mixture. It is noteworthy that none of these criteria are perfect, but they are complementary; and therefore, these criteria must be considered together for a comprehensive evaluation of sorbents.[10] These criteria reflect the performance of sorbents under equilibrium conditions and do not take into account the kinetics of adsorption and desorption processes. The experimental setup for measurement of gas mixture adsorption is complicated; and therefore, to calculate the evaluation criteria, IAST is usually used to predict the behaviour of a binary gas mixture from single-component isotherms.[10] As such, we used IAST to assess the performance of ALPs for CO_2 separation from flue gas and landfill gas by VSA and PSA. The evaluation criteria of ALPs were calculated from CO_2, CH_4, and N_2 adsorption isotherms collected at 298 K (Figures 3.24 and 3.36).

Table 3.7: Adsorbent evaluation criteria[a].

CO_2 uptake under adsorption conditions (mol kg^{-1})	$\boldsymbol{N_1^{ads}}$
Working CO_2 capacity (mol kg^{-1}), N_1^{ads} - N_1^{des}	$\boldsymbol{\Delta N_1}$
Regenerability (%), $(\Delta N_1/N_1^{ads}) \times 100$ %	**R**
Selectivity under adsorption conditions, $(N_1^{ads}/N_2^{ads}) \times (y_2/y_1)$	$\boldsymbol{\alpha_{12}^{ads}}$
Sorbent selection parameter, $(\alpha_{12}^{ads})^2/(\alpha_{12}^{des}) \times (\Delta N_1/\Delta N_2)$	***S***

[a]N: adsorbed amount. y: mole fraction in gas mixture. Subscripts 1 and 2 indicate the strongly adsorbed component (CO_2) and the weakly adsorbed component (CH_4 or N_2), respectively. Superscripts "ads" and "des" refer to adsorption and desorption conditions, respectively. α_{12}: selectivity of component 1 over component 2.

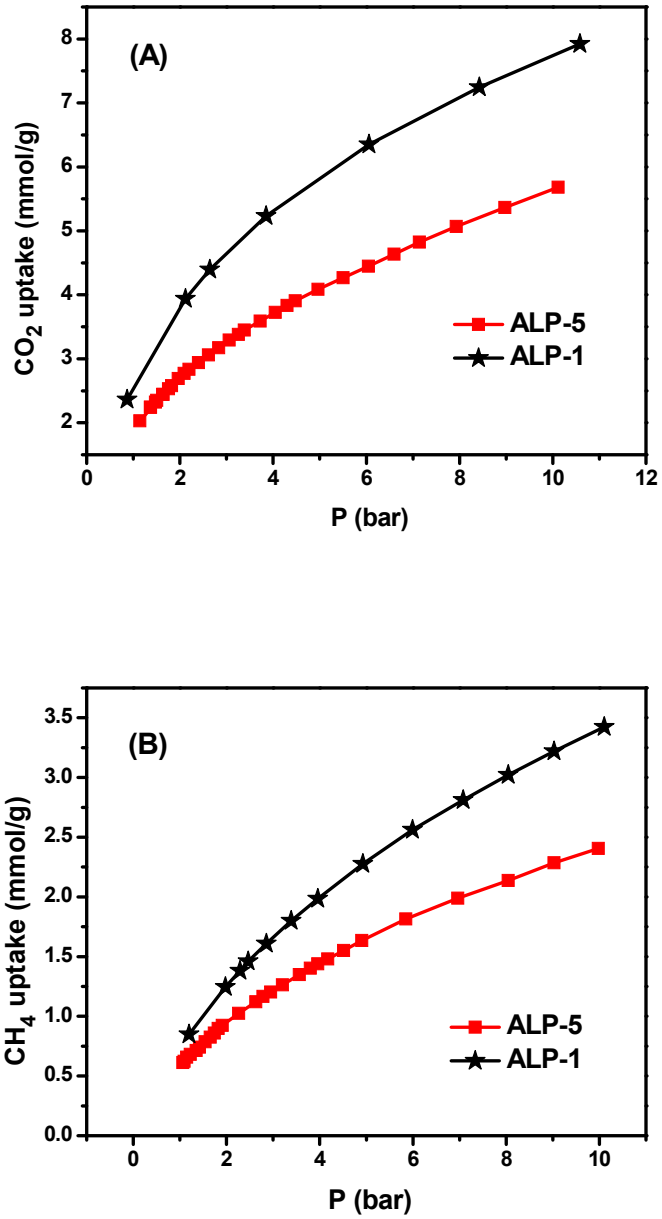

Figure 3.36: High-pressure total (absolute) CO_2 (A) and CH_4 (B) uptake of ALP-1 and ALP-5 at 298 K.

3.4.4.1 CO_2 Separation from Flue Gas using VSA

To evaluate the performance of ALPs in CO_2 separation from flue gas, the CO_2:N_2 mole ratio was assumed to be 10:90. The evaluation criteria were calculated by setting the adsorption pressure (P^{ads}) and desorption pressure (P^{des}) to 1.0 bar and 0.1 bar, respectively. Table 3.8 compares the performance of ALPs with those of different classes of promising porous sorbents. As seen in Table 3.8, ALP-5 has the highest working capacity among all ALPs. This can be attributed to the combined effects of its high Q_{st} for CO_2 and relatively high surface area.[10] Interestingly, although the surface area of ALP-5 (801 $m^2\ g^{-1}$) is much lower than that of ALP-1 (1235 $m^2\ g^{-1}$), it has a higher working capacity than ALP-1 (Table 3.8). This can be attributed to the higher Q_{st} of ALP-5 for CO_2 which results in higher CO_2 uptake at low pressures.[10]

Table 3.8: VSA evaluation criteria for CO_2 separation from flue gas[a].

Adsorbents	N_1^{ads}	ΔN_1	R	α_{12}^{ads}	S
ALP-1[2]	0.57	0.51	88.6	28.0	85.2
ALP-5	0.72	0.63	87.4	47.0	233.7
ALP-6	0.41	0.36	88.1	47.7	228.7
ALP-7	0.32	0.28	87.9	56.4	326.8
ALP-8	0.38	0.33	88.0	44.1	195.2
BILP-12[26]	0.55	0.49	88.7	27.1	72.6
TBILP-2[45]	0.67	0.59	88.3	42.1	192.3
SNU-Cl-sca[46]	0.58	0.51	88.5	17.0	88
ZIF-78[10]	0.60	0.58	96.3	34.5	396
HKUST-1[10]	0.62	0.55	89.0	20.4	46.2
Ni-MOF-74[10]	4.34	3.2	73.7	41.1	83.5
Zeolite-13X[10]	2.49	1.35	54.2	86.2	128

[a]CO_2:N_2= 10:90, T= 298K, P^{ads}= 1 bar, and P^{des} = 0.1 bar.

Other ALPs (ALP-6, -7, -8) have relatively low working capacities due to their low surface areas which lead to low CO_2 uptakes. The working capacity of ALP-5 (0.63) surpasses those of previously reported POPs such as BILPs (0.30-0.49)[26], SNU-Cls (0.41- 0.51)[46], and TBILPs (0.35-0.59)[45]. On the other hand, Ni-MOF-74 and Zeolite-13X have higher working capacities than ALP-5 due to their higher Q_{st} for CO_2 (~38 kJ mol^{-1}). It is worth mentioning that the high Q_{st} values of Ni-MOF-74 and Zeolite-13X for CO_2 result in low regenerability levels (Table 3.8).[11] In addition, Ni-MOF-74 and Zeolite-13X have much lower *S* values than ALP-5 due to their high working capacity for nitrogen (ΔN_2).

3.4.4.2 CO_2 Separation from Landfill Gas using VSA

While landfill gas is an important source of CH_4, it consists of approximately 40-60% CO_2.[11] This significant level of CO_2 results in low energy density of the fuel and also corrosion of pipelines and tanks used for transportation of CH_4.[47] Therefore, CO_2 separation from landfill gas is necessary before transportation and storage.[11, 48] To assess the performance of ALPs in CO_2 separation from landfill gas, we assumed the CO_2:CH_4 mole ratio to be 50:50 and set the adsorption and desorption pressure to 1 and 0.1 bar, respectively. As seen in Table 3.9, ALP-1 shows the highest working capacity among ALPs due to its higher surface area.[26] On the other hand, the working capacity of ALP-1 for separation of CO_2 from flue under VSA process is lower than that of ALP-5 despite its higher surface area (Table 3.8). It can be concluded that the effect of surface area on working capacity becomes more dominant when the partial pressure of CO_2 in binary gas mixtures increases.[10, 26] ALP-5 has the highest *S* value among all adsorbents listed in Table 3.9, due to its high working capacity for CO_2, high CO_2/CH_4 selectivity, and low working capacity for CH_4. ALP-5 outperforms previously reported POPs such as BILPs,[26] SNU-C1s,[46] and TBILPs[45] considering all evaluation criteria together for CO_2 separation from landfill gas by VSA. Due to

their moderate Q_{st} for CO_2 (29.2-32.5 kJ mol^{-1}), ALPs have high regenerability values of 81-85%, while adsorbents such as Ni-MOF-74 and Zelolite-13X which have high Q_{st} for CO_2(~38 kJ mol^{-1}) exhibit much lower regenerabilities of ~ 50% (Table 3.9).[10]

Table 3.9: VSA evaluation criteria for CO_2 separation from landfill gas[a]

Adsorbents	N_1^{ads}	ΔN_1	R	α_{12}^{ads}	S
ALP-1[2]	2.04	1.73	85.1	5.8	35.1
ALP-5	2.07	1.67	80.9	8.3	75.0
ALP-6	1.40	1.17	84.0	6.7	47.9
ALP-7	1.04	0.86	83.0	7.9	66.9
ALP-8	1.29	1.08	83.8	7.2	56.2
BILP-12[26]	2.01	1.71	85.3	6.0	33.7
TBILP-2[45]	2.20	1.84	83.7	7.6	62.5
SNU-Cl-sca[46]	1.99	1.60	80.4	7.5	38
ZIF-82[10]	1.42	1.20	84.9	5.6	20.5
HKUST-1[10]	2.81	1.90	67.5	5.5	19.8
Ni-MOF-74[10]	6.23	3.16	50.7	8.5	21.0
Zeolite-13X[10]	3.97	1.97	49.6	13.2	19.1

[a]CO_2:CH_4= 50:50, T= 298K, P^{ads}= 1 bar, and P^{des} = 0.1 bar.

3.4.4.3 CO_2 Separation from Landfill Gas using PSA

For PSA processes, high surface area adsorbents are more promising than those having low or moderate surface areas.[11, 26] Therefore, we have only evaluated the performance of ALP-1 and ALP-5 for CO_2 separation from landfill gas using PSA since both polymers have higher surface area than other ALPs. The CO_2:CH_4 mole ratio was assumed to be 50:50, and the adsorption and desorption pressures were set to 5 and 1 bar, respectively. The PSA evaluation criteria of ALPs for separation of CO_2 from landfill gas are summarized and compared with those of different classes

of adsorbents in Table 3.10. Most notably, ALP-5 has the highest CO_2/CH_4 selectivity under adsorption conditions (α_{12}^{ads}) and also the highest *S* value among all materials listed in Table 3.10. ALP-5 has lower working capacity than ALP-1, which can be attributed to its lower surface area and pore volume. Consistently, ALP-5 exhibits relatively low working capacity when compared to other POPs of higher surface area such as BILP-12[26] and TBILP-2[45] (1080-1479 $m^2\ g^{-1}$). It is important to note that ALP-5 has high working capacities for VSA processes compared to other POPs (Tables 3.8 and 3.9); however, it has a low working capacity under PSA process when compared to other POPs such as BILP-12 and TBILP-2 (Table 3.10).

Table 3.10: PSA evaluation criteria for CO_2 separation from landfill gas[a].

Adsorbents	N_1^{ads}	ΔN_1	*R*	α_{12}^{ads}	*S*
ALP-1[2]	4.27	2.49	58.2	6.8	38.3
ALP-5	3.22	1.68	52.3	9.0	46.5
BILP-12[26]	5.04	3.02	59.8	5.8	29.7
TBILP-2[45]	4.28	2.32	54.33	7.2	31.9
HKUST-1[10]	8.01	5.34	66.7	4.9	21.0
Ni-MOF-74[10]	8.48	2.25	26.5	2.93	1.05
Zeolite-13X[10]	5.37	1.40	26.1	4.2	2.0

[a]CO_2:CH_4= 50:50, T= 298K, P^{ads}= 5 bar, and P^{des} = 1 bar.

This is consistent with previous findings that one CO_2 adsorbent cannot simultaneously be optimized for all VSA and PSA processes.[10-11] In general, CO_2 adsorbents with moderate surface

area and high Q_{st} for CO_2 are more favourable for VSA processes; however, high surface area adsorbents with moderate Q_{st} for CO_2 are more efficient for PSA applications.[10, 26] Consistently, although Ni-MOF-74 and zeolite-13X are very promising candidates for CO_2 separation by VSA processes (Tables 3.8 and 3.9), they have very low working capacities for separation of CO_2 from landfill gas by PSA (Table 3.10) due to their high Q_{st} for CO_2 (~ 38 kJ mol^{-1}). On the other hand, HKUST-1 with a lower working capacities than Ni-MOF-74 and zeolite-13X for VSA processes, outperforms Ni-MOF-74 and zeolite-13X for separation of CO_2 from landfill gas by PSA due to its high surface area (1570 m^2 g^{-1}) and moderate Q_{st} for CO_2 (29 kJ mol^{-1}). Because of its high surface area, ALP-1 has high working capacity of 2.49 mol kg^{-1}, which is comparable to those of the best benzimidazole-linked polymers such as BILP-12 and TBILP-2 (Table 3.10).

3.5 Conclusions

We have synthesized four new porous azo-linked polymers (ALPs) and studied their performance in selective CO_2 capture over N_2 and CH_4. The CO_2 uptake capacity of ALPs is influenced by their surface area and Q_{st} value for CO_2. At very low pressures, the CO_2 uptake correlates more with Q_{st} for CO_2, while the CO_2 uptake at high pressures is more dependent on the surface area. One of the polymers, ALP-5, exhibits high Q_{st} for CO_2 (32.5 kJ mol^{-1}) which is the highest Q_{st} value among all reported azo-linked porous polymers. At 1 bar, ALP-5 shows CO_2 uptake capacities of 4.46 and 2.94 mmol g^{-1} at 273 and 298 K, respectively. This high uptake is due to high surface area and high Q_{st} for CO_2. At 298 K, all ALPs have high selectivities for CO_2/N_2 (44-56) but moderate selectivity for CO_2/CH_4 (7-8). Moreover, the CO_2 separation ability of ALPs from flue gas and landfill gas under VSA and PSA conditions was found to be influenced by surface area of ALPs and their Q_{st} for CO_2. The overall results show that ALPs which have moderate surface area and high Q_{st} for CO_2 are more favourable for VSA processes; whereas,

ALPs having high surface area and moderate Q_{st} for CO_2 perform better in PSA applications. The evaluation of ALPs for CO_2 separation from flue gas and landfill gas revealed that ALPs are among the most promising porous organic polymers for VSA and PSA processes.

References

1. Arab, P.; Parrish, E.; Islamoglu, T.; El-Kaderi, H. M., Synthesis and Evaluation of Porous Azo-Linked Polymers for Carbon Dioxide Capture and Separation. *Journal of Materials Chemistry A,* **2015**, *3*, 20586-20594.

2. Arab, P.; Rabbani, M. G.; Sekizkardes, A. K.; İslamoğlu, T.; El-Kaderi, H. M., Copper(I)-Catalyzed Synthesis of Nanoporous Azo-Linked Polymers: Impact of Textural Properties on Gas Storage and Selective Carbon Dioxide Capture. *Chemistry of Materials,* **2014**, *26*, 1385-1392.

3. Patel, H. A.; Je, S. H.; Park, J.; Chen, D. P.; Jung, Y.; Yavuz, C. T.; Coskun, A., Unprecedented High-Temperature CO_2 Selectivity in N_2-Phobic Nanoporous Covalent Organic Polymers. *Nature Communications,* **2013**, *4*, 1357.

4. Lu, J.; Zhang, J., Facile Synthesis of Azo-Linked Porous Organic Frameworks via Reductive Homocoupling for Selective CO_2 Capture. *Journal of Materials Chemistry A,* **2014**, *2*, 13831-13834.

5. Patel, H. A.; Je, S. H.; Park, J.; Jung, Y.; Coskun, A.; Yavuz, C. T., Directing the Structural Features of N_2-Phobic Nanoporous Covalent Organic Polymers for CO_2 Capture and Separation. *Chemistry – A European Journal,* **2014**, *20*, 772-780.

6. Nagaraja, C. M.; Haldar, R.; Maji, T. K.; Rao, C. N. R., Chiral Porous Metal–Organic Frameworks of Co(II) and Ni(II): Synthesis, Structure, Magnetic Properties, and CO_2 Uptake. *Crystal Growth & Design,* **2012**, *12*, 975-981.

7. Park, J.; Yuan, D.; Pham, K. T.; Li, J.-R.; Yakovenko, A.; Zhou, H.-C., Reversible Alteration of CO2 Adsorption upon Photochemical or Thermal Treatment in a Metal–Organic Framework. *Journal of the American Chemical Society,* **2012**, *134*, 99-102.

8. Dawson, R.; Cooper, A. I.; Adams, D. J., Chemical Functionalization Strategies for Carbon Dioxide Capture in Microporous Organic Polymers. *Polymer International,* **2013**, *62*, 345-352.

9. Wu, S.; Liu, Y.; Yu, G.; Guan, J.; Pan, C.; Du, Y.; Xiong, X.; Wang, Z., Facile Preparation of Dibenzoheterocycle-Functional Nanoporous Polymeric Networks with High Gas Uptake Capacities. *Macromolecules,* **2014**, *47*, 2875-2882.

10. Bae, Y.-S.; Snurr, R. Q., Development and Evaluation of Porous Materials for Carbon Dioxide Separation and Capture. *Angewandte Chemie International Edition,* **2011**, *50*, 11586-11596.

11. Wilmer, C. E.; Farha, O. K.; Bae, Y.-S.; Hupp, J. T.; Snurr, R. Q., Structure-Property Relationships of Porous Materials for Carbon Dioxide Separation and Capture. *Energy & Environmental Science,* **2012**, *5*, 9849-9856.

12. Moon, S.-Y.; Mo, H.-R.; Ahn, M.-K.; Bae, J.-S.; Jeon, E.; Park, J.-W., Organic Sol–Gel Synthesis of Microporous Molecular Networks Containing Spirobifluorene and Tetraphenylmethane Nodes. *Journal of Polymer Science Part A: Polymer Chemistry,* **2013**, *51*, 1758-1766.

13. Xu, K.; Economy, J., Hyperbranched Thermosetting Poly(imide−ester): Synthesis and Properties. *Macromolecules,* **2004**, *37*, 4146-4155.

14. Sun, F.; Zhang, G.; Zhang, D.; Xue, L.; Jiang, H., Aqueous Fluorescence Turn-on Sensor for Zn^{2+} with a Tetraphenylethylene Compound. *Organic Letters,* **2011**, *13*, 6378-6381.

15. Ma, S.; Zhou, H.-C., Gas Storage in Porous Metal-Organic Frameworks for Clean Energy Applications. *Chemical Communications,* **2010**, *46*, 44-53.

16. Zou, X.; Ren, H.; Zhu, G., Topology-Directed Design of Porous Organic Frameworks and their Advanced Applications. *Chemical Communications,* **2013**, *49*, 3925-3936.

17. Demirocak, D. E.; Ram, M. K.; Srinivasan, S. S.; Goswami, D. Y.; Stefanakos, E. K., A Novel Nitrogen Rich Porous Aromatic Framework for Hydrogen and Carbon Dioxide Storage. *Journal of Materials Chemistry A,* **2013**, *1*, 13800-13806.

18. Kaur, P.; Hupp, J. T.; Nguyen, S. T., Porous Organic Polymers in Catalysis: Opportunities and Challenges. *ACS Catalysis,* **2011**, *1*, 819-835.

19. Shen, C.; Bao, Y.; Wang, Z., Tetraphenyladamantane-Based Microporous Polyimide for Adsorption of Carbon Dioxide, Hydrogen, Organic and Water Vapors. *Chemical Communications,* **2013**, *49*, 3321-3323.

20. Wisser, F. M.; Eckhardt, K.; Wisser, D.; Böhlmann, W.; Grothe, J.; Brunner, E.; Kaskel, S., Tailoring Pore Structure and Properties of Functionalized Porous Polymers by Cyclotrimerization. *Macromolecules,* **2014**, *47*, 4210-4216.

21. Feng, X.; Ding, X.; Jiang, D., Covalent Organic Frameworks. *Chemical Society Reviews,* **2012**, *41*, 6010-6022.

22. Zhang, X.; Lu, J.; Zhang, J., Porosity Enhancement of Carbazolic Porous Organic Frameworks Using Dendritic Building Blocks for Gas Storage and Separation. *Chemistry of Materials,* **2014**, *26*, 4023-4029.

23. Lu, W.; Wei, Z.; Yuan, D.; Tian, J.; Fordham, S.; Zhou, H.-C., Rational Design and Synthesis of Porous Polymer Networks: Toward High Surface Area. *Chemistry of Materials,* **2014**, *26*, 4589-4597.

24. Ben, T.; Li, Y.; Zhu, L.; Zhang, D.; Cao, D.; Xiang, Z.; Yao, X.; Qiu, S., Selective Adsorption of Carbon Dioxide by Carbonized Porous Aromatic Framework (PAF). *Energy & Environmental Science,* **2012**, *5*, 8370-8376.

25. Ma, H.; Ren, H.; Zou, X.; Meng, S.; Sun, F.; Zhu, G., Post-Metalation of Porous Aromatic Frameworks for Highly Efficient Carbon Capture from $CO_2 + N_2$ and $CH_4 + N_2$ Mixtures. *Polymer Chemistry,* **2014**, *5*, 144-152.

26. Sekizkardes, A. K.; Islamoglu, T.; Kahveci, Z.; El-Kaderi, H. M., Application of Pyrene-Derived Benzimidazole-Linked Polymers to CO_2 Separation under Pressure and Vacuum Swing Adsorption Settings. *Journal of Materials Chemistry A,* **2014**, *2*, 12492-12500.

27. Li, G.; Zhang, B.; Yan, J.; Wang, Z., Tetraphenyladamantane-Based Polyaminals for Highly Efficient Captures of CO_2 and Organic Vapors. *Macromolecules,* **2014**, *47*, 6664-6670.

28. Arab, P.; Verlander, A.; El-Kaderi, H. M., Synthesis of a Highly Porous Bis(imino)pyridine-Linked Polymer and Its Postsynthetic Modification with Inorganic Fluorinated Ions for Selective CO_2 Capture. *The Journal of Physical Chemistry C,* **2015**, *119*, 8174-8182.

29. Lu, W.; Yuan, D.; Sculley, J.; Zhao, D.; Krishna, R.; Zhou, H.-C., Sulfonate-Grafted Porous Polymer Networks for Preferential CO_2 Adsorption at Low Pressure. *Journal of the American Chemical Society,* **2011**, *133*, 18126-18129.

30. Sung, S.; Suh, M. P., Highly Efficient Carbon Dioxide Capture with a Porous Organic Polymer Impregnated with Polyethylenimine. *Journal of Materials Chemistry A,* **2014**, *2*, 13245-13249.

31. Song, W.-C.; Xu, X.-K.; Chen, Q.; Zhuang, Z.-Z.; Bu, X.-H., Nitrogen-Rich Diaminotriazine-Based Porous Organic Polymers for Small Gas Storage and Selective Uptake. *Polymer Chemistry,* **2013**, *4*, 4690-4696.

32. Liu, B.; Smit, B., Comparative Molecular Simulation Study of CO_2/N_2 and CH_4/N_2 Separation in Zeolites and Metal−Organic Frameworks. *Langmuir,* **2009**, *25*, 5918-5926.

33. Byun, Y.; Coskun, A., Bottom-up Approach for the Synthesis of a Three-Dimensional Nanoporous Graphene Nanoribbon Framework and Its Gas Sorption Properties. *Chemistry of Materials,* **2015**, *27*, 2576-2583.

34. Patel, H. A.; Ko, D.; Yavuz, C. T., Nanoporous Benzoxazole Networks by Silylated Monomers, Their Exceptional Thermal Stability, and Carbon Dioxide Capture Capacity. *Chemistry of Materials,* **2014**, *26*, 6729-6733.

35. Li, G.; Wang, Z., Naphthalene-Based Microporous Polyimides: Adsorption Behavior of CO_2 and Toxic Organic Vapors and Their Separation from Other Gases. *The Journal of Physical Chemistry C,* **2013**, *117*, 24428-24437.

36. Liu, G.; Wang, Y.; Shen, C.; Ju, Z.; Yuan, D., A Facile Synthesis of Microporous Organic Polymers For Efficient Gas Storage and Separation. *Journal of Materials Chemistry A,* **2015**, *3*, 3051-3058.

37. Zhu, X., et al., Efficient CO_2 Capture by a Task-Specific Porous Organic Polymer Bifunctionalized with Carbazole and Triazine Groups. *Chemical Communications,* **2014**, *50*, 7933-7936.

38. Liao, Y.; Weber, J.; Faul, C. F. J., Fluorescent Microporous Polyimides Based on Perylene and Triazine for Highly CO_2-Selective Carbon Materials. *Macromolecules,* **2015**.

39. Saleh, M.; Kim, K. S., Highly Selective CO_2 Adsorption Performance of Carbazole Based Microporous Polymers. *RSC Advances,* **2015**, *5*, 41745-41750.

40. Islamoglu, T.; Gulam Rabbani, M.; El-Kaderi, H. M., Impact of Post-Synthesis Modification of Nanoporous Organic Frameworks on Small Gas Uptake and Selective CO_2 Capture. *Journal of Materials Chemistry A,* **2013**, *1*, 10259-10266.

41. Li, P.-Z.; Zhao, Y., Nitrogen-Rich Porous Adsorbents for CO_2 Capture and Storage. *Chemistry – An Asian Journal,* **2013**, *8*, 1680-1691.

42. Saleh, M.; Baek, S. B.; Lee, H. M.; Kim, K. S., Triazine-Based Microporous Polymers for Selective Adsorption of CO_2. *The Journal of Physical Chemistry C,* **2015**, *119*, 5395-5402.

43. Lee, J. H.; Lee, H. J.; Lim, S. Y.; Kim, B. G.; Choi, J. W., Combined CO_2-Philicity and Ordered Mesoporosity for Highly Selective CO_2 Capture at High Temperatures. *Journal of the American Chemical Society,* **2015**, *137*, 7210–7216.

44. Hu, X.-M.; Chen, Q.; Zhao, Y.-C.; Laursen, B. W.; Han, B.-H., Straightforward Synthesis of a Triazine-Based Porous Carbon with High Gas-Uptake Capacities. *Journal of Materials Chemistry A,* **2014**, *2*, 14201-14208.

45. Sekizkardes, A. K.; Altarawneh, S.; Kahveci, Z.; İslamoğlu, T.; El-Kaderi, H. M., Highly Selective CO_2 Capture by Triazine-Based Benzimidazole-Linked Polymers. *Macromolecules,* **2014**, *47*, 8328-8334.

46. Xie, L.-H.; Suh, M. P., High CO2-Capture Ability of a Porous Organic Polymer Bifunctionalized with Carboxy and Triazole Groups. *Chemistry – A European Journal,* **2013**, *19*, 11590-11597.

47. Farha, O. K.; Bae, Y.-S.; Hauser, B. G.; Spokoyny, A. M.; Snurr, R. Q.; Mirkin, C. A.; Hupp, J. T., Chemical Reduction of a Diimide Based Porous Polymer for Selective Uptake of Carbon Dioxide Versus Methane. *Chemical Communications,* **2010**, *46*, 1056-1058.

48. Bae, Y.-S.; Hauser, B. G.; Farha, O. K.; Hupp, J. T.; Snurr, R. Q., Enhancement of CO_2/CH_4 Selectivity in Metal-Organic Frameworks Containing Lithium Cations. *Microporous and Mesoporous Materials,* **2011**, *141*, 231-235.

Chapter 4

Synthesis of a Highly Porous Bis(imino)pyridine-Linked Polymer and its Post-Synthetic Modification with Inorganic Fluorinated Ions for Selective CO_2 Capture

This chapter is mainly taken from my recent article.[1] Adapted with permission from *The Journal of Physical Chemistry C,* **2015**, *119*, 8174–8182.

4.1 Abstract

A novel bis(imino)pyridine-linked porous polymer with high BET surface area of 1580 m^2 g^{-1} was synthesized via a facile condensation reaction between 2,6-pyridinedicarboxaldehyde and 1,3,5-tris(4-aminophenyl)benzene. The polymer was post-synthetically functionalized with $Cu(BF_4)_2$ through the complexation of copper cations with bis(imino)pyridine moieties of the polymer, where BF_4^- ions act as counter ions to balance the charge of copper cations. The effect of functionalization on CO_2 uptake capacity and selectivity was studied. The functionalization resulted in a 19% enhancement in CO_2 binding affinity and 200 % increase in CO_2 uptake capacity at 0.15 bar. Upon functionalization, CO_2/N_2 and CO_2/CH_4 selectivity values increased by a factor of up to 6. The functionalized network exhibits high CO_2/N_2 and CO_2/CH_4 selectivity values of 101 and 20, respectively.

4.2 Introduction

Surface modification of POPs with polar groups such as amine, nitro, hydroxyl, and halogens has been widely used to achieve high CO_2 uptake capacity and selectivity.[2-5] Recently, design and synthesis of fluorinated POPs and MOFs for CO_2 capture has attracted considerable attention.[6-10] Functionalization of the pores with fluoro moieties can lead to improvement in CO_2 uptake capacity and selectivity due to dipole-quadrupole interactions between fluoro sites and CO_2.[6, 11-12] Several MOFs and POPs functionalized with fluorocarbons exhibit enhanced CO_2 uptake capacity and high isosteric heat of adsorption (Q_{st}) for CO_2.[6-9, 11] Likewise, MOFs functionalized with fluorinated ions such as PF_6^-, SiF_6^{2-}, and BF_4^- show moderate to high Q_{st} values for CO_2 (34-45 kJ/mol).[13-15] By virtue of their metal-free nature, POPs can be designed to have a wide variety of chelating ligand sites, which can subsequently be used for framework metalation and pore functionalization.[16-18] In conventional synthetic strategies for the incorporation of metal binding sites into POPs, monomers containing chelating ligands are commonly used.[17] However, the preparation of such monomers usually involves tedious multi-step reactions. Moreover, polymerization of monomers featuring chelating sites can be complicated by their high tendency to bind to the metallic catalysts used for polymerization.[19] As a result, judicious choice of monomers and metallic catalysts is critical for the preparation of POPs possessing free metal binding functional groups, posing a limit to the scope of this approach. In order to circumvent these issues, in this work we have introduced a synthetic strategy that involves a bottom-up approach to produce the chelating sites, bis(imino)pyridines, *in situ* during the polymerization process under metal free conditions (Figure 4.1).

Herein, we report on the synthesis of the first highly porous bis(imino)pyridine linked polymer (BIPLP-1) and its post-synthetic modification with $Cu(BF_4)_2$ for enhanced selective CO_2

capture (Figure 4.1). We chose $Cu(BF_4)_2$ for functionalization of BIPLP-1 since post-synthetic modification of porous frameworks and porous molecular materials with fluorinated ions such as TiF_6^{2-} and BF_4^- has been shown to result in enhanced CO_2 uptake capacity.[20-21] This is attributed to Lewis acid-base interactions between CO_2 molecules and fluorinated ions.[21-23]

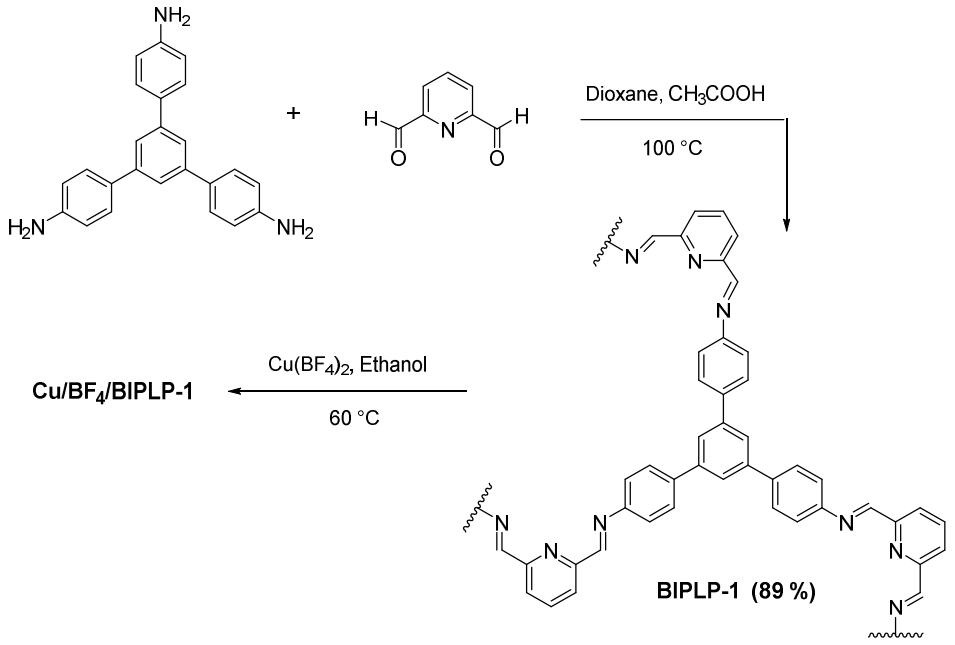

Figure 4.1: Synthesis of BIPLP-1 and its Post-Synthetic Modification with $Cu(BF_4)_2$.

4.3 Experimental Section

4.3.1 Materials and Methods

All chemicals were purchased from commercial suppliers (Acros Organics, Sigma-Aldrich, and Alfa Aesar) and used as received, unless otherwise noted. 2,6-Pyridinedicarboxaldehyde (PDCA) was obtained from Tokyo Chemical Industry (TCI). 1,3,5-Tris(4-aminophenyl)benzene (TAPB) was synthesized following the procedure reported in

literature.[24] Air sensitive or moisture sensitive materials and reactions were handled under a nitrogen atmosphere, using a glovebox or Schlenk line. Elemental analyses were performed by Midwest Microlab LLC. Thermogravimetric analysis (TGA) was carried out by a Perkin-Elmer Pyris 1 thermogravimetric analyzer under a nitrogen atmosphere with a heating rate of 10º C min^{-1}. For Scanning Electron Microscopy (SEM) imaging and Eenergy-Dispersive X-ray (EDX) studies, the samples were prepared by dispersing the material onto the surface of a sticky carbon attached to a flat aluminium sample holder. Then, the samples were coated with platinum at a pressure of 1×10^{-5} mbar in a N_2 atmosphere for 60 seconds before analysis. SEM images and EDX elemental mappings were obtained by a Hitachi SU-70 Scanning Electron Microscope. Powder X-ray diffraction patterns were obtained by using a Panalytical X'pert pro multipurpose diffractometer (MPD) with Cu Kα radiation. FT-IR spectra of the samples were obtained with a Nicolet-Nexus 670 spectrometer having an attenuated total reflectance accessory. Porosity and gas sorption measurements were carried out by a Quantachrome Autosorb iQ volumetric analyzer using UHP grade adsorbates. The samples were degassed at 110 °C under vacuum for 24 hours before gas sorption measurements. Pore size distribution (PSD) was calculated from Ar isotherms by non-local density functional theory (NLDFT) using a spherical/cylindrical pore (zeolite) NLDFT adsorption branch model. The pore volume of the samples were calculated from single point Ar uptake at P/Po=0.90. The X-ray photoelectron spectroscopy (XPS) analysis was performed on a Thermo Fisher Scientific ESCALAB 250 instrument having monochromatized Al Kα X-rays. To prepare the samples for XPS, the material was pressed into a piece of indium foil which was mounted on the sample holder using a double sided sticky tape. During XPS analysis, a combination of a low energy electron flood gun and an argon ion flood gun was utilized for charge compensation. The binding energy scale was calibrated by setting the C1s peak at 285.0

eV. The XPS data were analyzed with Thermo Avantage software (v4.84). For the determination of copper content, inductively coupled plasma optical emission spectroscopy (ICP-OES) analysis was carried out using a VISTA-MPX CCD Simultaneous ICP-OES. To prepare the sample for ICP-OES, 10 mg of the sample was dispersed in 10 mL of 70 % nitric acid and the mixture was stirred at ambient temperature for 24 h to dissolve the polymer. Then, the obtained solution was diluted for ICP analysis.

4.3.2 Synthetic Aspects

Synthesis of BIPLP-1. A Pyrex tube, having the outer diameter of 12 mm and inner diameter of 10 mm, was charged with 1,3,5-tris(4-aminophenyl)benzene (22 mg, 0.06 mmol, 2 eq) and 2,6-pyridinedicarboxaldehyde (12 mg, 0.09 mmol, 3 eq). Anhydrous 1,4-dioxane (3.0 mL) was added and the resulting mixture was sonicated for 1 min to dissolve the monomers. Afterwards, an aqueous solution of acetic acid (0.6 mL, 3.0 M) was added, resulting in immediate formation of a yellow precipitate. Then, the mixture was degassed by three freeze-pump-thaw cycles. Next, the tube was frozen at 77 K using liquid nitrogen bath, and it was flame-sealed under a reduced pressure (150 mTorr). Then, the tube was placed in an oven and the temperature was increased to 100 ºC with the rate of 0.1 ºC min^{-1}. The tube was kept at 100 ºC for 48 h yielding a yellow solid. The solid was isolated by filtration and washed with 1,4-dioxane, THF, and chloroform. After drying at 110 ºC and 150 mTorr, a yellow powder (Figure 4.2) was obtained which was denoted as BIPLP-1 (28 mg, 89% based on 1,3,5-tris(4-aminophenyl)benzene). Elemental analysis calcd (%) for $C_{69}H_{45}N_9$: C, 82.86; H, 4.54; N, 12.60. Found (%): C,79.22; H, 4.60; N, 12.33.

Synthesis of Cu/BF_4/BIPLP-1. A solution obtained by dissolving $Cu(BF_4)_2.6H_2O$ (80 mg, 0.23 mmol, excess) in absolute ethanol (15 mL) was added to 60 mg of BIPLP-1 under a nitrogen

atmosphere. The resulting mixture was stirred at 60 ºC for 18 h under N_2. Afterwards the resulting brownish solid was collected by filtration over a glass frit and washed with absolute ethanol. The obtained powder was soaked in absolute ethanol for 1 day during which the solvent was exchanged three times. Thereafter, the product was filtered and washed with ethanol. Finally, the resulting solid was dried at 110 ºC and 150 mTorr to give Cu/BF_4/BIPLP-1 as a brown powder (Figure 4.3). Elemental analysis calcd (%) for $C_{69}H_{45}N_9Cu_3B_6F_{24}$: C, 48.42; H, 2.65; N, 7.36. Found (%): C, 53.44; H, 3.35; N, 8.03.

Figure 4.2: Photo of BIPLP-1.

Figure 4.3: Photo of Cu/BF_4/BIPLP-1.

4.4 Result and Discussion

4.4.1 Synthesis and Characterization of BIPLP-1

BIPLP-1 was prepared via a condensation reaction between 2,6-pyridinedicarboxaldehyde and 1,3,5-tris(4-aminophenyl)benzene that leads to the formation of bis(imino)pyridine linkage, as illustrated in Figure 4.1. The bis(imino)pyridines of BIPLP-1 might have several conformations as shown in Figure 4.4.

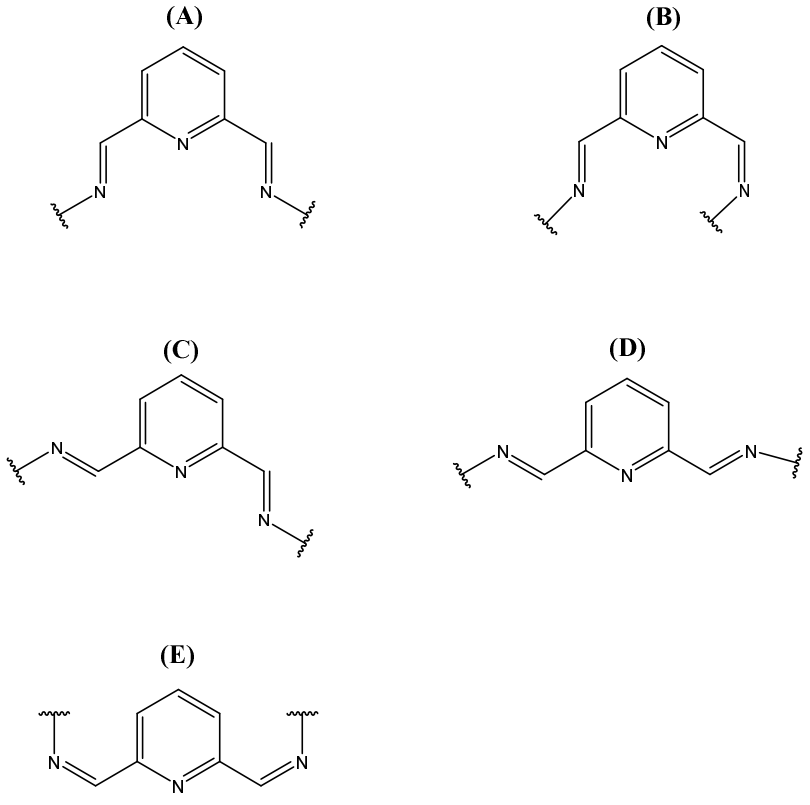

Figure 4.4: Some possible conformations of bis(imino)pyridine moiety in BIPLP-1.

The formation of the imine bond was first confirmed by the appearance of a characteristic peak for C=N vibration at 1625 cm^{-1} in the FT-IR spectrum of BIPLP-1 (Figure 4.5).[25] Upon polymerization, the intensity of the bands resulting from C=O vibrations in the aldehyde (~1715 cm^{-1}) and N-H stretches (~3420 and 3340 cm^{-1}) in the amine are significantly decreased (Figure 4.5).The residual signals at these wavenumbers are attributed to the presence of terminal aldehyde and amine groups on the surface of BIPLP-1's particles. BIPLP-1 is insoluble in common organic solvents such as DMF, THF, chloroform, acetone, and ethanol, showing its hyper-cross-linked structure as expected.

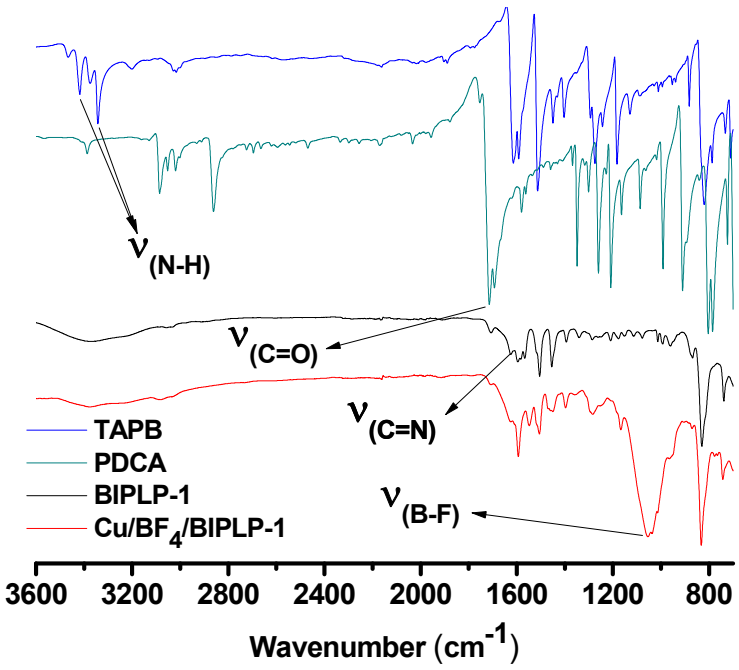

Figure 4.5: FT-IR spectra of BIPLP-1, Cu/BF_4/BIPLP-1, and monomers.

The PXRD pattern of BIPLP-1 is featureless indicating the amorphous nature of BIPLP-1 (Figure 4.6). The SEM images of BIPLP-1 (Figure 4.7) reveal that nanoscale fibers having diameter of ~20 nm are interwoven to form web-like particles of variable sizes (0.5 -2 μm). The fibrous morphology of imine-linked POPs has been proposed to be the result of reversible nature of imine bond.[26] This enables the dissolution of irregular polymer particles formed at the initial stage of the reaction followed by their re-precipitation as the energetically favored fibrous networks.[26]

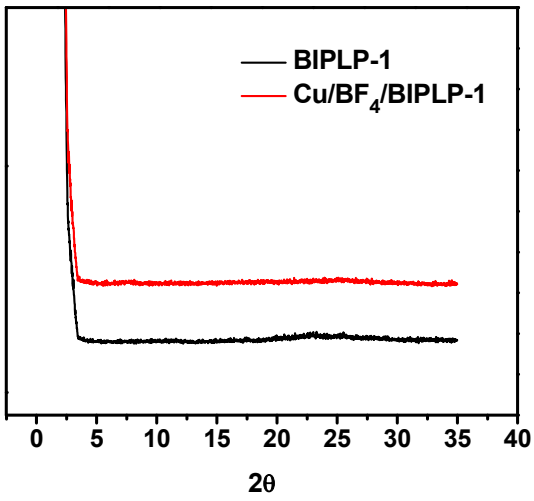

Figure 4.6: PXRD pattern of BIPLP-1 and Cu/BF_4/BIPLP-1.

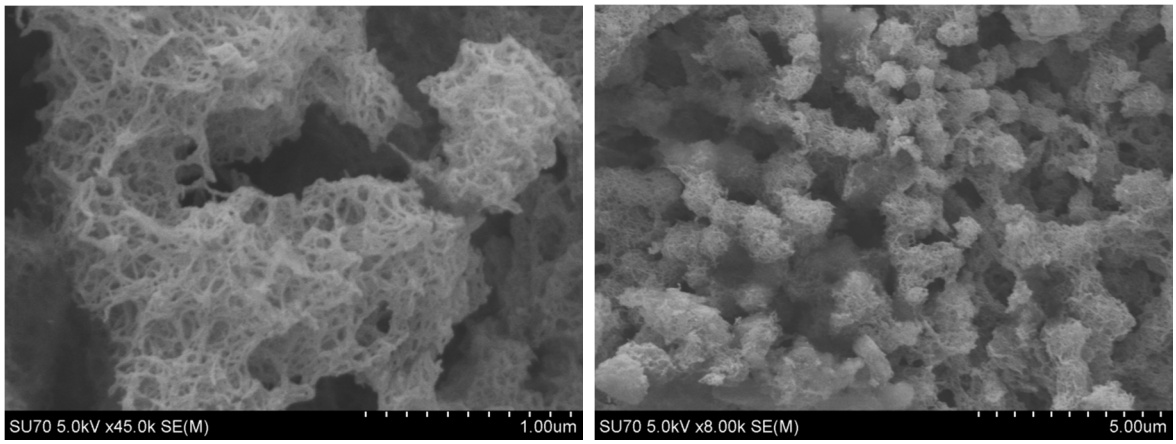

Figure 4.7: SEM images of BIPLP-1.

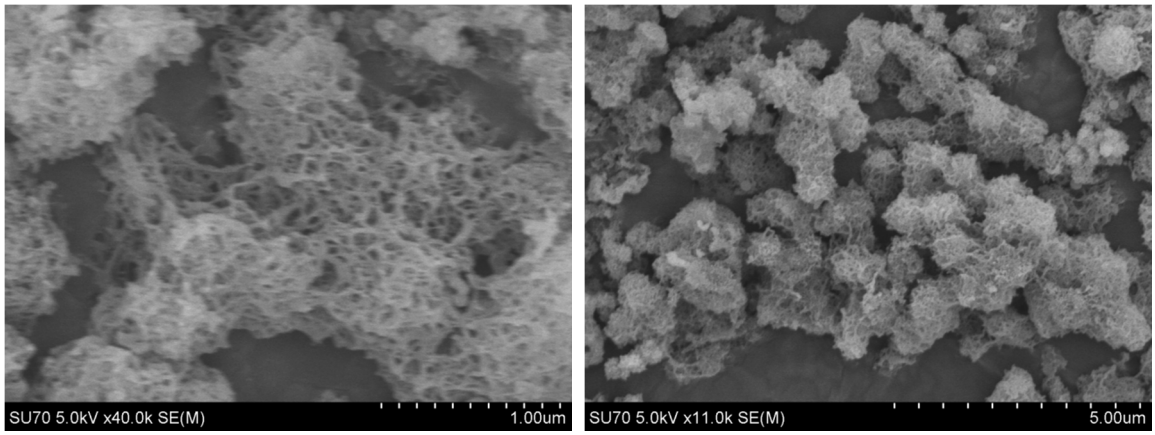

Figure 4.8: SEM images of Cu/BF_4/BIPLP-1.

Figure 4.9 shows the TGA of BIPLP-1 indicating that BIPLP-1 is stable up to ~ 400 ºC. Elemental analysis of BIPLP-1 shows some deviations from expected theoretical values. Differences between the experimental and theoretical elemental analysis values are common for porous organic polymers and can be attributed to incomplete polymerization and adsorption of moisture from air during handling, as previously reported for several POPs.[2]

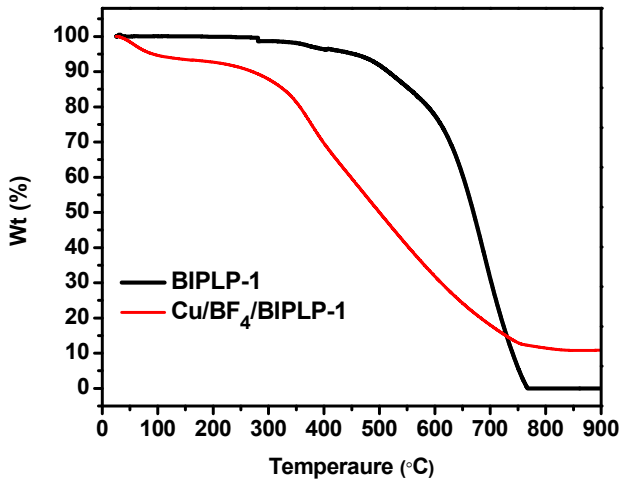

Figure 4.9 TGA traces of BIPLP-1 and Cu/BF4/BIPLP-1.

The porosity parameters of BIPLP-1 were studied by argon sorption at 87 K (Figure 4.10 A). The Ar isotherm of BIPLP-1 displays a rapid uptake at very low relative pressures due to microporosity, followed by a continuous gradual increase at *P/Po* of 0.05-0.9 due to the presence of mesopores.[2] At relative pressures above 0.9, a sharp increase in Ar uptake is observed which can be ascribed to Ar condensation in interparticle voids between agglomerated particles.[2] The specific surface area of BIPLP-1 was calculated from adsorption branch of Ar isotherm using the Brunauer-Emmett-Teller (BET) model and found to be 1580 $m^2 g^{-1}$ (Figure 4.11). The pore size distribution (PSD) of the polymer is calculated from nonlocal density functional theory (NLDFT) and depicted

in Figure 4.10 B. The PSD of BIPLP-1 shows two major peaks centered around 17 and 24 Å, as well as widely distributed pores in the range of 30-80 Å. The pore volume of BIPLP-1 was calculated from single point Ar uptake at *P/Po*=0.90 and found to be 1.37 cm^3 g^{-1}. The porosity parameters of BIPLP-1 are summarized in Table 4.1.

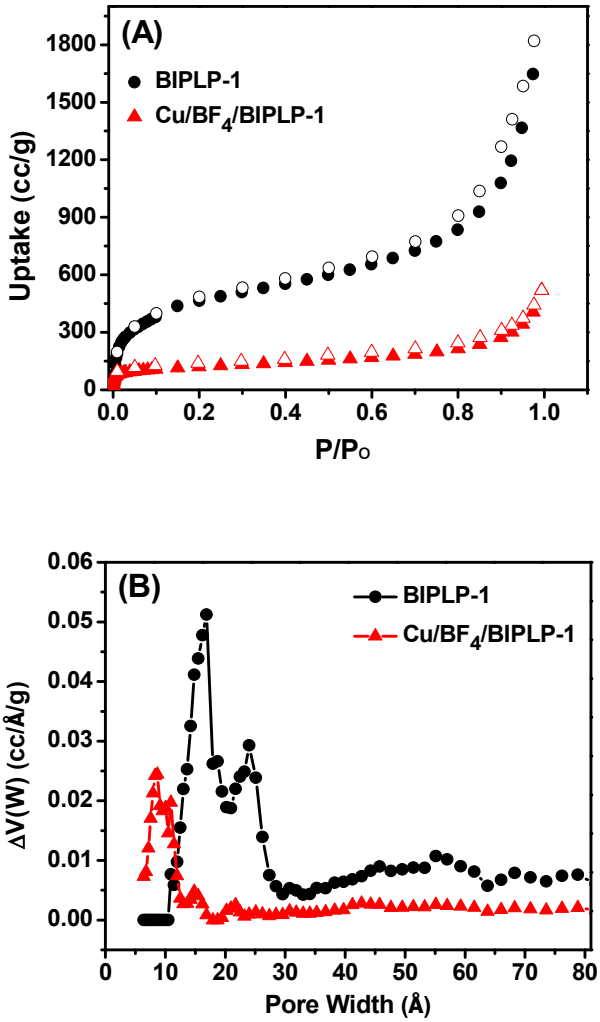

Figure 4.10: Ar uptake isotherms at 87 K (A) and pore size distribution (B) of BIPLP-1 and Cu/BF_4/BIPLP-1. Filled and open symbols represent adsorption and desorption, respectively.

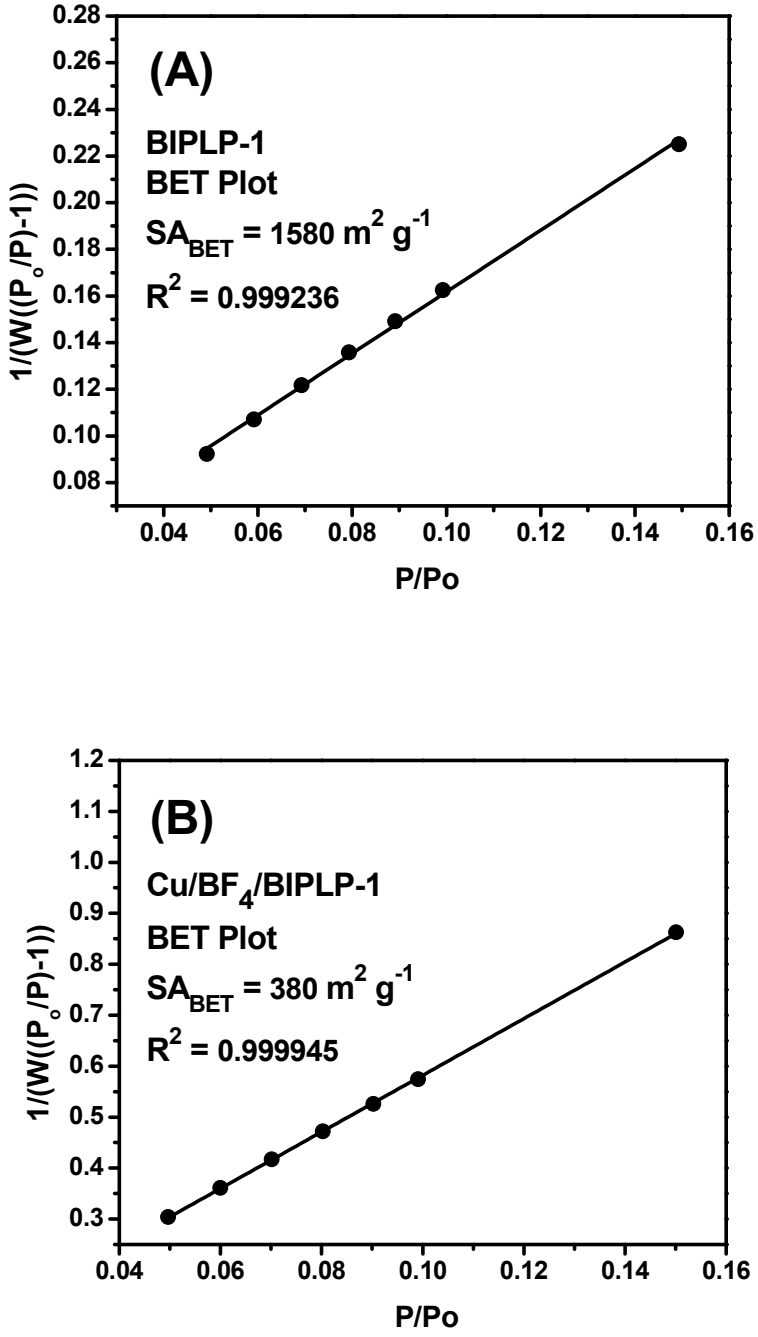

Figure 4.11: BET plots of BIPLP-1 and Cu/BF_4/BIPLP-1.

Table 4.1: Porosity Parameters of BIPLP-1 and Cu/BF_4/BIPLP-1

Polymer	SA_{BET}[a]	Dominant Pore Size[b]	V_{total}[c]
BIPLP-1	1580	17, 24	1.37
Cu/BF_4/BIPLP-1	380	8, 11	0.35

[a]Surface area (m^2g^{-1}) calculated from the argon adsorption branch based on the BET model. [b]Pore size distribution (Å) estimated from the adsorption branch of the argon isotherms using NLDFT. [c]Total pore volume ($cm^3\ g^{-1}$) calculated from single point argon uptake at P/P_o= 0.90.

4.4.2 Synthesis and Characterization of Cu/BF_4/BIPLP-1

Previous studies have shown the facile complexation of bis(imino)pyridine ligands with hydrated $Cu(BF_4)_2$, where BF_4^- ions act as counter ions to balance the charge of the copper cations.[27] Bis(imino)pyridines can complex with copper cations in bidentate or tridentate binding modes.[28] In a bidentate mode, coordination is achieved via the nitrogen of the pyridine and the nitrogen of one of the imine groups.[28] On the other hand, in a tridentate binding fashion, the pyridine and both imine groups participate in complexation.[28] Based on these studies, the functionalization of BIPLP-1 was achieved by treatment of BIPLP-1 with an ethanolic solution of $Cu(BF_4)_2.6H_2O$. The functionalization was confirmed by the appearance of characteristic peaks for Cu, B, and F atoms in the XPS spectrum of Cu/BF_4/BIPLP-1 (Figure 4.12 B). The complexation of copper cations with bis(imino)pyridine moieties was verified by comparison of N1s XPS spectra of Cu/BF_4/BIPLP-1 and BIPLP-1 (Figure 4.12 C). A shift of ~1 eV to higher binding energy was observed upon complexation. This significant shift in N1s binding energy clearly shows that the nitrogen atoms in Cu/BF_4/BIPLP-1 are coordinated to copper cations (Figure 4.12 C).[29] The oxidation state of copper atoms in Cu/BF_4/BIPLP-1 was studied with Cu2p XPS spectrum (Figure 4.12 D).

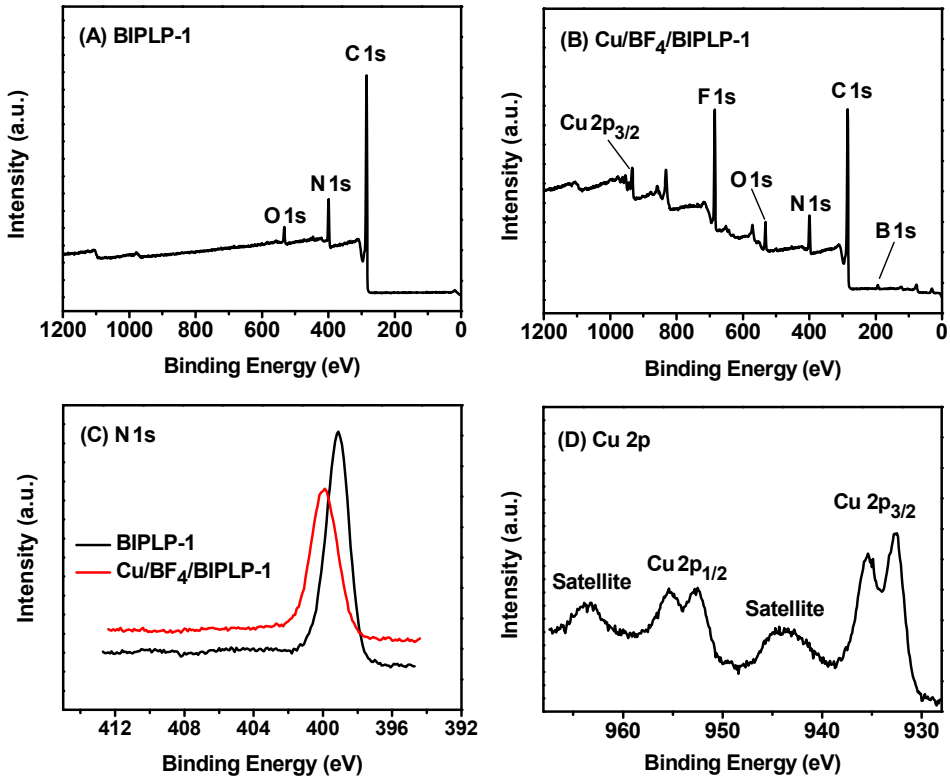

Figure 4.12: XPS survey spectra of BIPLP-1 (A) and Cu/BF_4/BIPLP-1 (B), comparison of N1s XPS spectra of BIPLP-1 and Cu/BF_4/BIPLP-1 (C), and Cu2p XPS spectrum of Cu/BF_4/BIPLP-1.

The Cu2p spectrum shows typical peaks for Cu(II) at ~935.4 and ~955.4 eV, as well as strong satellite peaks for Cu(II) at ~944 and ~963 eV.[29] The strong satellite peaks in the Cu2p spectrum are characteristic of Cu(II) atoms and can be used to differentiate copper oxidation states.[29] In addition to the peaks attributed to Cu(II), the Cu2p spectrum of Cu/BF_4/BIPLP-1 shows additional peaks centered at ~932.6 and 952.6 eV. These two peaks can be attributed to one of the following: i) presence of Cu(II) species with different coordination environment,[29] ii) spontaneous reduction of Cu(II) to Cu(I) during functionalization,[28] or iii) photoreduction of Cu(II) cations to Cu(I)

during XPS analysis.[30] It has been reported that Cu(I)-containing compounds give a peak at ~932.5 eV for 2p3/2 and at ~952.5 eV for 2p1/2.[30] The O1s XPS spectra of BIPLP-1 and Cu/BF_4/BIPLP-1 show similar peaks at ~532 eV which can be assigned to adsorbed moisture (Figure 4.13).[31]

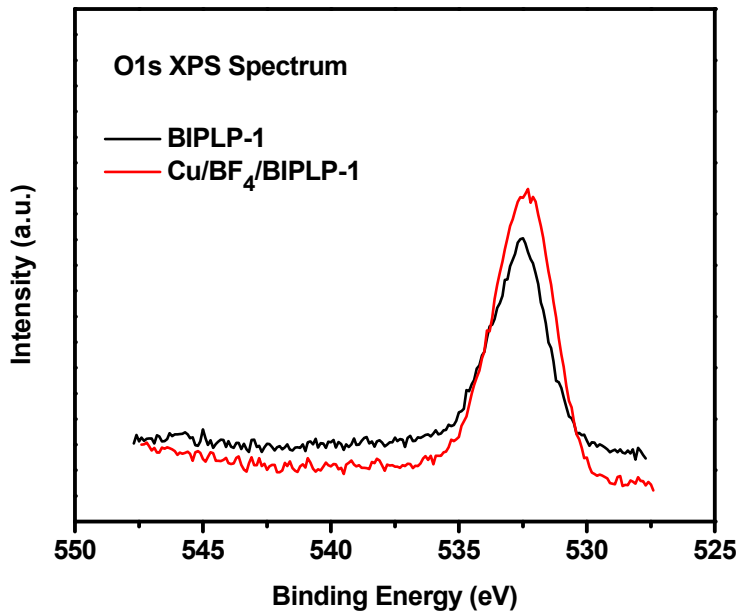

Figure 4.13: O1s XPS spectra of BIPLP-1 and Cu/BF_4/BIPLP-1.

IR studies further confirmed the functionalization of BIPLP-1 with $Cu(BF_4)_2$. A new strong band centering at around 1056 cm^{-1} appeared in the IR spectrum of Cu/BF_4/BIPLP-1 which is attributed to B-F vibrations in BF_4^- ions (Figure 4.5).[27] Energy-dispersive X-ray (EDX) elemental mapping also confirms the homogenous distribution of Cu, and F atoms in Cu/BF_4/BIPLP-1 (Figure 4.14).

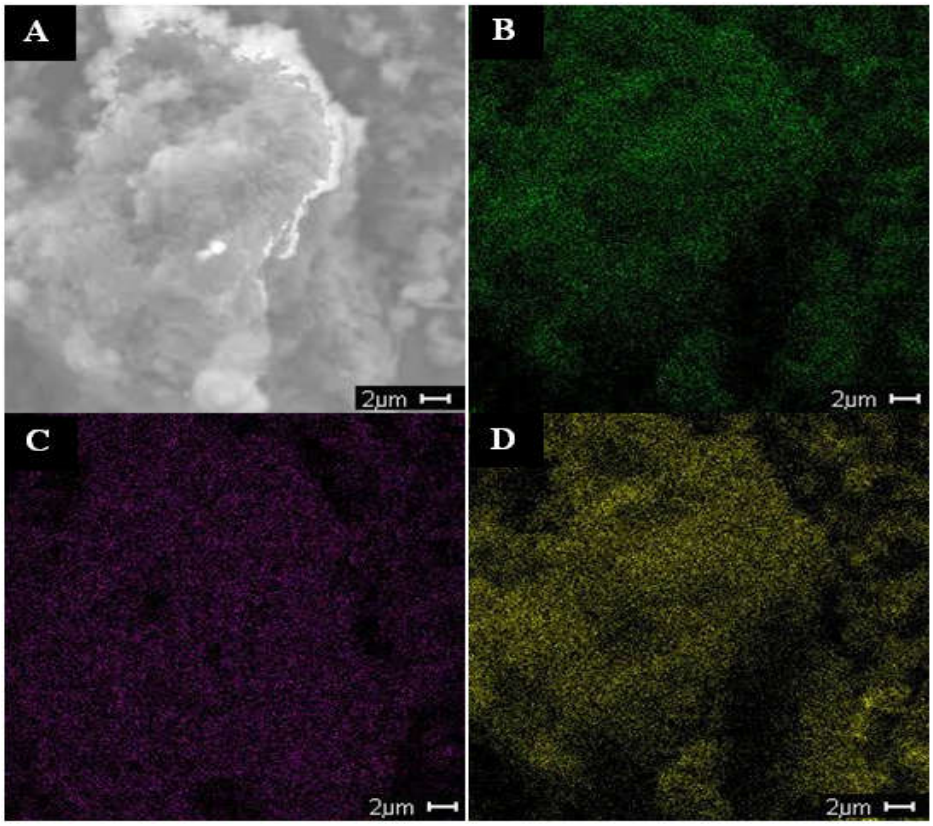

Figure 4.14: SEM image (A), and EDX elemental mapping of Cu/BF_4/BIPLP-1 for nitrogen (B), copper (C) and fluorine (D).

The copper content of Cu/BF_4/BIPLP-1 was determined by ICP and found to be 11.73 wt%. If all bis(imino)pyridine moieties of BIPLP-1 are functionalized with one $Cu(BF_4)_2$, the theoretical copper content in the functionalized polymer would equal to 11.14 wt%. Therefore, it can be

concluded that all bis(imino)pyridine moieties of the polymer are successfully functionalized. The porosity parameters of Cu/BF_4/BIPLP-1 were studied with Ar isotherm collected at 87 K (Figure 4.10 A) and compared to those of BIPLP-1 in Table 4.1. Cu/BF_4/BIPLP-1 has a BET surface area of 380 m^2 g^{-1} which is much lower than the surface area of BIPLP-1 (1580 m^2 g^{-1}). The PSD of Cu/BF_4/BIPLP-1, depicted in Figure 4.10 B, shows two major peaks centering at around 8 and 11 Å, as well as two small peaks at 15 and 21 Å. The pore volume of Cu/BF_4/BIPLP-1 was found to be 0.35 cm^3 g^{-1}, which is much lower than that of BIPLP-1 (1.37cm^3 g^{-1}). The decrease in surface area, pore size, and pore volume upon functionalization clearly indicates that the pores of Cu/BF_4/BIPLP-1 have been modified with $Cu(BF_4)_2$. The elemental analysis of Cu/BF_4/BIPLP-1 shows some deviations from corresponding theoretical values. These deviations can be attributed to adsorbed guest molecules (moisture, and gases) as evidenced by weight loss before 100 ºC in the TGA of Cu/BF_4/BIPLP-1 (Figure 4.9).[2, 32] In addition, partial reduction of Cu(II) to Cu(I) can lead to functionalization of some pores with $CuBF_4$ instead of $Cu(BF_4)_2$, resulting in some differences between experimental and theoretical elemental analysis values. The PXRD pattern and SEM images of Cu/BF_4/BIPLP-1 were found to be comparable to those of BIPLP-1 (Figures 4.6 and 4.8).

4.4.3 Impact of Functionalization on CO_2 Uptake Capacity and Selectivity

Bis(imino)pyridines can act as bidentate or tridentate ligands to coordinate to various transition metals;[33] and therefore, the incorporation of such moieties into POPs should allow for the functionalization of POPs with a wide variety of metallic species. Functionalization of porous frameworks with extraneous ions has been used as a means to modulate adsorbate-framework interactions to achieve high selectivity toward CO_2.[34] Higher CO_2 Q_{st} values have been observed upon functionalization of porous structures with inorganic salts.[14, 35] This could be due to

electrostatic interactions [36-37] and/or Lewis acid-base interactions [21] between CO_2 molecules and extraneous ions. In addition, surface modification with extraneous ions can be an effective method to reduce the size of the large pores in porous frameworks to achieve stronger affinity for CO_2 through multiple interactions between an adsorbed CO_2 molecule and pore walls.[35] Furthermore, both theoretical[22] and experimental[23] studies have shown Lewis acid-base interactions between CO_2 molecules and fluorinated ions (such as PF_6^- and BF_4^-), where the carbon atom of CO_2 acts as a Lewis acid and the fluorinated ion acts as a Lewis base. A wide variety of chelating ligand sites can be incorporated into POPs, allowing for further functionalization with inorganic salts via pre-synthetic and post-synthetic modification methods.[17] The applications of such metalated POPs in catalysis have been widely studied;[17] however, their potential use in CO_2 capture has been limited to only few studies on pre-synthetically metalated salen-based[38] and porphyrin-based[39] POPs. With these considerations in mind, we hypothesized that functionalization of BIPLP-1 with $Cu(BF_4)_2$ would lead to enhanced CO_2 capturing properties due to the altered physical and electronic nature of the pores. In order to study the effect of pore functionalization on CO_2 capture and selectivity, we collected CO_2, N_2, and CH_4 isotherms at 273 K and 298 K (Figure 4.15). The CO_2 and CH_4 isotherms of BIPLP-1 and Cu/BF_4/BIPLP-1 are reversible and show small hysteresis (Figures 4.16 and 4.17). This hysteresis can be attributed to slight structural changes of the frameworks upon gas adsorption due to the flexibility of the polymers.[40]

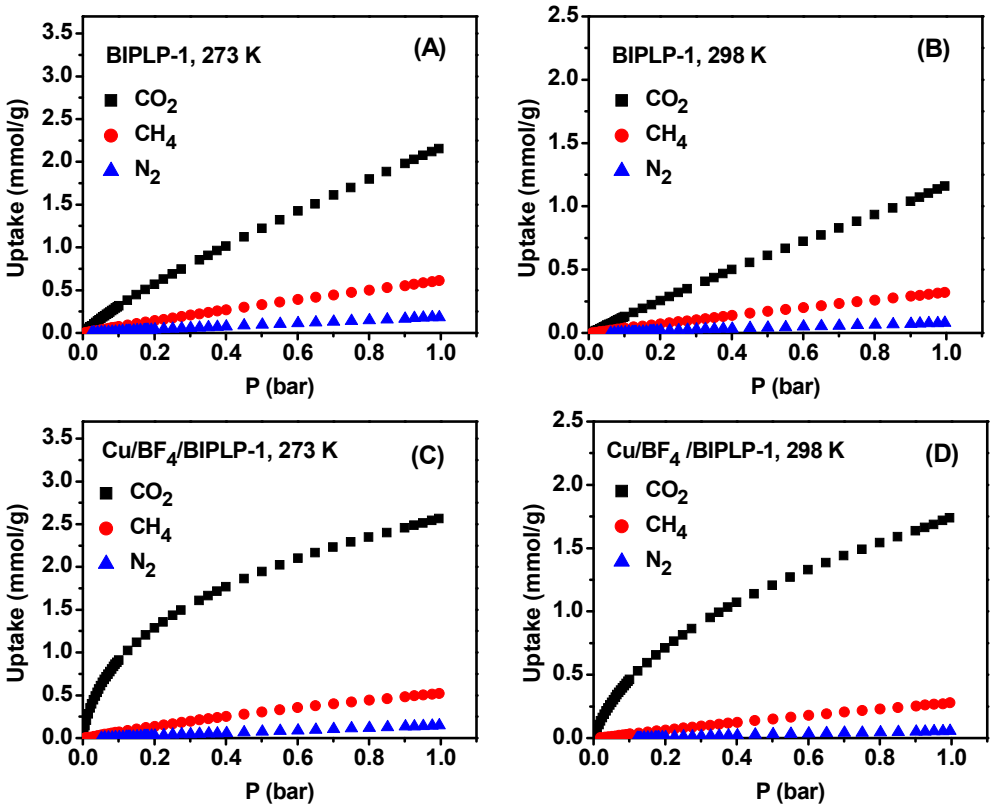

Figure 4.15: CO_2, CH_4 and N_2 adsorption isotherms of BIPLP-1 and Cu/BF_4/BIPLP-1 at 273 and 298 K.

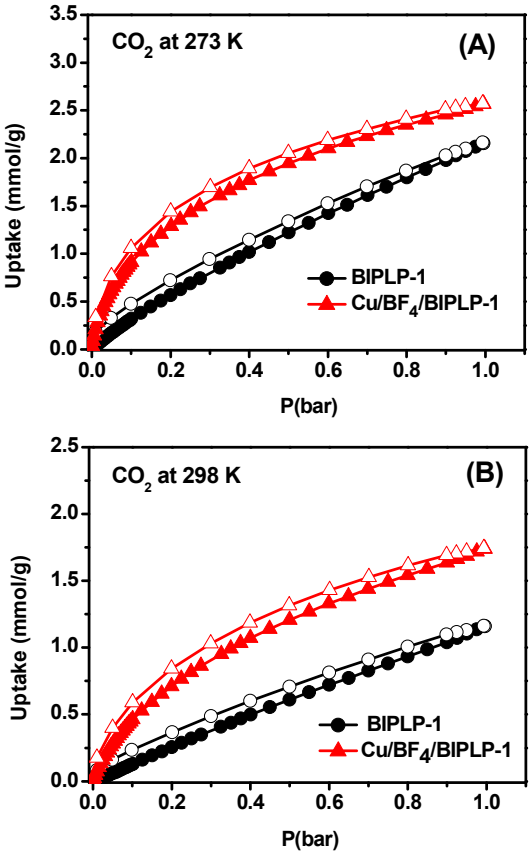

Figure 4.16: CO_2 uptake isotherms of BIPLP-1 and Cu/BF_4/BIPLP-1 at 273 K (A) and 298 K (B). Filled andopen symbols represent adsorption and desorption, respectively.

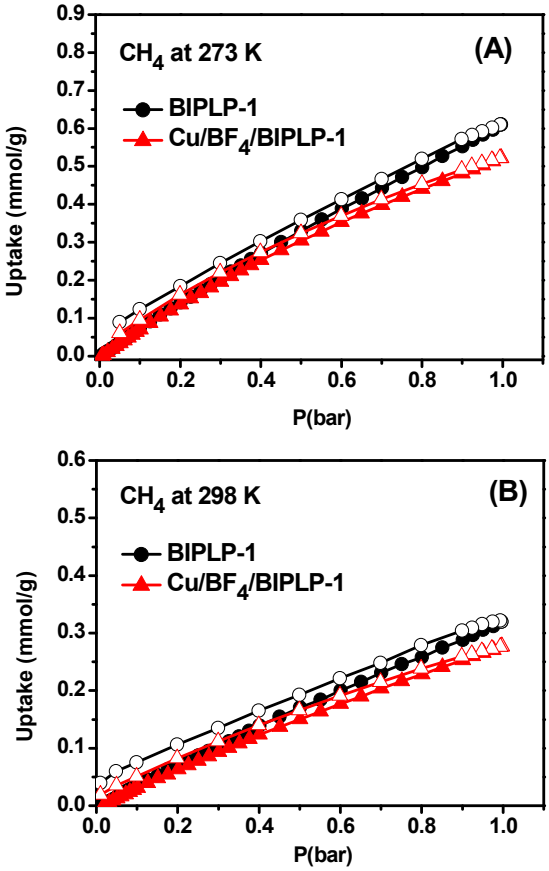

Figure.17: CH_4 uptake isotherms of BIPLP-1 and Cu/BF_4/BIPLP-1 at 273 K (A) and 298 K (B). Filled and open symbols represent adsorption and desorption, respectively.

While BIPLP-1 exhibits a linearly increasing CO_2 adsorption isotherm, the CO_2 adsorption isotherm of Cu/BF_4/BIPLP-1 shows a steep rise at low pressures (Figure 4.18). This change in CO_2 adsorption behavior indicates much stronger CO_2-framework interactions resulting in a drastic increase in CO_2 uptake capacity at 0.15 bar, which is the partial pressure of CO_2 in flue gas. Since flue gas usually contains ~15 % CO_2, the CO_2 uptake capacity at 0.15 bar is more relevant for realistic post-combustion applications.[41-42] At this pressure, Cu/BF_4/BIPLP-1 shows CO_2 uptake

capacities of 1.1 and 0.6 mmol g^{-1} at 273 and 298 K respectively (Figure 4.18). At 0.15 bar, the CO_2 uptake capacities of Cu/BF_4/BIPLP-1 at 273 and 298 K are 2.5 and 3 times those of BIPLP-1, respectively (Figure 4.18). Moreover, despite the decrease in surface area, the CO_2 uptake capacity at 1.0 bar and 298 K increased by 50% upon functionalization (Figure 4.18).

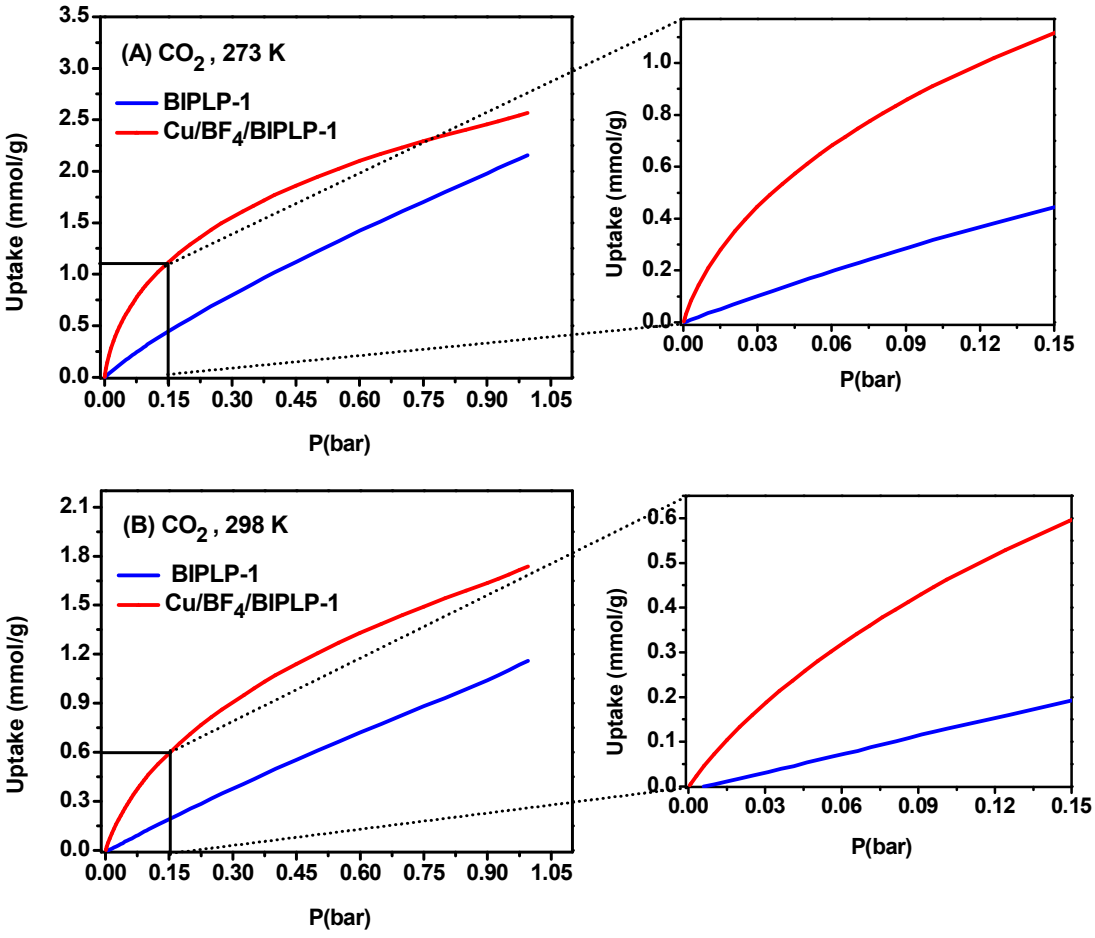

Figure 4.18: CO_2 adsorption isotherms of BIPLP-1 and Cu/BF_4/BIPLP-1 at 273 (A) and 298 K (B).

In contrast to the significant increase in CO_2 uptake capacity upon functionalization, the CH_4 and N_2 uptakes decreased after functionalization due to decreased specific surface area of the material (Figures 4.17 and 4.19). The CO_2 uptake capacity of Cu/BF_4/BIPLP-1 at 273 K and 1 bar (2.57 mmol g^{-1}) is comparable to that of many microporous POPs such as azo-POFs (1.92-2.98 mmol g^{-1}),[43] NPOFs (2.4-2.9 mmol g^{-1}),[44] box-COPs (2.14-3.17 mmol g^{-1}),[45] and azo-COPs (1.9-2.6 mmol g^{-1})[46] but lower than that of the best performing POPs such as ALP-1 (5.37 mmol g^{-1}),[2] BILP-4 (5.34 mmol g^{-1}),[47] and FCTF-1-600 (5.53 mmol g^{-1}).[6]

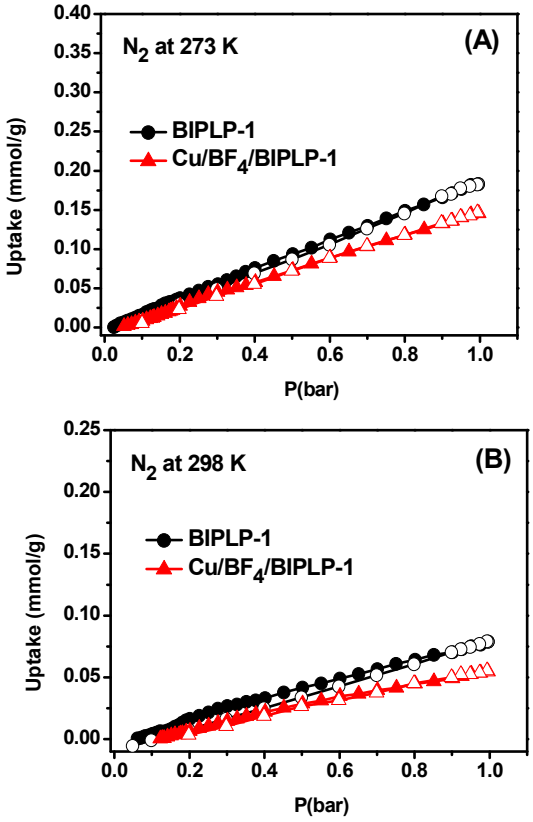

Figure 4.19: N_2 uptake isotherms of BIPLP-1 and Cu/BF_4/BIPLP-1 at 273 K (A) and 298 K (B).Filled andopen symbols represent adsorption and desorption, respectively.

To study the effect of functionalization on binding affinity for CO_2 and CH_4, we calculated the Q_{st} values by using the virial method (Figures 4.20 and 4.21). Upon functionalization, the Q_{st} for CO_2 at zero-coverage increased from 25.3 kJ mol^{-1} to 32.2 kJ mol^{-1} (Figure 4.21 A).The Q_{st} of Cu/BF_4/BIPLP-1 for CO_2 decreases from 32.3 kJ mol^{-1} at zero-coverage to 27.2 kJ mol^{-1} at higher loadings, which clearly indicates the presence of more favorable adsorption sites at low pressures. On the other hand, the Q_{st} of BIPLP-1 for CO_2 remains almost constant during the entire loading.

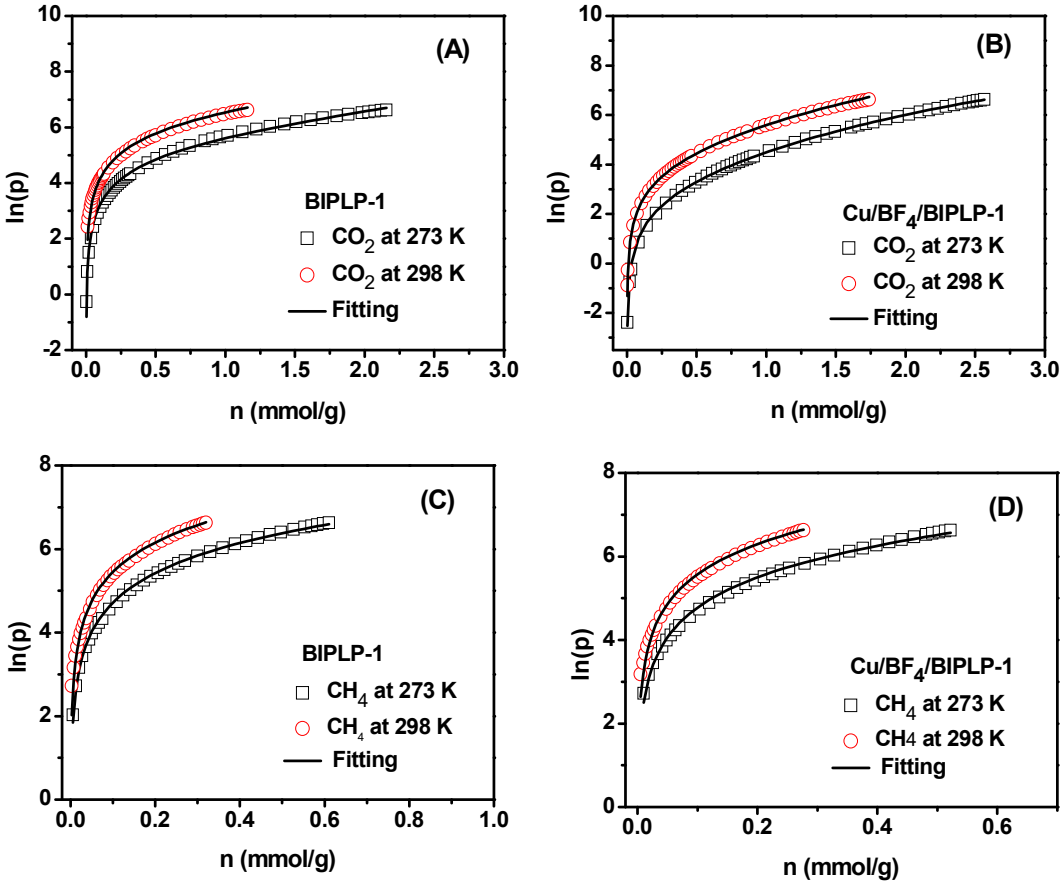

Figure 4.20: Experimental data (symbol) and corresponding virial fittings (solid line) of CH_4 and CO_2 adsorption isotherms for BIPLP-1 and Cu/BF_4/BIPLP-1.

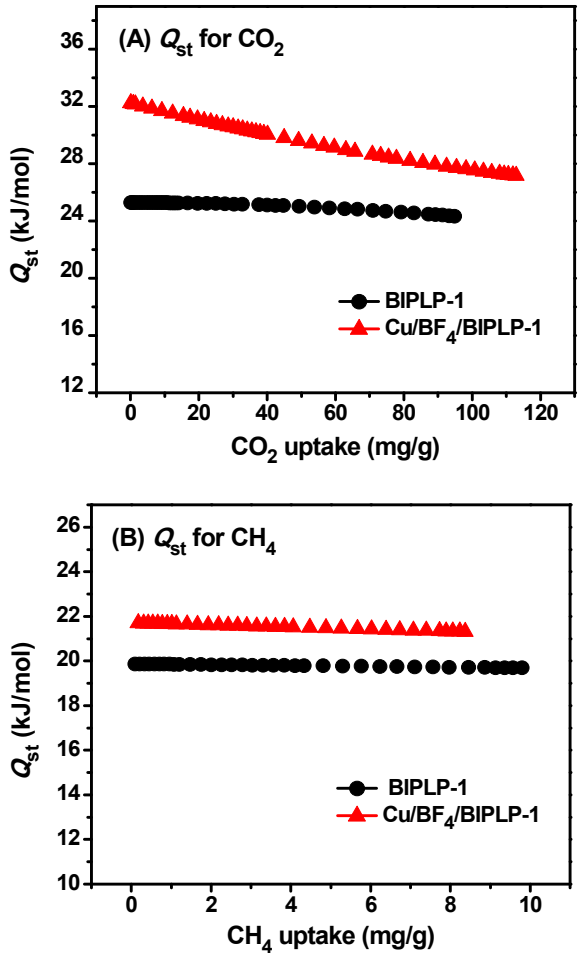

Figure 4.21: Isosteric heats of adsorption of BIPLP-1 and Cu/BF_4/BIPLP-1 for CO_2 (A) and CH_4 (B).

The Q_{st} of Cu/BF_4/BIPLP-1 for CO_2 is similar to that of a previously reported Cu$(BF_4)_2$-functionalized MOF (~34 kJ mol^{-1}at zero coverage),[14] while the Q_{st} of BIPLP-1 for CO_2 is comparable to those of non-functionalized microporous POPs such as NPOF-4 (23.2 kJ mol^{-1})[44] and mPAFs (24.5- 26 kJ mol^{-1}).[48] The enhanced CO_2 binding affinity and CO_2 uptake capacity of Cu/BF_4/BIPLP-1 can be attributed to the following factors: 1) strong Lewis acid-base interactions between BF_4^- ions and CO_2 molecules where the carbon atom of CO_2 acts as a Lewis acid and a BF_4^- ion acts as a Lewis base,[21] 2) pore size reduction upon functionalization which can lead to an

increase in the number of multiple interactions between the adsorbed CO_2 molecules and the pore walls,[35] 3) electrostatic interactions between CO_2 and copper cations.[36-37, 39] Our results are consistent with previously reported results by Yaghi and coworkers demonstrating that the functionalization of a 2,2′-bipyridine lined MOF with $Cu(BF_4)_2$ results in enhanced CO_2 uptake capacity and CO_2 binding affinity.[14] In addition, Nunez *et al.* have shown that the post-synthetic incorporation of BF_4^- ions into PCM-10, a MOF, resulted in a 24% enhancement in CO_2 binding affinity.[21] It is noteworthy that post-synthetic metalation of POPs with alkali and alkaline earth metal cations can lead to enhanced CO_2 Q_{st} values.[37, 41, 49] The Q_{st} for CH_4 at zero-coverage increased from 19.9 to 21.7 kJ mol^{-1} upon functionalization (Figure 4.21 B). This might be due to smaller pore size in Cu/BF_4/BIPLP-1, as well as the electrostatic interactions of CH_4 molecules with copper cations.[37]

In order to study the effect of pore functionalization on selective CO_2 capture over N_2 and CH_4, single component adsorption isotherms for CO_2, N_2, and CH_4 were collected at 273 and 298 K (Figure 4.15). The CO_2/N_2 and CO_2/CH_4 selectivities were estimated by initial slope method using the ratio of Henry's law constants of pure gas isotherms as summarized in Table 4.2 as well as Figures 4.22 and 4.23.

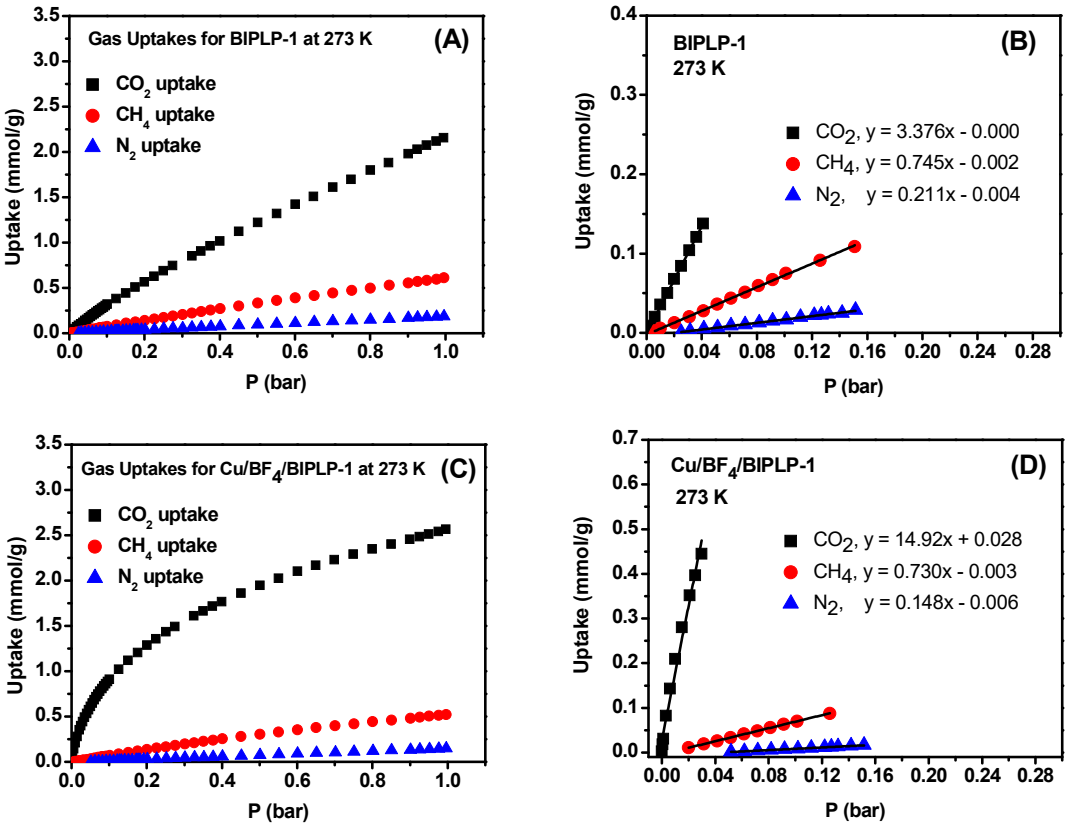

Figure 4.22: Gas uptakes and initial slope selectivity studies of BIPLP-1 and Cu/BF_4/BIPLP-1 at 273 K.

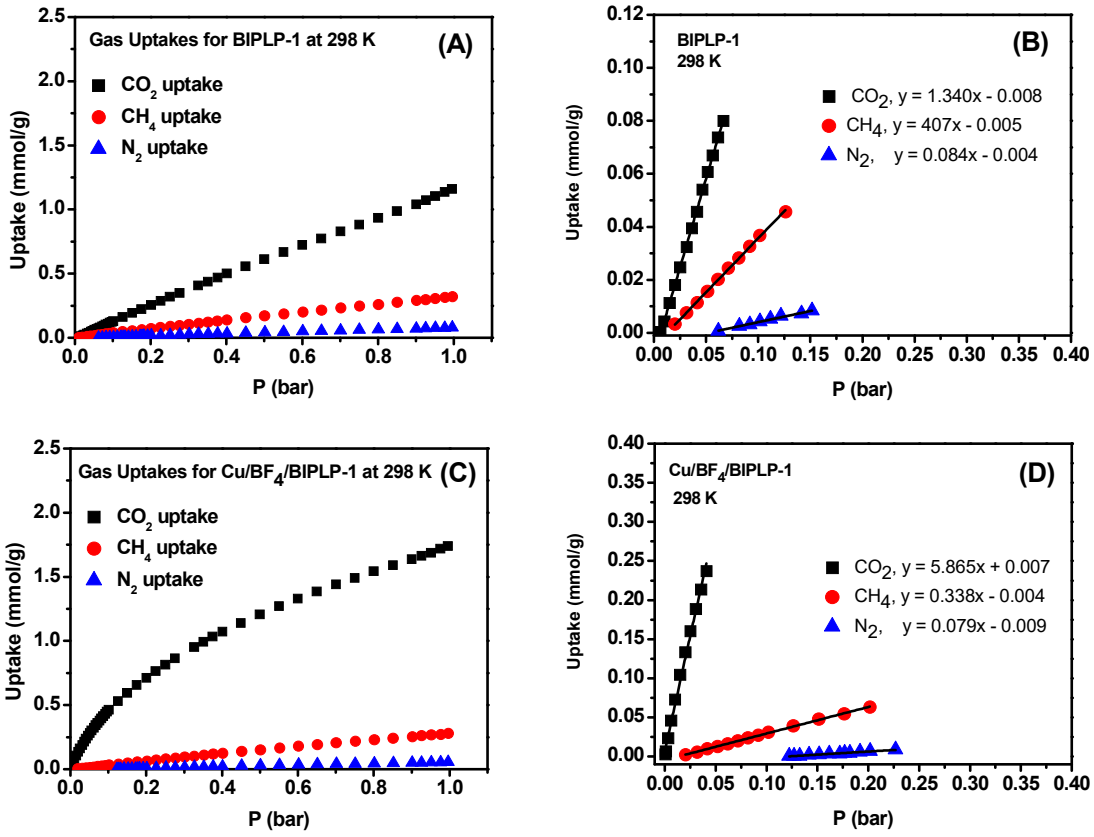

Figure 4.23: Gas uptakes and initial slope selectivity studies of BIPLP-1 and Cu/BF_4/BIPLP-1at 298 K.

Table 4.2: Selectivity Values of BIPLP-1 and Cu/BF_4/BIPLP-1[a]

	CO_2/N_2 Selectivity		CO_2/CH_4 Selectivity	
Polymer	273 K	298 K	273 K	298 K
BIPLP-1	16	16	5	3
Cu/BF_4/BIPLP-1	101	64	20	17

[a]Selectivities (mol mol^{-1}) were estimated by initial slope method.

The high binding affinity of Cu/BF_4/BIPLP-1 for CO_2 resulted in a steep rise in CO_2 uptake at low pressures which led to an increase in CO_2/N_2 and CO_2/CH_4 selectivity values by a factor of up to 6 (Table 4.2). Upon functionalization, the CO_2/N_2 selectivity at 273 K and 298 K increased from 16 to 101 and from 16 to 64, respectively. A significant enhancement for CO_2/CH_4 selectivities was also observed upon functionalization; the CO_2/CH_4 selectivities of 5 (273 K) and 3 (298 K) increased to 20 and 17, respectively. This drastic improvement in selectivity values is consistent with the results of the previous work studying the effect of functionalizing a 2,2′-bipyridine lined MOF with $Cu(BF_4)_2$ on CO_2/N_2 selectivity.[14] It is worth noting that the CO_2/N_2 and CO_2/CH_4 selectivities of Cu/BF_4/BIPLP-1 are comparable to those of the best performing porous organic polymers such a BILPs,[50] PANs,[51] and BLPs.[3]

4.5 Conclusions

We have introduced a facile synthetic route for the synthesis of a highly porous organic polymer (BIPLP-1) bearing metal free chelating sites, bis(imino)pyridines. BIPLP-1 was post-synthetically functionalized by treatment with $Cu(BF_4)_2$ via coordination of copper cations to bis(imino)pyridine moieties. We demonstrated that the coordination of metallic species to bis(imino)pyridine moieties of BIPLP-1 can be an effective means to achieve desired gas-framework interactions for selective CO_2 capture. The functionalization of BIPLP-1 with copper cations and tetrafluoroborate anions

resulted in enhancement in CO_2 binding affinity and CO_2 uptake capacity. Moreover, the functionalized network exhibits significantly enhanced CO_2/N_2 and CO_2/CH_4 selectivity values of 101 and 20, respectively.

References

1. Arab, P.; Verlander, A.; El-Kaderi, H. M., Synthesis of a Highly Porous Bis(imino)pyridine-Linked Polymer and Its Postsynthetic Modification with Inorganic Fluorinated Ions for Selective CO_2 Capture. *The Journal of Physical Chemistry C,* **2015**, *119*, 8174–8182.

2. Arab, P.; Rabbani, M. G.; Sekizkardes, A. K.; İslamoğlu, T.; El-Kaderi, H. M., Copper(I)-Catalyzed Synthesis of Nanoporous Azo-Linked Polymers: Impact of Textural Properties on Gas Storage and Selective Carbon Dioxide Capture. *Chemistry of Materials,* **2014**, *26*, 1385-1392.

3. Reich, T. E.; Behera, S.; Jackson, K. T.; Jena, P.; El-Kaderi, H. M., Highly Selective CO_2/CH_4 Gas Uptake by a Halogen-Decorated Borazine-Linked Polymer. *Journal of Materials Chemistry,* **2012**, *22*, 13524-13528.

4. Lu, W.; Sculley, J. P.; Yuan, D.; Krishna, R.; Zhou, H.-C., Carbon Dioxide Capture from Air Using Amine-Grafted Porous Polymer Networks. *The Journal of Physical Chemistry C,* **2013**, *117*, 4057-4061.

5. Shen, C.; Wang, Z., Tetraphenyladamantane-Based Microporous Polyimide and Its Nitro-Functionalization for Highly Efficient CO_2 Capture. *The Journal of Physical Chemistry C,* **2014**, *118*, 17585-17593.

6. Zhao, Y.; Yao, K. X.; Teng, B.; Zhang, T.; Han, Y., A Perfluorinated Covalent Triazine-Based Framework for Highly Selective and Water-Tolerant CO_2 Capture. *Energy & Environmental Science,* **2013**, *6*, 3684-3692.

7. Yang, Z.-Z.; Zhao, Y.; Zhang, H.; Yu, B.; Ma, Z.; Ji, G.; Liu, Z., Fluorinated Microporous Organic Polymers: Design and Applications in CO_2 Adsorption and Conversion. *Chemical Communications,* **2014**, *50*, 13910-13913.

8. Zhang, D.-S.; Chang, Z.; Li, Y.-F.; Jiang, Z.-Y.; Xuan, Z.-H.; Zhang, Y.-H.; Li, J.-R.; Chen, Q.; Hu, T.-L.; Bu, X.-H., Fluorous Metal-Organic Frameworks with Enhanced Stability and High H_2/CO_2 Storage Capacities. *Sci. Rep.,* **2013**, *3*, 3312-3318.

9. Xue, D.-X.; Cairns, A. J.; Belmabkhout, Y.; Wojtas, L.; Liu, Y.; Alkordi, M. H.; Eddaoudi, M., Tunable Rare-Earth fcu-MOFs: A Platform for Systematic Enhancement of CO_2 Adsorption Energetics and Uptake. *Journal of the American Chemical Society,* **2013**, *135*, 7660-7667.

10. Liu, D.-P.; Chen, Q.; Zhao, Y.-C.; Zhang, L.-M.; Qi, A.-D.; Han, B.-H., Fluorinated Porous Organic Polymers via Direct C–H Arylation Polycondensation. *ACS Macro Letters,* **2013**, *2*, 522-526.

11. Deria, P.; Mondloch, J. E.; Tylianakis, E.; Ghosh, P.; Bury, W.; Snurr, R. Q.; Hupp, J. T.; Farha, O. K., Perfluoroalkane Functionalization of NU-1000 via Solvent-Assisted Ligand Incorporation: Synthesis and CO_2 Adsorption Studies. *Journal of the American Chemical Society,* **2013**, *135*, 16801-16804.

12. Bae, Y.-S.; Farha, O. K.; Hupp, J. T.; Snurr, R. Q., Enhancement of CO_2/N_2 Selectivity in a Metal-Organic Framework by Cavity Modification. *Journal of Materials Chemistry,* **2009**, *19*, 2131-2134.

13. Noro, S.-i.; Fukuhara, K.; Hijikata, Y.; Kubo, K.; Nakamura, T., Rational Synthesis of a Porous Copper(II) Coordination Polymer Bridged by Weak Lewis-Base Inorganic Monoanions Using an Anion-Mixing Method. *Inorganic Chemistry,* **2013**, *52*, 5630-5632.

14. Bloch, E. D.; Britt, D.; Lee, C.; Doonan, C. J.; Uribe-Romo, F. J.; Furukawa, H.; Long, J. R.; Yaghi, O. M., Metal Insertion in a Microporous Metal−Organic Framework Lined with 2,2′-Bipyridine. *Journal of the American Chemical Society,* **2010**, *132*, 14382-14384.

15. Nugent, P., et al., Porous Materials with Optimal Adsorption Thermodynamics and Kinetics for CO_2 Separation. *Nature,* **2013**, *495*, 80-84.

16. Rose, M., Nanoporous Polymers: Bridging the Gap between Molecular and Solid Catalysts? *ChemCatChem,* **2014**, *6*, 1166-1182.

17. Kaur, P.; Hupp, J. T.; Nguyen, S. T., Porous Organic Polymers in Catalysis: Opportunities and Challenges. *ACS Catalysis,* **2011**, *1*, 819-835.

18. Chen, X.; Huang, N.; Gao, J.; Xu, H.; Xu, F.; Jiang, D., Towards Covalent Organic Frameworks with Predesignable and Aligned Open Docking Sites. *Chemical Communications,* **2014**, *50*, 6161-6163.

19. Weston, M. H.; Farha, O. K.; Hauser, B. G.; Hupp, J. T.; Nguyen, S. T., Synthesis and Metalation of Catechol-Functionalized Porous Organic Polymers. *Chemistry of Materials,* **2012**, *24*, 1292-1296.

20. Nugent, P. S.; Rhodus, V. L.; Pham, T.; Forrest, K.; Wojtas, L.; Space, B.; Zaworotko, M. J., A Robust Molecular Porous Material with High CO_2 Uptake and Selectivity. *Journal of the American Chemical Society,* **2013**, *135*, 10950-10953.

21. Nuñez, A. J.; Chang, M. S.; Ibarra, I. A.; Humphrey, S. M., Tuning the Host–Guest Interactions in a Phosphine Coordination Polymer through Different Types of post-Synthetic Modification. *Inorganic Chemistry,* **2013**, *53*, 282-288.

22. Bhargava, B. L.; Balasubramanian, S., Probing Anion–Carbon Dioxide Interactions in Room Temperature Ionic Liquids: Gas phase Cluster Calculations. *Chemical Physics Letters,* **2007**, *444*, 242-246.

23. Kazarian, S. G.; Briscoe, B. J.; Welton, T., Combining Ionic Liquids and Supercritical Fluids: ATR-IR Study of CO Dissolved in Two Ionic Liquids at High Pressures. *Chemical Communications,* **2000**, 2047-2048.

24. Bao, C.; Lu, R.; Jin, M.; Xue, P.; Tan, C.; Xu, T.; Liu, G.; Zhao, Y., Helical Stacking Tuned by Alkoxy Side Chains in π-Conjugated Triphenylbenzene Discotic Derivatives. *Chemistry – A European Journal,* **2006**, *12*, 3287-3294.

25. Chen, G.; Wang, F.; Wang, Y.; Zhang, X.; Qin, H.; Zou, H.; Xu, J., Imine-Linked Conjugated Organic Polymer Bearing Bis(imino)pyridine Ligands and its Catalytic Application in C–C Coupling Reactions. *Chinese Journal of Catalysis,* **2014**, *35*, 540-545.

26. Huang, W.; Jiang, Y.; Li, X.; Li, X.; Wang, J.; Wu, Q.; Liu, X., Solvothermal Synthesis of Microporous, Crystalline Covalent Organic Framework Nanofibers and Their Colorimetric Nanohybrid Structures. *ACS Applied Materials & Interfaces,* **2013**, *5*, 8845-8849.

27. Davis, R. N.; Tanski, J. M.; Adrian Jr, J. C.; Tyler, L. A., Variations in the Coordination Environment of Co^{2+}, Cu^{2+} and Zn^{2+} Complexes Prepared From a Tridentate (imino)pyridine Ligand and Their Structural Comparisons. *Inorganica Chimica Acta,* **2007**, *360*, 3061-3068.

28. Holland, J. M.; Liu, X.; Zhao, J. P.; Mabbs, F. E.; Kilner, C. A.; Thornton-Pett, M.; Halcrow, M. A., Copper Complexes of 2,6-Bis(iminomethyl)pyridine Derivatives and of 1,3-

Bis(pyridin-2-yl)pyrazole. Effects of Ligand Bulk and Conformational Strain on the Ground State of a Six-co-ordinate Copper(II) Ion. *Journal of the Chemical Society, Dalton Transactions,* **2000**, 3316-3324.

29. Clarke, R.; Latham, K.; Rix, C.; Hobday, M.; White, J., Supramolecular Bidentate Amine Derivatives of Copper(II) Organophosphonates. *CrystEngComm.,* **2004**, *6*, 42-50.

30. Yano, Y.; Nakano, M.; Takakura, D., The X-Ray Photoelectron Spectroscopy of Copper Complxes in the Interlayer Space of Clay Minerals. *Analytical Sciences,* **1997**, *13*, 355-358.

31. Pirhashemi, M.; Habibi-Yangjeh, A., Preparation of AgCl–ZnO Nanocomposites as Highly Efficient Visible-Light Photocatalysts in Water by One-pot Refluxing Method. *Journal of Alloys and Compounds,* **2014**, *601*, 1-8.

32. Ren, S.; Bojdys, M. J.; Dawson, R.; Laybourn, A.; Khimyak, Y. Z.; Adams, D. J.; Cooper, A. I., Porous, Fluorescent, Covalent Triazine-Based Frameworks Via Room-Temperature and Microwave-Assisted Synthesis. *Advanced Materials,* **2012**, *24*, 2357-2361.

33. Gibson, V. C.; Redshaw, C.; Solan, G. A., Bis(imino)pyridines: Surprisingly Reactive Ligands and a Gateway to New Families of Catalysts. *Chemical Reviews,* **2007**, *107*, 1745-1776.

34. Evans, J. D.; Sumby, C. J.; Doonan, C. J., Post-Synthetic Metalation of Metal-Organic Frameworks. *Chemical Society Reviews,* **2014**, *43*, 5933-5951.

35. Zhang, Z.; Gao, W.-Y.; Wojtas, L.; Ma, S.; Eddaoudi, M.; Zaworotko, M. J., Post-Synthetic Modification of Porphyrin-Encapsulating Metal–Organic Materials by Cooperative Addition of Inorganic Salts to Enhance CO_2/CH_4 Selectivity. *Angewandte Chemie International Edition,* **2012**, *51*, 9330-9334.

36. Kong, L.; Zou, R.; Bi, W.; Zhong, R.; Mu, W.; Liu, J.; Han, R. P. S.; Zou, R., Selective Adsorption of CO_2/CH_4 and CO_2/N_2 within a Charged Metal-Organic Framework. *Journal of Materials Chemistry A,* **2014**, *2*, 17771-17778.

37. Ma, H.; Ren, H.; Zou, X.; Meng, S.; Sun, F.; Zhu, G., Post-Metalation of Porous Aromatic Frameworks for Highly Efficient Carbon Capture from $CO_2 + N_2$ and $CH_4 + N_2$ Mixtures. *Polymer Chemistry,* **2014**, *5*, 144-152.

38. Xie, Y.; Wang, T.-T.; Liu, X.-H.; Zou, K.; Deng, W.-Q., Capture and Conversion of CO_2 at Ambient Conditions by a Conjugated Microporous Polymer. *Nature Communications,* **2013**, *4*, 1960–1966.

39. Wang, Z.; Yuan, S.; Mason, A.; Reprogle, B.; Liu, D.-J.; Yu, L., Nanoporous Porphyrin Polymers for Gas Storage and Separation. *Macromolecules,* **2012**, *45*, 7413-7419.

40. Ritter, N.; Antonietti, M.; Thomas, A.; Senkovska, I.; Kaskel, S.; Weber, J., Binaphthalene-Based, Soluble Polyimides: The Limits of Intrinsic Microporosity. *Macromolecules,* **2009**, *42*, 8017-8020.

41. Lu, W.; Yuan, D.; Sculley, J.; Zhao, D.; Krishna, R.; Zhou, H.-C., Sulfonate-Grafted Porous Polymer Networks for Preferential CO_2 Adsorption at Low Pressure. *Journal of the American Chemical Society,* **2011**, *133*, 18126-18129.

42. Sung, S.; Suh, M. P., Highly Efficient Carbon Dioxide Capture with a Porous Organic Polymer Impregnated with Polyethylenimine. *Journal of Materials Chemistry A,* **2014**, *2*, 13245-13249.

43. Lu, J.; Zhang, J., Facile Synthesis of Azo-Linked Porous Organic Frameworks via Reductive Homocoupling for Selective CO_2 Capture. *Journal of Materials Chemistry A,* **2014**, *2*, 13831-13834.

44. Islamoglu, T.; Gulam Rabbani, M.; El-Kaderi, H. M., Impact of Post-Synthesis Modification of Nanoporous Organic Frameworks on Small Gas Uptake and Selective CO_2 Capture. *Journal of Materials Chemistry A,* **2013**, *1*, 10259-10266.

45. Patel, H. A.; Ko, D.; Yavuz, C. T., Nanoporous Benzoxazole Networks by Silylated Monomers, Their Exceptional Thermal Stability, and Carbon Dioxide Capture Capacity. *Chemistry of Materials,* **2014**, *26*, 6729-6733.

46. Patel, H. A.; Je, S. H.; Park, J.; Chen, D. P.; Jung, Y.; Yavuz, C. T.; Coskun, A., Unprecedented High-Temperature CO_2 Selectivity in N_2-Phobic Nanoporous Covalent Organic Polymers. *Nature Communications,* **2013**, *4*, 1357.

47. Rabbani, M. G.; El-Kaderi, H. M., Synthesis and Characterization of Porous Benzimidazole-Linked Polymers and Their Performance in Small Gas Storage and Selective Uptake. *Chemistry of Materials,* **2012**, *24*, 1511-1517.

48. Errahali, M., et al., Microporous Hyper-Cross-Linked Aromatic Polymers Designed for Methane and Carbon Dioxide Adsorption. *The Journal of Physical Chemistry C,* **2014**, *118*, 28699-28710.

49. Xiang, Z.; Cao, D.; Wang, W.; Yang, W.; Han, B.; Lu, J., Postsynthetic Lithium Modification of Covalent-Organic Polymers for Enhancing Hydrogen and Carbon Dioxide Storage. *The Journal of Physical Chemistry C,* **2012**, *116*, 5974-5980.

50. Sekizkardes, A. K.; Altarawneh, S.; Kahveci, Z.; İslamoğlu, T.; El-Kaderi, H. M., Highly Selective CO_2 Capture by Triazine-Based Benzimidazole-Linked Polymers. *Macromolecules,* **2014**, *47*, 8328-8334.

51. Li, G.; Zhang, B.; Yan, J.; Wang, Z., Tetraphenyladamantane-Based Polyaminals for Highly Efficient Captures of CO_2 and Organic Vapors. *Macromolecules,* **2014**, *47*, 6664-6670.

Chapter 5

Concluding Remarks

Novel synthetic strategies were introduced for synthesis of two new classes of porous organic polymers functionalized with CO_2-philic groups. The potential applications of our azo-linked and bis(imino)pyridine linked porous polymers for selective CO_2 capture from industrially-relevant gas mixtures such as flue gas, natural gas, landfill gas were evaluated.

In our first work, we developed a new synthetic rout for the synthesis of nanoporous azo-linked polymers (ALPs) by homocoupling of two-dimensional and three-dimensional amine-based monomers. The polymerization was achieved by linking aniline-like monomers through a copper(I)-catalyzed oxidative reaction to form azo an bond. We have shown that the choice of polymerization conditions such as temperature, catalyst amount, and solvent play important roles in porosity parameters of this class of porous polymers. ALPs are mainly microporous and have high BET surface areas of up to 1235 m^2 g^{-1}. ALPs have high stabilities in acidic and basic conditions as well as high temperatures. Notably, the surface areas of ALPs (up to 1235 m^2 g^{-1}) are much higher than those of other azo-linked polymers such as azo-COPs and azo-POFs (<750 m^2 g^{-1}). Due to their higher surface areas, ALPs exhibit almost twice the CO_2 uptake capacities of azo-COPs and azo-POFs.

One of our polymers, ALP-1, has a high CO_2 uptake capacity (5.37 mmol g^{-1} at 273 K and 1 bar) which is among the best-performing porous organic polymers for CO_2 capture. ALPs have moderate biding affinities for CO_2 (~ 30 kJ mol^{-1}); and therefore, they can adsorb CO_2 molecules through physisorption. As a result, the adsorbed CO_2 in ALPs can be easily desorbed upon lowering the pressure without applying heat. ALPs show good CO_2/N_2 selectivity values (up to 43) and moderate CO_2/CH_4 selectivities (5-8). ALPs have larger pores and higher surface areas than azo-COPs. As a result, the CO_2/N_2 selectivities of ALPs (35-44) are lower than those of azo-COPs (64-110). Moreover, the selectivity of ALPs decreases upon increase in adsorption temperature; whereas, azo-COPs show enhanced selectivity values upon increase in temperature. Accordingly, we have shown that the CO_2 capturing ability of azo-linked polymers is a function of their textural properties such as pore size and surface area.

In our second work, we applied new nitrogen-rich monomers for the synthesis of novel ALPs having both high CO_2 uptake capacity and selectivity simultaneously. The CO_2 capturing performance of new ALPs was compared in detail with those of other azo-linked polymers such as azo-COPs, azo-POFs, and our previously reported ALPs. Moreover, we evaluated the potential applications of our new ALPs for pre-combustion and post-combustion CO_2 capture systems under pressure swing adsorption (PSA) and vacuum swing adsorption (VSA) settings. Consistent with previous works, our result show that ALPs with smaller pore sizes exhibit higher binding affinity (Q_{st}) values for CO_2. One of our new polymers, ALP-5, shows very high binding affinity for CO_2 (32.5 kJ mol^{-1}), which is the highest Q_{st} value among all classes of porous azo-linked polymers. Thanks to its high biding affinity of CO_2, ALP-5 outperforms the best previously reported azo-linked polymer, ALP-1, in both CO_2 uptake capacity and selectivity. We demonstrated that the CO_2 uptake capacity of ALPs is a function their surface area and their

binding affinity for CO_2. The CO_2 uptake capacity of ALPs at very low pressures is more dependent on their Q_{st} for CO_2. On the other hand, at high pressures, the CO_2 uptake capacity of ALPs correlates more with their surface areas. The evaluation of ALPs for CO_2 separation under VSA and PSA settings reveals that the CO_2 separation ability of ALPs is influenced by their surface areas and binding affinities for CO_2. Interestingly, our results show that the CO_2 capturing properties of a sorbent cannot be simultaneously optimized for all VSA and PSA applications. ALPs with high surface areas and moderate binding affinities for CO_2 are more suitable for pre-combustion applications under PSA applications. On the other hand, ALPs with moderate surface areas and high binding affinities for CO_2 are favorable for post-combustion applications under VSA settings. Our overall results show that ALPs are among the promising porous organic polymers for CO_2 separation by VSA and PSA due to their high working capacity, regenerability, and sorbent selection parameter values.

Finally, we introduced a facile synthetic route for construction of a highly porous bis(imino)pyridine-linked polymer (BIPLP-1). Due to the metal-free polymerization conditions, the bis(imino)pyridines of polymer are available for post-synthetic modifications with transition metals. We successfully functionalized BIPLP-1 with $Cu(BF_4)_2$ to improve the CO_2 capturing ability of the polymer. The functionalization of the polymer was first confirmed by appearance of characteristics peaks for Cu, F, and B atoms in XPS spectrum of the functionalized polymer. The complexation of copper cations to bis(imino)pyridines of the polymer was confirmed by observing ~1eV shift to higher binding energy in N 1S XPS peak of the polymer upon functionalization. The ICP studies showed that all bis(imino)pyridines of the polymer are successfully functionalized with $Cu(BF_4)_2$. EDX imaging studies exhibits homogenous distribution of copper cations in functionalized polymer. Importantly, the size of the pores

significantly decreased upon functionalization which confirms the pores are completely functionalized with $Cu(BF_4)_2$. The effect of functionalization on CO_2 capturing ability of the polymer was evaluated for CO_2 separation from flue gas and natural gas. Due to Lewis acid-base interactions between CO_2 molecules and BF_4^- ions, 19 % enhancement in binding affinity for CO_2 was observed upon functionalization. This resulted in a significant increase (200 %) in CO_2 uptake capacity at 0.15 bar after functionalization. The CO_2/N_2 and CO_2/CH_4 selectivities increased by a factor of up to 6. The functionalized polymer shows high CO_2/N_2 and CO_2/CH_4 selectivity values of 101 and 20, respectively. We have shown that post-synthetic functionalization of BIPLP-1 with extraneous ions can be an effective strategy to tune adsorbate-framework interactions for selective CO_2 capture. Due to the high reactivity of its bis(imino)pyridine moieties, BIPLP-1 can be functionalized with a wide variety of transition metals for selective gas capture and catalytic applications.